



2016-05-01

Lateral Resistance of H-Piles and Square Piles Behind an MSE Wall with Ribbed Strip and Welded Wire Reinforcements

Andrew I. Luna
Brigham Young University

Follow this and additional works at: <https://scholarsarchive.byu.edu/etd>

 Part of the [Civil and Environmental Engineering Commons](#)

BYU ScholarsArchive Citation

Luna, Andrew I., "Lateral Resistance of H-Piles and Square Piles Behind an MSE Wall with Ribbed Strip and Welded Wire Reinforcements" (2016). *All Theses and Dissertations*. 6346.
<https://scholarsarchive.byu.edu/etd/6346>

This Thesis is brought to you for free and open access by BYU ScholarsArchive. It has been accepted for inclusion in All Theses and Dissertations by an authorized administrator of BYU ScholarsArchive. For more information, please contact scholarsarchive@byu.edu, ellen_amatangelo@byu.edu.

Lateral Resistance of H-Piles and Square Piles Behind an MSE
Wall with Ribbed Strip and Welded Wire Reinforcements

Andrew I. Luna

A thesis submitted to the faculty of
Brigham Young University
in partial fulfillment of the requirements for the degree of
Master of Science

Kyle M. Rollins, Chair
Kevin W. Franke
Fernando S. Fonseca

Department of Civil and Environmental Engineering
Brigham Young University
May 2016

Copyright © 2016 Andrew I. Luna

All Rights Reserved

ABSTRACT

Lateral Resistance of H-Piles and Square Piles Behind an MSE Wall with Ribbed Strip and Welded Wire Reinforcements

Andrew I. Luna

Department of Civil and Environmental Engineering, BYU
Master of Science

Bridges often use pile foundations behind MSE walls to help resist lateral loading from seismic and thermal expansion and contraction loads. Overdesign of pile spacing and sizes occur owing to a lack of design code guidance for piles behind an MSE wall. However, space constraints necessitate the installation of piles near the wall. Full scale lateral load tests were conducted on piles behind an MSE wall. This study involves the testing of four HP12X74 H-piles and four HSS12X12X5/16 square piles. The H-piles were tested with ribbed strip soil reinforcement at a wall height of 15 feet, and the square piles were tested with welded wire reinforcement at a wall height of 20 feet. The H-piles were spaced from the back face of the MSE wall at pile diameters 4.5, 3.2, 2.5, and 2.2. The square piles were spaced at pile diameters 5.7, 4.2, 3.1, and 2.1. Testing was based on a displacement control method where load increments were applied every 0.25 inches up to three inches of pile deflection. It was concluded that piles placed closer than 3.9 pile diameters have a reduction in their lateral resistance. P-multipliers were back-calculated in LPILE from the load-deflection curves obtained from the tests. The p-multipliers were found to be 1.0, 0.85, 0.60, and 0.73 for the H-piles spaced at 4.5, 3.2, 2.5, and 2.2 pile diameters, respectively. The p-multipliers for the square piles were found to be 1.0, 0.77, 0.63, and 0.57 for piles spaced at 5.7, 4.2, 3.1, and 2.1 pile diameters, respectively. An equation was developed to estimate p-multipliers versus pile distance behind the wall. These p-multipliers account for reduced soil resistance, and decrease linearly with distance for piles placed closer than 3.9 pile diameters.

Measurements were also taken of the force induced in the soil reinforcement. A statistical analysis was performed to develop an equation that could predict the maximum induced reinforcement load. The main parameters that went into this equation were the lateral pile load, transverse distance from the reinforcement to the pile center normalized by the pile diameter, spacing from the pile center to the wall normalized by the pile diameter, vertical stress, and reinforcement length to height ratio where the height included the equivalent height of the surcharge. The multiple regression equations account for 76% of the variation in observed tensile force for the ribbed strip reinforcement, and 77% of the variation for the welded wire reinforcement. The tensile force was found to increase in the reinforcement as the pile spacing decreased, transverse spacing from the pile decreased, and as the lateral load increased.

Keywords: laterally loaded piles, MSE wall, p-multiplier, welded wire reinforcement, ribbed strip reinforcement, p-y curve, tensile force, reinforcement load

ACKNOWLEDGEMENTS

Funding for this project has been provided for by FHWA pooled sponsors. These Department of Transportation sponsors were from the states of Utah (the lead agency with Jason Richards as the project manager), Florida, Iowa, Kansas, Massachusetts, Minnesota, Montana, New York, Oregon, and Texas. In-kind donations were made from Reinforced Earth Company which provided the ribbed strip reinforcement, and SSL, Inc. which provided the welded wire reinforcement. Other in-kind donations included Atlas Tube, Spartan Steel, and Skyline Steel whom provided the pile foundations, and Desert Deep Foundations, Inc. whom provided the pile driving. The opinions, conclusions, and recommendations of this project does not necessarily represent those of the sponsoring organizations.

I would like to thank Geneva Rock for providing the test site for this project, and Hadco Construction for building the wall. My appreciation also goes out to David Anderson and Rodney Mayo for their assistance in the pile testing. Others involved in the project that I would like to thank are Cody Hatch, Jarell Han, Guillermo Bustamante, Jason Besendorfer, Ryan Budd, Dalin Russell, Rawley Selk, and Kyle Chavez.

I would like to express my gratefulness and appreciation to Dr. Kyle M. Rollins for giving me the opportunity to pursue my master's degree at BYU, and for everything he has taught me. I would also like to thank Dr. Kevin W. Franke and Dr. Fernando S. Fonseca for their help on my graduate committee, and for the things they have taught me. I would love to thank my parents, Leo and Yanina, for all of their help and support during my time at BYU. Last, but certainly not least, I would love to thank my wife Gloria for believing in me and helping me accomplish my goals.

TABLE OF CONTENTS

LIST OF TABLES	ix
LIST OF FIGURES	xii
1 Introduction.....	1
1.1 Objectives	3
1.2 Scope.....	3
1.3 Thesis Organization	4
2 Literature Review	5
2.1 MSE Wall Design (Berg, Christopher, & Samtani, 2009).....	5
2.2 Pullout Resistance Factor Tests	18
2.3 Laterally Loaded Pile Design (Isenhower & Wang, 2015)	23
2.4 Previous Related Testing and Research.....	30
2.4.1 Tests with Drilled Shafts and Geogrid Reinforcement (Pierson, Parsons, Han, Brown, & Thompson, 2009)	30
2.4.2 Tests with Driven Pipe Piles and Metallic Reinforcements (Rollins, Price, & Nelson, 2013).....	34
2.4.3 Lateral Load Tests on Pipe Piles Behind an MSE Wall with Metallic Reinforcement (Hatch, 2014; Han, 2014; Besendorfer, 2015; Budd, 2016)	41
3 Test Layout	47
3.1 MSE Wall and Soil Reinforcement	48
3.1.1 Backfill.....	53
3.1.2 Surcharge	60
3.2 Piles.....	60
3.3 Loading Apparatus.....	63
3.3.1 Data Acquisition	66
4 Instrumentation.....	67

4.1	Load Cell and Pressure Transducers.....	67
4.2	String Potentiometers.....	67
4.3	Strain Gauges.....	71
4.3.1	Soil Reinforcement Strain Gauges.....	72
4.3.2	Pile Strain Gauges.....	74
4.4	Shape Arrays.....	74
4.5	Digital Image Correlation (DIC).....	75
4.6	Surveying.....	76
5	Lateral Load Testing	77
5.1	Load Displacement Curves.....	77
5.1.1	H-Piles.....	77
5.1.2	Square Piles.....	82
5.2	Soil Reinforcement Performance.....	85
5.2.1	H-Piles.....	85
5.2.2	Square Piles.....	92
5.3	Statistical Analysis of Load in the Reinforcement	98
5.3.1	Ribbed Strip Soil Reinforcement.....	98
5.3.2	Welded Wire Soil Reinforcement.....	110
5.4	Ground Displacement	119
5.4.1	H-Piles.....	119
5.4.2	Square Piles.....	126
5.5	Wall Panel Displacement.....	132
5.5.1	H-Piles.....	132
5.5.2	Square Piles.....	146
5.6	Bending Moment versus Depth Curves	159

5.6.1	H-Piles.....	159
5.6.2	Square Piles.....	163
6	Lateral Pile Load Analysis	168
6.1	Material Properties.....	169
6.1.1	H-Piles.....	169
6.1.2	Square Piles.....	171
6.2	Results of LPILE Analysis	174
6.2.1	H-Piles.....	174
6.2.2	Square Piles.....	182
6.2.3	P-Multipliers versus Pile Spacing Curves.....	188
6.2.4	Pile Head Load versus Rotation Curves	197
6.2.4.1	H-Piles	197
6.2.4.2	Square Piles	200
6.2.5	Bending Moment versus Depth Curves	202
6.2.5.1	H-Piles	202
6.2.5.2	Square Piles	205
7	Conclusion	209
7.1	Conclusions Relative to Lateral Pile Resistance.....	209
7.2	Conclusions Relative to Force Induced in the Reinforcements.....	211
7.3	Recommendations for Further Research.....	211
	REFERENCES.....	213
	Appendix A. Capacity to Demand Ratio Against Pullout Calculations.....	216
	Ribbed Strip Reinforcement	217
	Welded Wire Reinforcement	218
	Appendix B. Geneva Rock Laboratory Test Reports	219

Phase 1	219
Phase 2	220
Appendix C. Load Displacement Curves.....	221
H-Piles	222
Square Piles.....	224
Appendix D. Induced Force in the Reinforcement Curves.....	226
H-Piles	227
4.5D Soil Reinforcement Curves	227
3.2D Soil Reinforcement Curves	229
2.5D Soil Reinforcement Curves	231
2.2D Soil Reinforcement Curves	233
Square Piles.....	235
5.7D Soil Reinforcement Curves	235
4.2D Soil Reinforcement Curves	238
3.1D Soil Reinforcement Curves	240
2.1D Soil Reinforcement Curves	242
Appendix E. Statistical Analysis Data of Pipe Piles Within Ribbed Strip Reinforcement	244
Appendix F. Vertical Ground Displacement Curves	252
H-Piles	253
Square Piles.....	255
Appendix G. Maximum Reinforcement Force Against H-Pile and Square Pile Head Displacement Curves	257
H-Piles	258
Square Piles.....	260
Appendix H. Pile Driving Blowcounts	262

Appendix I.	Plug Depths	264
Appendix J.	Horizontal Spacing of Pipe Piles	265
Appendix K.	RECo MSE Wall Plans	266
Appendix L.	SSL MSE Wall Plans	271

LIST OF TABLES

Table 2-1. Pullout Resistance Factor Welded Wire Grid Testing Parameters.....	19
Table 2-2. Shaft Distances and Capacity from Pierson (2009).....	32
Table 2-3. Summary Table for Piles Tested by Rollins et al. (2013)	36
Table 2-4. P-multipliers of Test Piles from Price (2012) and Nelson (2013).....	39
Table 2-5. Summary Table for Piles Tested in Ribbed Metal Strip Reinforcement (Han, 2014 & Besendorfer, 2015).....	45
Table 2-6. Summary Table for Piles Tested in Welded Wire Reinforcement (Hatch, 2014 & Budd, 2016).....	46
Table 3-1. Welded Wire Orientation Details	52
Table 3-2. Sieve Size and Percent Passing	53
Table 3-3. Phase 1 and Phase 2 Soil Parameters	54
Table 3-4. Average Soil Measurements for Phase 1	56
Table 3-5. Average Soil Measurements for Phase 2.....	56
Table 3-6. Adjacent Spacing of H-piles.....	61
Table 3-7. Adjacent Spacing of Square Piles.....	62
Table 3-8. H-pile and Square Pile Diameter Spacing	63
Table 4-1. H-pile String Potentiometer Locations	71
Table 4-2. Square Pile String Potentiometer Locations.....	71
Table 4-3. H-pile Strain Gauge Locations	73
Table 4-4. Square Pile Strain Gauge Locations	73
Table 4-5. Location of Shape Arrays	75
Table 5-1. Statistical Analysis of Ribbed Strip Reinforcement.....	100
Table 5-2. Term Elimination with the Change of R^2 and Adjusted R^2 for Ribbed Strip Reinforcement.....	101
Table 5-3. ANOVA for Ribbed Strip Reinforcement.....	101

Table 5-4. Confidence Interval Values for Ribbed Strip Reinforcement	102
Table 5-5. Numerical Range of Parameters for Ribbed Strip Reinforcement Statistical Analysis.....	110
Table 5-6. Statistical Analysis of Welded Wire Reinforcement.....	111
Table 5-7. Term Elimination with the Change of R^2 and Adjusted R^2 for Welded Wire Reinforcement.....	111
Table 5-8. ANOVA for Welded Wire Reinforcement.....	112
Table 5-9. Confidence Interval Values for Welded Wire Reinforcement	112
Table 5-10. Numerical Range of Parameters for Welded Wire Reinforcement Statistical Analysis.....	119
Table 5-11. H-Pile String Potentiometers for Wall Displacement at Peak Loads	133
Table 5-12. Transverse Distance from Nearest Panel Joint to Center of H-Pile	134
Table 5-13. H-Pile Shape Array Transverse Distances	134
Table 5-14. Square Pile String Potentiometers for Wall Displacement at Peak Loads	146
Table 5-15. Transverse Distance from Nearest Panel Joint to Center of Square Pile	147
Table 5-16. Square Pile Shape Array Transverse Distances.....	147
Table 6-1. LPILE Pile Materials for H-Piles	169
Table 6-2. LPILE Soil Profile for H-Piles with no Surcharge.....	170
Table 6-3. LPILE Soil Profile for H-Piles with Surcharge.....	171
Table 6-4. LPILE Pile Materials for Square Piles	172
Table 6-5. LPILE Soil Profile for Square Piles	173
Table 6-6. LPILE Soil Profile for Square Piles with Surcharge.....	173
Table 6-7. Comparison of Friction Angles from LPILE of Different Studies.....	173
Table 6-8. P-multipliers for H-Piles from LPILE.....	176
Table 6-9. P-multipliers for Square Piles from LPILE.....	183
Table 6-10. Summary of P-multipliers	196

Table E-1. Statistical Analysis Data of Ribbed Strip Reinforcement of Pipe Piles.....	244
Table E-2. Term Elimination with the Change of R^2 and Adjusted R^2 of Pipe Piles Data....	244
Table E-3. ANOVA for Ribbed Strip Reinforcement Data of Pipe Piles.....	245
Table E-4. Confidence Interval Values for Ribbed Strip Reinforcement Data of Pipe Piles.....	245
Table E-5. Numerical Range of Parameters for Ribbed Strip Reinforcement Statistical Analysis for Pipe Piles.....	251
Table H-1. Pile Driving Blow Counts for the H-Piles.....	262
Table H-2. Pile Driving Blow Counts for the Square Piles.....	263
Table I-1. Plug Depths for Pipe and Square Piles.....	264
Table J-1. Adjacent Spacing of Pipe Piles on the Ribbed Strip Side.....	265
Table J-2. Adjacent Spacing of Pipe Piles on the Welded Wire Side.....	265

LIST OF FIGURES

Figure 1-1. Cross-section of abutment piles behind an MSE wall.	2
Figure 2-1. The reinforced soil zone (modified from Berg et al., 2009).	7
Figure 2-2. Relative displacement versus L/H ratio (Berg et al., 2009).	8
Figure 2-3. External failure modes of MSE walls (Berg et al., 2009).	9
Figure 2-4. Reinforcement active and resistant zones (Berg et al., 2009).	10
Figure 2-5. Visual description of reinforcement width and horizontal spacing (Berg et al., 2009).	11
Figure 2-6. MSE soil profile with equivalent surcharge.	13
Figure 2-7. Depth versus K_r/K_a ratio (Berg et al., 2009).	14
Figure 2-8. Default values for pullout friction factor (<i>AASHTO LRFD Bridge Design Specifications</i> , 2012).	20
Figure 2-9. Depth of fill versus pullout resistance factor for ribbed steel strips (Jayawickrama et al., 2015).	21
Figure 2-10. Depth of fill versus normalized pullout resistance factor for welded wire grids (Jayawickrama et al., 2015).	22
Figure 2-11. Reaction of stresses after lateral deflection of pile (Isenhower et al., 2015).	24
Figure 2-12. Model showing how LPILE models p-y curves (Isenhower et al., 2015).	25
Figure 2-13. Failure wedge of pile in sand near ground surface (Isenhower et al., 2015).	26
Figure 2-14. Ultimate lateral resistance coefficients versus angle of friction (Isenhower et al., 2015).	28
Figure 2-15. Initial modulus of subgrade reaction versus friction angle and relative density (Isenhower et al., 2015).	29
Figure 2-16. Single shaft peak load versus displacement curves for shafts spaced at 1, 2, 3 and 4 pile diameters (D) behind the MSE wall (Pierson, 2009).	32
Figure 2-17. Peak load versus displacement for single, group, and short shafts installed at 2 pile diameters behind the MSE wall (Pierson et al., 2009).	33

Figure 2-18. Horizontal wall deflection for Shaft C (Pierson et al., 2009).....	34
Figure 2-19. US Highway 89 location showing pile head load versus pile head deflection, peak data points for TP1 and TP2 (Price, 2012).	37
Figure 2-20. Pioneer Crossing location showing pile head load versus pile head deflection, peak data points for TP3, TP4, and TP5 (Price, 2012).	38
Figure 2-21. Provo Center Street location showing pile head load versus pile head deflection, peak data points for TP6, TP7, and TP8 (Nelson, 2013).	38
Figure 2-22. Normalized induced load versus normalized distance for welded wire reinforcement (Price, 2012).	40
Figure 2-23. Normalized induced load versus normalized distance for ribbed strip reinforcement (Nelson, 2013).	41
Figure 2-24. P-multipliers versus normalized distance from wall (modified from Budd, 2016).	44
Figure 3-1. Test site location (GOOGLE EARTH, 2013).	47
Figure 3-2. Elevation view of MSE wall.	49
Figure 3-3. Photograph of the completed MSE wall.	50
Figure 3-4. Panel configuration for the ribbed strip reinforcement side of the MSE wall.....	51
Figure 3-5. Panel configuration for the welded wire reinforcement side of the MSE wall.....	51
Figure 3-6. Soil percent passing versus grain size.	54
Figure 3-7. Depth versus relative compaction, Phase 1.....	57
Figure 3-8. Depth versus relative compaction, Phase 2.....	57
Figure 3-9. Depth versus moisture content, Phase 1.....	58
Figure 3-10. Depth versus moisture content, Phase 2.....	58
Figure 3-11. Depth versus moist unit weight, Phase 1.	59
Figure 3-12. Depth versus moist unit weight, Phase 2.	59
Figure 3-13. Plan view of MSE wall.	62
Figure 3-14. Reaction beam with hemispherical end platen and struts.	64

Figure 3-15. Loading apparatus, reaction beam, and surcharge blocks.....	64
Figure 3-16. Loading apparatus.	65
Figure 3-17. Cross-section through the MSE wall.....	65
Figure 4-1. String potentiometers attached to a square pile at the load cell level.	68
Figure 4-2. String potentiometer attached three feet above the pile.	69
Figure 4-3. String potentiometers attached to stakes for horizontal ground displacement readings.....	70
Figure 4-4. DIC setup in front of the MSE wall.	76
Figure 5-1. Pile head load versus deflection curves for H-piles at peak.....	79
Figure 5-2. Pile head load versus deflection curves for H-piles at one-minute average.	80
Figure 5-3. Pile head load versus deflection curves for H-piles at five-minute average.	80
Figure 5-4. Pile head load versus pile head rotation for all H-piles and the H-pile reaction pile.....	82
Figure 5-5. Pile head load versus deflection curves for square piles at peak.	83
Figure 5-6. Pile head load versus deflection curves for square piles at one-minute average.	84
Figure 5-7. Pile head load versus deflection curves for square piles at five-minute average.	84
Figure 5-8. Pile head load versus pile head rotation for all square piles and the square reaction pile.....	85
Figure 5-9. Reinforcement force versus distance from back face of MSE wall (H-pile 3.2D, 15-inch depth, strip #4, transverse spacing 52.6 inches).	88
Figure 5-10. Interaction between MSE wall, soil, and reinforcement.	89
Figure 5-11. Maximum reinforcement force for each instrumented ribbed strip versus pile head load for H-pile 4.5D.	90
Figure 5-12. Maximum reinforcement force for each instrumented ribbed strip versus pile head load for H-pile 3.2D.	91
Figure 5-13. Maximum reinforcement force for each instrumented ribbed strip versus pile head load for H-pile 2.5D.	91

Figure 5-14. Maximum reinforcement force for each instrumented ribbed strip versus pile head load for H-pile 2.2D.	92
Figure 5-15. Reinforcement force versus distance from back face of MSE wall (square pile 5.7D, 45-inch depth, welded wire #26, transverse spacing 28.5 inches).....	94
Figure 5-16. Maximum reinforcement force for each instrumented welded wire versus pile head load for square pile 5.7D.	95
Figure 5-17. Maximum reinforcement force for each instrumented welded wire versus pile head load for square pile 4.2D.	96
Figure 5-18. Maximum reinforcement force for each instrumented welded wire versus pile head load for square pile 3.1D.	96
Figure 5-19. Maximum reinforcement force for each instrumented welded wire versus pile head load for square pile 2.1D.	97
Figure 5-20. Log measured maximum tensile force versus log predicted maximum tensile force, ribbed strip reinforcement.	104
Figure 5-21. Measured maximum tensile force versus predicted maximum tensile force, ribbed strip reinforcement.....	105
Figure 5-22. Log residual versus pile load, ribbed strip reinforcement.....	106
Figure 5-23. Log residual versus normalized transverse distance, ribbed strip reinforcement.	107
Figure 5-24. Log residual versus vertical stress, ribbed strip reinforcement.....	107
Figure 5-25. Log residual versus normalized spacing, ribbed strip reinforcement.	108
Figure 5-26. Log residual versus L/H ratio, ribbed strip reinforcement.	108
Figure 5-27. Log residual versus log predicted maximum tensile force, ribbed strip reinforcement.	109
Figure 5-28. Log measured maximum tensile force versus log predicted maximum tensile force, welded wire reinforcement.....	114
Figure 5-29. Measured maximum tensile force versus predicted maximum tensile force, welded wire reinforcement.	115
Figure 5-30. Log residual versus pile load, welded wire reinforcement.	116
Figure 5-31. Log residual versus normalized transverse distance, welded wire reinforcement.	116

Figure 5-32. Log residual versus vertical stress, welded wire reinforcement.	117
Figure 5-33. Log residual versus normalized spacing, welded wire reinforcement.	117
Figure 5-34. Log residual versus L/H ratio, welded wire reinforcement.....	118
Figure 5-35. Log residual versus log predicted maximum tensile force, welded wire reinforcement.	118
Figure 5-36. Horizontal ground displacement versus distance from the back face of the MSE wall, 4.5D H-pile.	120
Figure 5-37. Horizontal ground displacement versus distance from the back face of the MSE wall, 3.2D H-pile.	121
Figure 5-38. Horizontal ground displacement versus distance from the back face of the MSE wall, 2.5D H-pile.	121
Figure 5-39. Horizontal ground displacement versus distance from the back face of the MSE wall, 2.2D H-pile.	122
Figure 5-40. Horizontal ground displacement versus distance from the back face of the MSE wall without omitting the data point closest to the pile, 2.5D H-pile.....	122
Figure 5-41. Horizontal ground displacement normalized by the displacement at the pile face extrapolated to the ground surface versus normalized distance from pile face for all H-piles for the 2" load increment.	124
Figure 5-42. Horizontal ground displacement normalized by the displacement at the pile face extrapolated to the ground surface versus normalized distance from pile face for all H-piles for the 0.25", 0.5", 1", 2", and 3" load increments with the best fit line.....	124
Figure 5-43. Vertical ground displacement versus distance from the back face of the MSE wall for all H-piles.	125
Figure 5-44. Horizontal ground displacement versus distance from the back face of the MSE wall, 5.7D square pile.	126
Figure 5-45. Horizontal ground displacement versus distance from the back face of the MSE wall, 4.2D square pile.	127
Figure 5-46. Horizontal ground displacement versus distance from the back face of the MSE wall, 3.1D square pile.	127
Figure 5-47. Horizontal ground displacement versus distance from the back face of the MSE wall, 2.1D square pile.	128

Figure 5-48. Horizontal ground displacement versus distance from the back face of the MSE wall without omitting data the point closest to the pile, 3.1D square pile.....	128
Figure 5-49. Horizontal ground displacement normalized by the displacement at the pile face extrapolated to the ground surface versus normalized distance from pile face for all square piles for the 3” load increment.	130
Figure 5-50. Horizontal ground displacement normalized by the displacement at the pile face extrapolated to the ground surface versus normalized distance from pile face for all square piles for the 0.25”, 0.5”, 1”, 2”, and 3” load increments with the best fit line.....	130
Figure 5-51. Square and H-pile comparison of the best fit lines of the horizontal ground displacement normalized by the displacement at the pile face extrapolated to the ground surface versus normalized distance from pile.....	131
Figure 5-52. Vertical ground displacement versus distance from the back face of the MSE wall for all square piles.....	132
Figure 5-53. DIC wall displacement for the 4.5D H-pile at the 44.1 kip and 3” load increment.....	135
Figure 5-54. DIC wall displacement for the 3.2D H-pile at the 43.8 kip and 3” load increment.....	135
Figure 5-55. DIC wall displacement for the 2.5D H-pile at the 30.4 kip and 2.25” load increment.....	136
Figure 5-56. DIC wall displacement for the 2.2D H-pile at the 37.8 kip and 2” load increment.....	136
Figure 5-57. Wall deflection at reinforcement locations and top of wall versus pile head load, 4.5D H-pile.....	139
Figure 5-58. Wall deflection at reinforcement locations and top of wall versus pile head load , 3.2D H-pile.....	139
Figure 5-59. Wall deflection at reinforcement locations and top of wall versus pile head load , 2.5D H-pile.....	140
Figure 5-60. Wall deflection at reinforcement locations and top of wall versus pile head load, 2.2D H-pile.....	140
Figure 5-61. Depth from the 15-foot ground surface versus peak wall displacement at the 3” load increment for 4.5D H-pile.....	141
Figure 5-62. Depth from the 15-foot ground surface versus peak wall displacement at the 3” load increment for 3.2D H-pile.....	142

Figure 5-63. Depth from the 15-foot ground surface versus peak wall displacement at the 2.25" load increment for 2.5D H-pile.	142
Figure 5-64. Depth from the 15-foot ground surface versus peak wall displacement at the 2" load increment for 2.2D H-pile.	143
Figure 5-65. Depth from the 15-foot ground surface versus wall deflection from shape array for 3" load increment, 4.5D H-pile.	144
Figure 5-66. Depth from the 15-foot ground surface versus wall deflection from shape array for 3" load increment, 3.2D H-pile.	144
Figure 5-67. Depth from the 15-foot ground surface versus wall deflection from shape array for 2.25" load increment, 2.5D H-pile.	145
Figure 5-68. Depth from the 15-foot ground surface versus wall deflection from shape array for 2" load increment, 2.2D H-pile.	145
Figure 5-69. DIC wall displacement for the 5.7D square pile at the 51.9 kip and 3" load increment.	148
Figure 5-70. DIC wall displacement for the 4.2D square pile at the 46.4 kip and 3" load increment.	148
Figure 5-71. DIC wall displacement for the 3.1D square pile at the 42.6 kip and 3" load increment.	149
Figure 5-72. DIC wall displacement for the 2.1D square pile at the 40.1 kip and 3" load increment.	149
Figure 5-73. Wall deflection at reinforcement locations and top of wall versus pile head load, 5.7D square pile.	151
Figure 5-74. Wall deflection at reinforcement locations and top of wall versus pile head load, 4.2D square pile.	152
Figure 5-75. Wall deflection at reinforcement locations and top of wall versus pile head load, 3.1D square pile.	152
Figure 5-76. Wall deflection at top of wall versus pile head load, 2.1D square pile.	153
Figure 5-77. Depth from the 20-foot ground surface versus wall deflection from shape array for 3" load increment, 5.7D square pile.	154
Figure 5-78. Depth from the 20-foot ground surface versus wall deflection from shape array for 3" load increment, 4.2D square pile.	155
Figure 5-79. Depth from the 20-foot ground surface versus wall deflection from shape array for 3" load increment, 3.1D square pile.	155

Figure 5-80. Depth from the 20-foot ground surface versus wall deflection from shape array for 3” load increment, 2.1D square pile.....	156
Figure 5-81. Depth from the 20-foot ground surface versus wall deflection from shape array for 3” load increment, 5.7D square pile.....	157
Figure 5-82. Depth from the 20-foot ground surface versus wall deflection from shape array for 3” load increment, 4.2 square pile.....	157
Figure 5-83. Depth from the 20-foot ground surface versus wall deflection from shape array for 3” load increment at 5-minute hold, 3.1D square pile.	158
Figure 5-84. Depth from the 20-foot ground surface versus wall deflection from shape array for 3” load increment, 2.1D square pile.....	158
Figure 5-85. Bending moment versus depth curves for four load levels during test of 4.5D H-pile.	161
Figure 5-86. Bending moment versus depth curves for four load levels during test of 3.2D H-pile.	161
Figure 5-87. Bending moment versus depth curves for three load levels during test of 2.5D H-pile.	162
Figure 5-88. Bending moment versus depth curves for three load levels during test of 2.2D H-pile.	162
Figure 5-89. Maximum moment corresponding to the 0.5-, 1-, 2-, and 3-inch pile displacement normalized by pile head load versus distance from MSE wall normalized by pile diameter for H-piles.	163
Figure 5-90. Square pile rotation needing correction for calculating pile bending moments.....	164
Figure 5-91. Bending moment versus depth curves for four load levels during test of 5.7D square pile.	165
Figure 5-92. Bending moment versus depth curves for four load levels during test of 4.2D square pile.	165
Figure 5-93. Bending moment versus depth curves for four load levels during test of 3.1D square pile.	166
Figure 5-94. Bending moment versus depth curves for four load levels during test of 2.1D square pile.	166

Figure 5-95. Maximum moment corresponding to the 0.5-, 1-, 2-, and 3-inch pile displacement normalized by pile head load versus distance from MSE wall normalized by pile diameter for square piles.	167
Figure 6-1. Comparison of measured pile head load versus deflection curve for the 4.5D H-pile with curves computed using LPILE assuming no surcharge and 600 psf surcharge.	176
Figure 6-2. Comparison of measured pile head load versus deflection curve for the 3.2D H-pile with curves computed using LPILE assuming no surcharge and 600 psf surcharge.	177
Figure 6-3. Comparison of measured pile head load versus deflection curve for the 2.5D H-pile with curves computed using LPILE assuming no surcharge and 600 psf surcharge.	177
Figure 6-4. Comparison of measured pile head load versus deflection curve for the 2.2D H-pile with curves computed using LPILE assuming no surcharge and 600 psf surcharge.	178
Figure 6-5. Comparison of load-deflection curve for 4.5D H-pile with curves for pipe piles at the similar spacing of the nominal 5D distance.	179
Figure 6-6. Comparison of load-deflection curve for 3.2D H-pile with curves for pipe piles at the similar spacing of the nominal 4D distance.	180
Figure 6-7. Comparison of load-deflection curve for 2.5D H-pile with curves for pipe piles at the similar spacing of the nominal 3D distance.	180
Figure 6-8. Comparison of load-deflection curve for 2.2D H-pile with curves for pipe piles at the similar spacing of the nominal 2D distance.	181
Figure 6-9. Comparison of the most comparable spacing for 3.2D H-pile and curves for pipe piles.	181
Figure 6-10. Comparison of measured pile head load versus deflection curve for the 5.7D square pile with curves computed using LPILE assuming no surcharge and 600 psf surcharge.	183
Figure 6-11. Comparison of measured pile head load versus deflection curve for the 4.2D square pile with curves computed using LPILE assuming no surcharge and 600 psf surcharge.	184
Figure 6-12. Comparison of measured pile head load versus deflection curve for the 3.1D square pile with curves computed using LPILE assuming no surcharge and 600 psf surcharge.	184

Figure 6-13. Comparison of measured pile head load versus deflection curve for the 2.1D square pile with curves computed using LPILE assuming no surcharge and 600 psf surcharge.	185
Figure 6-14. Comparison of load-deflection curve for 5.7D square pile with curves for pipe piles at the similar spacing of the nominal 5D distance.....	186
Figure 6-15. Comparison of load-deflection curve for 4.2D square pile with curves for pipe piles at the similar spacing of the nominal 4D distance.....	186
Figure 6-16. Comparison of load-deflection curve for 3.1D square pile with curves for pipe piles at the similar spacing of the nominal 3D distance.....	187
Figure 6-17. Comparison of load-deflection curve for 2.1D square pile with curves for pipe piles at the similar spacing of the nominal 2D distance.....	187
Figure 6-18. Comparison of p-multiplier versus normalized distance from MSE wall from data from Price (2012), Nelson (2013), Hatch (2014), Han (2014), Besendorfer (2015), Budd (2016), and this study with the best fit line with data points used for Equation (6-1a) and within the bounds of Equation (6-1b).	189
Figure 6-19. Comparison of p-multiplier versus normalized distance from MSE wall from data from Price (2012), Nelson (2013), Hatch (2014), Han (2014), Besendorfer (2015), Budd (2016), and this study without the aberrations with the best fit line with data points used for Equation (6-2a) and within the bounds of Equation (6-2b).....	191
Figure 6-20. P-multiplier versus normalized distance from wall comparing L/H ratios from data from Price (2012), Nelson (2013), Hatch (2014), Han (2014), Besendorfer (2015), Budd (2016), and this study.....	192
Figure 6-21. P-multiplier versus normalized distance from wall comparing reinforcement types from data from Price (2012), Nelson (2013), Hatch (2014), Han (2014), Besendorfer (2015), Budd (2016), and this study.	193
Figure 6-22. P-multiplier versus normalized distance from wall comparing wall systems from data from Price (2012), Nelson (2013), Hatch (2014), Han (2014), Besendorfer (2015), Budd (2016), and this study.	193
Figure 6-23. P-multiplier versus normalized distance from wall comparing pile shapes from data from Price (2012), Nelson (2013), Hatch (2014), Han (2014), Besendorfer (2015), Budd (2016), and this study.	194
Figure 6-24. P-multiplier versus normalized distance from wall comparing pile diameters from data from Price (2012), Nelson (2013), Hatch (2014), Han (2014), Besendorfer (2015), Budd (2016), and this study.	194

Figure 6-25. P-multiplier versus normalized distance from wall comparing pile locations behind the panel center or joint from data from Price (2012), Nelson (2013), Hatch (2014), Han (2014), Besendorfer (2015), Budd (2016), and this study.....	195
Figure 6-26. Comparison of measured pile head load versus pile head rotation curve for the 4.5D H-pile with curves computed using LPILE assuming no surcharge and 600 psf surcharge.	198
Figure 6-27. Comparison of measured pile head load versus pile head rotation curve for the 3.2D H-pile with curves computed using LPILE assuming no surcharge and 600 psf surcharge.	198
Figure 6-28. Comparison of measured pile head load versus pile head rotation curve for the 2.5D H-pile with curves computed using LPILE assuming no surcharge and 600 psf surcharge.	199
Figure 6-29. Comparison of measured pile head load versus pile head rotation curve for the 2.2D H-pile with curves computed using LPILE assuming no surcharge and 600 psf surcharge.	199
Figure 6-30. Comparison of measured pile head load versus pile head rotation curve for the 5.7D square pile with curves computed using LPILE assuming no surcharge and 600 psf surcharge.....	200
Figure 6-31. Comparison of measured pile head load versus pile head rotation curve for the 4.2D square pile with curves computed using LPILE assuming no surcharge and 600 psf surcharge.....	201
Figure 6-32. Comparison of measured pile head load versus pile head rotation curve for the 3.1D square pile with curves computed using LPILE assuming no surcharge and 600 psf surcharge.....	201
Figure 6-33. Comparison of measured pile head load versus pile head rotation curve for the 2.1D square pile with curves computed using LPILE assuming no surcharge and 600 psf surcharge.....	202
Figure 6-34. Comparison of depth from the ground surface versus pile bending moment curve and LPILE curves of both with the surcharge model and without the surcharge model for the 4.5D H-pile.	203
Figure 6-35. Comparison of depth from the ground surface versus pile bending moment curve and LPILE curves of both with the surcharge model and without the surcharge model for the 3.2D H-pile.	204
Figure 6-36. Comparison of depth from the ground surface versus pile bending moment curve and LPILE curves of both with the surcharge model and without the surcharge model for the 2.5D H-pile.	204

Figure 6-37. Comparison of depth from the ground surface versus pile bending moment curve and LPILE curves of both with the surcharge model and without the surcharge model for the 2.2D H-pile.	205
Figure 6-38. Comparison of depth from the ground surface versus pile bending moment curve and LPILE curves of both with the surcharge model and without the surcharge model for the 5.7D square pile.	206
Figure 6-39. Comparison of depth from the ground surface versus pile bending moment curve and LPILE curves of both with the surcharge model and without the surcharge model for the 4.2D square pile.	207
Figure 6-40. Comparison of depth from the ground surface versus pile bending moment curve and LPILE curves of both with the surcharge model and without the surcharge model for the 3.1D square pile.	207
Figure 6-41. Comparison of depth from the ground surface versus pile bending moment curve and LPILE curves of both with the surcharge model and without the surcharge model for the 2.1D square pile.	208
Figure C-1. Pile head load versus pile head deflection comparing peak, 1-minute hold, and 5-minute hold for 4.5D H-pile.	222
Figure C-2. Pile head load versus pile head deflection comparing peak, 1-minute hold, and 5-minute hold for 3.2D H-pile.	222
Figure C-3. Pile head load versus pile head deflection comparing peak, 1-minute hold, and 5-minute hold for 2.5D H-pile.	223
Figure C-4. Pile head load versus pile head deflection comparing peak, 1-minute hold, and 5-minute hold for 2.2D H-pile.	223
Figure C-5. Pile head load versus pile head deflection comparing peak, 1-minute hold, and 5-minute hold for 5.7D square pile.	224
Figure C-6. Pile head load versus pile head deflection comparing peak, 1-minute hold, and 5-minute hold for 4.2D square pile.	224
Figure C-7. Pile head load versus pile head deflection comparing peak, 1-minute hold, and 5-minute hold for 3.1D square pile.	225
Figure C-8. Pile head load versus pile head deflection comparing peak, 1-minute hold, and 5-minute hold for 2.1D square pile.	225
Figure D-1. Reinforcement force versus distance from back face of MSE wall (H-pile 4.5D, 15-inch depth, strip #3, transverse spacing 34.1 inches).	227

Figure D-2. Reinforcement force versus distance from back face of MSE wall (H-pile 4.5D, 15-inch depth, strip #4, transverse spacing 8.6 inches).	227
Figure D-3. Reinforcement force versus distance from back face of MSE wall (H-pile 4.5D, 45-inch depth, strip #16, transverse spacing 32.6 inches).	228
Figure D-4. Reinforcement force versus distance from back face of MSE wall (H-pile 4.5D, 45-inch depth, strip #11, transverse spacing 8.1 inches).	228
Figure D-5. Reinforcement force versus distance from back face of MSE wall (H-pile 3.2D, 15-inch depth, strip #3, transverse spacing 27.1 inches).	229
Figure D-6. Reinforcement force versus distance from back face of MSE wall (H-pile 3.2D, 15-inch depth, strip #4, transverse spacing 52.6 inches).	229
Figure D-7. Reinforcement force versus distance from back face of MSE wall (H-pile 3.2D, 45-inch depth, strip #16, transverse spacing 28.1 inches).	230
Figure D-8. Reinforcement force versus distance from back face of MSE wall (H-pile 3.2D, 45-inch depth, strip #11, transverse spacing 53.1 inches).	230
Figure D-9. Reinforcement force versus distance from back face of MSE wall (H-pile 2.5D, 15-inch depth, strip #8, transverse spacing 34.6 inches).	231
Figure D-10. Reinforcement force versus distance from back face of MSE wall (H-pile 2.5D, 15-inch depth, strip #7, transverse spacing 9.1 inches).	231
Figure D-11. Reinforcement force versus distance from back face of MSE wall (H-pile 2.5D, 45-inch depth, strip #14, transverse spacing 33.6 inches).	232
Figure D-12. Reinforcement force versus distance from back face of MSE wall (H-pile 2.5D, 45-inch depth, strip #15, transverse spacing 8.1 inches).	232
Figure D-13. Reinforcement force versus distance from back face of MSE wall (H-pile 2.2D, 15-inch depth, strip #8, transverse spacing 23.6 inches).	233
Figure D-14. Reinforcement force versus distance from back face of MSE wall (H-pile 2.2D, 15-inch depth, strip #7, transverse spacing 49.1 inches).	233
Figure D-15. Reinforcement force versus distance from back face of MSE wall (H-pile 2.2D, 45-inch depth, strip #14, transverse spacing 25.1 inches).	234
Figure D-16. Reinforcement force versus distance from back face of MSE wall (H-pile 2.2D, 45-inch depth, strip #15, transverse spacing 51.1 inches).	234
Figure D-17. Reinforcement force versus distance from back face of MSE wall (square pile 5.7D, 15-inch depth, welded wire #5, transverse spacing 21.5 inches).	235

Figure D-18. Reinforcement force versus distance from back face of MSE wall (square pile 5.7D, 15-inch depth, welded wire #4, transverse spacing 38.5 inches).....	235
Figure D-19. Reinforcement force versus distance from back face of MSE wall (square pile 5.7D, 45-inch depth, welded wire #26, transverse spacing 28.5 inches).....	236
Figure D-20. Reinforcement force versus distance from back face of MSE wall (square pile 5.7D, 45-inch depth, welded wire #27, transverse spacing 31 inches).....	236
Figure D-21. Reinforcement force versus distance from back face of MSE wall (square pile 5.7D, 75-inch depth, welded wire #21, transverse spacing 27 inches).....	237
Figure D-22. Reinforcement force versus distance from back face of MSE wall (square pile 5.7D, 105-inch depth, welded wire #17, transverse spacing 34.5 inches).....	237
Figure D-23. Reinforcement force versus distance from back face of MSE wall (square pile 4.2D, 15-inch depth, welded wire #4, transverse spacing 13 inches).....	238
Figure D-24. Reinforcement force versus distance from back face of MSE wall (square pile 4.2D, 15-inch depth, welded wire #3, transverse spacing 47.5 inches).....	238
Figure D-25. Reinforcement force versus distance from back face of MSE wall (square pile 4.2D, 45-inch depth, welded wire #27, transverse spacing 21 inches).....	239
Figure D-26. Reinforcement force versus distance from back face of MSE wall (square pile 4.2D, 45-inch depth, welded wire #28, transverse spacing 39.5 inches).....	239
Figure D-27. Reinforcement force versus distance from back face of MSE wall (square pile 3.1D, 15-inch depth, welded wire #3, transverse spacing 15.5 inches).....	240
Figure D-28. Reinforcement force versus distance from back face of MSE wall (square pile 3.1D, 15-inch depth, welded wire #2, transverse spacing 44 inches).....	240
Figure D-29. Reinforcement force versus distance from back face of MSE wall (square pile 3.1D, 45-inch depth, welded wire #28, transverse spacing 23.5 inches).....	241
Figure D-30. Reinforcement force versus distance from back face of MSE wall (square pile 3.1D, 45-inch depth, welded wire #29, transverse spacing 37 inches).....	241
Figure D-31. Reinforcement force versus distance from back face of MSE wall (square pile 2.1D, 15-inch depth, welded wire #2, transverse spacing 23.5 inches).....	242
Figure D-32. Reinforcement force versus distance from back face of MSE wall (square pile 2.1D, 15-inch depth, welded wire #1, transverse spacing 37.5 inches).....	242
Figure D-33. Reinforcement force versus distance from back face of MSE wall (square pile 2.1D, 45-inch depth, welded wire #29, transverse spacing 30 inches).....	243

Figure D-34. Reinforcement force versus distance from back face of MSE wall (square pile 2.1D, 45-inch depth, welded wire #30, transverse spacing 37.5 inches.	243
Figure E-1. Log measured maximum tensile force versus log predicted maximum tensile force, ribbed strip reinforcement of pipe piles.	246
Figure E-2. Measured maximum tensile force versus predicted maximum tensile force, ribbed strip reinforcement of pipe piles.	247
Figure E-3. Log residual versus pile load, ribbed strip reinforcement of pipe piles.....	248
Figure E-4. Log residual versus normalized transverse distance, ribbed strip reinforcement of pipe piles.	248
Figure E-5. Log residual versus vertical stress, ribbed strip reinforcement of pipe piles.....	249
Figure E-6. Log residual versus normalized spacing, ribbed strip reinforcement of pipe piles.	249
Figure E-7. Log residual versus L/H ratio, ribbed strip reinforcement of pipe piles.....	250
Figure E-8. Log residual versus log predicted maximum tensile force, ribbed strip reinforcement of pipe piles.	250
Figure F-1. Vertical ground displacement versus distance from back face of MSE wall, H-pile 4.5D.	253
Figure F-2. Vertical ground displacement versus distance from back face of MSE wall, H-pile 3.2D.	253
Figure F-3. Vertical ground displacement versus distance from back face of MSE wall, H-pile 2.5D.	254
Figure F-4. Vertical ground displacement versus distance from back face of MSE wall, H-pile 2.2D.	254
Figure F-5. Vertical ground displacement versus distance from back face of MSE wall, square pile 5.7D.	255
Figure F-6. Vertical ground displacement versus distance from back face of MSE wall, square pile 4.2D.	255
Figure F-7. Vertical ground displacement versus distance from back face of MSE wall, square pile 3.1D.	256
Figure F-8. Vertical ground displacement versus distance from back face of MSE wall, square pile 2.1D.	256

Figure G-1. Maximum reinforcement force for each instrumented ribbed strip versus pile head displacement for H-pile 4.5D.	258
Figure G-2. Maximum reinforcement force for each instrumented ribbed strip versus pile head displacement for H-pile 3.2D.	258
Figure G-3. Maximum reinforcement force for each instrumented ribbed strip versus pile head displacement for H-pile 2.5D.	259
Figure G-4. Maximum reinforcement force for each instrumented ribbed strip versus pile head displacement for H-pile 2.2D.	259
Figure G-5. Maximum reinforcement force for each instrumented welded wire versus pile head displacement for square pile 5.7D.	260
Figure G-6. Maximum reinforcement force for each instrumented welded wire versus pile head displacement for square pile 4.2D.	260
Figure G-7. Maximum reinforcement force for each instrumented welded wire versus pile head displacement for square pile 3.1D.	261
Figure G-8. Maximum reinforcement force for each instrumented welded wire versus pile head displacement for square pile 2.1D.	261

1 INTRODUCTION

Integral bridge abutments are often supported by piles near a Mechanically Stabilized Earth wall (MSE wall). These piles are within the zone of soil reinforcement. They support the axial load induced from the bridge abutment caps, and also the lateral loading induced from thermal expansion and contraction and earthquake loads. Figure 1-1 shows a cross-section of how abutment piles would be configured behind an MSE wall. However, the proximity of these piles to the MSE wall affects their capacity to resist lateral loads. Little information is available for capacity reduction in laterally loaded piles close to the MSE wall. Designers may ignore soil resistance entirely which leads to a conservative design and potential increase in pile size or the number of piles. Designers may also place the piles far enough from the wall to eliminate interactions, and thus install their piles six to eight pile diameters from the wall. This may be too conservative due to increased costs from longer bridge spans. Designers may instead still place the piles close to the MSE wall but use some reduction factor based on engineering judgment to account for reduction which increases the number of piles and/or the pile diameters if the reduction factor is conservatively too low. This again may be too conservative due to added foundation costs, and the reduction factors are not verified.

The earliest full-scale lateral load tests relating to this topic was performed by Pierson (2009). Cast-in-place shafts with geosynthetic soil reinforcement were tested. Further tests were performed by Rollins (2013) which included pipe piles loaded laterally at various distances from the MSE wall. Metallic reinforcement of ribbed strips and welded wire were used as well. The

main conclusion deduced from these tests was that pile capacity decreases as the pile spacing also decreases. Rollins also determined p-multipliers that could be multiplied by the pile resistance to reduce it. These p-multipliers seemed to be factors of spacing from the wall normalized by the pile diameter and reinforcement length. Rollins tested the piles at a reinforcement length to wall height ratio (L/H) ranging from 1.0 to 1.4. This study is a part of another full-scale project in determining further conclusions of lateral loaded piles near an MSE wall. Pipe piles, square piles, and H-piles with spacing ranging from two to five nominal pile diameters were tested with ribbed strip and welded wire soil reinforcement. Half of the piles were tested at an L/H ratio of 0.90 and half of the piles were tested at an L/H ratio of 0.72. The lower L/H ratios will help determine further how relative this ratio really is in determining a reduction in pile resistance for piles near MSE walls. This study deals primarily with the H-piles in ribbed strip reinforcement with an L/H equal to 0.90 and the square piles in welded wire reinforcement with an L/H equal to 0.72.

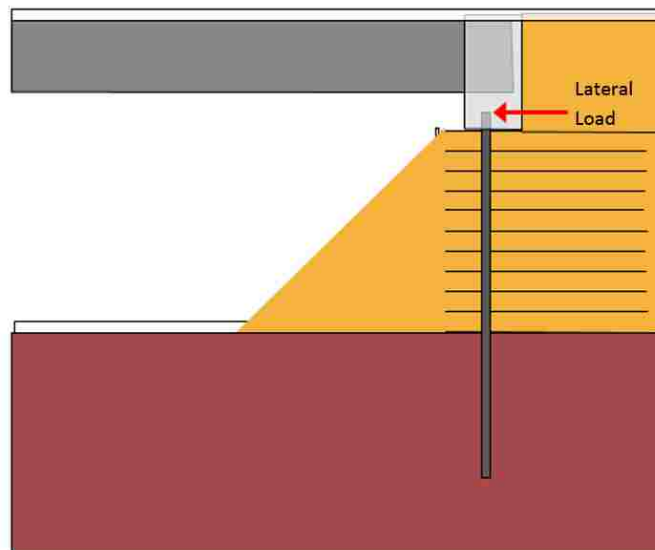


Figure 1-1. Cross-section of abutment piles behind an MSE wall.

1.1 Objectives

One of the main objectives of this research is to measure lateral pile resistance against pile displacement for piles at various distances behind an MSE wall. A second objective is to find p-multipliers which can accurately account for reduced lateral load resistance depending on the pile spacing, and to develop an equation to predict a p-multiplier for a given pile spacing behind an MSE wall. A third objective is to measure the tensile force distribution in the soil reinforcement induced by the pile loaded laterally. A final objective is to define an equation to accurately predict the maximum tensile force induced in the soil reinforcement. The achievement of these objectives will help designers properly space and install piles so as to minimize costs and still meet the lateral load demands.

1.2 Scope

To accomplish the research objectives, a full-scale MSE abutment wall was constructed to conduct research on laterally loaded steel piles near MSE wall faces. The wall was constructed in two phases using welded wire grid and steel ribbed strip reinforcements so that the performance of the two reinforcement systems could be evaluated separately but with comparable backfill conditions. Lateral load tests were first conducted at an L/H ratio of 0.90 (15-foot wall height) which might be typical for seismic conditions, and then at an L/H ratio of 0.72 (20-foot wall height) which is more typical for static conditions. Tests at these different ratios made it possible to evaluate the influence of the reinforcement ratio on lateral pile resistance and induced tensile force. This systematic examination of the interaction between piles and MSE walls has been the focus of four other theses, namely Hatch (2014), Han (2014), Besendorfer (2015), and Budd (2016). All of the other theses have investigated the behavior of pipe piles behind an MSE wall. Half of these

pipe piles were located within sand reinforced with ribbed strip soil reinforcement and the other half were within welded wire soil reinforcement.

One unique aspect of this study involved full-scale lateral load testing of H-piles and square piles. The purpose for using H-piles and square piles was to compare their behavior with that of the pipe piles. These square and H-piles were spaced at distances ranging from approximately two to five pile widths behind the wall face to investigate how distance and lateral resistance relate to each other. The piles were instrumented to record data on pile deflection, rotation, and bending moment. In addition, reinforcements were instrumented to measure the distribution of forces induced by pile loading. The tests with square and H-piles also involved two different L/H ratios (0.72 and 0.90) and two different reinforcement types (welded wire and ribbed strip) so that these factors affecting lateral resistance could be evaluated. This study details the tests that were performed, the results that were obtained, and the analyses that were performed to achieve the research objectives.

1.3 Thesis Organization

Following this introduction, a review of related literature is given in Chapter 2. In Chapter 3, an explanation of the test layout is provided which includes the MSE wall, soil reinforcement, backfill, surcharge, piles, and loading apparatus. The instrumentation plan is summarized in Chapter 4. Instrumentation was done so as to gather data on the pile deflection, pile moment, pile rotation, the soil reinforcement load, the horizontal and vertical displacement, and the wall displacement. Chapter 5 discusses the results of the tests for both the H-piles and square piles, after which an analysis of the lateral pile load tests using LPILE is presented in Chapter 6. This study then ends with observations and conclusions based on the results of the study along with recommendations for additional research in Chapter 7.

2 LITERATURE REVIEW

The design of Mechanically Stabilized Earth (MSE) walls have been more common in recent years because of their cost effectiveness. This literature review begins with an overview of MSE wall design as it relates to the pullout resistance of the soil reinforcement. An important factor in calculating pullout resistance is the pullout resistance factor. The second section explains a two-part study involving the analysis of the pullout resistance factor of ribbed strip and welded wire soil reinforcement. Also relating to MSE walls is the lateral load design of piles behind an MSE wall. These designs can be modeled in the program LPILE, and a review of LPILE is given next. However, little guidance is given on the lateral resistance of piles behind an MSE wall. This chapter then reviews the research of drilled shafts with geogrid soil reinforcement, and pipe piles with ribbed strip and welded wire reinforcement at several locations.

2.1 MSE Wall Design (Berg, Christopher, & Samtani, 2009)

Conventional gravity or cantilever retaining walls have been used for many years; however, the cost of these retaining walls significantly increases as wall height increases and poor soil conditions are encountered. Thus, Mechanically Stabilized Earth (MSE) walls have been implemented in more recent years because of their inherent cost effectiveness for high walls and their higher settlement tolerance which in turn reduces the cost of the structure substantially. In general, an MSE wall is a retaining wall consisting of thin wall facing panels with reinforced soil

backfill. The reinforced soil backfill is generally composed of multiple layers of inclusions. Inclusions are man-made elements such as steel ribbed strips, steel welded wire grids, or geotextile sheets. The actual wall is usually made up of segmental precast square blocks about 6 inches thick with surface areas ranging from about 25 to 60 ft². Interface friction between the backfill soil and the inclusion provides lateral resistance for the vertical wall face while the facing panels prevent raveling of the backfill at the wall surface. The reinforced soil zone along with the segmental panels give MSE walls greater flexibility and a higher differential settlement tolerance.

In addition to the cost effectiveness of MSE walls, other advantages include: less site preparation required, faster construction procedures, feasible heights of at least 100 feet, and they do not need a rigid foundation support because of their high deformation tolerance.

There are three types of reinforcement geometry: (1) linear unidirectional which includes smooth or ribbed steel strips, (2) composite unidirectional which includes welded wire grids or bar mats, and (3) planar bi-directional which includes geosynthetics. The reinforcement material is either metallic (usually mild, galvanized steel) or nonmetallic which consists of polymeric materials. The reinforcement is either inextensible or extensible. Ribbed strips and welded wire grids are inextensible because the reinforcement at failure deforms less than the soil while geosynthetic sheets are extensible and deform with the soil. The three major parts of an MSE wall are the reinforcing elements, the facing system, and the reinforced fill as shown in Figure 2-1. The zone of reinforcement is where the reinforcing fill is placed, and the adjacent soil is called the retained soil which is the cause of the earth pressures that must be resisted.

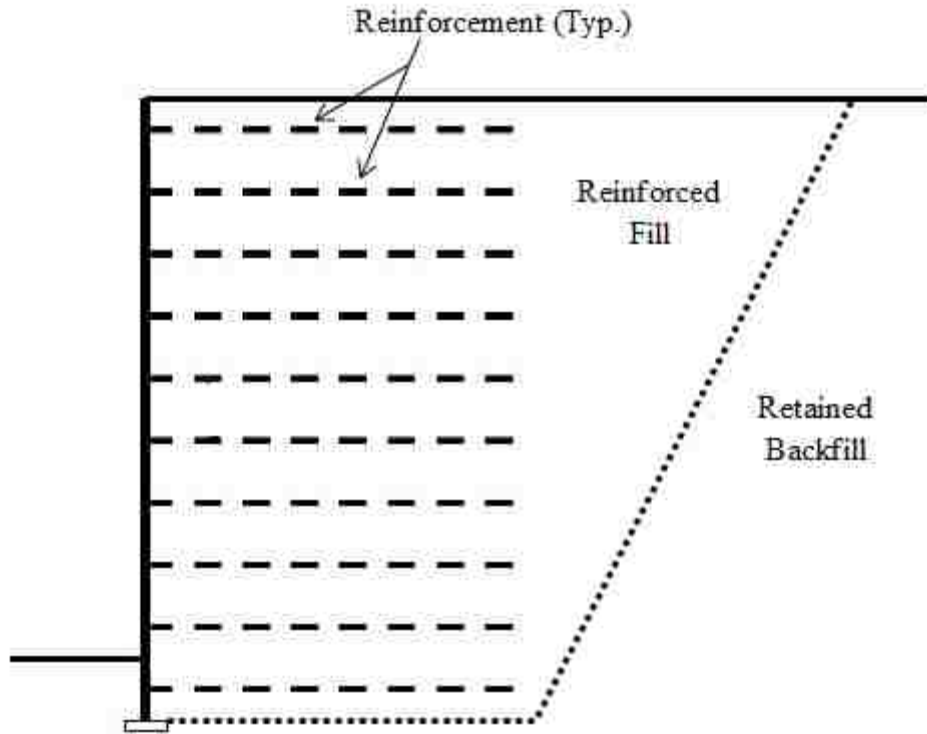


Figure 2-1. The reinforced soil zone (modified from Berg et al., 2009).

There is no definitive way to predict lateral wall displacements, which are due to compaction effects, reinforcement extensibility, facing system, connection details of the reinforcement and the panels, and the reinforcement length. However, lateral displacements can be estimated as a function of the reinforcement length to wall-height ratio as shown in Figure 2-2. For metallic reinforcement, the displacement is about 0.5 inches for every 10 feet of wall height for an L/H ratio equal to 0.7. As shown in Figure 2-2, relative settlement increases quite significantly for L/H ratios less than 0.7; therefore, there is a minimum $0.7H$ reinforcement length.

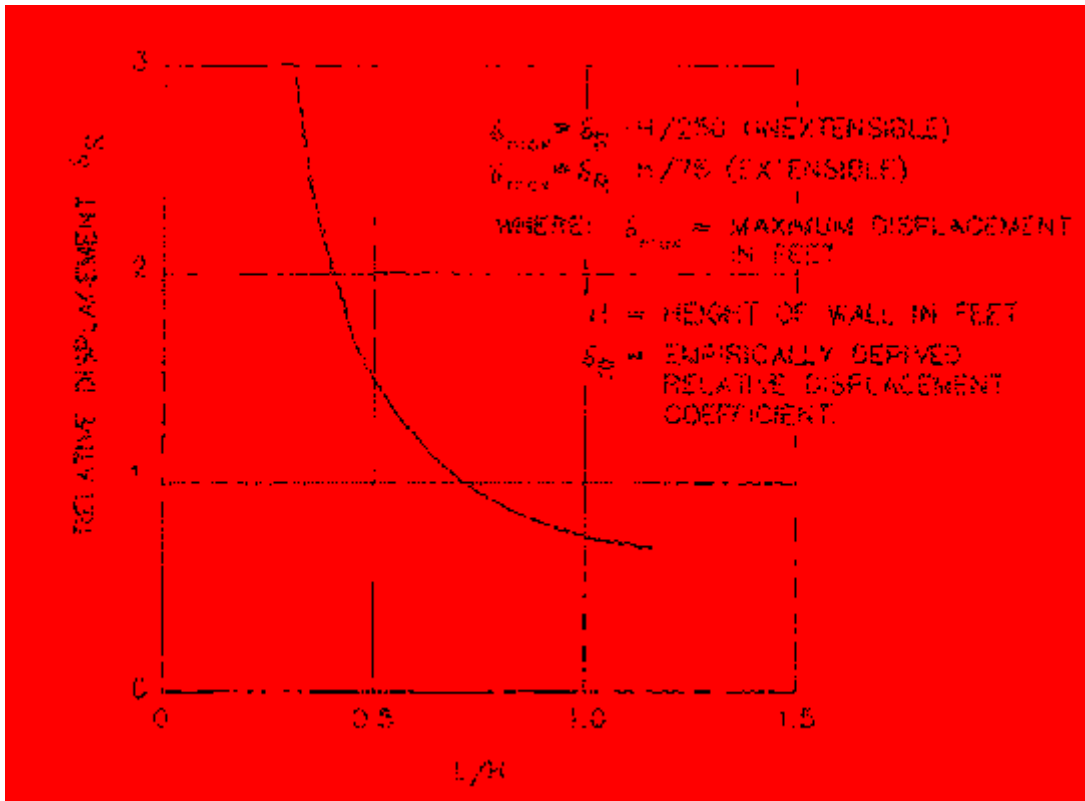


Figure 2-2. Relative displacement versus L/H ratio (Berg et al., 2009).

In years past, walls have been designed using the allowable stress design (ASD) method. However, the load and resistance factor design (LRFD) method is now used by the FHWA and AASHTO. This method accounts for uncertainty in loads with a load factor (γ) and in material resistance with a resistance factor (ϕ). The four limit states are strength, serviceability, extreme event, and fatigue limit states. When sizing MSE walls, both external and internal failure modes must be considered. External failure modes include sliding, limiting eccentricity (overturning), and bearing failure as shown in Figure 2-3.

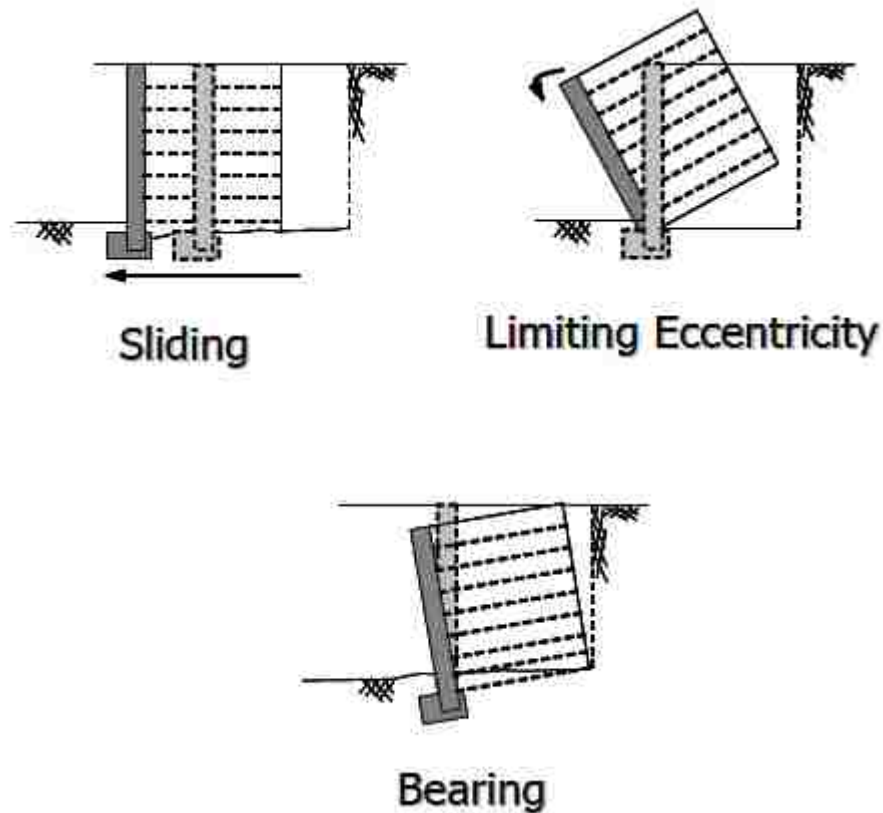


Figure 2-3. External failure modes of MSE walls (Berg et al., 2009).

There are two types of internal stability failures: (1) excessive elongation or breakage of reinforcements, and (2) pullout of the reinforcements. Each of these failure modes are due to the tensile forces becoming too large, thus whether the soil is inextensible or not will make a difference in resistance. For metallic (inextensible) reinforcement, elongation failure is negligible, but tensile failure must be considered. To ensure pullout failure does not occur, the factored maximum tensile force, T_{MAX} , must be less than the factored reinforcement pullout resistance, T_r . Pullout resistance is only considered to act behind a bi-linear failure surface dividing the reinforcement active zone with the resistant zone (see Figure 2-4). Calculation of the maximum tensile force is crucial to evaluate these failure modes.

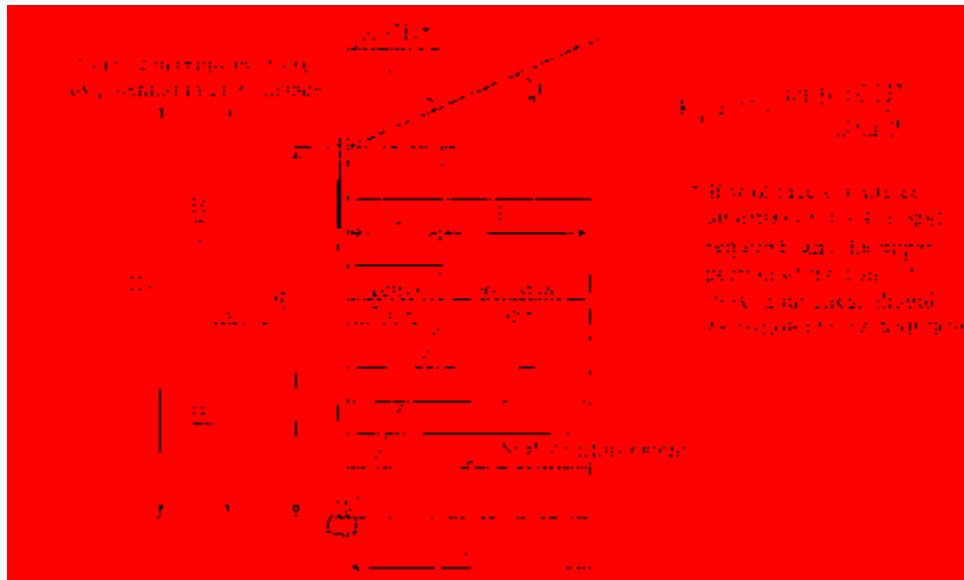


Figure 2-4. Reinforcement active and resistant zones (Berg et al., 2009).

The maximum factored applied tensile force per unit width, T_{max} , for each layer is given by the equation:

$$T_{MAX} = \sigma_H S_v \quad (2-1)$$

where σ_H = horizontal earth pressure at the level of reinforcement, and

S_v = vertical reinforcement spacing.

However, for discrete reinforcements such as ribbed strips and welded wire grids, the maximum factored tensile force may be calculated per unit width of reinforcement (UWR) as follows:

$$P_{TMAX-UWR} = \frac{\sigma_H S_v}{R_c} \quad (2-2)$$

where $P_{TMAX-UWR}$ = maximum tensile force per unit width of reinforcement, and

R_c = coverage ratio.

The coverage ratio is defined in the following equation:

$$R_c = \frac{b}{S_h} \quad (2-3)$$

where b = width of reinforcement as shown in Figure 2-5 for ribbed strips and welded wire, and

S_h = center-to-center horizontal spacing of the reinforcement as described in Figure 2-5.

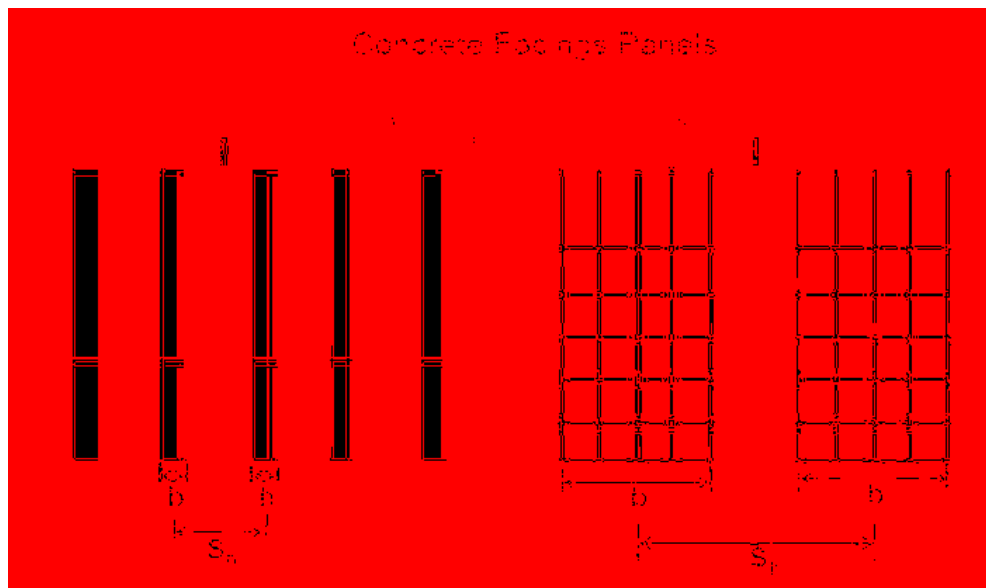


Figure 2-5. Visual description of reinforcement width and horizontal spacing (Berg et al., 2009).

The maximum factored force, T_{\max} , may also be calculated in just force units as follows:

$$T_{MAX} = \sigma_H A_{trib} \quad (2-4)$$

where $A_{trib} = S_v S_h$.

The generic horizontal stress, σ_H , is calculated by the following equation:

$$\sigma_H = K_r \sigma_V + \Delta\sigma_H \quad (2-5)$$

where K_r = coefficient of lateral earth pressure

σ_V = vertical earth pressure at desired depth, and

$\Delta\sigma_H$ = horizontal stress due to surcharge.

If surcharge is included as a dead load and the maximum load factor was applied (with no horizontal surcharge) as shown in Figure 2-6, then the horizontal stress would be calculated as shown below:

$$\sigma_H = K_r (\gamma_r (Z + h_{eq}) \gamma_{EV-MAX}) \quad (2-6)$$

where $\gamma_r (Z + h_{eq}) \gamma_{EV-MAX} = \sigma_V$

γ_r = moist unit weight of the reinforced backfill

Z = height from the top of the wall to the desired depth

h_{eq} = equivalent soil height of the surcharge calculated by dividing the surcharge pressure by the equivalent moist unit weight of the reinforced backfill, γ_{eq} , which is assumed to be equal to γ_r , and

$\gamma_{EV-MAX} = 1.35$ for the maximum load factor of vertical earth pressure from the dead load of earth fill for a retaining wall.

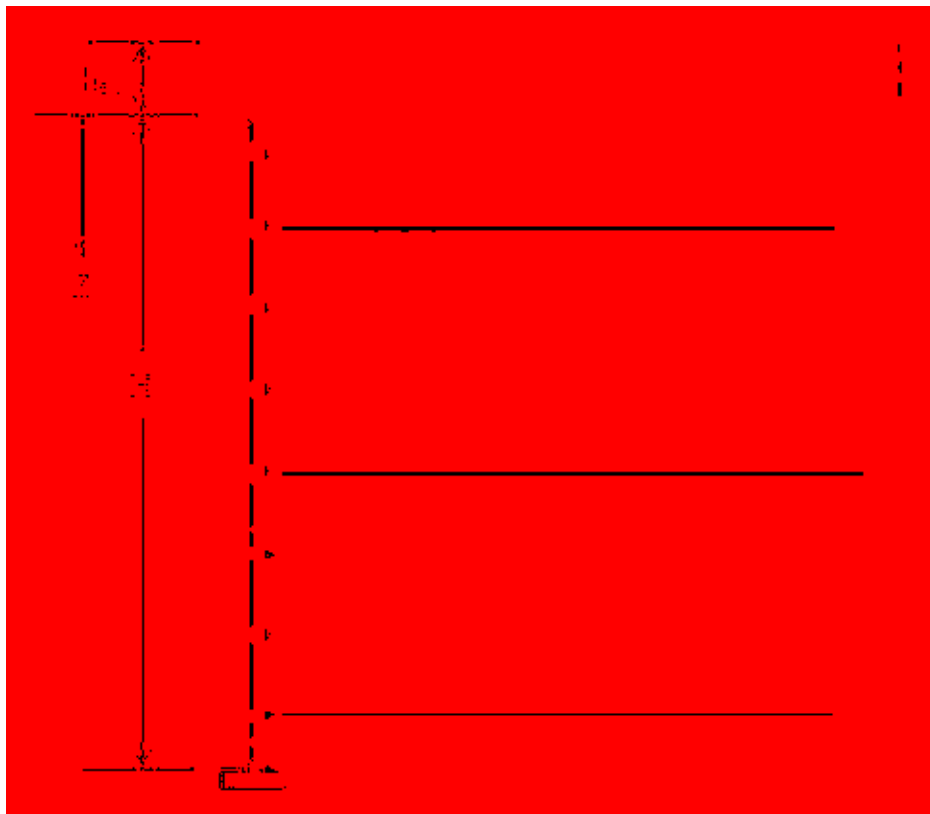


Figure 2-6. MSE soil profile with equivalent surcharge.

The coefficient of lateral earth pressure is calculated by multiplying the ratio K_r/K_a taken from Figure 2-7 by the active earth pressure coefficient given in the following equation:

$$K_a = \tan^2\left(45 - \frac{\phi'_r}{2}\right) \tag{2-7}$$

where K_a = active earth pressure coefficient, and

ϕ'_r = friction angle of the reinforced backfill.

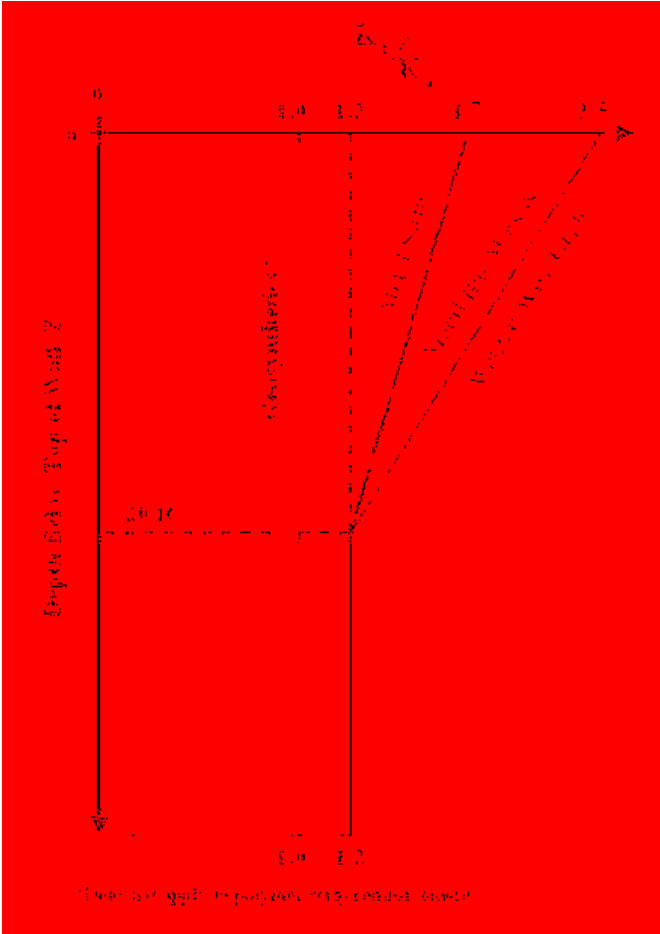


Figure 2-7. Depth versus K_r/K_a ratio (Berg et al., 2009).

The capacity of the reinforcement to resist tensile forces is affected by the length of embedment in the resisting zone. The following equation is used to calculate the minimum length of embedment needed to resist against pullout failure:

$$\phi L_e \geq \frac{T_{MAX}}{F^* \alpha \sigma_v C R_c} \quad (2-8)$$

where ϕ = resistance factor, 0.9 for pullout

L_e = embedment length in the resisting zone

T_{MAX} = maximum factored tensile force per length from Equation (2-1)

F^* = pullout resistance factor

α = scale correction factor (generally 1.0 for metallic reinforcements)

σ_v = unfactored vertical stress of the desired reinforcement level including external surcharges

C = 2 for metallic strips and welded wire grids, and

R_c = coverage ratio from Equation (2-3).

However, for a given embedment length, to calculate the actual nominal pullout resistance in units of force, P_r , to check against the unfactored maximum tensile force using Equation (2-4), the following equation is used:

$$P_r = F^* \alpha \sigma_v L_e C_b \quad (2-9)$$

To obtain the pullout resistance per unit width of reinforcement, the term “b” would need to be dropped from Equation (2-9) and be checked against Equation (2-2) unfactored.

The calculation of the pullout resistance factor, F^* , is different for steel ribbed reinforcement (metal strips) than it is for welded wire grid reinforcement. F^* is interpolated from the top of the structure until a depth of 20 feet. The maximum F^* at the top of the structure is given by Equation (2-10) for steel ribbed reinforcement. The minimum F^* at a depth of 20 feet and below is calculated in Equation (2-11).

For steel ribbed strip reinforcement:

$$F^* = 1.2 + \log C_u \leq 2.0 \quad (2-10)$$

$$F^* = \tan \phi \quad (2-11)$$

where C_u = uniformity coefficient of the backfill, and

ϕ = friction angle of the reinforced backfill.

For the welded wire reinforcement, the maximum F^* at the top of the structure is given by Equation (2-12), and the minimum F^* at a depth of 20 feet and below is calculated in Equation (2-13).

For welded wire reinforcement:

$$F^* = 20(t/S_t) \quad (2-12)$$

$$F^* = 10(t/S_t) \quad (2-13)$$

where t = thickness of the transverse bars, and

S_t = transverse spacing.

From the equations above, it is shown that a larger embedment length, which is the length of reinforcement past the active zone measuring away from the wall, means that the soil reinforcement can take on greater tensile force before failing in pullout. The total length of reinforcement, L , needed when constructing MSE walls is shown in the following equation:

$$L = L_a + L_e \quad (2-14)$$

Where L = total length of reinforcement

L_a = length of reinforcement in the active zone, and

L_e = embedment length of the reinforcement in the resisting zone.

The determination of L_a is dependent on whether the reinforcement is inextensible or not and the depth of the layer of interest in relation to the wall. Equation (2-15) below is for inextensible reinforcement for the bottom half of the MSE wall (incorporating the equivalent surcharge height in the total height if applicable) and Equation (2-16) is for the upper half:

$$L_a = 0.6(H - Z) \quad (2-15)$$

$$L_a = 0.3H \quad (2-16)$$

where H = height of the MSE wall plus the equivalent surcharge height, and

Z = depth to the reinforcement level from the top of the wall.

After L_a is determined, the total length of reinforcement per layer can be calculated using Equation (2-14).

2.2 Pullout Resistance Factor Tests

Recently, additional research was performed on both ribbed strip and welded wire inextensible reinforcements to investigate the pullout resistance factor, F^* , for various soil types and confining pressures. The first phase of the research involved testing the reinforcement embedded in sandy backfill (Lawson, Jayawickrama, Wood, & Surles, 2013), and the second phase of the research involved testing the reinforcement embedded in gravelly backfill (Jayawickrama, Lawson, Wood, & Surles, 2015). For Phase 1, 99 pullout tests were performed with strips, and 195 pullout tests were performed with welded wire reinforcements. Phase 2 had 73 pullout tests on steel strips, and 214 pullout tests on the welded wire reinforcements. The sandy backfill for Phase 1 had a coefficient of uniformity (C_u) of 4.7 with a maximum dry unit weight of 124.5 pcf. The friction angle was not given. Phase 2 tests were performed with crushed limestone gravel with a friction angle of 53 degrees and an average dry unit weight of about 116 pcf (the maximum dry unit weight nor the coefficient of uniformity were not provided). The strips tested were about 2 inches wide and 0.157 inches thick. Table 2-1 shows the different welded wire sizes and spacing

that were tested when evaluating the transverse and longitudinal effects. There were always three longitudinal bars for every welded wire grid pullout test.

Table 2-1. Pullout Resistance Factor Welded Wire Grid Testing Parameters

Test	Transverse			Longitudinal		
	Size	Diameter [in]	Spacing [in]	Size	Diameter [in]	Spacing [in]
Transverse Testing	W7.5, W11, W15	0.31, 0.37, 0.44	6, 12, 18, 24	W20	0.5	9
Longitudinal Testing	W11	0.37	12	W9.5, W20	0.35, 0.50	2, 6, 9, 12

An MSE Test Box was used that was 12 feet wide by 12 feet long by 4 feet deep. A reaction frame was used to simulate overburden pressures of up to about 40 feet which was then used to determine the depth of fill. The pullout testing was done with a 60-ton hollow core hydraulic jack. The systems used to measure the pullout force were the annular load cell and the pressure transducer. The reinforcement was pulled to 1.5 inches, however the data measured for the 0.75-inch displacement was used for calculations. Figure 2-8 shows the default values for the pullout resistance factor according to AASHTO as a function of depth. Figure 2-9 and Figure 2-10 show the depth of fill versus the pullout resistance factor calculated from the pullout forces measured from the testing along with the default AASHTO curve. Figure 2-9 shows the data for ribbed steel strips in both the sandy and gravel backfill. Figure 2-10 shows the data for the normalized pullout resistance factor for the welded steel grids in both the sandy and gravel backfill. The friction factor was normalized by dividing F^* by t/S_t (transverse bar diameter divided by transverse spacing) because AASHTO has the resistance factor vary linearly with t/S_t .

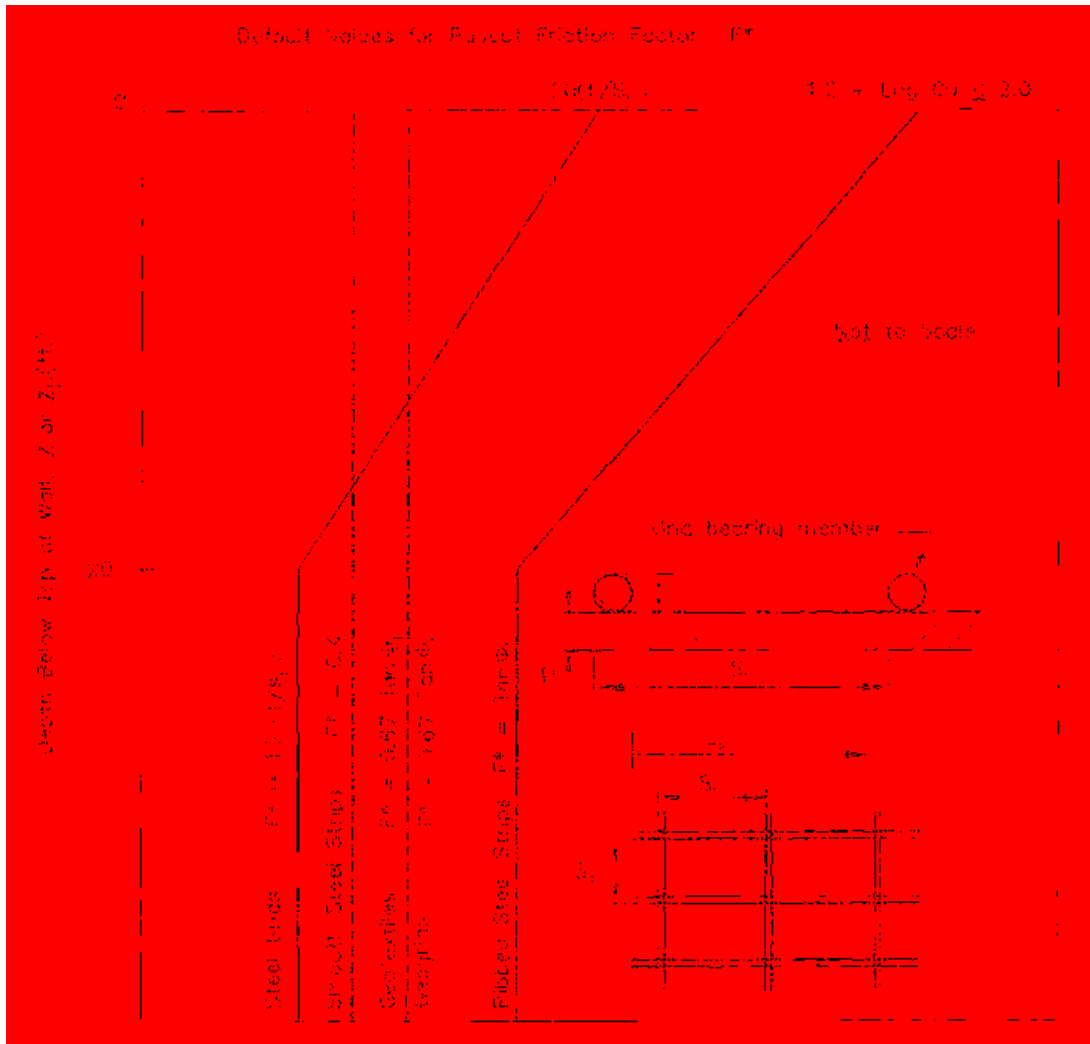


Figure 2-8. Default values for pullout friction factor (AASHTO LRFD Bridge Design Specifications, 2012).

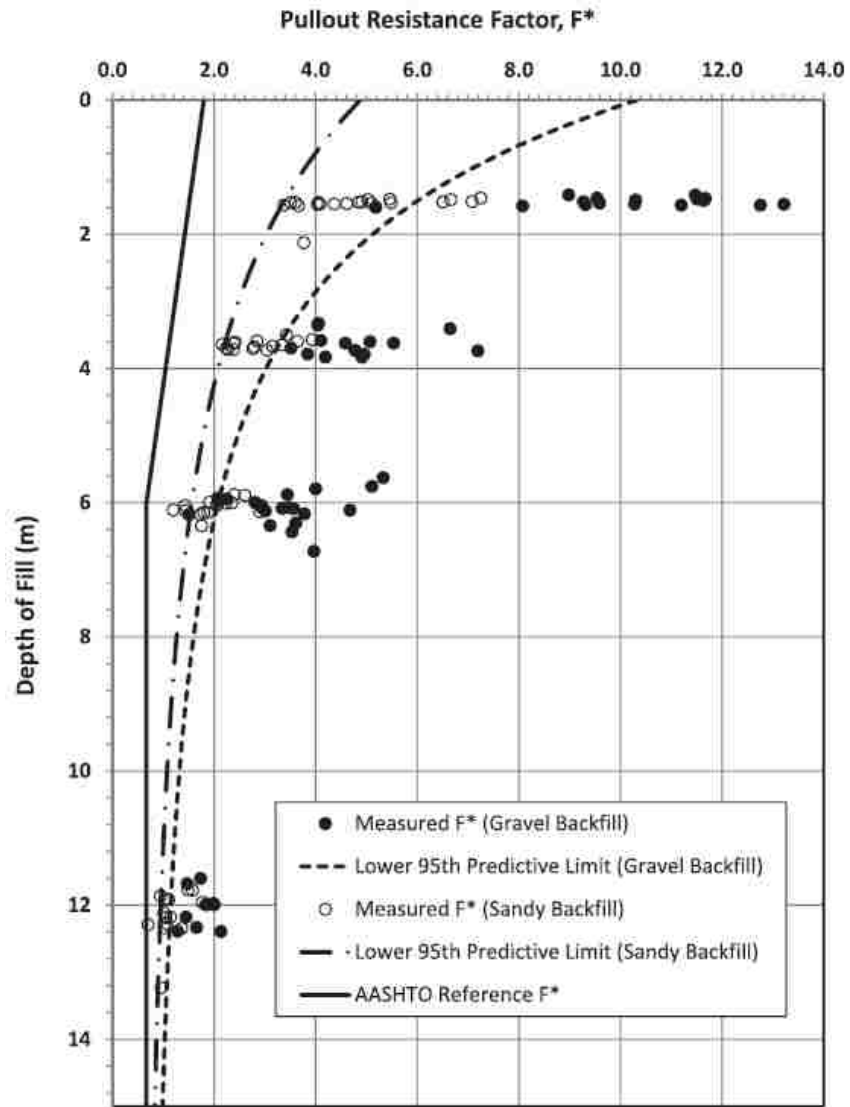


Figure 2-9. Depth of fill versus pullout resistance factor for ribbed steel strips (Jayawickrama et al., 2015).

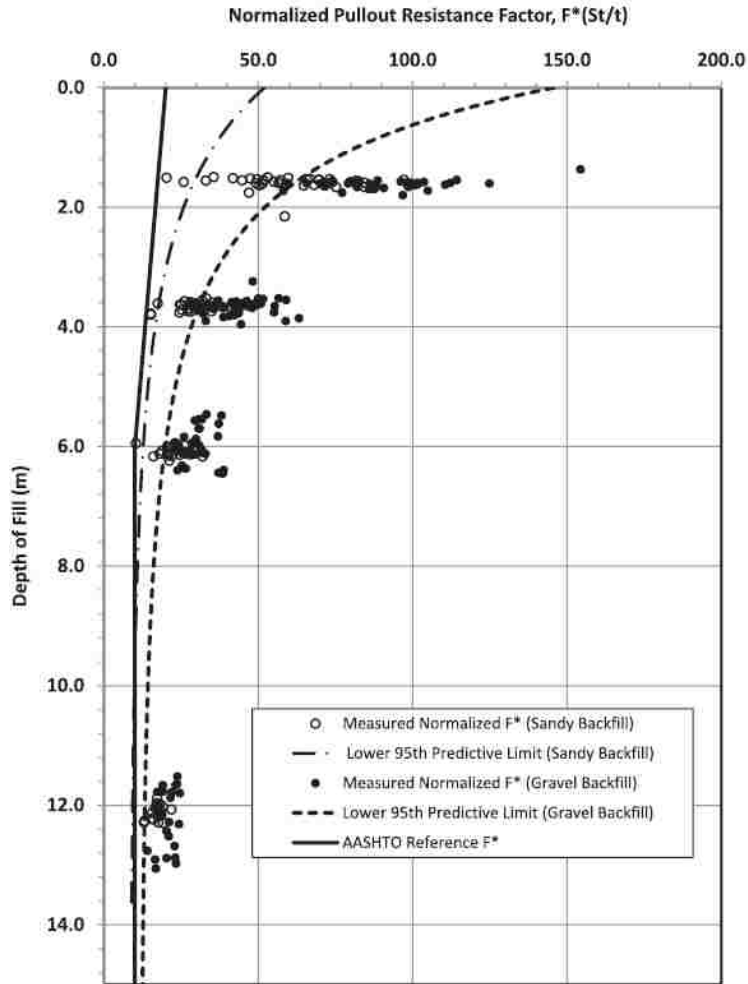


Figure 2-10. Depth of fill versus normalized pullout resistance factor for welded wire grids (Jayawickrama et al., 2015).

The AASHTO design line in Figure 2-9 and Figure 2-10 is typically close to the lower 95th predictive limits for other pullout tests a part of other research. All of the data yields F^* values higher than the AASHTO reference line, with the margin being greatest at shallow depths. The tests performed in gravel backfill yielded higher values than the tests performed in sandy backfill. The statistical analysis performed was a nonlinear regression and an analysis of variance (ANOVA). The variables used for the metal strips were depth of fill, embedment length, test layer, and overburden stress ratio. The variables used for the welded wire grids were the same with the

addition of transverse and longitudinal bar spacing and diameter. The statistical analysis was performed after the F^* data was transformed into the natural log of F^* using the Box-Cox transformation to satisfy the uniformity of variance condition. The results in Figure 2-9 and Figure 2-10 indicate that there is considerable scatter in the measured friction factor for a given material type. This scatter is more apparent at lower confining pressures and decreases with depth. It was found that in the sandy backfill, compaction strongly influences pullout resistance such that slightly lower compaction greatly decreases the pullout resistance. This observation may be influenced by the effect of dilation at low confining pressures which becomes less important at deeper depths. It was also concluded that the pullout resistance factor increases with transverse bar diameter, but decreases with longitudinal bar spacing. The pullout resistance factor was found to not be affected by the embedment length. From the Jayawickrama (2015) research, it was concluded that the pullout resistance factor increases with increased transverse bar spacing and longitudinal diameter size. However, it decreases with increased longitudinal bar spacing and inversely decreases with increased transverse diameter size.

2.3 Laterally Loaded Pile Design (Isenhower & Wang, 2015)

Abutment piles for bridges are subjected to lateral loads due to earthquakes as well as thermal expansion and contraction. Lateral load analysis is routinely performed in engineering practice using a p-y curve approach when the surrounding soil extends horizontally or at a slope away from the pile. The program LPILE Plus is a widely used computer program which analyzes piles under lateral loading. The piles are treated as a beam-column while the nonlinear response of the soil is defined by p-y curves within a finite difference model. For a given load, the program

computes the pile deflection, bending moment, and shear in the pile as a function of depth. The loading is two-dimensional. Soil behavior is modeled with p-y curves (soil resistance p versus pile deflection y) along the depth of the entire pile. Figure 2-11 shows how the radial stresses normal to the pile (soil resistance p) increases on the side opposite of the loading after there has been enough lateral loading to deflect the pile a distance of y. The figure shows how the stresses become non-uniform. The p-y method LPILE uses is the Winkler model; a series of discrete springs that are nonlinear. The springs being nonlinear means that the soil resistance versus the pile deflection is a nonlinear function. Figure 2-12 shows how LPILE represents the nonlinearity of the p-y curves.



Figure 2-11. Reaction of stresses after lateral deflection of pile (Isenhower et al., 2015).

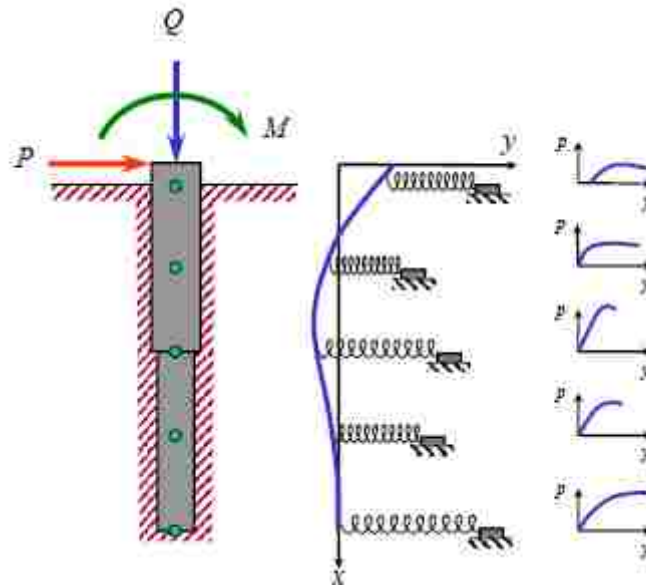


Figure 2-12. Model showing how LPILE models p-y curves (Isenhower et al., 2015).

LPILE has a number of built-in p-y curves that a user can select for various soil types; however, because most backfill soils behind bridge abutments are composed of cohesionless soil, this review will focus on the American Petroleum Institute (API) model for sand. This model is described in the American Petroleum Institute manual for recommended practice for designing fixed offshore platforms (*API RP 2A-WSD*, 2010). For the API sand model, the initial slope of the p-y curve is linear where the initial stiffness is a function of the confining pressure and magnitude of shearing strain. Also, there is zero resistance at the ground surface for any value of deflection. Since the ultimate resistance for piles in sand is different near the ground surface than deeper into the soil, LPILE uses two models to account for that difference. Figure 2-13 shows the assumed passive wedge failure near the ground surface. The total lateral force is found by taking the difference between the passive force and the active force. The active force is determined by the Rankine theory and the passive force is determined by assuming the Mohr-Coulomb failure condition for the vertical and sloping wedges. As shown in Figure 2-13, the width of the wedge

fans out from the pile pile width at an angle α which is equal to half of the friction angle. At deeper depths, the soil is assumed to flow around the pile.

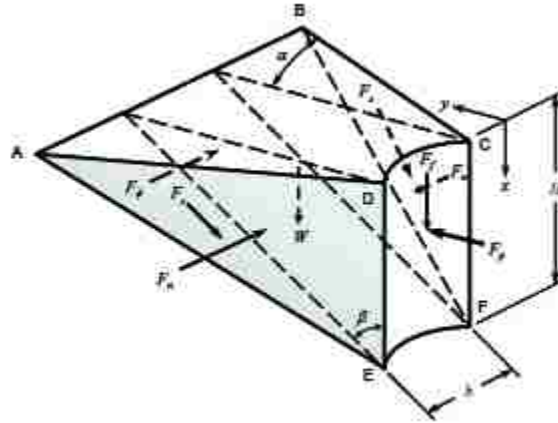


Figure 2-13. Failure wedge of pile in sand near ground surface (Isenhower et al., 2015).

The main parameters that are needed for this method are the angle of internal friction, the effective unit weight of soil, and the pile diameter. The next step is to calculate the ultimate soil resistance at a desired depth. Equation (2-17) is for the wedge failure at shallow depths, while Equation (2-18) is for the flow-around failure at deeper depths.

$$p_{us} = (C_1x + C_2b)\gamma'x \quad (2-17)$$

$$p_{ud} = C_3b\gamma'x \quad (2-18)$$

where p_{us} = ultimate soil resistance for shallow depths (lb./in.)

p_{ud} = ultimate soil resistance for deep depths, (lb./in.)

γ' = effective soil weight, (lb./in.³)

x = depth of interest (in.)

b = average pile diameter (in.), and

C_1, C_2, C_3 = coefficients as determined from Figure 2-14, or by using the following equations:

$$\text{where } C_1 = \tan \beta \left\{ K_p \tan \alpha + K_0 \left[\tan \phi \sin \beta \left(\frac{1}{\cos \alpha} + 1 \right) - \tan \alpha \right] \right\}$$

$$C_2 = K_p - K_A, \text{ and}$$

$$C_3 = K_p^2 (K_p + K_0 \tan \phi) - K_A$$

$$\text{where } \alpha = \frac{\phi}{2}$$

$$\beta = 45^\circ + \frac{\phi}{2}$$

ϕ = angle of internal friction, degrees

$$K_0 = 0.4$$

$$K_A = \tan^2 \left(45^\circ - \frac{\phi}{2} \right), \text{ and}$$

$$K_p = \tan^2 \left(45^\circ + \frac{\phi}{2} \right).$$

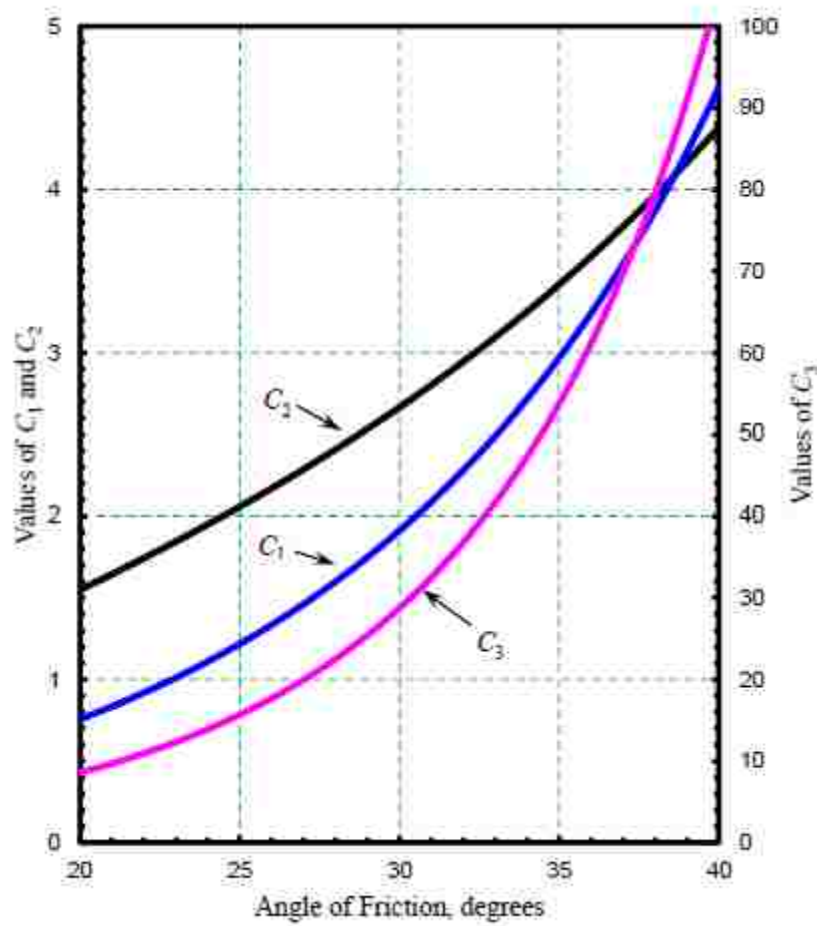


Figure 2-14. Ultimate lateral resistance coefficients versus angle of friction (Isenhower et al., 2015).

The ultimate resistance must be computed for both the deep and shallow conditions. The lower value is then used to compute the p-y (load-deflection) curve according to the following equation where p is a function of y:

$$p = Ap_u \tanh\left(\frac{kx}{Ap_u} y\right) \quad (2-19)$$

where p = soil resistance (lb.)

A = factor to account for cyclic or static loading

where $A = 0.9$ for cyclic loading, and

$$A = \left(3.0 - 0.8 \frac{x}{b} \right) \geq 0.9 \text{ for static loading.}$$

p_u = lower of the ultimate resistance values of shallow or deep depths

k = initial modulus of subgrade reaction determined from Figure 2-15 (lb./in.³)

x = depth of interest (in.), and

y = lateral deflection of pile (in.).

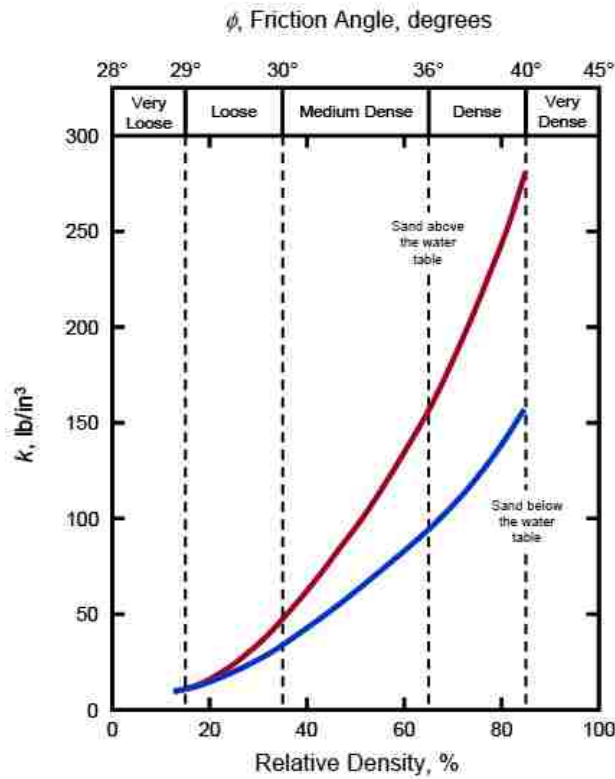


Figure 2-15. Initial modulus of subgrade reaction versus friction angle and relative density (Isenhower et al., 2015).

2.4 Previous Related Testing and Research

This section describes the lateral load testing of shafts and piles. The first subsection describes the full-scale lateral load test of drilled shafts behind an MSE wall with extensible geogrid soil reinforcement. The following subsections explain multiple full-scale lateral load tests of piles behind an MSE wall with inextensible metallic soil reinforcement. The conclusions and limitations are also included therein.

2.4.1 Tests with Drilled Shafts and Geogrid Reinforcement (Pierson, Parsons, Han, Brown, & Thompson, 2009)

The research study by Pierson et al. (2009) was performed to determine how laterally loaded drilled shaft foundations for light poles constructed behind an MSE wall behaved under lateral loading. The test site was located at an interchange in Kansas with sloping ground over shallow limestone bedrock. To perform the tests, an MSE wall 20 feet tall and 140 feet long was constructed with modular block facing. Geogrids by Tensar International were used as the soil reinforcement. This reinforcement classifies as a non-metallic, extensible geosynthetic. Eight 36-inch diameter shafts installed at different distances from the wall were laterally loaded and analyzed. Five of these shafts were tested independent of the other shafts at distances of one to four diameters from the wall measured from the back face of the wall to the center of the shaft. All five of these shafts were considered to act as “short” shafts (length/width < 10) because they were only typically installed to a depth of 20 feet or less into the ground and were likely to rotate at the base during lateral loading. However, one shaft (BS) was shorter than the others by being installed only 15 feet into the ground as opposed to 20 feet (installation depth of all the other shafts). Three

other shafts (each two diameters from the wall and spaced 15' apart) were tested as a group (BG) to compare lateral resistance of the group to that of the single piles. Table 2-2 shows the distances and ultimate load applied to each of the shafts. The center shaft of the group testing (BG2) is shown in the table below. The geogrids were 14 feet in length. UX1500 geogrids were used for the bottom four layers and the UX1400 geogrids were used for the top six layers. The geogrids were placed in the fill spaced at two feet vertically. Lateral pile deflections were measured versus depth with an inclinometer. Strain gauges were placed along the geogrids at different distances from the wall in the top four layers. At the back of the MSE wall, total pressure cells (TPC) were installed to measure induced pressure. Deflections of the wall were also measured using photogrammetry techniques.

Figure 2-16 shows the peak load versus displacement curves for the single shafts. For the single full depth shafts, an increase in distance from the wall yielded increased lateral load capacity as well. Shaft BS, which was only installed to a depth of 15 feet, displaced more than a similar shaft installed to a depth of 20 feet at the same distance behind the wall.

Figure 2-17 shows a comparison of the peak load versus displacement curves for the single full depth shaft, the group shafts, and the short shaft all at a distance of two shaft diameters behind the wall. It is interesting to note that the short shaft (BS) has the lowest lateral resistance while the full depth shaft has the highest. Loading the shafts as a group decreased the lateral resistance relative to that for a single shaft loaded independently.

Table 2-2. Shaft Distances and Capacity from Pierson (2009)

Shaft	Distance from Wall Facing [in]	Pile Diameters	Ultimate Capacity [kip]
A	36	1D	34
B	72	2D	90
C	108	3D	116
D	144	4D	194
BS	72 (15' length)	2D	55
BG2	72 (15' spacing)	2D	85

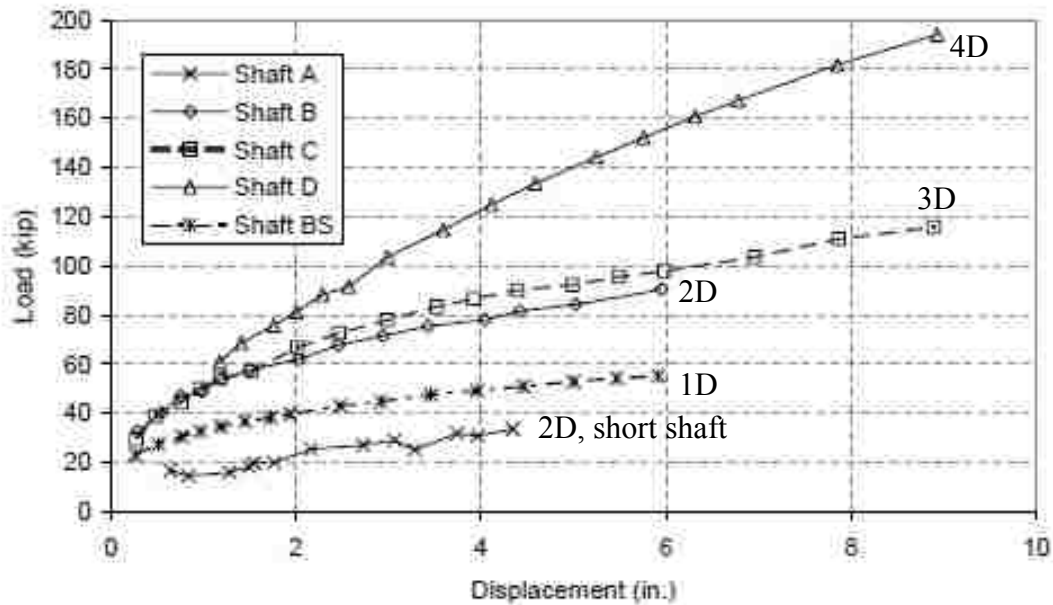


Figure 2-16. Single shaft peak load versus displacement curves for shafts spaced at 1, 2, 3 and 4 pile diameters (D) behind the MSE wall (Pierson, 2009).

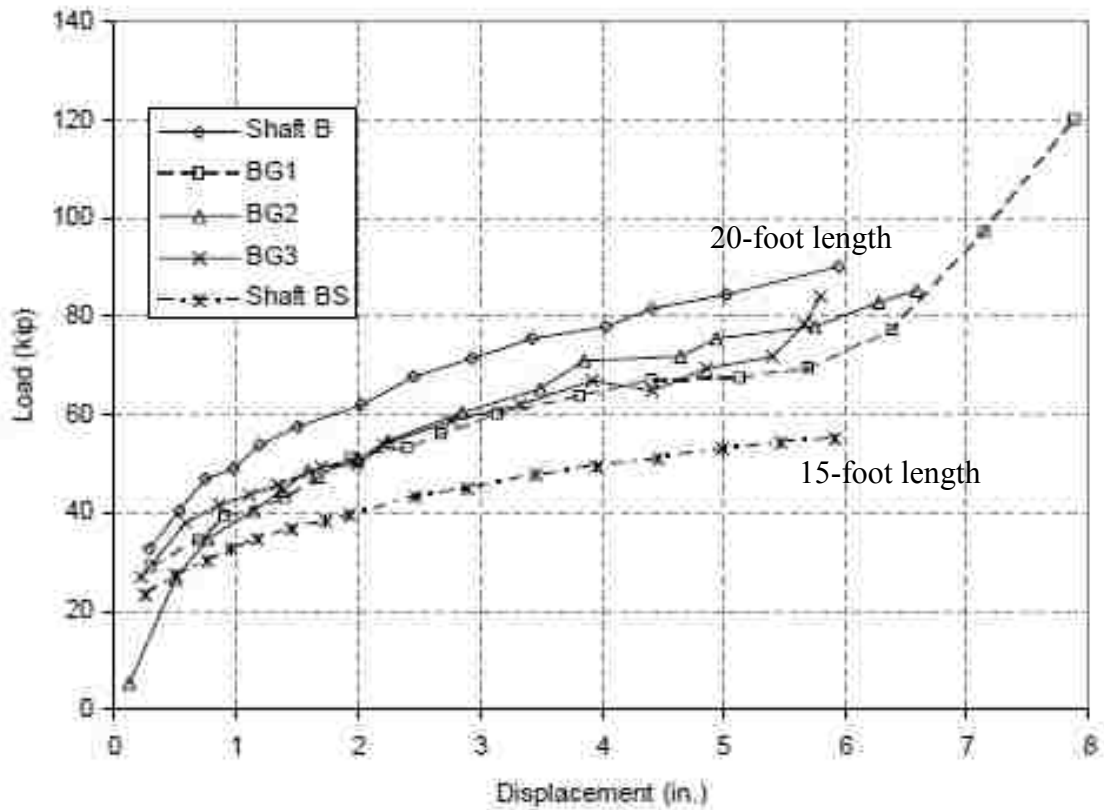


Figure 2-17. Peak load versus displacement for single, group, and short shafts installed at 2 pile diameters behind the MSE wall (Pierson et al., 2009).

Wall deflection was also measured with photogrammetry using targets placed on the wall and a digital camera placed on a tripod. Figure 2-18 shows that the wall deflected over six inches from the center of Shaft C when it was loaded to a displacement of nine inches. This shows that the wall does not help resist lateral loads applied to the shaft.

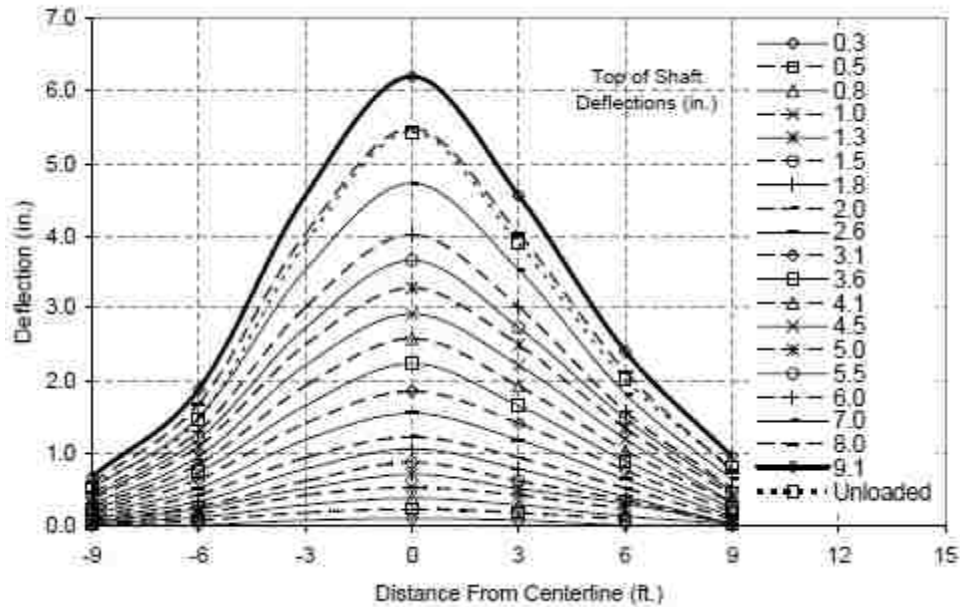


Figure 2-18. Horizontal wall deflection for Shaft C (Pierson et al., 2009).

Since this test was the first of its kind, results were limited due to short drilled shafts being used as opposed to longer driven piles with different shapes. Results were also limited owing to extensible geogrids and a block wall being used as opposed to other soil reinforcement, particularly metallic, inextensible reinforcement which is more typical of bridge abutments.

2.4.2 Tests with Driven Pipe Piles and Metallic Reinforcements (Rollins, Price, & Nelson, 2013)

The tests reported by Pierson et al. (2009) were the first of their kind. However, additional research was necessary to evaluate behavior of longer driven piles and inextensible, metallic reinforcement. The objective of the research presented by Rollins et al. (2013) was to determine how much reduction in lateral resistance would be measured for steel pipe piles with metallic reinforcements. Rollins et al. (2013) tested eight pipe piles behind MSE walls in 3 different locations in Utah County. These site locations were the US Highway 89 in Pleasant Grove, Pioneer

Crossing in Lehi, and Provo Center Street in Provo; all of which had sandy gravel as the backfill material. As opposed to Pierson et al. (2009) which used short shafts which did not extend below the base of the wall, these piles were typically driven 50 to 60 feet below the bottom of the MSE wall. Another contrast is that all eight of these piles had inextensible soil reinforcement for the MSE wall. The two types of inextensible reinforcement were welded wire grids with Price (2012) and metallic ribbed strips with Nelson (2013). The distance from the back face of the MSE wall to the center of the piles ranged from 1.3-7.2 pile diameters. At the Pioneer Crossing site, three 16-inch diameter pipe piles were tested each with 10-mil thick high-density polyethylene (HDPE) wrapped around each pile to reduce downdrag effects. A sloped soil surcharge load was incorporated at this site for one of the piles. However, a tracker hoe, loader, or dozer was also placed on top of the soil to help support the lateral loading apparatus. This site used welded wire soil reinforcement. At the US Highway 89 location, there were two pipe piles 12.75 inches in diameter tested, and the soil was reinforced with welded wire grids. A sloped soil surcharge load was also in place during testing for these piles. The test site at Provo Center Street had three 12.75-inch diameter pipe piles. However, the reinforcement type was ribbed metal strips. A dozer was also placed on top of the soil for two of the pile testing to help support the lateral loading apparatus. Table 2-3 provides a summary of the test pile and reinforcement geometry at all three different test site locations. The table includes, among other criteria, the normalized spacing by pile diameter from the center of the piles to the back face of the wall (S/D), the reinforcement length to the total height of the wall which includes the equivalent height of the surcharge (L/H ratio), the surcharge load, and the moist unit weight of the soil. The L/H ratio ranges from about 1.0 to 1.4, and, as mentioned above, the normalized spacing ranges from about 1.3D to 7.2D.

Table 2-3. Summary Table for Piles Tested by Rollins et al. (2013)

Test Pile	US Highway 89		Pioneer Crossing			Provo Center Street		
	TP1	TP2	TP3	TP4	TP5	TP6	TP7	TP8
Outside Pile Diameter [in]	12.75	12.75	16	16	16	12.75	12.75	12.75
Pile Wall Thickness [in]	0.375	0.375	0.375	0.375	0.375	0.375	0.375	0.375
Wrapped with HDPE? If Yes, Thickness [mm]	No	No	Yes, 10	Yes, 10	Yes, 10	No	No	No
Distance from Back Wall Face to Center of Pile [ft]	7.7	4.0	3.8	6.9	2.2	1.3	2.8	6.7
Normalized Pile Spacing [pile diameters]	7.2D	3.8D	2.9D	5.2D	1.6D	1.3D	2.7D	6.3D
Wall Height at Time of Testing [ft]	20.5	20.5	29.8	37.7	34.7	23.25	23.25	23.25
Reinforcement Length [ft]	33	33	50	42	39	28	28	28
Reinforcement Length-to-Height of Wall (including surcharge)	1.29	1.42	1.27	0.98	0.97	1.03	1.20	1.03
Wall Facing Type	Single Stage: Concrete Panel		Single Stage: Concrete Panel			Two Stage: Welded Wire Covered with Geo Fabric		
Inextensible Reinforcement Type	Welded Wire		Welded Wire			Ribbed Strips		
Vertical Spacing of Reinforcement [ft]	2.5		2.5			2		
Surcharge Load [psf]	708	383	1363	735	808	657	135	657
Wall Panel Dimensions [ft]	5x12		5x10			4.8x9.75		
Backfill Material	Sandy Gravel		Sandy Gravel			Sandy Gravel		
Moist Unit Weight of Soil [pcf]	141.8		142.0			134.9		

The lateral pile load tests were controlled by their displacements as was the case with Pierson et al. (2009). In other words, the piles were loaded laterally until the desired displacement was obtained, then the actuator was locked off. Figure 2-19, Figure 2-20, and Figure 2-21 show the pile head load versus the pile head deflection curves for the peak data points of site locations US Highway 89, Pioneer Crossing, and Provo Center Street, respectively. With the exception of Figure 2-19, the graphs confirm that the lateral pile resistance decreases the closer a pile is to the wall. Possible reasons mentioned by Price (2012) for the exception of TP1 and TP2 was that those piles may have been far enough away from the wall such that a reduction in lateral resistance may not have applied. Another reason is that the relatively long reinforcements may have been sufficient to compensate for pile-wall interaction effects, or it may have been some combination of both effects.

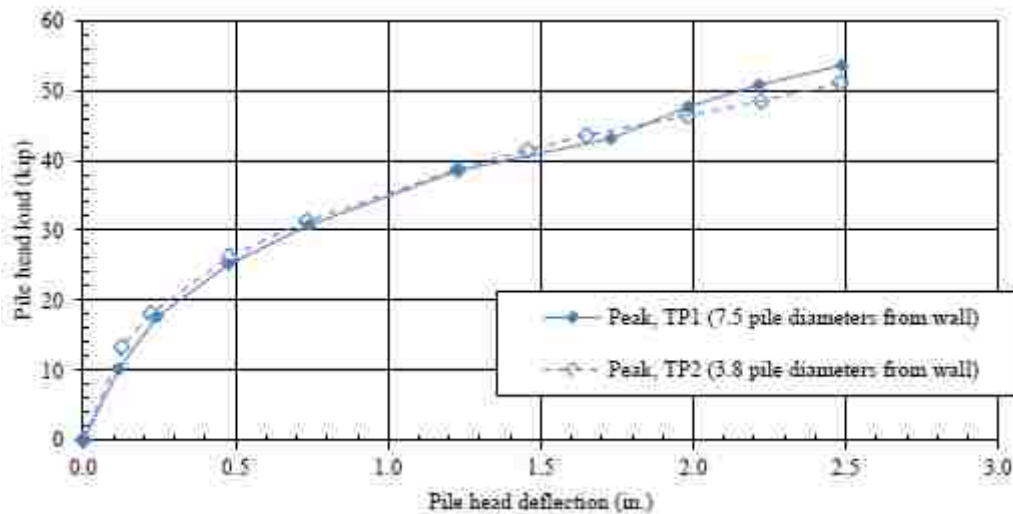


Figure 2-19. US Highway 89 location showing pile head load versus pile head deflection, peak data points for TP1 and TP2 (Price, 2012).

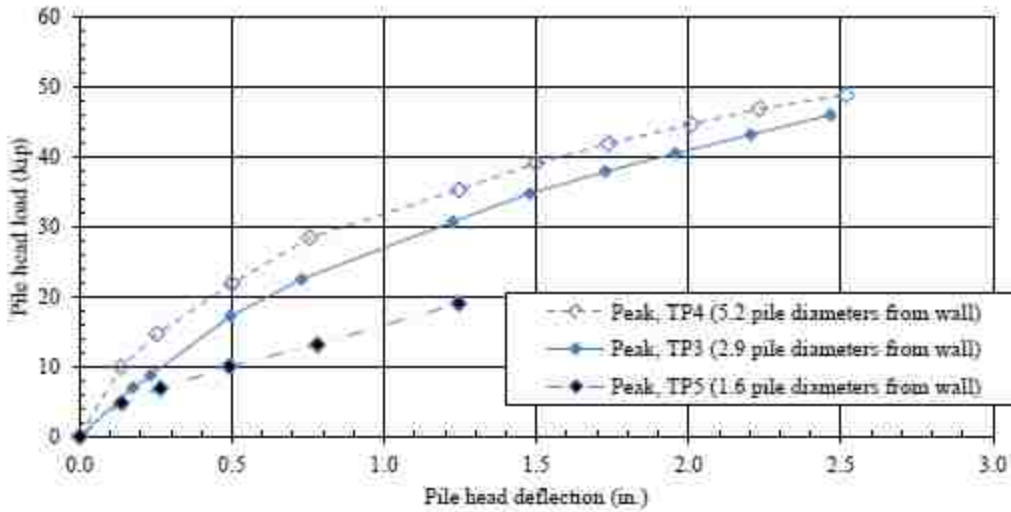


Figure 2-20. Pioneer Crossing location showing pile head load versus pile head deflection, peak data points for TP3, TP4, and TP5 (Price, 2012).

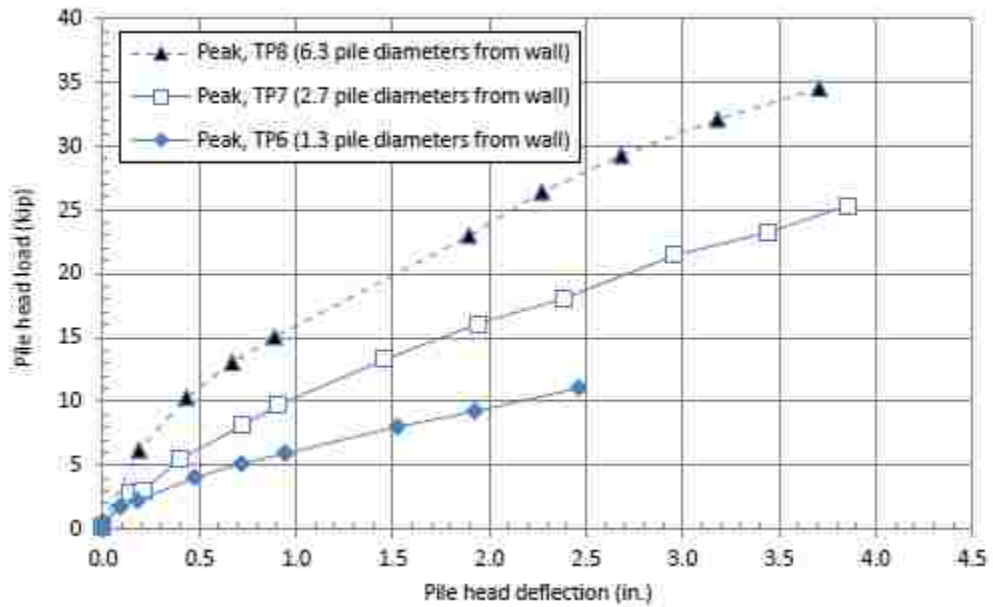


Figure 2-21. Provo Center Street location showing pile head load versus pile head deflection, peak data points for TP6, TP7, and TP8 (Nelson, 2013).

The computer program LPILE was used to back-calculate p-multipliers for each of the test sites. Generally, the pile farthest from the wall at each site was analyzed and the soil properties necessary to match the measured load-deflection curve was determined. These soil parameters were then held constant for each pile, and a constant p-multiplier was used to produce agreement with the measured load-deflection curve. These p-multipliers are factors that are multiplied by the normal lateral soil resistance to account for the reduced lateral pile resistance for piles near an MSE wall. Table 2-4 shows the back-calculated p-multipliers for each test pile along with their respective normalized pile diameter (S/D) and the reinforcement length-to-wall height (L/H) ratio. The L/H ratio includes the equivalent height of any surcharge used. In general, the p-multipliers decreased as the distance to the MSE wall decreased, thus showing that the piles have a reduction in lateral resistance as they get closer to the MSE wall. The Pioneer Crossing site also had the larger pile diameters and HDPE plastic wrapping, although it didn't strongly affect the p-multipliers.

Table 2-4. P-multipliers of Test Piles from Price (2012) and Nelson (2013)

Test Pile	Location	S/D	P-multiplier	L/H
TP1	US Highway 89	7.2	1	1.3
TP2	US Highway 89	3.8	1	1.4
TP3	Pioneer Crossing	2.9	0.80	1.3
TP4	Pioneer Crossing	5.2	1	1.0
TP5	Pioneer Crossing	1.6	0.25	1.0
TP6	Provo Center Street	1.3	0.16	1.0
TP7	Provo Center Street	2.7	0.51	1.2
TP8	Provo Center Street	6.3	1	1.0

Soil reinforcement performance was also calculated by obtaining tensile force in the reinforcements using strain gauges. These strain gauges were attached to the reinforcements at

several distances along the length of the reinforcements to define the variation of tensile force along the length of the reinforcement. Strain was measured at distances from the back face of the MSE wall ranging from 0.5 to 18 feet. Reinforcing elements were instrumented at various transverse distances from the piles and at various depths. The transverse distances ranged from as low as about 4 inches to as high as over 5 feet. The depth of instrumented soil reinforcements ranged from as shallow as 15 inches to as deep as over 5 feet. From Price (2012), it was found that piles closer to the wall experienced higher loads in the reinforcement. On a similar note, Nelson (2013) concluded that the greater the lateral load, the greater the induced force was in the reinforcement. It was also concluded that as the transverse spacing of the reinforcement increases, the induced force decreases exponentially. This can be shown in Figure 2-22 and Figure 2-23 which shows the normalized induced load versus the normalized distance for welded wire and ribbed strip reinforcement, respectively. To accommodate the scatter in the data, both mean and upper bound curves were provided in each figure.

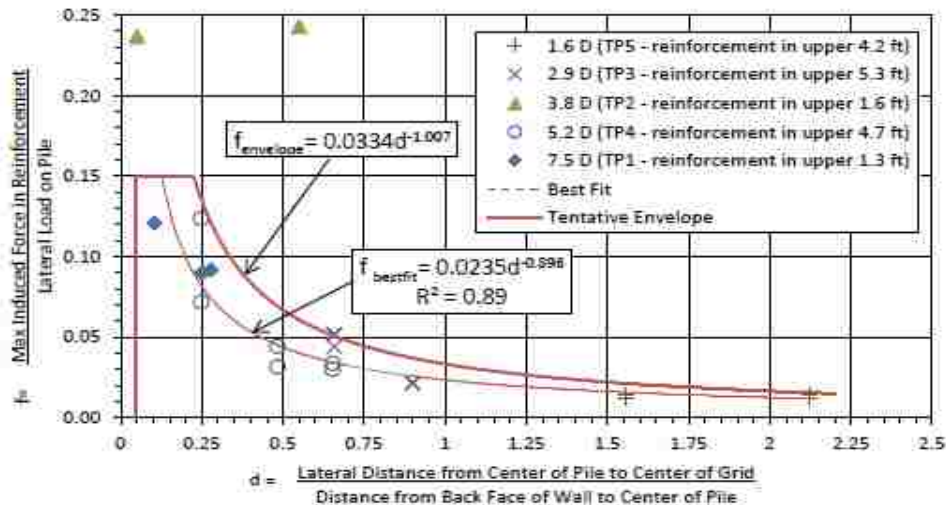


Figure 2-22. Normalized induced load versus normalized distance for welded wire reinforcement (Price, 2012).

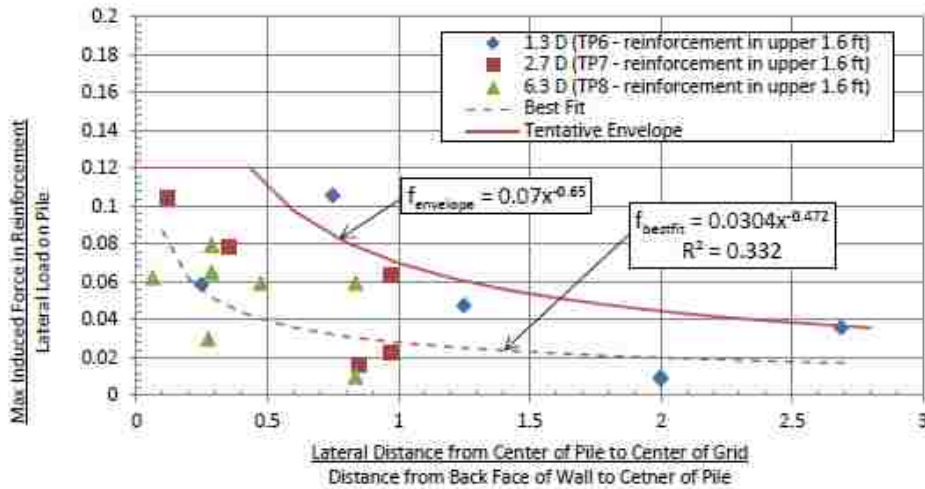


Figure 2-23. Normalized induced load versus normalized distance for ribbed strip reinforcement (Nelson, 2013).

Rollins et al. (2013) concluded that lateral pile resistance reduction was a function of the normalized distance behind the MSE wall. It was also concluded that the reinforcement-to-height ratio affected the lateral pile resistance. This research was limited to the L/H ratio only being at least one, and thus the uncertainty in the effect of the L/H ratio on the lateral pile resistance needed to be further investigated.

2.4.3 Lateral Load Tests on Pipe Piles Behind an MSE Wall with Metallic Reinforcement (Hatch, 2014; Han, 2014; Besendorfer, 2015; Budd, 2016)

Similar to the full-scale pile testing conducted by Nelson (2013) and Price (2012), another series of tests was performed on a simulated MSE wall abutment. Tests were performed for wall heights of 15 and 20 ft and for both ribbed strip and welded wire reinforcements. This was intended to evaluate the effect of reinforcement type and reinforcement length-to-height ratio (L/H) on the

results. These tests involved pipe piles with nominal spacing of two to five pile diameters from the wall. Hatch (2014) and Budd (2016) investigated the behavior of pipe piles with welded wire reinforcement, while Han (2014) and Besendorfer (2015) investigated behavior of pipe piles with ribbed strip reinforcement. The MSE wall was constructed of concrete panels nominally 10 ft wide by 5 ft tall. The AASHTO soil classification for the backfill of the MSE wall was A-1-a with the average moist unit weight ranging from 126.2 pcf to 127.5 pcf. A surcharge of 600 psf was also applied, using concrete blocks, to simulate the weight of the abutment on the wall. Pile moment and the induced reinforcement load was measured using strain gauges attached along the piles and reinforcements, respectively. Hatch (2014), Han (2014), Besendorfer (2015) and Budd (2016) completed research on four 12.75" pipe piles each. The computer program LPILE was once again used to back-calculate p-multipliers for each test. This p-multiplier was part of the research to analyze how much reduction occurred in lateral load capacity for piles behind MSE walls.

Table 2-5 and Table 2-6 provide a summary of all the different tests for this MSE wall project. Figure 2-24 shows all of the p-multipliers versus the normalized distance from the wall (in pile diameters) of the data from Rollins et al. (2013), Hatch (2014), Han (2014), Besendorfer (2015), and Budd (2016). The legend has been modified from Budd (2016). It was generally found that piles placed farther than about 4.0 pile diameters from the MSE wall did not have their lateral resistance reduced. The R^2 value was found to be 79%, but neglecting two aberrations, the R^2 increases to 89%.

The following equation has been developed for piles spaced closer than 3.9 pile diameters corresponding to the R² of 89%:

$$p_{mult} = 0.32 \frac{S}{D} - 0.23 \quad \text{for} \quad \frac{S}{D} < 3.9 \quad (2-20a)$$

$$p_{mult} = 1.0 \quad \text{for} \quad \frac{S}{D} > 3.9 \quad (2-20b)$$

where p_{mult} = p-multiplier

S = distance from the back face of the MSE wall to the center of the pile, and

D = pile diameter.

The results generally show that the p-multipliers were not strongly affected by the L/H ratio nor by reinforcement type. It was again found with confidence that pile resistance decreases as the pile moves closer to the MSE wall. A limitation of the research performed was that it did not analyze the effect of different pile shapes. This thesis further investigates the effect the L/H ratio and reinforcement type, as well as the effect of square piles and H-piles on lateral resistance. Table 2-5 represents a summary of the parameters for the ribbed strip reinforcement tests of Han (2014) and Besendorfer (2015). Table 2-6 represents a summary of the parameters for the welded wire reinforcement tests of Hatch (2014) and Budd (2016).

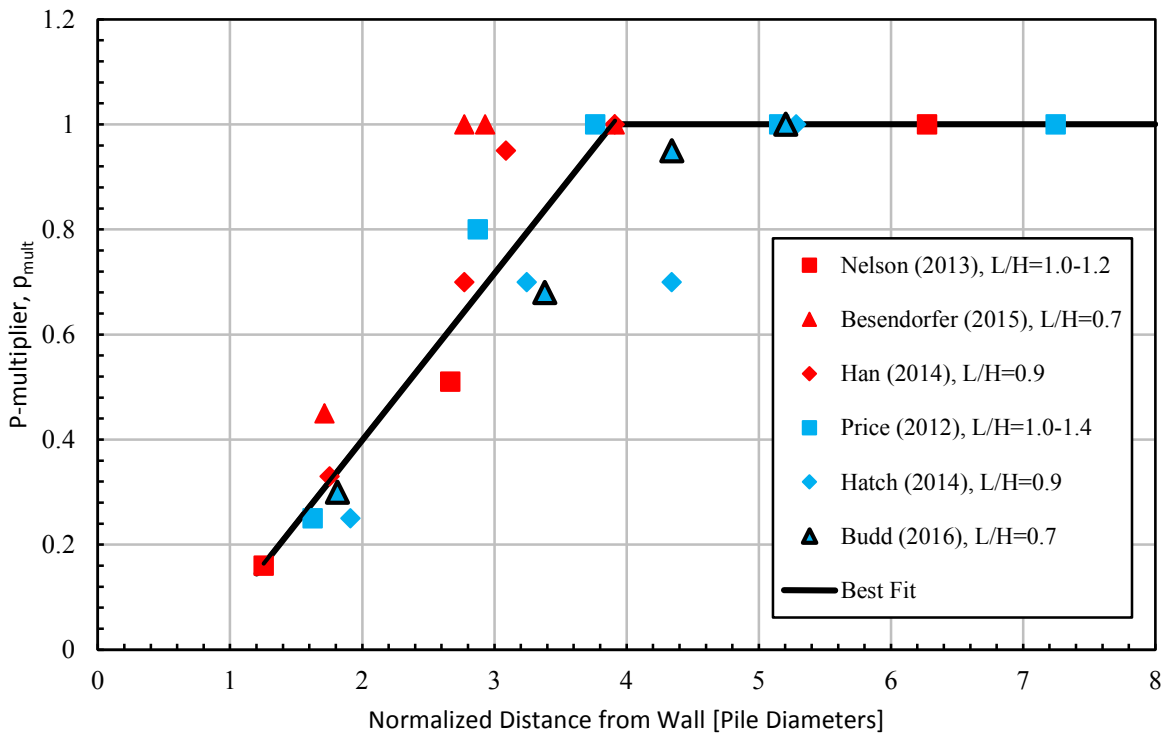


Figure 2-24. P-multipliers versus normalized distance from wall (modified from Budd, 2016).

**Table 2-5. Summary Table for Piles Tested in Ribbed Metal Strip Reinforcement
(Han, 2014 & Besendorfer, 2015)**

Researcher	Han				Besendorfer			
Test Pile Type	Pipe				Pipe			
Pile Shape Name	HSS12.750X0.375				HSS12.750X0.375			
Outside Pile Diameter [in]	12.75				12.75			
Distance from Back Face of Wall to Center of Pile [in]	22.4	35.4	39.4	49.9	21.9	35.4	37.4	49.9
Nominal Distance from Back Face of Wall to Center of Pile [diameters]	2D	3D	4D	5D	2D	3D	4D	5D
Normalized Spacing Between Back Face of Wall to Center of Pile	1.8D	2.8D	3.1D	3.9D	1.7D	2.8D	2.9D	3.9D
Nominal C-C Spacing Between Piles [ft]	5				5			
Pile Depth Below Base of Wall [ft]	18				18			
Wall Height at Time of Testing [ft]	15				20			
Reinforcement Length [ft]	18				18			
Length-to-Height Ratio with Surcharge	0.90				0.72			
Wall Facing Type	Single Stage: Concrete Panel				Single Stage: Concrete Panel			
Wall Panel Dimensions [ft]	9.84'X4.92'				9.84'X4.92'			
Inextensible Reinforcement Type	Strip				Strip			
Nominal Vertical Spacing of Reinforcement [ft]	2.5				2.5			
Nominal C-C Spacing Between Reinforcement [ft]	2.5				2.5			
Surcharge Load [psf]	600				600			
Backfill Material	A-1-a SM				A-1-a SP-SM			
Compacted Backfill Density [pcf]	127.5				126.2			

**Table 2-6. Summary Table for Piles Tested in Welded Wire Reinforcement
(Hatch, 2014 & Budd, 2016)**

Researcher	Hatch				Budd			
Test Pile Type	Pipe				Pipe			
Pile Shape Name	HSS12.750X0.375				HSS12.750X0.375			
Outside Pile Diameter [in]	12.75				12.75			
Distance from Back Face of Wall to Center of Pile [in]	24.4	41.4	55.4	67.4	23.1	43.1	55.4	66.4
Nominal Distance from Back Face of Wall to Center of Pile [diameters]	2D	3D	4D	5D	2D	3D	4D	5D
Normalized Spacing Between Back Face of Wall to Center of Pile	1.9D	3.2D	4.3D	5.3D	1.8D	3.4D	4.3D	5.2D
Nominal C-C Spacing Between Piles [ft]	5				5			
Pile Depth Below Base of Wall [ft]	18				18			
Wall Height at Time of Testing [ft]	15				20			
Reinforcement Length [ft]	18				18			
Length-to-Height Ratio with Surcharge	0.90				0.72			
Wall Facing Type	Single Stage: Concrete Panel				Single Stage: Concrete Panel			
Wall Panel Dimensions [ft]	9.84'X4.92'				9.84'X4.92'			
Inextensible Reinforcement Type	Welded Wire				Welded Wire			
Nominal Vertical Spacing of Reinforcement [ft]	2.5				2.5			
Nominal C-C Spacing Between Reinforcement [ft]	5				5			
Surcharge Load [psf]	600				600			
Backfill Material	A-1-a SM				A-1-a SP-SM			
Compacted Backfill Density [pcf]	127.5				126.2			

3 TEST LAYOUT

This study is a part and continuation of the previous full-scale lateral load testing performed on piles behind an MSE wall with soil reinforcement (Hatch, 2014; Han, 2014; Besendorfer, 2015; Budd, 2016). This research took place in Lehi, Utah near a place informally called the Point of the Mountain between Salt Lake County and Utah County just east of the Interstate-15 (see Figure 3-1). The project was located on Geneva Rock property. The test piles that deal with this project are the H-piles and square piles behind the MSE wall at nominal distances of two, three, four, and five pile diameters.



Figure 3-1. Test site location (GOOGLE EARTH, 2013).

3.1 MSE Wall and Soil Reinforcement

The MSE wall is a single stage wall, and was constructed with the help of both SSL, LLC and Reinforced Earth Company (RECo). (See Appendix K for RECo's MSE wall plans and Appendix L SSL's MSE wall plans). The piles behind the MSE wall are discussed subsequently. The MSE wall was split into two halves, with the west (left side looking from the front) half being designed by RECo using ribbed metal strip soil reinforcement and the east (right side looking from the front) half designed by SSL using welded wire soil reinforcement. The MSE wall was constructed in two phases. In the first phase, the wall was built up to 15 feet and in the second phase the wall was built up an additional 5 feet bringing the wall to a height of 20 feet. In accordance with standard practice, the MSE wall was constructed with a leveling pad 1 foot in width and 6 inches in thickness at its base. About 2 ft of backfill soil ($\approx 0.1H$) was added above the top of the leveling in front of the MSE wall. The back of the MSE wall had backfill soil up to the top of the wall and the backfill extended 25 ft behind the wall.

Backfill soil properties are explained below, but the design friction angle was 34 degrees and the design unit weight was 131 pcf. The length of the wall came to a total of about 180 ft with a slip joint dividing the wall in half for the ribbed strip and welded wire sides. The length of the ribbed strip side of the MSE wall is a total of 89.56 ft (including the slip joint that divides the two halves of the wall). There is 49.90 ft length of full height wall followed by 39.66 ft of a 2:1 (H:V) down slope. The welded wire side is similar (90 ft long wall); having a 50 ft length of full height wall section followed by 40 ft of a 2:1 (H:V) down slope. Figure 3-2 and Figure 3-3 provide an elevation view of the wall. The actual wall was constructed to a total of 20 ft high above the

leveling pad (after Phase 2) made up of concrete panels 9.84 ft in length and 4.92 ft in height (dimensions include the 0.75-inch panel joints). Starting from the bottom, every other column of panels started with panels cut in half horizontally so that per column the panels are staggered by half a panel as shown in Figure 3-4. On the welded wire side, a similar approach is taken. However, on the top of the wall, instead of installing half of a panel every other column on the top 2.5 ft of the wall, the panels were just extended from below, bringing the height of every other panel to approximately 7.5 ft as shown in Figure 3-5.

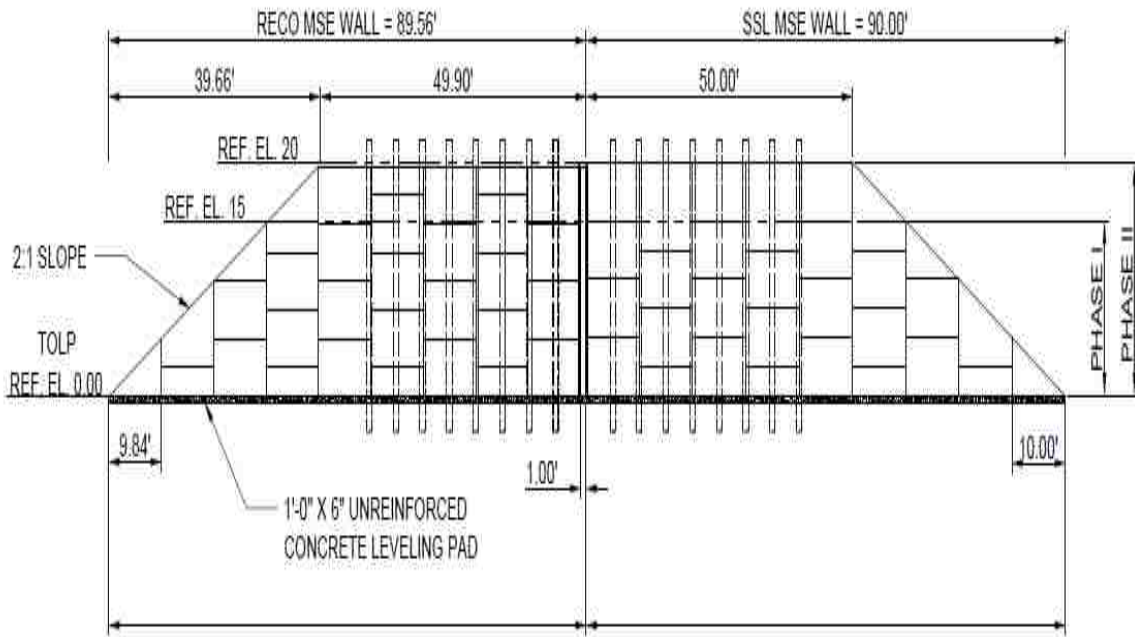


Figure 3-2. Elevation view of MSE wall.



Figure 3-3. Photograph of the completed MSE wall.

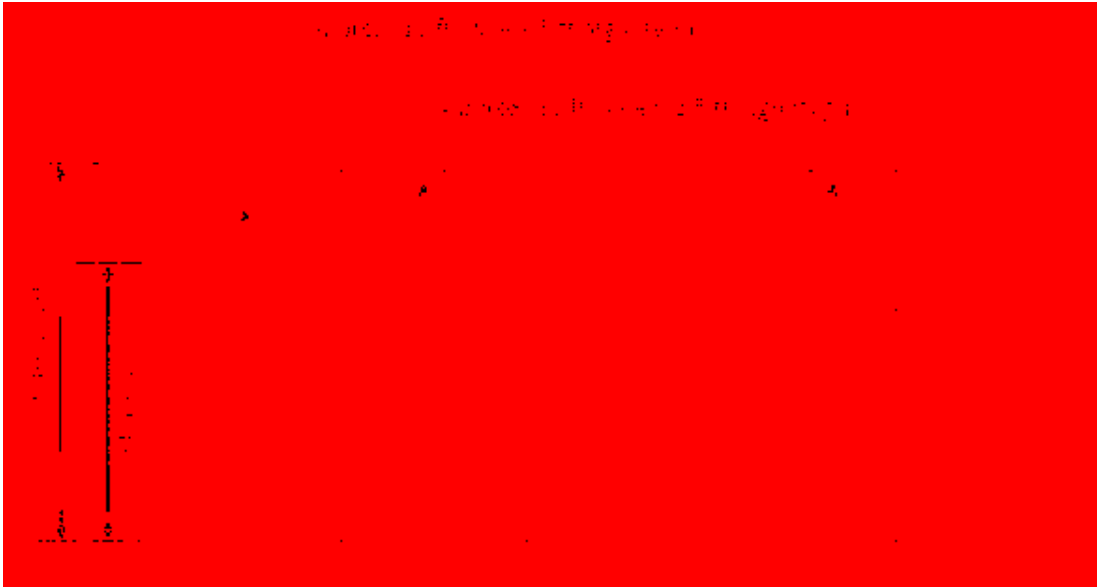


Figure 3-4. Panel configuration for the ribbed strip reinforcement side of the MSE wall.

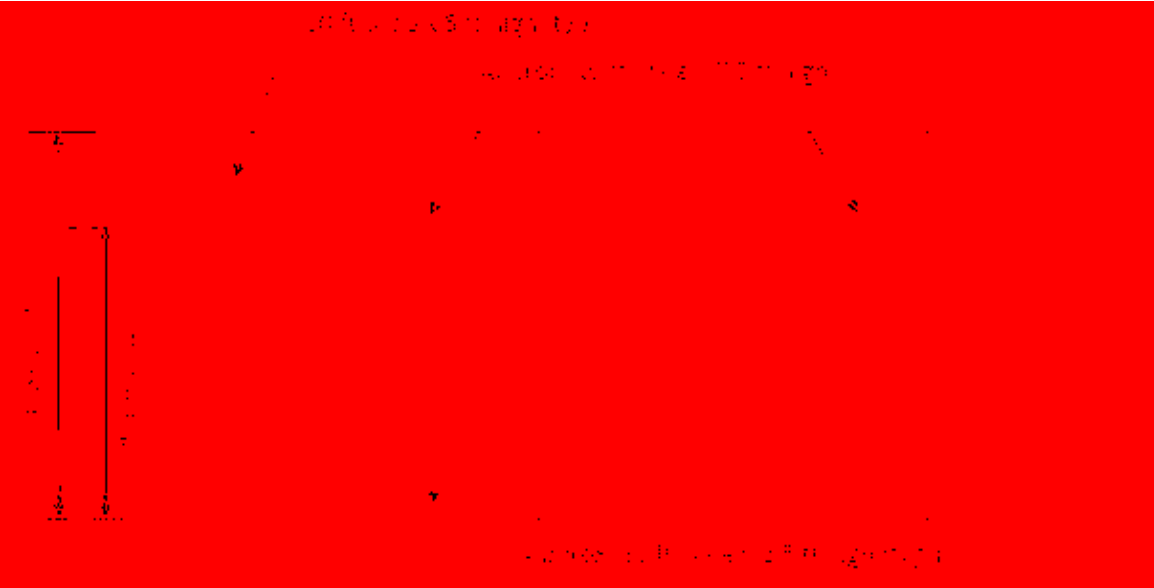


Figure 3-5. Panel configuration for the welded wire reinforcement side of the MSE wall.

The RECO side had inextensible ribbed metal strips 50 mm wide and 4 mm thick. The steel was Grade 65 ($F_y = 65,000$ psi) and was galvanized for corrosion protection. A typical panel has two rows and four columns of strips, making eight strips per panel. They were spaced at about 2.5

ft both horizontally and vertically on average. As described subsequently in Chapter 4, selected strips were instrumented along the length and height of the wall to determine the distribution and magnitude of tensile forces induced by pile loading. The strips were all 18 ft in length. On the full height section of the wall, the top layer started 1.25 ft from the top of the wall.

SSL installed 18 ft long inextensible welded wire reinforcements with a yield strength of 65,000 psi. On the full height section of the SSL side, eight layers of welded wire grids were installed starting at 1.25 ft from the top of the wall. Both the transverse and longitudinal wires were size W11 (0.374 in. diameter) for all layers. The top layer had six longitudinal wires with a longitudinal spacing of eight inches (which longitudinal spacing is typical for all of the layers) and the transverse wires had a transverse spacing of six inches along the length of the reinforcement. The next four layers below had only five longitudinal wires with the transverse wires spaced at 12 inches. The last three (bottom) layers had six longitudinal wires also with the transverse wires spaced at 12 inches. See Table 3-1 for welded wire orientation. The horizontal spacing per section of wire mesh was about 5 ft on average. The vertical spacing was 2.5 ft all along the height of the wall.

Table 3-1. Welded Wire Orientation Details

Grid Layer (From Top of Wall)	Depth From Top of Wall [ft]	Longitudinal Wires			Transverse Wires	
		Number	Size	Spacing [in]	Size	Spacing [in]
1	1.25	6	W11	8	W11	6
2	3.75	5	W11	8	W11	12
3	6.25	5	W11	8	W11	12
4	8.75	5	W11	8	W11	12
5	11.25	5	W11	8	W11	12
6	13.75	6	W11	8	W11	12
7	16.25	6	W11	8	W11	12
8	18.75	6	W11	8	W11	12

3.1.1 Backfill

Twenty feet of backfill was used for the whole height of the MSE wall. The backfill differed slightly between each phase. Phase 1 had 63% sand and only 23% gravel thus classifying the soil as sand. The fines content was 14%. The soil classification for Phase 1 was A-1-a material according to AASHTO and SM (silty sand with gravel) according to the Unified Soil Classification System (USCS). Phase 2 was similar and the soil was still classified as A-1-a material according to AASHTO, except that the USCS classification was SP-SM (poorly graded sand with silt and gravel) owing to the fact that it had less than 11.5% fines and a coefficient of uniformity (C_u) value of 4.5. The coefficient of curvature (C_u) value for Phases 1 and 2 are 60 and 50, respectively. Table 3-2 shows the sieve size and percent passing of the two phases and Table 3-3 shows selected parameters obtained from the grain-size distribution curves. Figure 3-6 is a graph of the percent passing vs. grain size for both phases of the project.

Table 3-2. Sieve Size and Percent Passing

Phase 1		Phase 2	
Sieve Size [mm]	% Passing	Sieve Size [mm]	% Passing
9.5	100	9.5	100
4.75	77	4.75	79
2.36	52	2.36	51
1.18	37	1.18	33
0.6	30	0.6	25
0.3	25	0.3	20
0.15	20	0.15	16
0.075	14	0.075	11.5

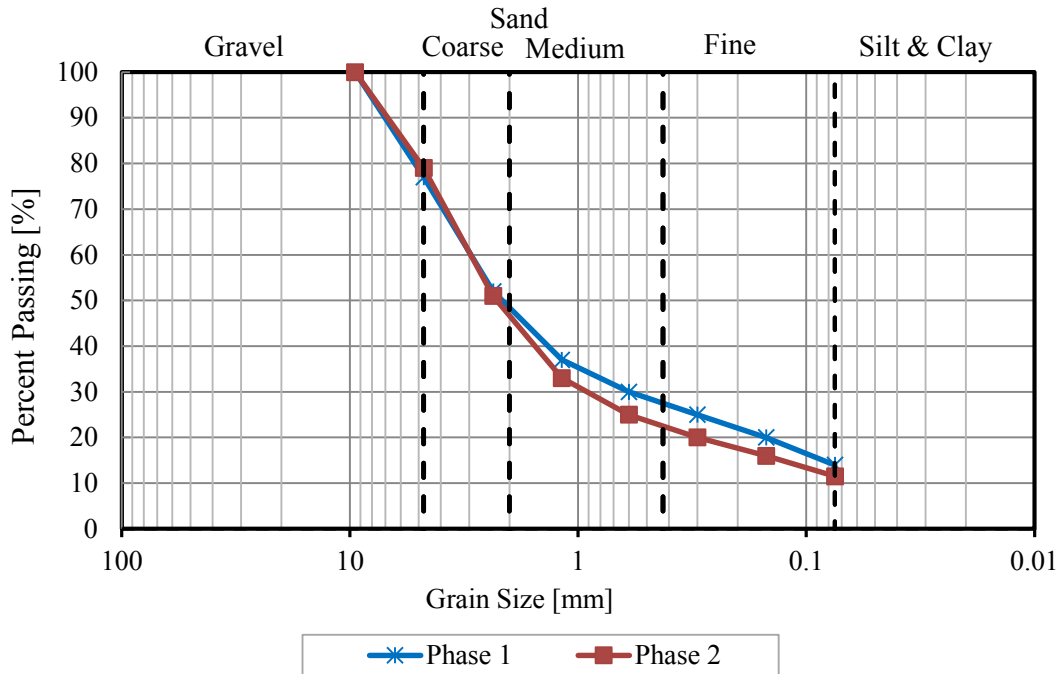


Figure 3-6. Soil percent passing versus grain size.

Table 3-3. Phase 1 and Phase 2 Soil Parameters

	Phase 1	Phase 2
D₁₀	0.05	0.06
D₃₀	0.9	0.6
D₆₀	3	3
C_c	5.4	2.0
C_u	60	50

For the backfill soil in Phase 1, the maximum standard proctor density was measured as 128 pcf with an optimum moisture content of 7.8%. For Phase 2, neither the maximum standard proctor nor optimum moisture content were measured. However, the maximum modified proctor density was measured as 131.7 pcf with an optimum moisture content of 8.7%. Behind the piles, a vibratory roller was used to compact the soil to a target relative compaction of 95%, while a plate

compactor was used to compact the soil around and in front of the piles near the wall face. This procedure is typically mandated in engineering practice to prevent the wall panels from displacing outward during compaction. The moisture content, dry unit weight, moist unit weight, and relative compaction were measured using a nuclear density gauge with tests performed by Brigham Young University students. Nuclear density gauge tests were performed between the test piles and the MSE wall and also behind the test piles for both phases. The average moist unit weight for all of Phase 1 was calculated to be 127.5 pcf, while Phase 2 had an average moist unit weight calculated to be 126.2 pcf. Averaging all of the data yielded a moist unit weight of 126.7 pcf.

Table 3-4 and Table 3-5 show average measurements of the data behind the test piles, between the wall and the test piles, and the combination of all the data for Phase 1 and Phase 2, respectively. Figure 3-7 and Figure 3-8 show the scatter of the relative compaction versus depth for Phase 1 and Phase 2, respectively. The relative compaction behind the tests piles was consistently higher than 95%; however, in front of the test piles the relative compaction varied between 88% and 94% as a result of the differing compaction procedures. In an effort to improve compaction near the wall face, lift thicknesses of six inches were used rather than the typical 12 inch lifts with the roller compactor. Nevertheless, the relative compaction was still lower near the wall even after multiple passes. Figure 3-9 and Figure 3-10 show the scatter of the moisture content versus depth for Phase 1 and Phase 2, respectively. Figure 3-11 and Figure 3-12 show the scatter of the moist unit weight versus depth for Phase 1 and Phase 2, respectively. (Appendix B shows the Geneva Rock laboratory test reports).

Table 3-4. Average Soil Measurements for Phase 1

Between Test Piles and Wall				
	Moisture Content [%]	Dry Unit Weight [pcf]	Moist Unit Weight [pcf]	Relative Compaction [%]
Average	6.5	114.6	122.1	89.5
Standard Deviation	1.80	1.52	2.49	1.22
Coefficient of Variation	0.275	0.013	0.020	0.014
Behind Test Piles				
Average	6.6	122.5	130.6	95.7
Standard Deviation	1.66	1.20	2.90	0.93
Coefficient of Variation	0.252	0.010	0.022	0.010
Combined				
Average	6.6	122.5	130.6	95.7
Standard Deviation	1.66	1.20	2.90	0.93
Coefficient of Variation	0.252	0.010	0.022	0.010

Table 3-5. Average Soil Measurements for Phase 2

Between Test Piles and Wall				
	Moisture Content [%]	Dry Unit Weight [pcf]	Moist Unit Weight [pcf]	Relative Compaction [%]
Average	4.6	117.7	123.1	92.9
Standard Deviation	1.08	3.33	4.23	2.63
Coefficient of Variation	0.233	0.028	0.034	0.028
Behind Test Piles				
Average	5.0	123.7	129.9	97.7
Standard Deviation	1.06	1.94	2.41	1.53
Coefficient of Variation	0.214	0.016	0.019	0.016
Combined				
Average	5.0	123.7	129.9	97.7
Standard Deviation	1.06	1.94	2.41	1.53
Coefficient of Variation	0.214	0.016	0.019	0.016

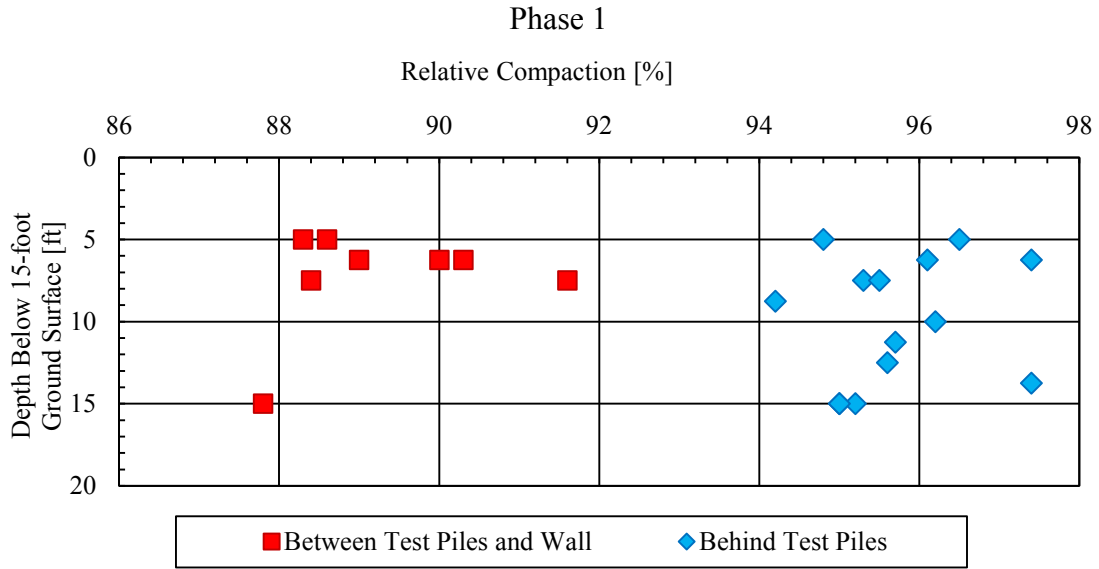


Figure 3-7. Depth versus relative compaction, Phase 1.

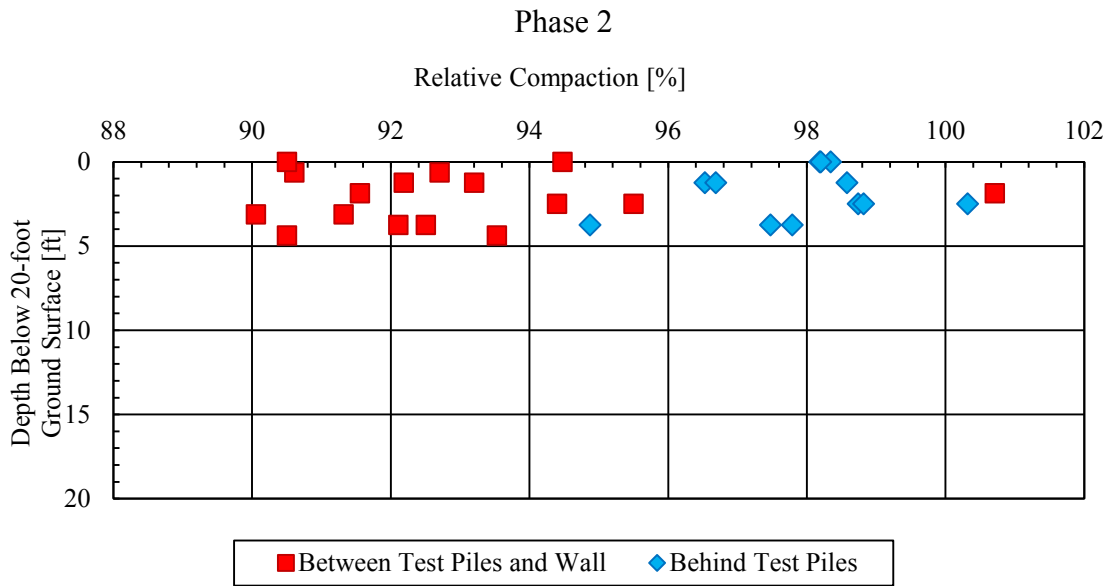


Figure 3-8. Depth versus relative compaction, Phase 2.

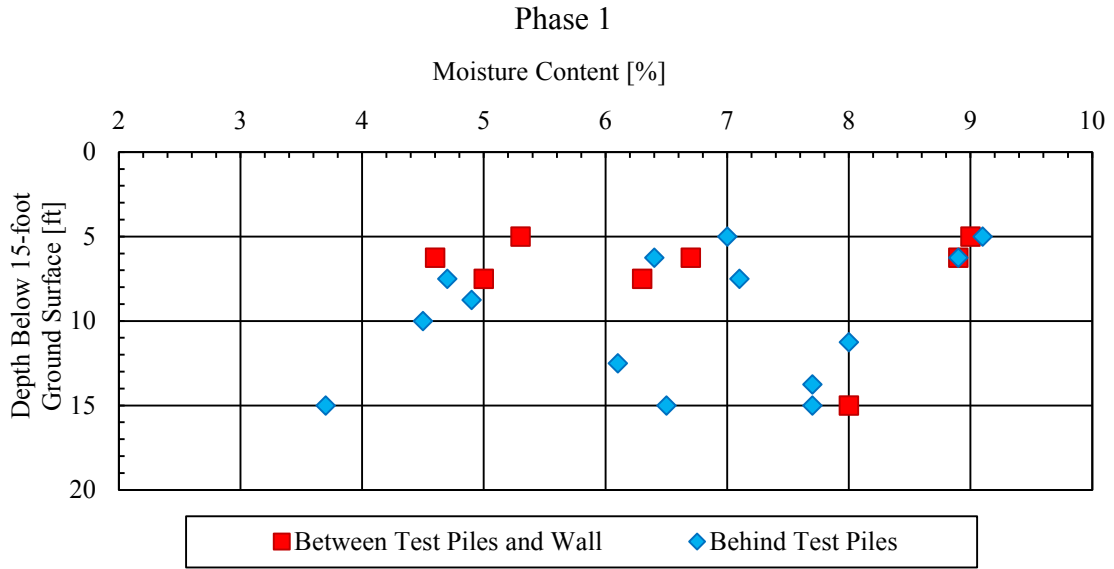


Figure 3-9. Depth versus moisture content, Phase 1.

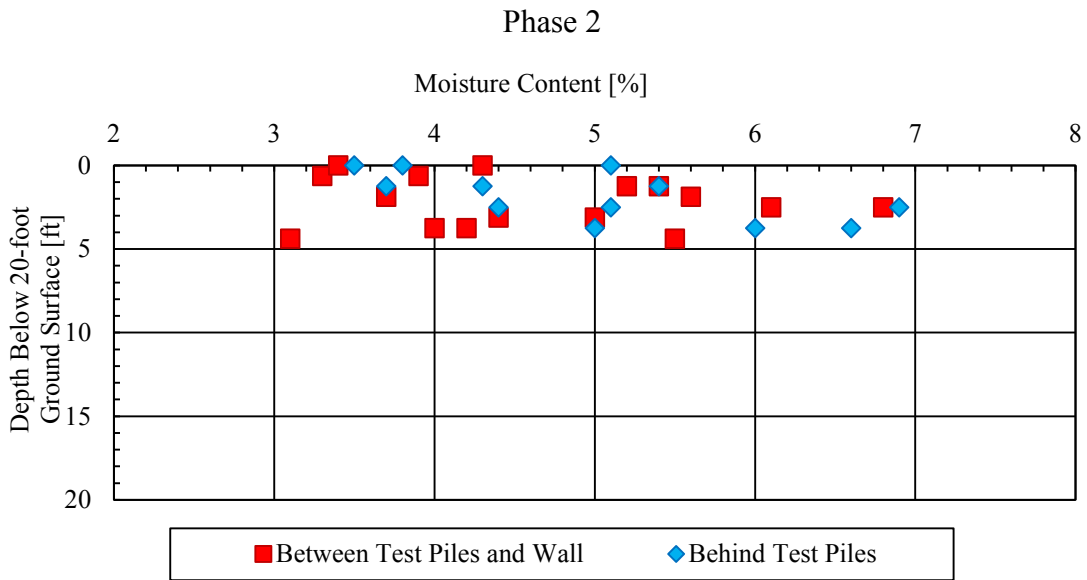


Figure 3-10. Depth versus moisture content, Phase 2.

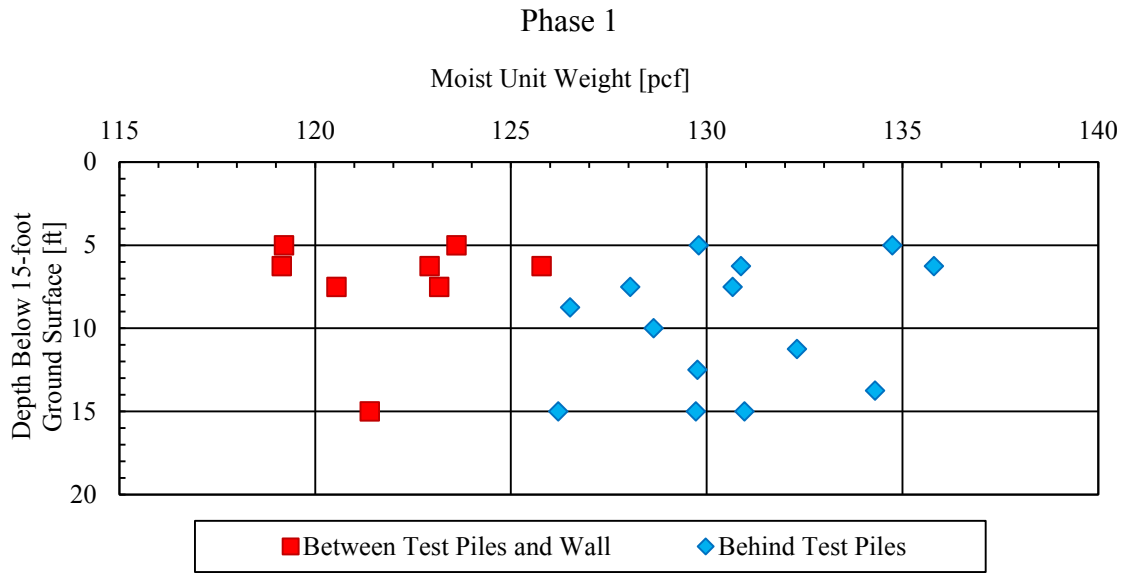


Figure 3-11. Depth versus moist unit weight, Phase 1.

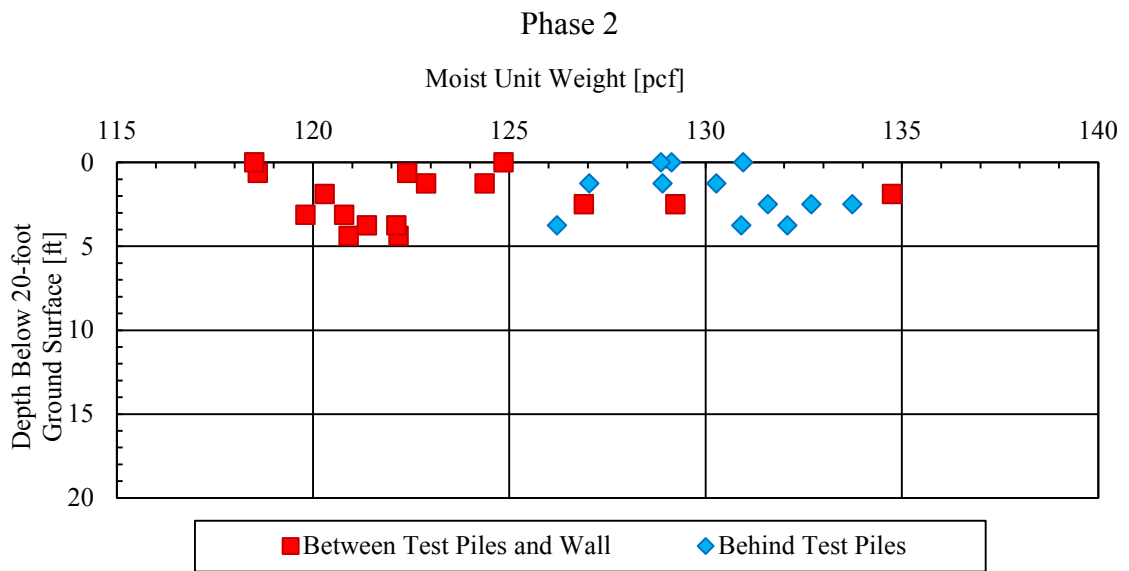


Figure 3-12. Depth versus moist unit weight, Phase 2.

3.1.2 Surcharge

To simulate to some extent the weight of an abutment pile cap atop the MSE wall, a 600 psf surcharge was applied adjacent to both sides of the pile being loaded laterally. Without the surcharge, the pullout resistance of the upper reinforcement would be significantly underestimated. The surcharge consisted of multiple 2'x2'x6' pre-cast concrete blocks. Concrete was assumed to weigh 150 pcf. The surcharge was 3 blocks (6 ft) wide on either side of the test pile and two blocks (4 ft) high. The blocks laid along the length of the soil reinforcement behind the pile. Using an average soil moist unit weight of 127.5 pcf for Phase 1, an equivalent height of soil fill was calculated to be about 4.75 ft from the 600 psf surcharge (see Figure 3-13 for a plan view). For Phase 2, the equivalent height of soil fill was calculated to be about 4.71 ft using the average moist unit weight of 126.2 pcf. However, an equivalent soil height of 5 ft was used for the L/H ratios.

3.2 Piles

There were sixteen piles near the MSE wall. The piles were driven by Desert Deep Foundations using an ICE I-030V2 diesel hammer prior to the construction of the MSE wall. The piles were 40 feet in length and were driven 18 feet below the base of the wall. A record of the blow counts is shown in Appendix H. The square and pipe piles were driven open-ended and the depth of the plug in each pile is indicated in Appendix I. Reaction piles were also driven behind the reinforced soil zone so as not to affect the tensile forces on the reinforcement. The reaction piles were loaded transverse to the MSE wall face to examine the effect of pile shape on lateral resistance (Bustamante, 2014 & Russell, 2016). They were also used to provide lateral resistance against the reaction beam as each of the test piles were loaded laterally normal to the MSE wall (see Figure 3-13). The ribbed strip side of the wall had four pipe piles and four H-piles while the welded wire side had four pipe piles and four square piles. During Phase 1 (15-foot wall height),

all eight pipe piles and the H-piles were loaded and analyzed. During Phase 2 (20-foot wall height) the same eight pipe piles were tested again along with the four square piles. Tests on the pipe piles allowed a direct comparison of the effect of reinforcement type and L/H ratio on pile performance. Additional tests on the square and H-piles allowed a comparison of the reduction in load resistance between these pile shapes and the pipe piles. As indicated previously, this study deals with the testing and analysis of the H-piles and square piles.

The pipe piles were HSS12.75X0.375 (A252 Grade 3) with an outside diameter of 12.75 inches and a wall thickness of 0.375 inches. The square piles were HSS12X12X5/16 with a width of 12 inches. The H-piles were HP12X74. They were loaded about the weak axis on the web and thus the outside diameter used was the flange width which was 12.2 inches. Table 3-6 and Table 3-7 show the horizontal spacing of the H-piles and square piles, respectively. See Appendix J for the horizontal spacing of the pipe piles. Generally, the piles were spaced about 5 feet on center from each other. Figure 3-13 shows a plan view layout of the piles, MSE wall, and reaction piles. All of the piles were nominally spaced at two, three, four, and five pile diameters from the back face of the MSE wall to the center of the pile. Actual spacing varied owing to complications of driving the piles into place. Table 3-8 shows the nominal, normalized, and actual spacing of the square and H-piles.

Table 3-6. Adjacent Spacing of H-piles

	5D Pipe (strip side) to 5D H-pile (strip side)	5D to 4D H-pile	4D to 3D H-pile	3D to 2D H-pile	2D H-pile (strip side) to 2D Square (wire side)
Adjacent Spacing [in]	59	62	58	58	123

Table 3-7. Adjacent Spacing of Square Piles

	2D H-pile (strip side) to 2D Square (wire side)	2D to 3D Square	3D to 4D Square	4D to 5D Square	5D Square (wire side) to 5D Pipe (wire side)
Adjacent Spacing [in]	123	70	64	51	68.5

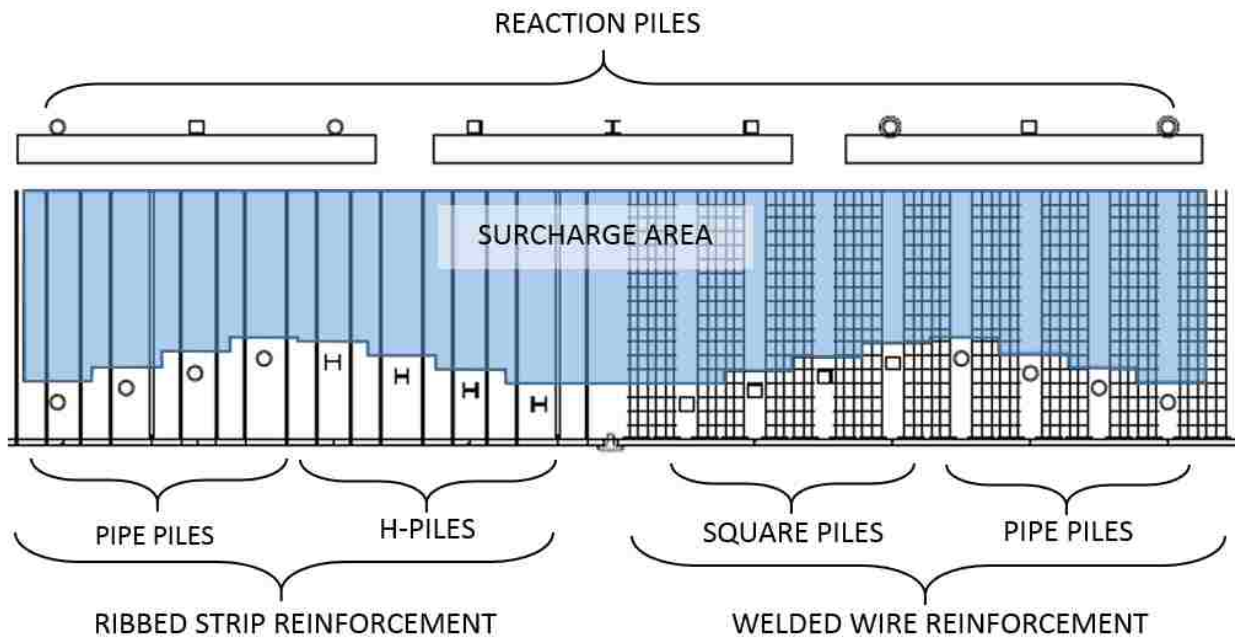


Figure 3-13. Plan view of MSE wall.

Table 3-8. H-pile and Square Pile Diameter Spacing

Test Pile Type	Square				H-Piles			
Pile Shape Name	HSS12X12X5/16				HP12X74			
Outside Pile Diameter [in]	12				12.2			
Distance from Back Face of Wall to Center of Pile [in]	25.0	37.5	50.5	68.8	26.4	30.4	38.6	55.1
Nominal Distance from Back Face of Wall to Center of Pile [diameters]	2D	3D	4D	5D	2D	3D	4D	5D
Normalized Spacing Between Back Face of Wall to Center of Pile	2.1D	3.1D	4.2D	5.7D	2.2D	2.5D	3.2D	4.5D

3.3 Loading Apparatus

A hydraulic jack was used to load all of the piles laterally. It was loaded against a W36X150 reaction beam. This reaction beam was placed against the back reaction piles. A variable length strut was placed between the reaction beam and the test pile in the gap between the pre-cast concrete blocks as shown in Figure 3-14. To reduce eccentricity, hemispherical load platens were used between the reaction beam and the hydraulic jack. A load cell was positioned between the pile and the hydraulic jack. Load was applied at a height of 12 inches above the ground surface with a pinned-head connection. See Figure 3-15 and Figure 3-16 for how the loading apparatus was applied for lateral testing. Figure 3-17 shows an overall configuration of a cross-section through the MSE wall.



Figure 3-14. Reaction beam with hemispherical end platen and struts.

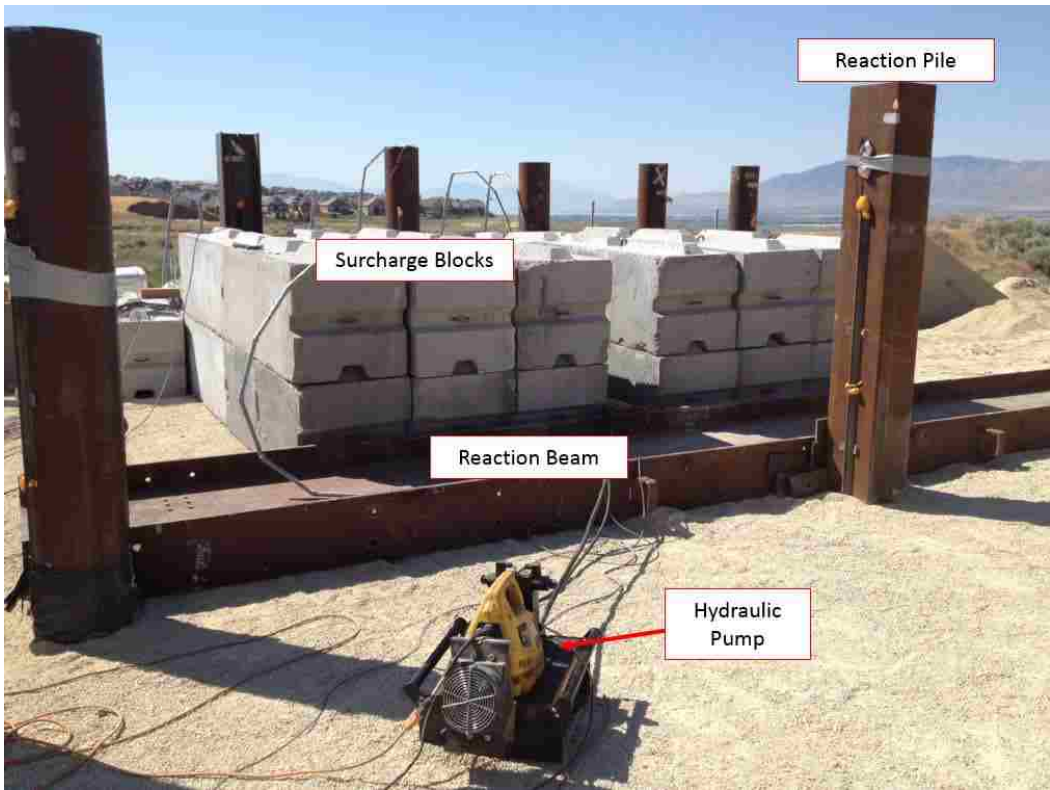


Figure 3-15. Loading apparatus, reaction beam, and surcharge blocks.

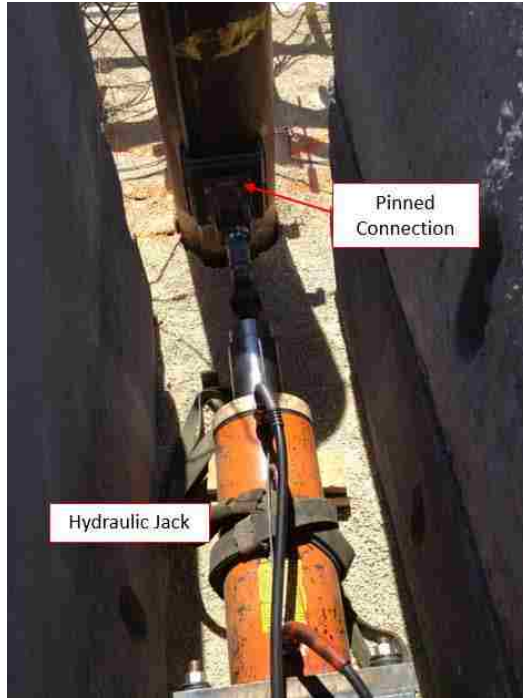


Figure 3-16. Loading apparatus.

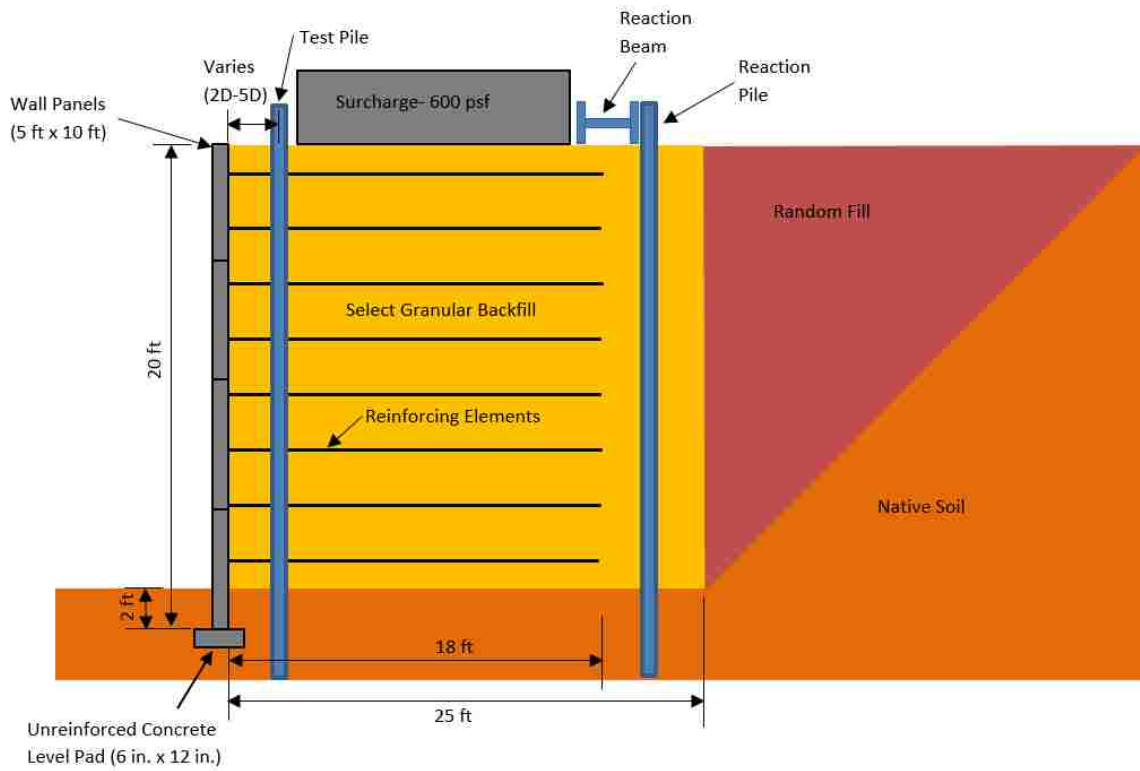


Figure 3-17. Cross-section through the MSE wall.

3.3.1 Data Acquisition

The data was acquired using a displacement control approach. The hydraulic ram loaded each pile until it displaced at quarter-inch increments from 0.25 inches up until 3.0 inches, with the initial push starting at 0.125 inches. At each quarter-inch increment, the load was held for five minutes, in which the load would decrease slightly before applying a greater load again until the next quarter-inch increment. Readings were taken every half-second from the hydraulic jack for the string potentiometers and strain gauges (see Chapter 4). The values taken immediately after each cycle (the peak), the one-minute average, and the five-minute average of the load being held at each increment were used to analyze the data. The one minute and five minute averages were taken by averaging the data 30 seconds following. Wall displacement recordings and images were only taken at the peak and five-minute hold of each quarter-inch load increment. Ground surface heaving was measured before and after each test for each pile (see Sec. 4.6).

4 INSTRUMENTATION

An instrumentation plan was implemented to be able to measure the behavior of the piles and backfill during lateral load testing. Pile behavior such as deflection and moment were able to be determined using the load cell and pressure transducers, string potentiometers, and strain gauges. The reinforcement behavior was also able to be determined with the strain gauges. The soil behavior such as vertical and horizontal heaving was also measured through the string potentiometers as well as with conventional surveying techniques. Soil reinforcement behavior was also able to be determined with the strain gauges. Lastly, wall displacement was also recorded as explained in this chapter.

4.1 Load Cell and Pressure Transducers

The pile load was measured in two ways, through the load cell and through the pressure transducers attached to the pump for the hydraulic jack. For the H-piles, the load from the hydraulic pressure transducer was used. However, for the square piles, the load cell was used because the pressure transducer began producing erratic results.

4.2 String Potentiometers

String potentiometers were used to acquire the horizontal pile deflection, horizontal ground displacement, and pile rotation after the piles were loaded laterally. The string potentiometers were attached to an independent reference frame with supports located 7 feet from the loaded piles. This

provided a reference datum for when ground movement occurred during lateral testing. The tensioned string in the potentiometers was attached to various reference points and deflection was measured as the string moved in or out of the potentiometer. To measure the pile deflection, one string potentiometer had its line attached horizontally to a magnetic eyebolt attached to the pile one foot above the ground. This kept it at the same elevation as the load cell (see Figure 4-1).

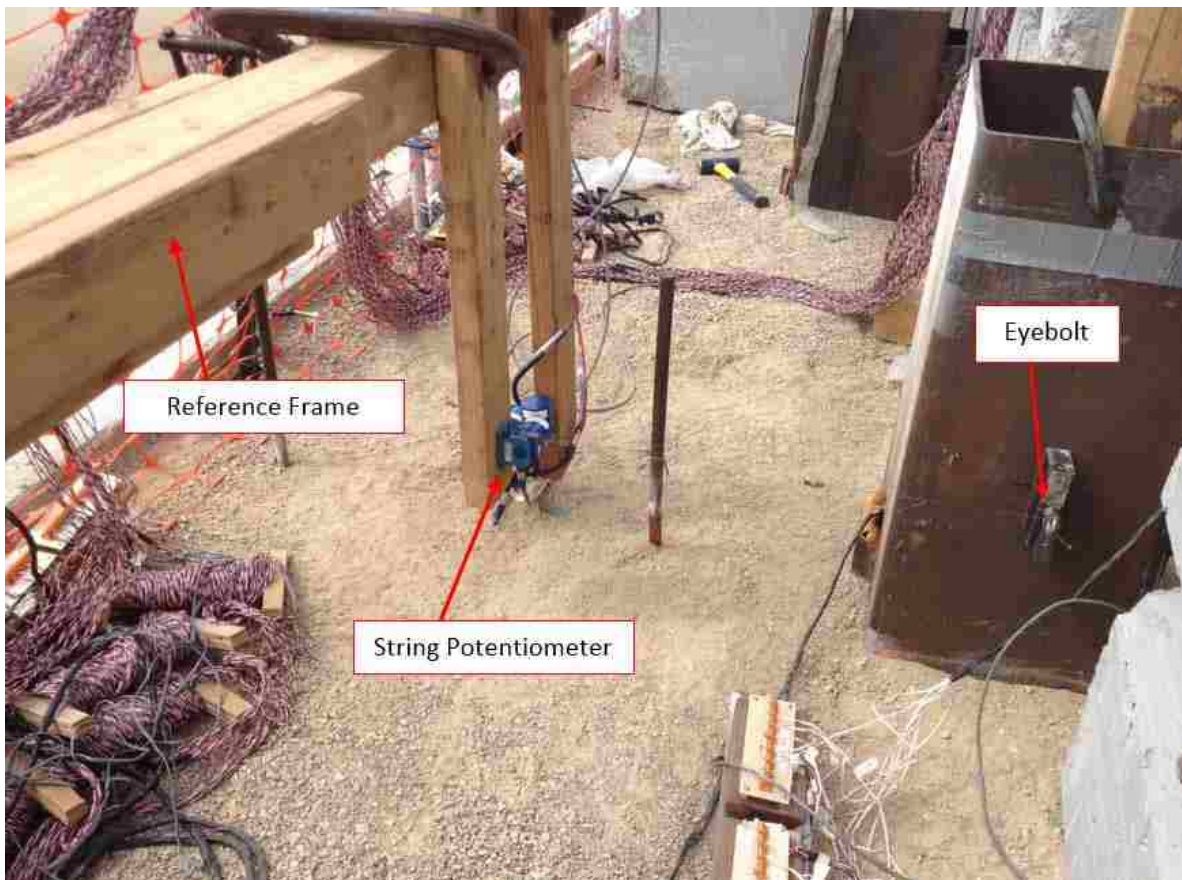


Figure 4-1. String potentiometers attached to a square pile at the load cell level.

To calculate the pile rotation, another string potentiometer had its line extended and attached to an eyebolt located 2 feet directly above the magnetic eyebolt and consequently 3 feet above the ground (see Figure 4-2). In this way, the difference between the two linear displacements

at each load increment could be taken to calculate the angle of pile rotation using the following equation:

$$\theta = \sin^{-1}\left(\frac{\delta_{3ft} - \delta_{lp}}{36in}\right) \quad (4-1)$$

where θ = pile head rotation (degrees)

δ_{3ft} = string potentiometer deflection at three feet above the load point (in.), and

δ_{lp} = string potentiometer deflection at the load point (in.).



Figure 4-2. String potentiometer attached three feet above the pile.

To record the ground displacements, steel stakes were driven into the ground at about 1 foot increments starting from the face of the pile towards the MSE wall. The strings of each of the string potentiometers were hooked onto the stakes horizontally as shown in Figure 4-3. Table 4-1 and Table 4-2 show the locations of all of the string potentiometers used for the H-piles and square piles, respectively.

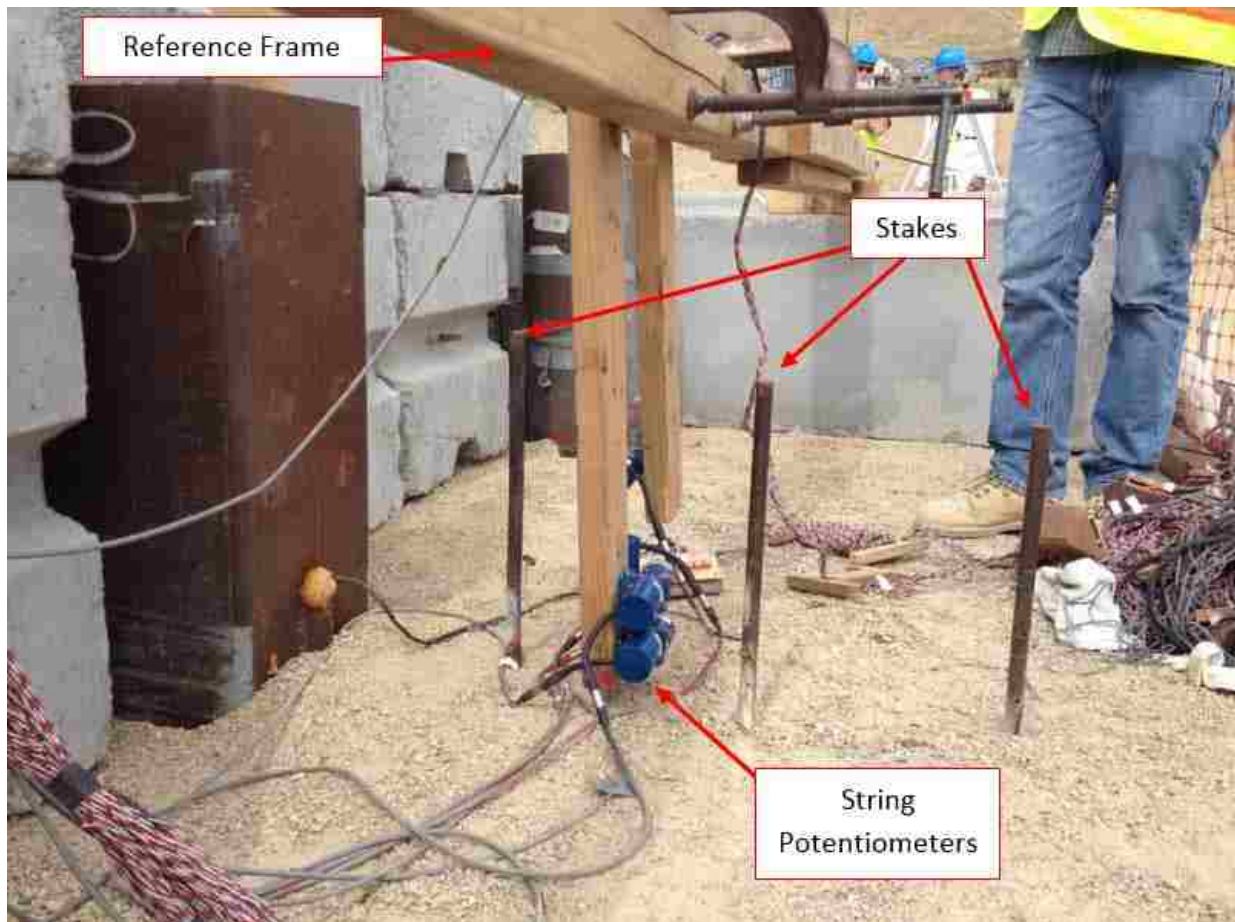


Figure 4-3. String potentiometers attached to stakes for horizontal ground displacement readings.

Table 4-1. H-pile String Potentiometer Locations

Test	Load Point	3ft Above Load Point	Top of Wall	1ft from Pile Face	2ft from Pile Face	3ft from Pile Face	4ft from Pile Face	Other
2.2D	SP36	SP35	SP34 (20.25" from pile face)	-	-	-	-	SP 39 (0.5ft)
2.5D	SP35	SP36	SP34 (24.25" from pile face)	-	-	-	-	SP37 (0.5ft), SP 39 (1.5ft)
3.2D	SP36	SP35	SP34 (32.5" from pile face)	SP37	SP39	-	-	-
4.5D	SP36	SP35	SP34 (49" from pile face)	SP40	SP37	SP39	-	-

Table 4-2. Square Pile String Potentiometer Locations

Test	Load Point	3ft Above Load Point	Top of Wall	1ft from Pile Face	2ft from Pile Face	3ft from Pile Face	4ft from Pile Face
2.1D	SP36	SP37	SP32 (19" from pile face)	SP38 (12.5" from pile face)	-	-	-
3.1D	SP36	SP37	SP38 (31.5" from pile face)	SP31	SP32	-	-
4.2D	SP36	SP37	SP34 (44.5" from pile face)	SP31	SP32	SP38	-
5.7D	SP36	SP37	SP35 (62.75" from pile face)	SP31	SP32	SP38	SP34

4.3 Strain Gauges

Both the soil reinforcement and the piles were instrumented with strain gauges to measure strain to be able to compute the bending moment for the piles, and the induced force in the reinforcements.

4.3.1 Soil Reinforcement Strain Gauges

Strain gauges were used to monitor the strain on the soil reinforcement. Strain gauges were applied to the top two layers of reinforcement for both the H-piles and square piles. The only exception was the 5.7D square pile where four layers were instrumented. This is because the third and fourth layers from the top of the 20-foot wall height were already instrumented from when the adjacent 5D pipe pile was tested at the 15-foot wall height (Hatch, 2016). Layer 1 started 15 inches from the top of the MSE wall. The soil reinforcements were spaced vertically at 30 inches for both the ribbed strip (H-piles) and welded wire (square piles) reinforcements, and thus Layer 2 was at 45 inches, Layer 3 was at 75 inches, and Layer 4 was at 105 inches from the top of the 20-foot wall height. (Layer 3 and Layer 4 only apply to the 5.7D square pile). The strain gauges were applied on the top and bottom of the reinforcement to account for bending effects. Strain gauge pairs were positioned at distances of 0.5, 2, 3, 5, 8, 11, and 14 feet from the back face of the MSE wall. The strain gauges were protected with epoxy coating to prevent water damage and the lead wires were protected with electrical tape. The wires ran along the reinforcement towards the wall and into a PVC pipe which extended to the ground surface against the wall. Generally, two reinforcements located at different transverse distances adjacent to each test pile at a given reinforcement level were instrumented. Table 4-3 shows which reinforcement ID applied to which H-piles as well as the location of the strain gauges on the reinforcement from the center of the test pile looking towards the back of the MSE wall. The location gives the direction and the spacing in inches. Table 4-4 shows the same, but for the square piles.

Table 4-3. H-pile Strain Gauge Locations

		H-Pile 2.2D	H-Pile 2.5D	H-Pile 3.2D	H-Pile 4.5D
Layer 1 (15 in. depth)	Strip #	7	7	4	4
	Location	Left 49.1"	Right 9.1"	Left 52.6"	Right 8.6"
	Strip #	8	8	3	3
	Location	Left 23.6"	Right 34.6"	Left 27.1"	Right 34.1"
Layer 2 (45 in. depth)	Strip #	15	15	11	11
	Location	Left 51.1"	Right 8.1"	Left 53.1"	Right 8.1"
	Strip #	14	14	16	16
	Location	Left 25.1"	Right 33.6"	Left 28.1"	Right 32.6"

Table 4-4. Square Pile Strain Gauge Locations

		Square 2.1D	Square 3.1D	Square 4.2D	Square 5.7D
Layer 1 (15 in. depth)	Welded Wire #	1	2	3	4
	Location	Left 37.5"	Left 44"	Left 47.5"	Left 38.5"
	Welded Wire #	2	3	4	5
	Location	Right 23.5"	Right 15.5"	Right 13"	Right 21.5"
Layer 2 (45 in. depth)	Welded Wire #	30	29	28	27
	Location	Left 37.5"	Left 37"	Left 39.5"	Left 31"
	Welded Wire #	29	28	27	26
	Location	Right 30"	Right 23.5"	Right 21"	Right 28.5"
Layer 3 (75 in. depth)	Welded Wire #				21
	Location	-	-	-	Right 27"
Layer 4 (105 in. depth)	Welded Wire #				17
	Location	-	-	-	Right 34.5"

4.3.2 Pile Strain Gauges

Water-proof electrical resistance type strain gauges also bonded with epoxy were instrumented along the length of the piles at various depths. The depths starting from the final backfill ground surface at the 20' level were 2, 4, 6, 9, 12, 15, and 18 feet for the square piles. The H-pile strain gauge depths reference the 15' level (Phase 1), and thus the depths of the strain gauges are 1, 4, 7, 10, and 13 feet. This is because no testing was done for the H-piles at the 20' level. The strain gauges were mounted along both the back and front pile faces in the direction of loading and were protected by L1-1/2X1-1/2X1/8 angle irons. The angle irons were also filled with expanding foam for further protection against possible water damage.

4.4 Shape Arrays

Measurand ShapeAccelArray (Shape Arrays) were used to measure the MSE wall deformation during lateral load testing. They are an array of rigid segments that measure tilt along three axes within those segments with microelectromechanical systems (MEMS) gravity sensors (i.e. accelerometers) (“Measurand ShapeAccelArray (SAA) Specifications”). The Shape Arrays were inserted vertically along the back face of the MSE wall into PVC pipes which would then measure wall displacements during lateral loading along the height of the wall. Table 4-5 shows the locations of the Shape Arrays in relation to the center of the pile looking towards the back of the wall.

Table 4-5. Location of Shape Arrays

Test Pile		Array Number			
		45134	45104	45115	45112
H-Piles	4.5D	53" right	6" right	93.5" right	25" right
	3.2D	11" left	87.5" right	29.5" right	56.5" right
	2.5D	94.5" right	56" right	31" right	0"
	2.2D	0"	25" left	56" left	83" left
Square Piles	5.7D	4" right	29.5" left	65.5" left	88" left
	4.2D	64" left	94" left	10" left	32.5" left
	3.1D	4" left	34" left	56" left	98" left
	2.1D	63.5" right	33.5" right	11.5" right	30.5" left

4.5 Digital Image Correlation (DIC)

Digital Image Correlation (DIC) was also used to measure the MSE wall displacement throughout load testing. DIC is an image analysis system that uses a 3D optical technique to measure displacement and strain over a surface (“Measurement Principles of (DIC)”). Two cameras at a fixed distance apart on a metal frame are set up on a tripod and calibrated at a distance of about 40 ft from the face of the MSE wall. The system is then focused on the MSE wall before lateral loading as shown in Figure 4-4 with a field of view that is about 10 ft high and 20 ft wide. The DIC system uses a computer algorithm to track the movement of thousands of points on the wall face. To facilitate this tracking procedure, the MSE wall was painted with a black and white grid to create more distinct points where the variation in the wall deformations could be obtained during the lateral load testing. The cameras would take baseline images immediately prior to testing and then at each load increment to determine the change in movement as the test progressed. See Sec. 3.3.1 for more information on the data acquisition.



Figure 4-4. DIC setup in front of the MSE wall.

4.6 Surveying

Measurements of ground surface heave and settlement before and after pile loading were performed using conventional surveying techniques. Surveying was performed using an automatic level on a tripod and a surveying rod with an accuracy of about 0.01 ft. Measurements of elevation were taken generally at the string potentiometer locations between the pile and the MSE wall.

5 LATERAL LOAD TESTING

Lateral load testing for the H-piles (Phase 1) occurred from July 10, 2014 through July 15, 2014 and testing for the square piles (Phase 2) occurred from August 12, 2014 through August 14, 2014. Using a displacement control approach, the hydraulic ram loaded each pile until it displaced at quarter-inch increments from 0.25 inches up until 3.0 inches. At each quarter-inch increment, the fluid flow into the jack was locked-off for five minutes, during which the load was allowed to relax and come into equilibrium with the displacement before applying load again to reach the next quarter-inch increment. Recordings were taken at one minute and five minutes after the peak load was reached at each increment. A recording was also taken at the initial 0.125-inch displacement for each test to better define the initial segment of the load-deflection curve.

5.1 Load Displacement Curves

5.1.1 H-Piles

The pile head load is plotted against the pile head deflections for all four H-piles in Figure 5-1, Figure 5-2, and Figure 5-3. The first figure shows the peak load versus deflection curve. The second and third figures show the average pile head load deflection curves for one-minute and five-minutes after the peak load. To smooth out noise in the data, load and deflection for the one- and five-minute hold plots are averages over a 30 second window. Appendix C shows the load versus deflection curves for the peak, one-minute, and five-minute intervals separated for each of

the H-piles. Two types of pile head load readings could be used; the load from the hydraulic pressure reading in the jack and the in-line load cell reading in the tie-rod. The hydraulic load readings were used for the H-piles because of lab tests which indicated some erratic behavior of the tie-rod load cells. Research from Russell (2016) and Bustamante (2014) involved reaction piles tested as a part of a companion study to this project. The reaction pile curve in the figures mentioned above is the average of H-pile reaction piles loaded parallel to the wall tested prior to loading transverse to the wall. This curve was added as a reference. The farthest H-pile (4.5D) is about 78.9% of this curve.

The average one-minute data was chosen as the basis for most results in this chapter. At this point, the pile head load has generally come into static equilibrium after pushing the pile to the desired displacement. The peak load versus displacement curves in Figure 5-1 show how erratic the load can be immediately after the push. However, after one-minute the load had stabilized. There is a decrease of an average of 21.9% from the peak load to the one-minute load, but only an average of 3.2% decrease from the one-minute to five-minute hold.

In all cases, the load-deflection curve for the “reaction pile” located behind the reinforced soil zone was significantly higher than for the four piles near the MSE wall. This difference is likely a result of the difference in relative compaction as described previously in Chapter 3. The average relative compaction for both Phase 1 and Phase 2 near the reaction piles was 96.6%, while the relative compaction between the test piles and the wall averaged at 91.8%. As explained previously, the lower relative compaction near the MSE wall face is typical of real construction practice where only plate compactors are used near the wall face, while roller compactors are used away from the wall. Generally, the results are consistent with previous data; that the closer the pile is to the MSE wall, then the lower the load is for a given deflection. The exception here is the 2.2D

H-pile which is closer to the wall, but which resists more load than the 2.5D H-pile. One possible explanation for this discrepancy is that soil compaction might have been higher for the 2.2D pile. As explained previously, variation in relative compaction was much greater near the wall face as a result of the compaction procedure. The last three data points for H-pile 2.5D and the last two data points for H-pile 2.2D are omitted owing to inaccurate results. To provide a more quantitative indication of the decrease in resistance of the H-piles as they are placed closer to the wall, the loads at the 2.0 inch displacement were compared for most results.

The average decrease in lateral resistance from the 4.5D to the 2.5D H-pile is 27.4%. The average decrease in lateral resistance from the 4.5D to the closest H-pile to the wall (2.2D) is 19.4%. Of course, the decrease in lateral soil resistance is actually greater than this percentage because part of the lateral pile resistance is provided by the flexural stiffness of the pile which remains constant and is not affected by the presence of the wall.

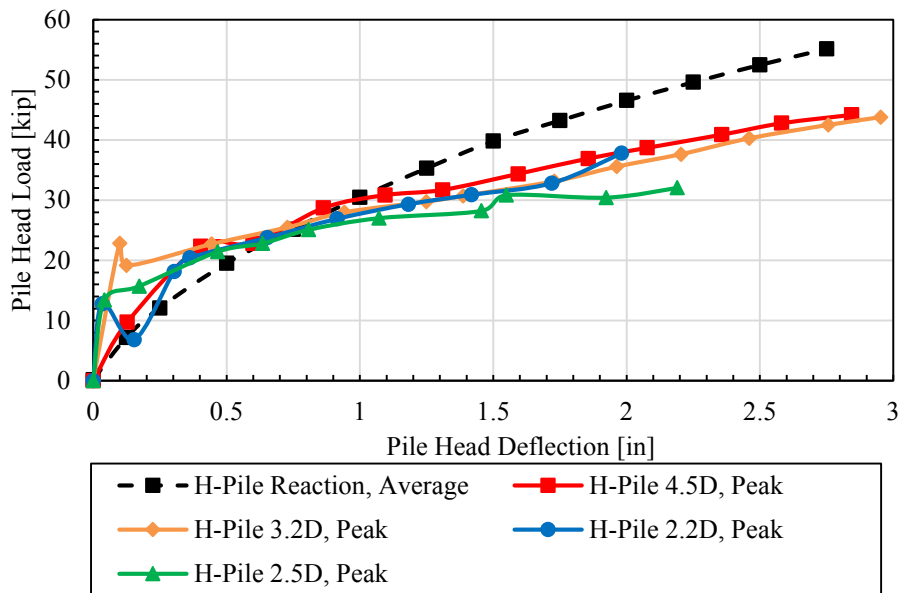


Figure 5-1. Pile head load versus deflection curves for H-piles at peak.

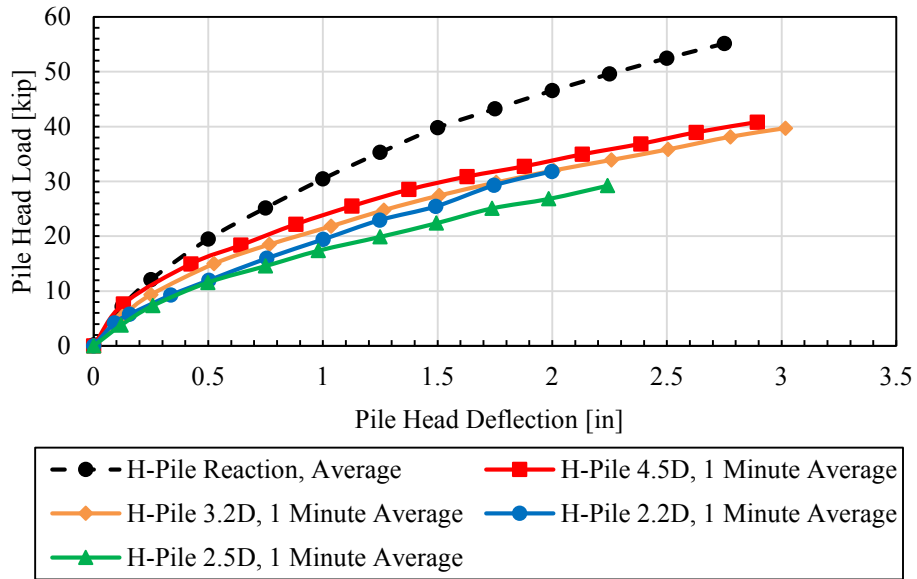


Figure 5-2. Pile head load versus deflection curves for H-piles at one-minute average.

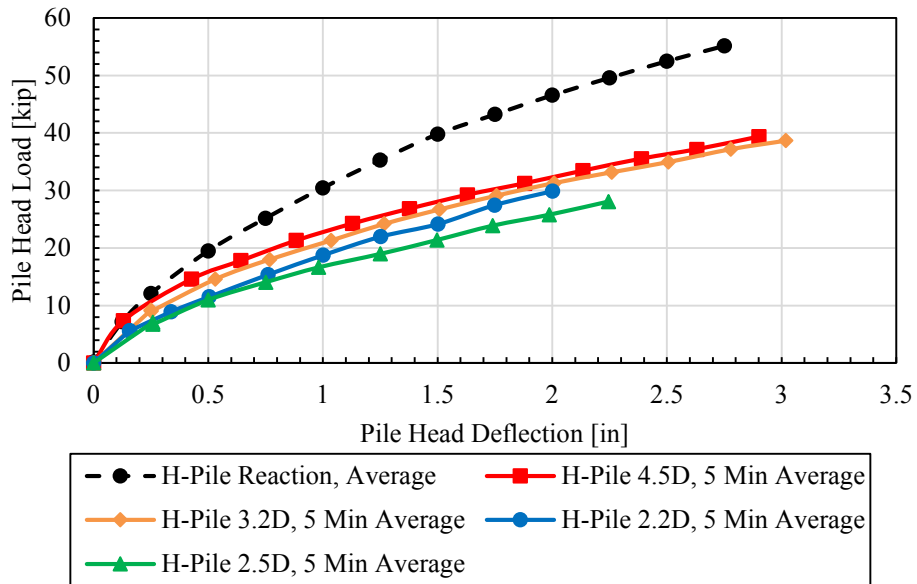


Figure 5-3. Pile head load versus deflection curves for H-piles at five-minute average.

The pile head rotation was also calculated as a function of pile head load. Section 4.2 describes how the string potentiometers were used to measure the displacement of the pile to calculate rotation. Pile head rotation (θ) in degrees was computed using the equation:

$$\theta = \sin^{-1}\left(\frac{\delta_{3ft} - \delta_{lp}}{36in}\right) \quad (5-1)$$

where θ = pile head rotation, degrees

δ_{3ft} = string potentiometer deflection at three feet above the load point, in.

δ_{lp} = string potentiometer deflection at the load point, in.

Figure 5-4 shows the pile head load versus the pile head rotation. The reaction H-pile curve is also included from Russell (2016). The other H-pile from Bustamante (2014) that was used for the load versus deflection curves was not included for an average due to the unavailability of the data.

Generally, the H-pile rotations increase for a given load as the piles move closer to the wall with the exception of the 2.2D H-pile. This is consistent with the behavior observed from the load-deflection curve. This shows that an H-pile seems to be more resistant to pile rotation as the pile is placed farther away from the MSE wall face.

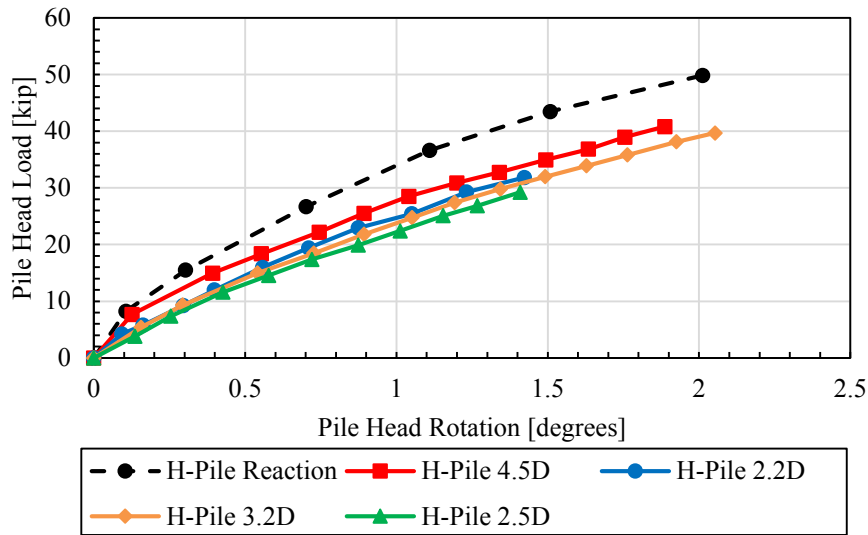


Figure 5-4. Pile head load versus pile head rotation for all H-piles and the H-pile reaction pile.

5.1.2 Square Piles

The pile head load plotted against the pile head deflections of all four square piles are shown in Figure 5-5, Figure 5-6, and Figure 5-7. The first figure shows the peak load versus deflection curve. The second and third figures show the average pile head load deflection curves for one-minute and five-minutes after the peak load. To smooth out noise in the data, load and deflection for the one- and five-minute hold plots are averages over a 30 second window. Appendix C shows the load versus deflection curves for the peak, one-minute, and five-minute interval separated for each of square pile. Two types of pile head load readings could be used; the load from the hydraulic pressure reading in the jack and the in-line load cell reading in the tie-rod. The in-line load cell readings were used in this case because of the erratic behavior of the hydraulic jack. The reaction pile curve in the figures mentioned above is the average of the square reaction piles loaded parallel to the wall tested prior to loading transverse to the wall from Bustamante

(2014). This curve was added as a reference. The farthest square pile (5.7D) is about 73.3% of this curve.

As stated for the H-piles, the average one-minute data was chosen as the basis for the square piles for most results in this chapter. Typically, there is a decrease of an average of 5.7% from the peak load to the one-minute load, and an average of 1.9% decrease from the one-minute to five-minute hold. In all cases, the load-deflection curve for the “reaction pile” located behind the reinforced soil zone was significantly higher than for the four piles near the MSE wall, as was the case for the H-piles. Generally, the results are consistent with previous data; that the closer the pile is to the MSE wall, then the lower the load is for a given deflection. The average decrease in lateral resistance from the 5.7D to the 2.1D square pile is 33.8%.

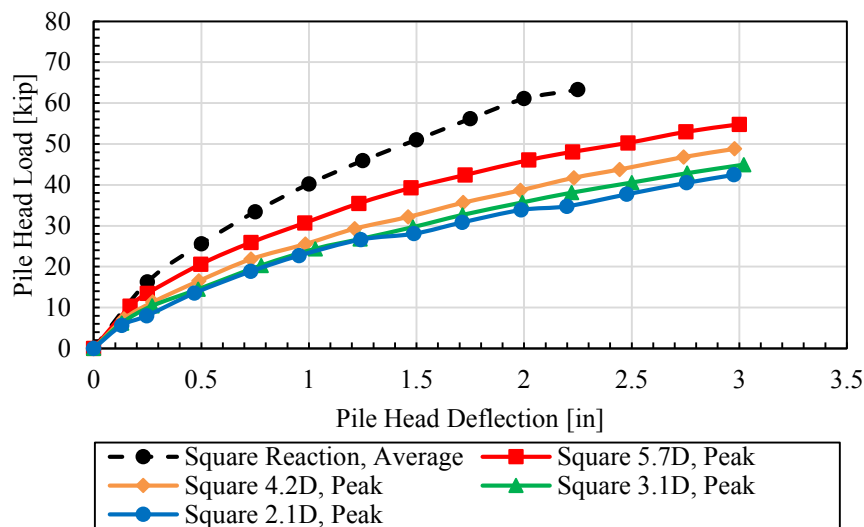


Figure 5-5. Pile head load versus deflection curves for square piles at peak.

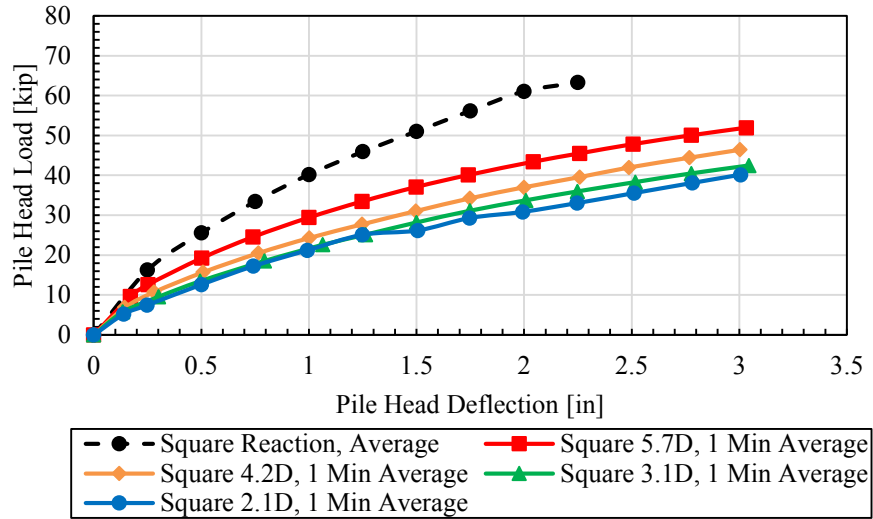


Figure 5-6. Pile head load versus deflection curves for square piles at one-minute average.

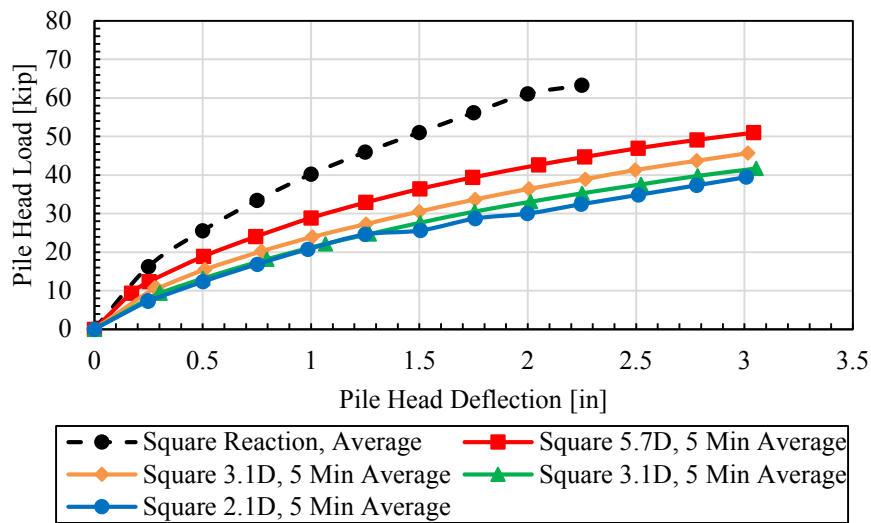


Figure 5-7. Pile head load versus deflection curves for square piles at five-minute average.

Figure 5-8 shows the pile head load versus the pile head rotation. The square pile reaction curve is not included owing to the unavailability of the data from Bustamante (2014). The equation used is the same as Equation (5-1). As expected, the closer the square pile gets to the wall, the

more rotation there is for a given load. This shows that the closer piles are less capable of resisting the load and thus the rotation increases.

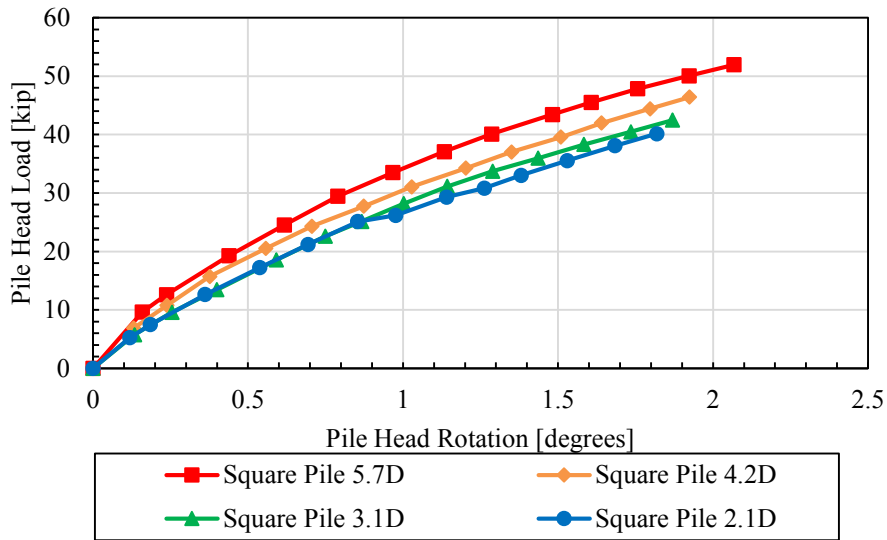


Figure 5-8. Pile head load versus pile head rotation for all square piles and the square reaction pile.

5.2 Soil Reinforcement Performance

5.2.1 H-Piles

The tensile force in the soil reinforcement was calculated with the data recorded from the strain gauges. As explained in section 4.3.1, the reinforcement was instrumented with strain gauges on both the top and bottom, and thus each location along the length of the reinforcement specified in 4.3.1 had two strain gauges. The average strain reading was then used to calculate the induced force in the reinforcement at various distances from the back face of the MSE wall. At times, the strain gauges were damaged or failed to give accurate readings. When this would happen, an average strain could not be determined and the strain was based on only one value. When both the

top and bottom strain gauges were damaged, then the whole reinforcement force was deleted for that given location. The average strain was actually given in micro-strain and thus needed to be multiplied by 10^{-6} to be obtain pure strain. The induced force in the soil reinforcement was calculated by the following equation:

$$T = EA \left(\frac{\mu\varepsilon_t + \mu\varepsilon_b}{n} \right) (10^{-6}) \quad (5-2)$$

where T = induced reinforcement load at a particular location of a given reinforcement strip (kip)

E = modulus of elasticity (2,900 ksi)

A = cross-sectional area of reinforcement (0.31 in² for ribbed strips)

$n = 2$ when neither strain reading was omitted, or 1 when one strain reading was omitted

$\mu\varepsilon_t$ = micro strain of the top strain gauge, and

$\mu\varepsilon_b$ = micro strain of the bottom strain gauge.

Due to the strain gauges being installed with the wrong side of the waterproof wafer against the pile, all of the soil reinforcement values were multiplied by a factor to obtain the correct value. Strain gauges were laboratory tested and it was concluded that the incorrect installation underestimated the correct soil reinforcement force by a factor of 1.7.

The reinforcement force for distances of 0.5 feet to 14 feet from the back face of the MSE wall was calculated for every load increment. Table 4-3 shows which ribbed strips were used for each of the H-piles for the top two layers and their locations. Figure 5-9 shows the reinforcement force versus distance from the back face of the MSE wall for one of the instrumented ribbed strips.

Using the FHWA equations (Equation 2-8) (Berg et al., 2009), the ultimate pullout resistance for ribbed strips is also plotted as an additional reference. (See Appendix A for the capacity to demand ratio against pullout calculations for the ribbed strip reinforcement).

Figure 5-9 is representative of how the induced reinforcement force developed along the length of the reinforcement. It shows curves for selected load increments corresponding to approximately the 0.5-, 1-, 2-, and 3-inch pile head deflection. Obviously, the higher deflection meant a higher induced load, and thus the induced reinforcement loads increase as the deflections increase. For many of the H-piles (see Appendix D for all strain gauge data relating to reinforcement load versus distance from back face of the MSE wall for the H-piles) the maximum reinforcement load developed near the pile or within approximately 2 feet behind the center of the pile. The induced force gradually increased from the back wall face up until the maximum force. After the maximum induced force, the load began to taper off to zero by the end of the reinforcement length (18 feet from the MSE wall). Also, the figure shows that higher induced forces developed for the higher pile head loads. As the applied pile load increased, the force in the reinforcements began to approach the line defining the pull-out resistance defined by the FHWA equation. The FHWA equation assumes that tensile force remains constant within $0.3H$ (or about 5.9 feet for the 15-foot wall height) behind the wall face for a wall without pile load. However, in this case, the force is actually decreasing towards the wall face. If the FHWA pull-out resistance were extrapolated to the wall face, the maximum tensile force would be about 8.6 kips. Theoretically, the induced load on the pile along any part of the soil reinforcement for any of the recorded deflection should be below the FHWA line which represents the pullout capacity of the soil reinforcement.

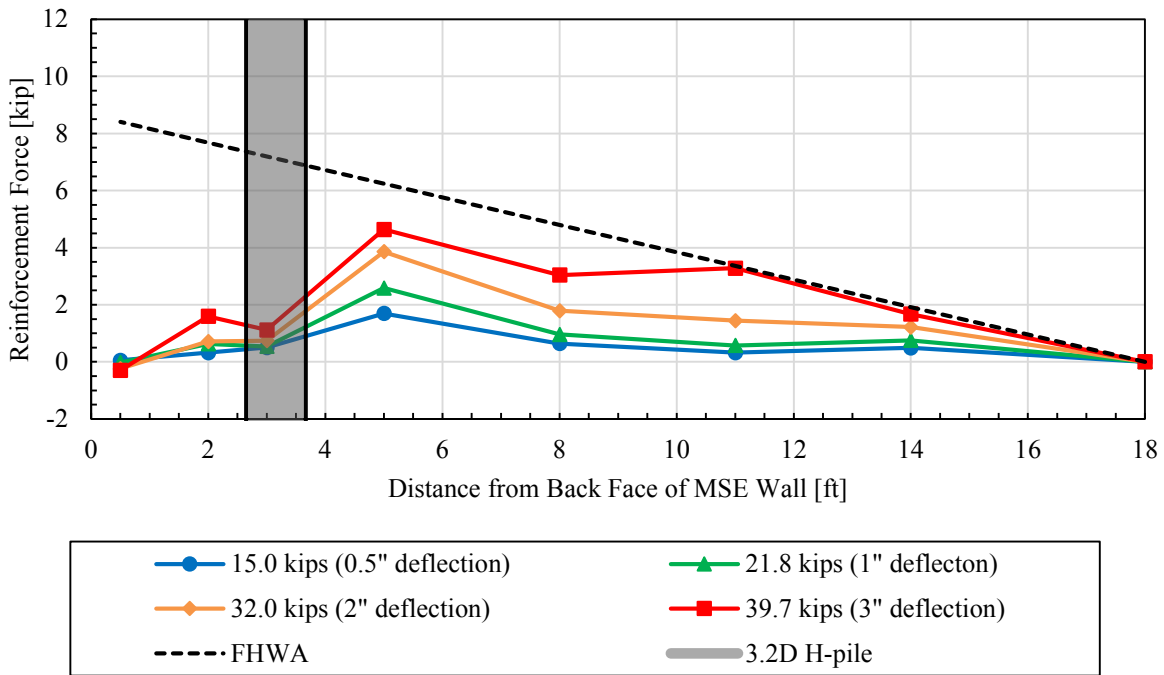


Figure 5-9. Reinforcement force versus distance from back face of MSE wall (H-pile 3.2D, 15-inch depth, strip #4, transverse spacing 52.6 inches).

Figure 5-10 shows a schematic diagram which may help explain the distribution of force in the reinforcement. In front of the pile, the soil moves left relative to the reinforcement which creates a friction force on the reinforcement that increases the tensile force in the reinforcement. Behind the pile, the reinforcement moves to the left relative to the soil as it resists pullout. Therefore, the skin friction on the reinforcement develops in the opposite direction (to the right) which decreases the tensile force in the reinforcement. From both sides of the pile, the induced load increases as the reinforcement approaches the pile. There may be some load at the back face of the MSE wall probably due to the earth pressure on the wall.

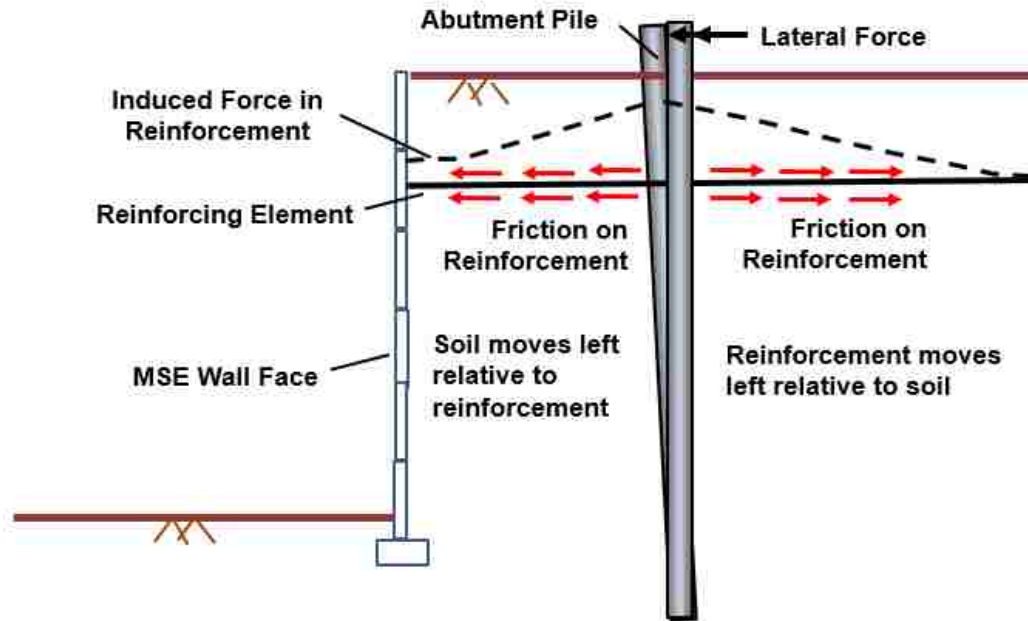


Figure 5-10. Interaction between MSE wall, soil, and reinforcement.

Figure 5-11, Figure 5-12, Figure 5-13, and Figure 5-14 show the relationship for the maximum induced reinforcement forces versus the pile head load for each pile. (Appendix G shows the relationship for the maximum induced reinforcement forces versus the pile head displacement for each H-pile). For each H-pile, the top two layers at depths of 15” and 45” were instrumented and measured, and they correspond with Layer 3 and Layer 4, respectively, as explained in Chapter 4. For each test pile, reinforcement forces in two different ribbed strips for each layer were determined from the strain gauges. Two lines in the figures are dashed to represent the farther strain gauge from the center of the pile of interest, and two other lines are solid to represent the closer strain gauge from the center of the pile. Black lines represent 15” below the ground surface, and gray lines represent 45” below the ground surface. The location from the back face of the MSE wall is shown to indicate where along the reinforcement length was the maximum induced force.

Generally, the maximum reinforcement forces occur within five feet from the wall. For the 4.5D and 3.2D H-piles, the greater induced forces occurred at the 15” depth, showing that the reinforcement force is affected by vertical stress. The shallower the depth of the reinforcement develops more induced tensile force. However, this was not the case for the 2.5D and 2.2D H-piles. For each level of each H-pile tested (with the exception of the 3.2D H-pile at the 15” depth), a higher induced force was developed for the “near” reinforcement as opposed to the “far” reinforcement of the same level. Thus, the closer in proximity the reinforcement is to the pile, then a higher induced force will be present.

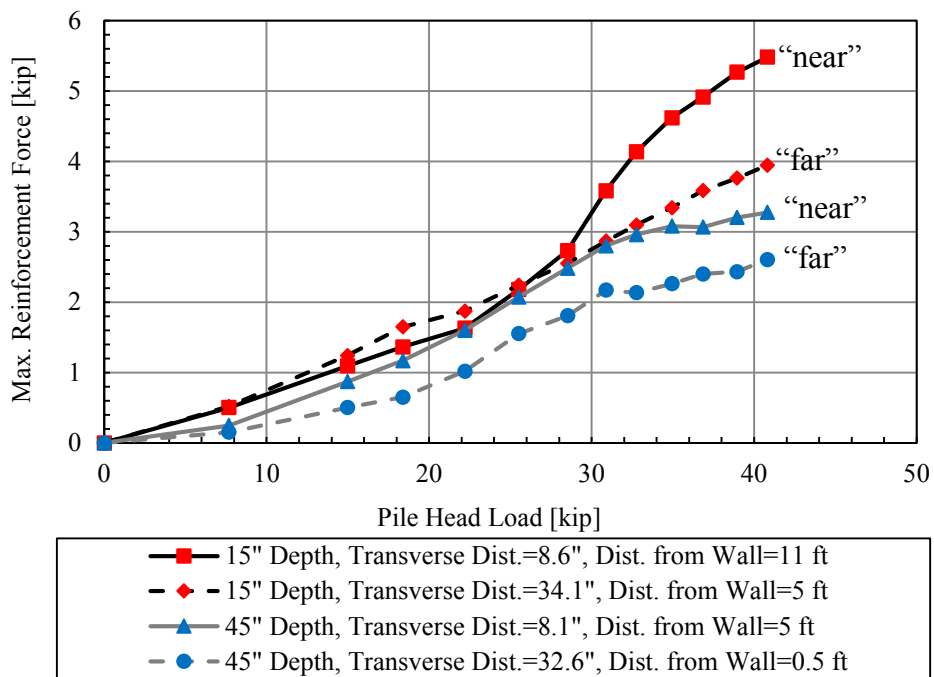


Figure 5-11. Maximum reinforcement force for each instrumented ribbed strip versus pile head load for H-pile 4.5D.

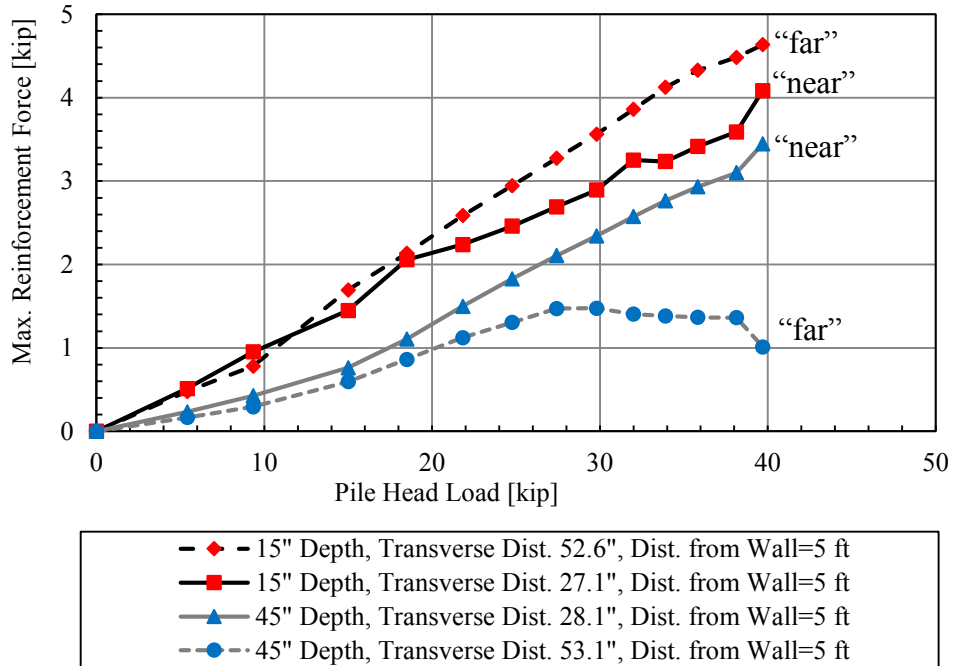


Figure 5-12. Maximum reinforcement force for each instrumented ribbed strip versus pile head load for H-pile 3.2D.

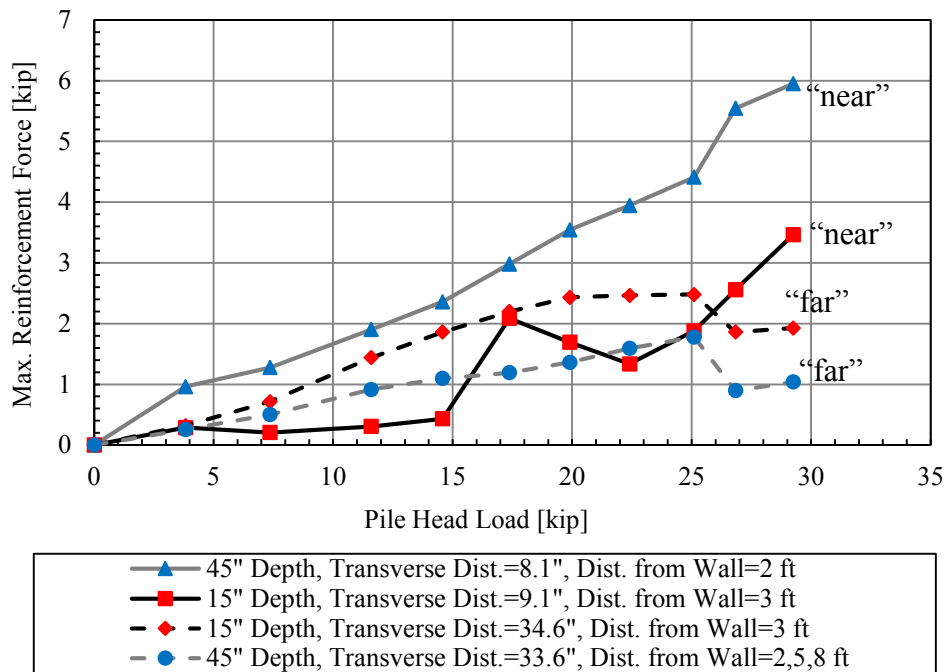


Figure 5-13. Maximum reinforcement force for each instrumented ribbed strip versus pile head load for H-pile 2.5D.

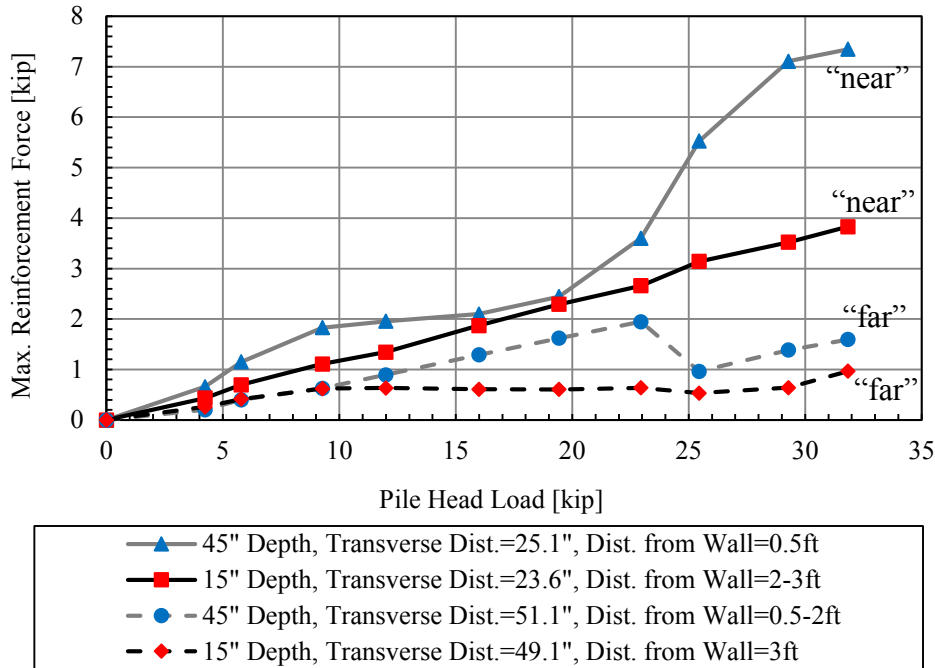


Figure 5-14. Maximum reinforcement force for each instrumented ribbed strip versus pile head load for H-pile 2.2D.

5.2.2 Square Piles

The tensile force for the square piles was calculated using a similar equation for the H-piles. Since the induced load is for the whole wire grid, the equation below is also multiplied by the number of tributary areas, which is one less than the number of longitudinal bars. The tributary areas for the end wires do not extend beyond the width of the grid, because obviously the transverse wires do not extend beyond the width of the grid. The induced load on the soil reinforcement was calculated as follows:

$$T = EA \left(\frac{\mu \varepsilon_t + \mu \varepsilon_b}{n} \right) (10^{-6}) (B - 1) \tag{5-3}$$

where T = induced reinforcement load at a particular location of a given reinforcement grid (kip)

E = modulus of elasticity (2,900 ksi)

A = cross-sectional area of one longitudinal welded wire (0.11 in²)

n = 2 when neither strain reading was omitted, or 1 when one strain reading was omitted

$\mu\epsilon_t$ = micro strain of the top strain gauge

$\mu\epsilon_b$ = micro strain of the bottom strain gauge, and

B = number of longitudinal wires of the grid.

Table 4-4 shows which welded wire reinforcement was used for each of the square piles for Layers 1 through 4 and their locations. Layer 1 is referenced at the top of the 20-foot wall height. Figure 5-15 shows the reinforcement force versus distance from the back face of the MSE wall for one of the instrumented welded wire reinforcements. It is a representative plot and shows curves for selected load increments corresponding to approximately the 0.5-, 1-, 2-, and 3-inch pile head deflection. Appendix D shows all strain gauge data relating to reinforcement load versus distance from the back face of MSE wall for the square piles. The ultimate pullout resistance for welded wire reinforcement is also plotted as an addition reference (as it was for the ribbed strips for the H-piles). (See Appendix A for the capacity to demand ratio against pullout calculations for the welded wire reinforcement). The shape of the curves in Figure 5-15 is similar to the H-piles and the idealized schematic diagram of Figure 5-10, except that the maximum reinforcement force occurs closer to the pile center. The induced force gradually increased from the back wall face up until the maximum force. After the maximum induced force, the load began to taper off to zero by the end of the reinforcement length. The FHWA equation assumes that tensile force remains constant within 0.3H (or about 7.4 ft for the 20-foot wall height) behind the wall face for a wall without pile load. The load decreases towards the wall face, but it does not decrease to 0 kips. If

the FHWA pull-out resistance were extrapolated to the wall face, the maximum tensile force would be about 110 kips.

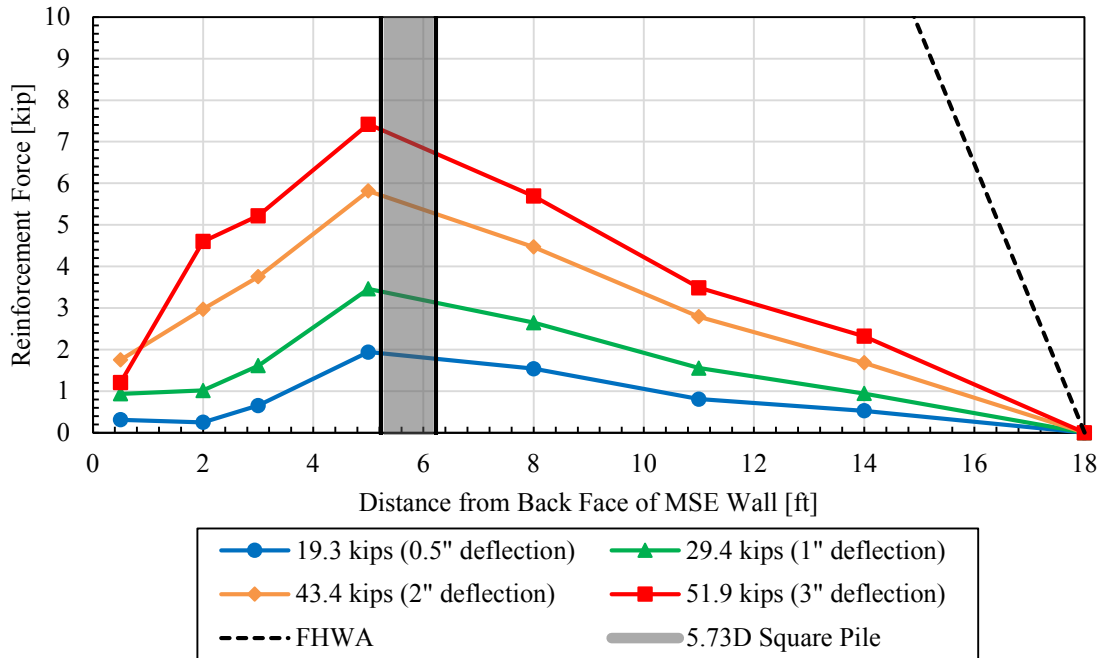


Figure 5-15. Reinforcement force versus distance from back face of MSE wall (square pile 5.7D, 45-inch depth, welded wire #26, transverse spacing 28.5 inches).

Figure 5-16, Figure 5-17, Figure 5-18, and Figure 5-19 show the relationship for the maximum induced reinforcement forces versus the pile head load for each pile. (Appendix G shows the relationship for the maximum induced reinforcement forces versus the pile head displacement for each square pile). For each square, the top two layers at depths of 15” and 45” were instrumented and measured, in addition to two more layers at depths of 75” and 105” for the 5.7D square pile, as explained in Chapter 4. For each test pile, reinforcement forces in two different welded wires (second from the right looking towards the front of the wall) for each layer were determined from the strain gauges. Generally, two lines in the figures are dashed to represent the

farther strain gauge from the center of the pile of interest, and two other lines are solid to represent the closer strain gauge from the center of the pile. Black lines represent the 15” below the ground surface, and gray lines represent 45” below the ground surface. The location from the back face of the MSE wall is shown to indicate where along the reinforcement length was the maximum induced force.

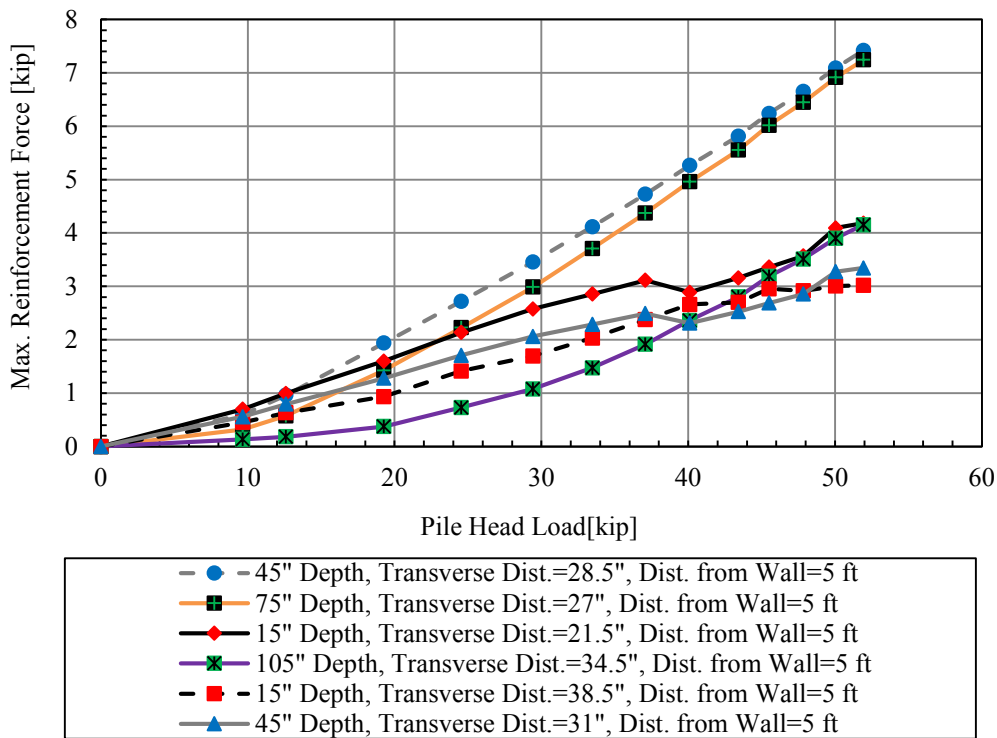


Figure 5-16. Maximum reinforcement force for each instrumented welded wire versus pile head load for square pile 5.7D.

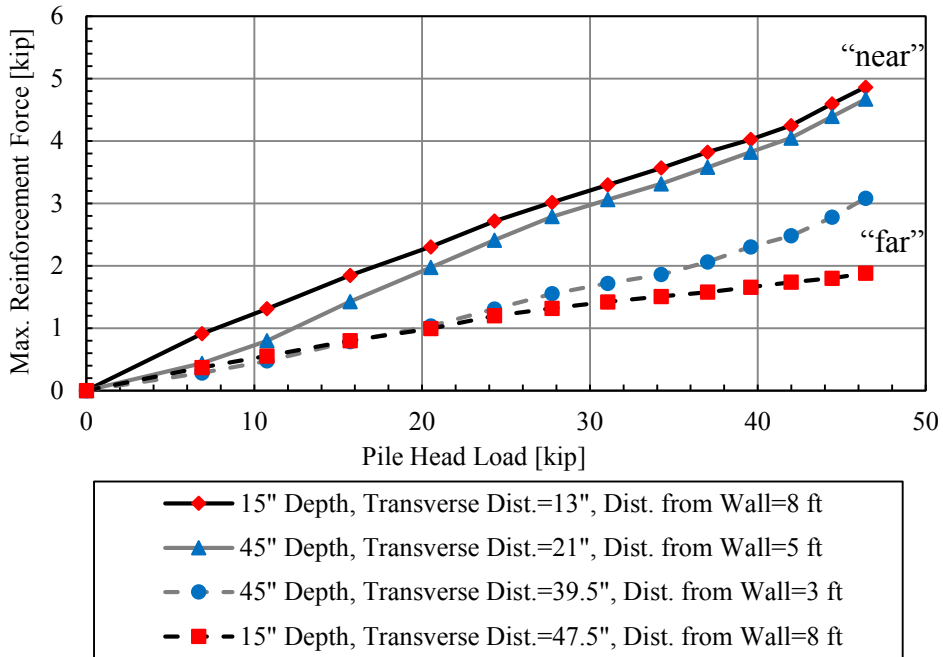


Figure 5-17. Maximum reinforcement force for each instrumented welded wire versus pile head load for square pile 4.2D.

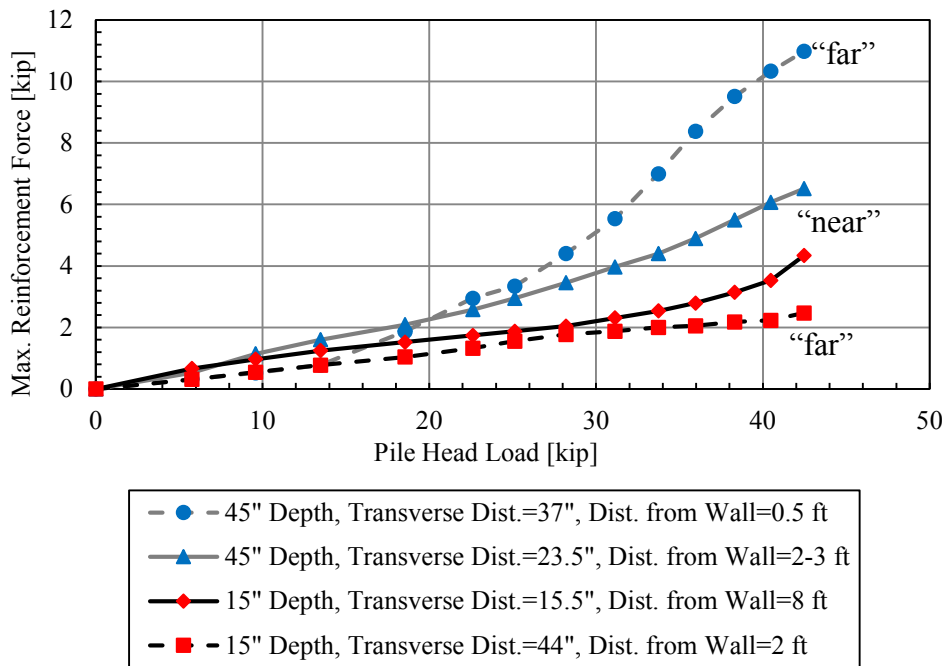


Figure 5-18. Maximum reinforcement force for each instrumented welded wire versus pile head load for square pile 3.1D.

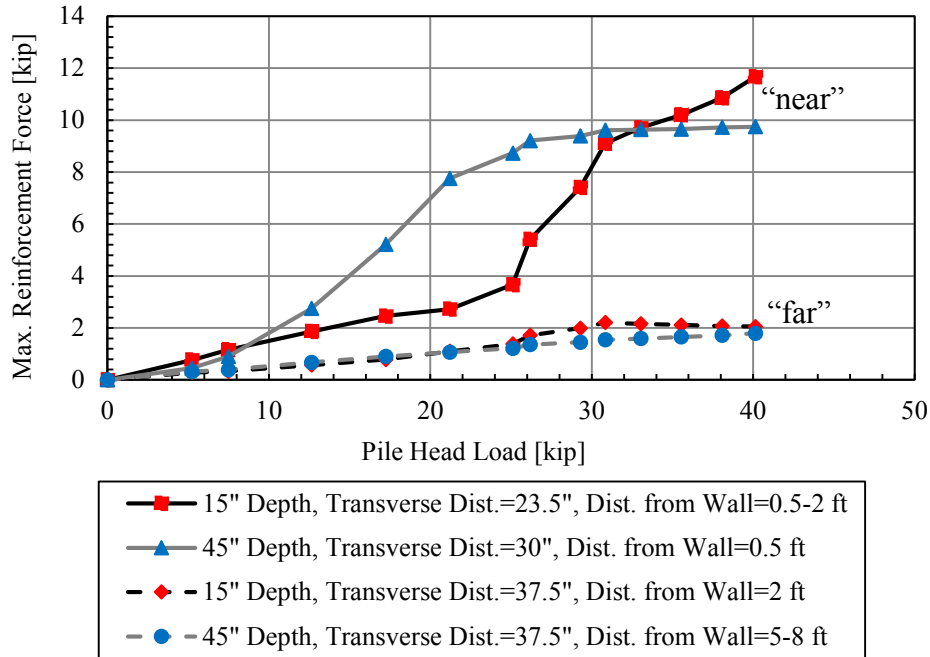


Figure 5-19. Maximum reinforcement force for each instrumented welded wire versus pile head load for square pile 2.1D.

Figure 5-16 does not seem to have a pattern as to whether or not the increased vertical stress reduces the induced reinforcement force. However, the maximum force occurs at 5 feet from the wall face for each of the six instrumented reinforcement. The other figures have the majority of the maximum reinforcement force occur anywhere from 0.5 feet to 5 feet behind the wall, with the exception of a few of the forces that occur 8 feet behind the wall. It is interesting to note that the maximum forces are unusually large for where the maximum forces occur about 0.5 feet from the wall. However, this only happens for the 3.1D and 2.1D square piles. The close proximity of these piles to the wall might interfere with the induced force readings from the strain gauges. These maximum induced forces occurring in front of the piles are in agreement with most of the other strain gauge reinforcement data presented in both the H-piles and square piles.

5.3 Statistical Analysis of Load in the Reinforcement

5.3.1 Ribbed Strip Soil Reinforcement

The load developed in an MSE wall reinforcement during lateral pile loading is a complex soil-structure interaction problem. This problem involves soil-pile, soil-reinforcement, pile-reinforcement, soil-wall, and wall-reinforcement interactions. Owing to this complexity, there are no equations in literature to guide engineers in estimating the maximum tensile force that would be induced on the reinforcement when a pile is loaded laterally. On some projects, finite element analyses are performed to estimate these forces; however, these analyses have not been calibrated to field performance and their accuracy is uncertain. To investigate the factors influencing the maximum tensile force in MSE reinforcements during lateral pile loading and to develop an equation to predict these forces, a statistical analysis was performed with the assistance of Dr. Dennis L. Eggett of the Department of Statistics at Brigham Young University (BYU). As shown in Section 5.2, strain in the reinforcements was measured and then the maximum tensile force was calculated for those reinforcements which were instrumented with strain gauges. The data set used in this analysis specifically consisted of forces measured in ribbed strip reinforcements in this study (the H-pile tests), along with forces measured by Besendorfer (2015), Han (2014), and Nelson (2013) for pipe piles. Because the data appeared to be log-normally distributed, the common logarithm of the tensile force was the dependent variable. A numerical value of +1 was also applied to all of the tensile force values so that the application of the common logarithm could be possible when the force equaled zero. A total of 942 data observations were used for this analysis. Initially a wide range of possible independent variables were evaluated to examine their statistical significance in predicting the maximum force. Two-way interactions for inclusion in an

equation were also checked for significance using the General Linear Model (GLM) procedure in the Statistical Analysis System (SAS) software program performed by Dr. Eggett.

Based on this statistical analysis, the primary independent values having statistical significance were the pile load, the transverse distance normalized by the pile diameter, the vertical stress, the pile spacing normalized by the pile diameter, and the reinforcement length to the total wall height (including the equivalent surcharge height) ratio. Depth and surcharge were not included as independent variables because they are both incorporated within the vertical stress. The values for pile load and maximum tensile force were based on the measurements for the one-minute hold for each load increment. The transverse distance was measured from the pile center to the strain gauge on the reinforcement of interest. The spacing of the piles was measured from the pile center to the back face of the MSE wall.

Table 5-1 shows the results from the statistical analysis of the main variables along with the most significant combination of any two variables. These variables are the terms in the equation created to predict the maximum tensile force in the reinforcement. The table also shows the coefficient estimates, the standard errors, the t-values, and the p-values. A review of Table 5-1 indicates that there are a number of parameters where the p-value is less than 0.01 indicating the statistical significance of the variable in the regression equation. Table 5-2 shows each term that was subsequently eliminated from the original equation obtained from Dr. Eggett. The combined term with the highest P-value was removed first, unless one of the main variables was higher and had no other combination left in the equation. The table also shows the R^2 and adjusted R^2 values and by how much they decrease with each term that is eliminated. The last term to remain (not included in the table) was the pile load, P. To simplify the regression equation, the first three terms in Table 5-2 were removed which simplified the resulting equation without significantly lowering

the R^2 value. The equation could be made simpler by eliminating more terms; however, the R^2 would start decreasing more rapidly. The final R^2 value was 76.2% and the adjusted R^2 value was 76.0%. The R^2 values are according to the common logarithm being applied to the data. This indicates that approximately 76% of the variation in the measured maximum tensile force is explained by the variables in the equation. The standard error value was 0.129. Table 5-3 shows the Analysis of Variance (ANOVA) output. The confidence interval used was 95% and Table 5-4 shows those values with their respective parameters. (See Appendix E for the statistical analysis on the same data minus the H-piles data. This represents all of the data for the ribbed strip reinforcement for pipe piles only).

Table 5-1. Statistical Analysis of Ribbed Strip Reinforcement

Parameter	Coefficients	Standard Error	t Stat	P-value
Intercept	-4.6093988330	0.39008	-11.81659	<0.00001
Pile Load, P	0.0277300731	0.00104	26.73446	<0.00001
Normalized Transverse Distance, T/D	-0.0090185405	0.00623	-1.44678	0.14830
Vertical Stress, σ_v	0.0031963922	0.00030	10.63629	<0.00001
Normalized Spacing, S/D	-0.0350237573	0.00364	-9.61879	<0.00001
Length to Height Ratio, L/H	7.1734028012	0.67238	10.66870	<0.00001
(L/H) ²	-2.7621763827	0.30443	-9.07322	<0.00001
$\sigma_v \cdot (L/H)$	-0.0022441570	0.00022	-10.31877	<0.00001
σ_v^2	-0.0000005846	<0.00001	-9.09627	<0.00001
P*(T/D)	-0.0020735059	0.00022	-9.48349	<0.00001
P ²	-0.0002019493	0.00002	-12.04534	<0.00001

Table 5-2. Term Elimination with the Change of R² and Adjusted R² for Ribbed Strip Reinforcement

Term Removed	Adjusted R²	Decrease in Adjusted R²	R²	Decrease in R²
None	77.16%	None	77.47%	None
P*(S/D) ⁺	77.01%	0.15%	77.30%	0.17%
P*(L/H) ⁺	76.82%	0.19%	77.09%	0.21%
(S/D)*(L/H) ⁺	75.99%	0.83%	76.24%	0.85%
(L/H) ²	73.89%	2.10%	74.14%	2.10%
σ_v *(L/H)	72.94%	0.95%	73.17%	0.97%
σ_v^2	72.21%	0.73%	72.41%	0.75%
σ_v	71.31%	0.90%	71.49%	0.92%
L/H	71.08%	0.23%	71.23%	0.26%
S/D	69.05%	2.03%	69.18%	2.05%
P*(T/D)	66.91%	2.14%	67.01%	2.17%
P ²	62.41%	4.50%	62.49%	4.52%
T/D	52.52%	9.89%	52.57%	9.92%

⁺Terms removed for the regression equation.

Table 5-3. ANOVA for Ribbed Strip Reinforcement

	Degrees of Freedom	Sum-of-Squares	Mean Squares	F Ratio	Significance F
Regression	10	49.80086	4.98009	298.75180	<0.00001
Residual	931	15.51944	0.01667		
Total	941	65.32030			

Table 5-4. Confidence Interval Values for Ribbed Strip Reinforcement

Parameter	Lower 95%	Upper 95%
Intercept	-5.37493	-3.84386
Pile Load, P	0.02569	0.02977
Normalized Transverse Distance, T/D	-0.02125	0.00321
Vertical Stress, σ_v	0.00261	0.00379
Normalized Spacing, S/D	-0.04217	-0.02788
Length to Height Ratio, L/H	5.85385	8.49296
$(L/H)^2$	-3.35963	-2.16472
$\sigma_v * (L/H)$	-0.00267	-0.00182
σ_v^2	<0.00001	<0.00001
P*(T/D)	-0.00250	-0.00164
P ²	-0.00023	-0.00017

The number of significant figures for the regression equation was reduced to two for every coefficient, but the R² value remained nearly the same at 75.9%. Applying the parameters and the coefficients from Table 5-1, the equation for the maximum tensile force was found to be:

$$\begin{aligned}
 F = 10^{(-4.6 + 0.028P - 2.0 \times 10^{-4} P^2 - 0.0090 \frac{T}{D} - 0.0021P \frac{T}{D} + 0.0032\sigma_v} \\
 - 5.8 \times 10^{-7} \sigma_v^2 + 7.2 \frac{L}{H} - 2.8 \left(\frac{L}{H} \right)^2 - 0.0022\sigma_v \frac{L}{H} - 0.035 \frac{S}{D}) - 1
 \end{aligned}
 \tag{5-4}$$

where F = maximum predicted tensile force (kip)

P = pile head load (kip)

T = transverse distance from reinforcement to pile center (in.)

D = pile diameter (in.)

σ_v = vertical stress (psf)

S = spacing from pile center to back face of MSE wall (in.)

L = length of reinforcement (ft.), and

H = total wall height including the equivalent height of surcharge (ft.).

MSE walls with an L/H ratio of 1.0 can be typical for seismic conditions. Equation (5-5) is similar to Equation (5-4), except that the L/H ratio is equal to 1.0, as shown below:

$$F = 10^{(-0.20 + 0.028P - 2.0 \times 10^{-4} P^2 - 0.0090 \frac{T}{D} - 0.0021P \frac{T}{D} + 0.0010 \sigma_v - 5.8 \times 10^{-7} \sigma_v^2 - 0.035 \frac{S}{D}) - 1} \quad (5-5)$$

MSE walls with an L/H ratio of 0.7 is more typical for static conditions. Equation (5-6) is similar to Equation (5-4), except that the L/H ratio is equal to 0.7, as shown below:

$$F = 10^{(-0.932 + 0.028P - 2.0 \times 10^{-4} P^2 - 0.0090 \frac{T}{D} - 0.0021P \frac{T}{D} + 0.00166 \sigma_v - 5.8 \times 10^{-7} \sigma_v^2 - 0.035 \frac{S}{D}) - 1} \quad (5-6)$$

Applying Equation (5-4), the predicted tensile force was calculated for every data observation. Figure 5-20 shows the measured tensile force versus the predicted tensile force in log-log form. Figure 5-21 shows the same relationship after transforming the data from the logarithm state (taking the measured data to the power of 10, subtracting 1, and applying Equation (5-4) for the predicted data). The red line shows that any point on this line would mean that the measured force equals the predicted force. Also included in the figure are mean plus and minus one and two standard deviation (σ) lines. Although there is significant scatter about the best-fit line, the

statistical parameters allow one to use the range of the standard deviations to account for variation if desired.

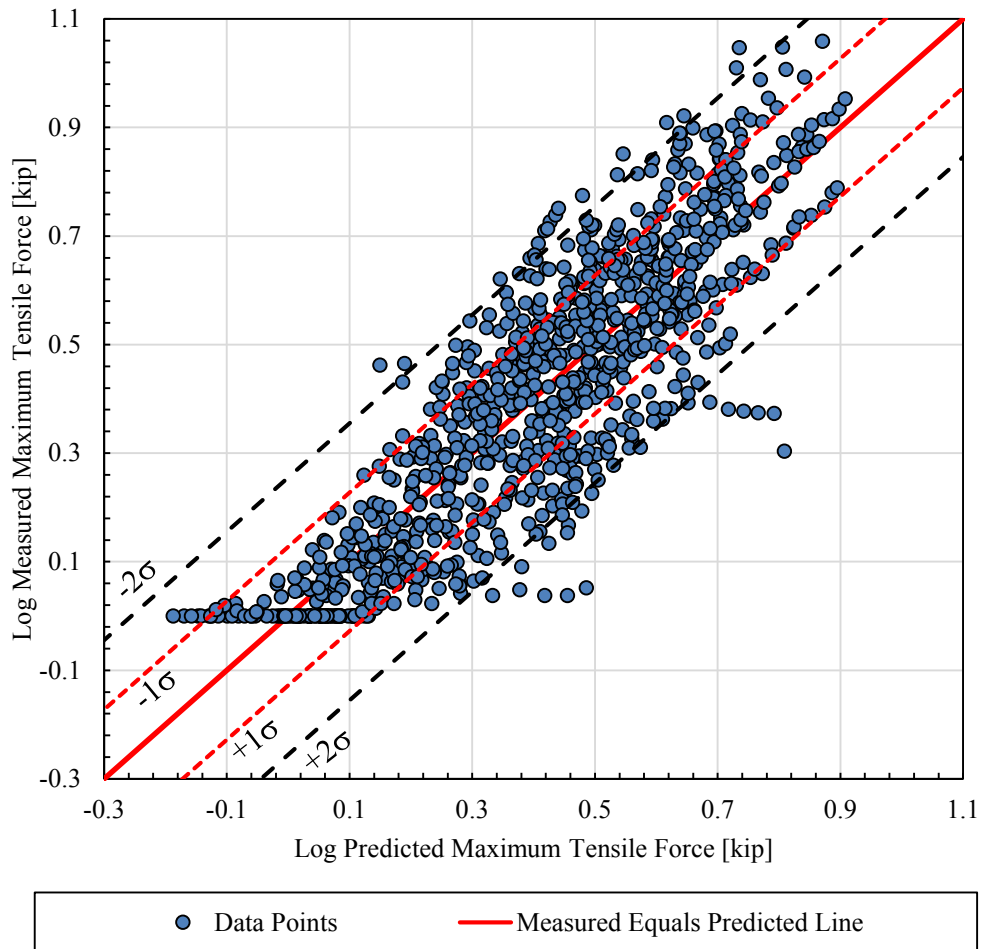


Figure 5-20. Log measured maximum tensile force versus log predicted maximum tensile force, ribbed strip reinforcement.

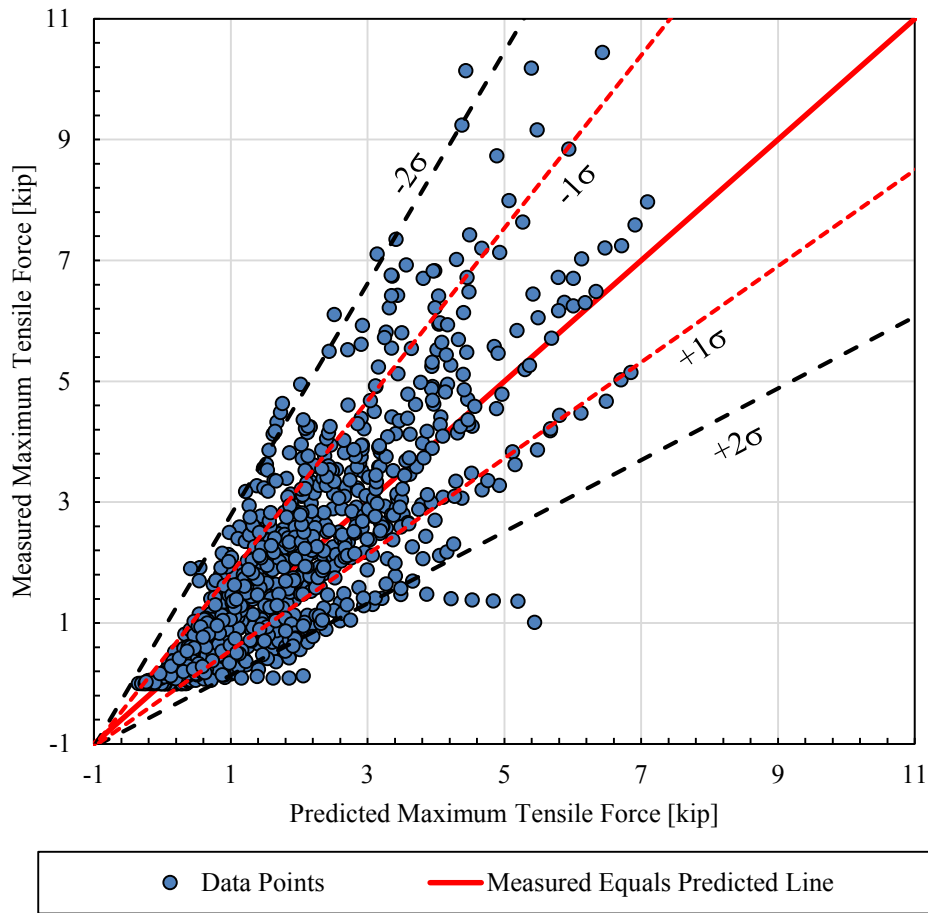


Figure 5-21. Measured maximum tensile force versus predicted maximum tensile force, ribbed strip reinforcement.

Figure 5-22, Figure 5-23, Figure 5-24, Figure 5-25, and Figure 5-26 show the common logarithm residual (called “log residual”) versus the main parameters. Figure 5-27 shows the logarithm residual versus the logarithm form of the predicted maximum tensile force. The residual, R , for each parameter was calculated using the equation:

$$R = \log(F_{measured} + 1) - \log(F_{predicted} + 1) \quad (5-7)$$

where R = residual

$F_{measured}$ = maximum tensile force measured (kip), and

$F_{predicted}$ = maximum tensile force predicted (kip).

Equation (5-7) provides a measure of the deviation from the best-fit line. Any point on the best-fit line means that there is no difference between the measured tensile force and the predicted tensile force. Most of the residuals fall between -0.2 and 0.2, but there are some in the -0.4 to 0.4 range. The values of the residuals appear to be uniformly divided with respect to zero indicating that Equation (5-4) is providing an appropriate fit to the data relative to each parameter of interest.

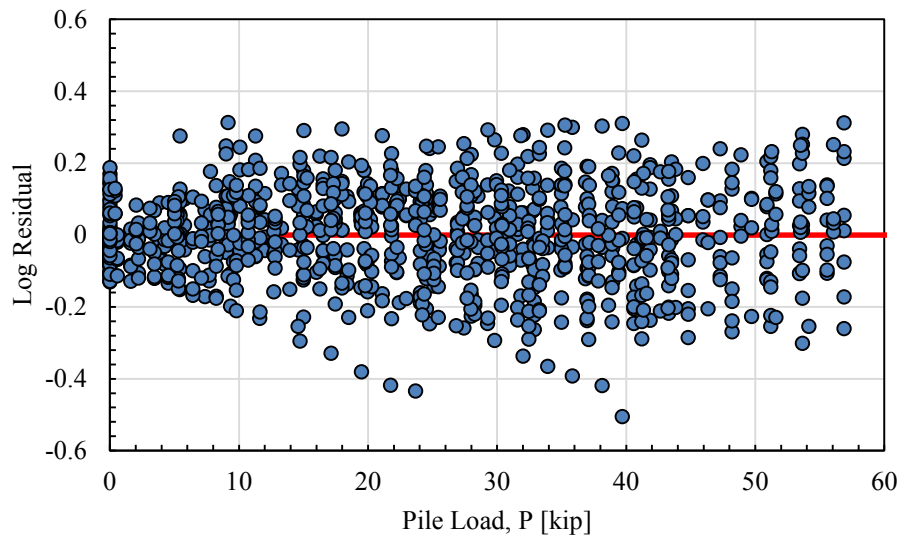


Figure 5-22. Log residual versus pile load, ribbed strip reinforcement.

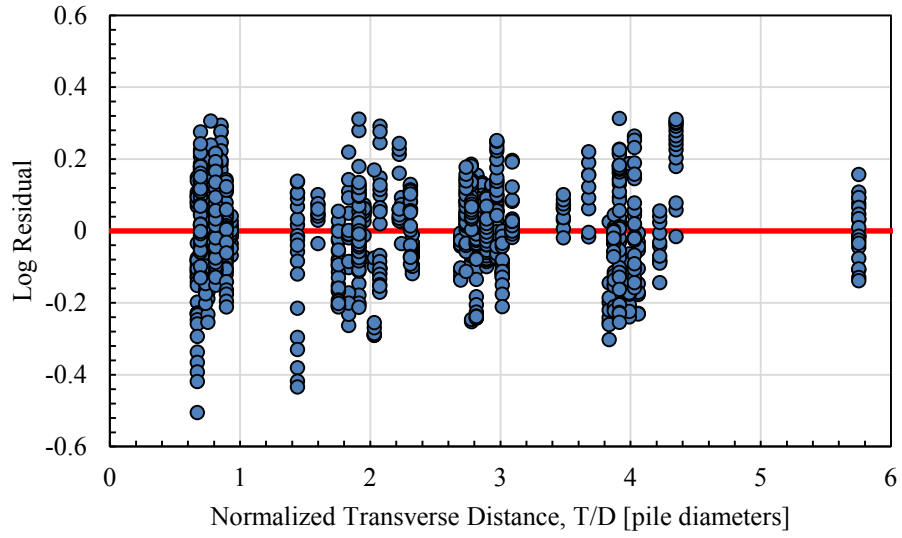


Figure 5-23. Log residual versus normalized transverse distance, ribbed strip reinforcement.

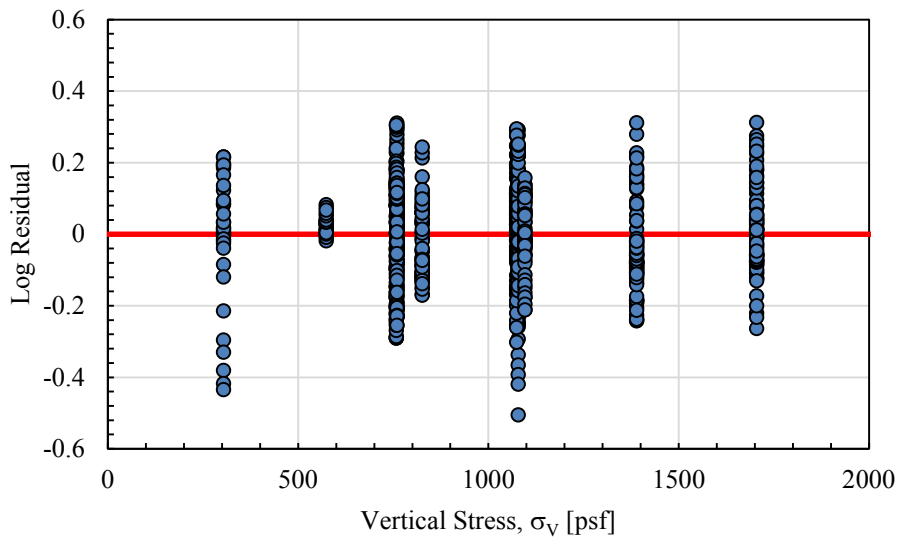


Figure 5-24. Log residual versus vertical stress, ribbed strip reinforcement.

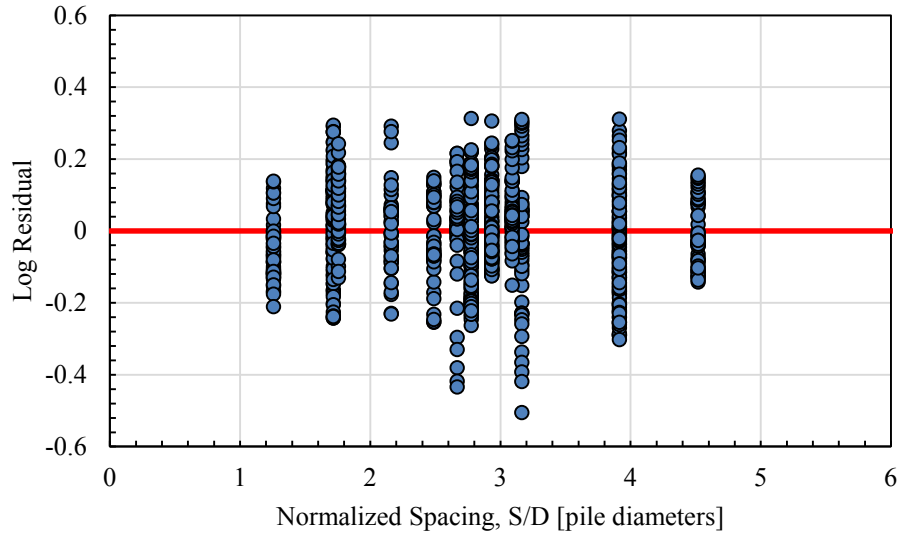


Figure 5-25. Log residual versus normalized spacing, ribbed strip reinforcement.

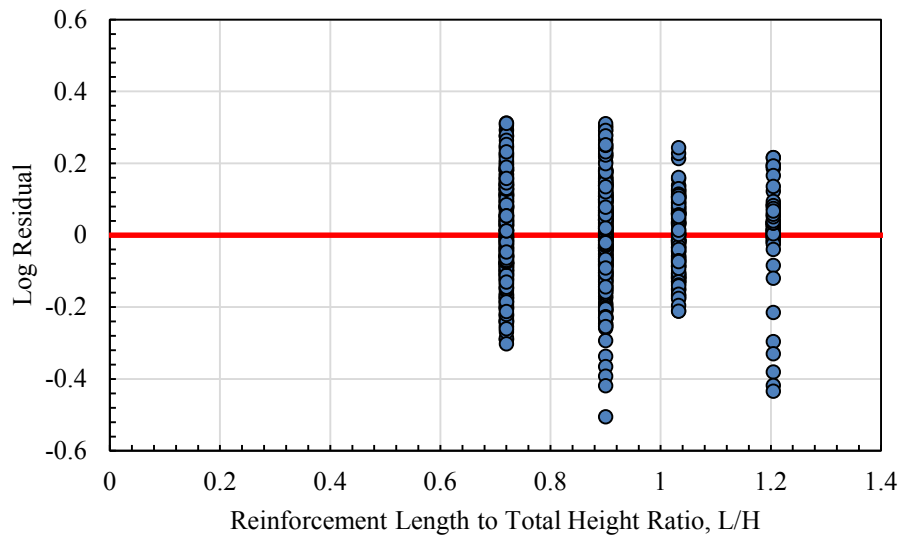


Figure 5-26. Log residual versus L/H ratio, ribbed strip reinforcement.

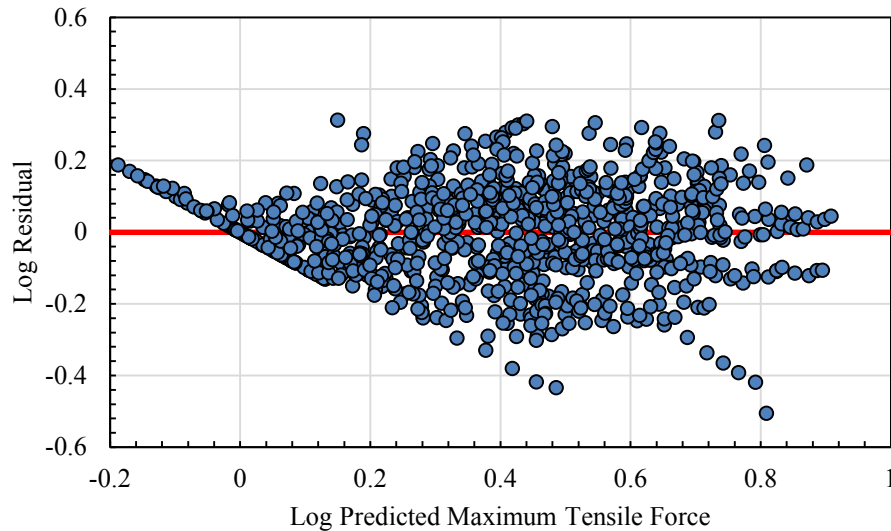


Figure 5-27. Log residual versus log predicted maximum tensile force, ribbed strip reinforcement.

Table 5-5 shows the minimum and maximum ranges of the main variables used in this statistical analysis. This is given to show that values out of this range may not be as accurate when using the predicted tensile force equation. The highest measured tensile force used to develop the predicted tensile force equation was 10.4 kips. Pile shape, panel size, wall facing type, and location of the pile behind a panel joint or center was not found to be significant compared to the other parameters. Pile diameter was taken into account at least partially and implicitly through the normalization of the pile and reinforcement spacing. However, the diameter range was too small to determine if this normalization is appropriate for a wide range of piles. At this stage, the equations should probably not be used for piles larger than about 18 inches in diameter. Future testing and analysis could better determine the significance of these parameters in predicting the maximum tensile force.

Table 5-5. Numerical Range of Parameters for Ribbed Strip Reinforcement Statistical Analysis

Parameter	Range
Measured Maximum Tensile Force, F_{measured}	0 kip – 10.4 kip
Pile Load, P	0 kip – 56.9 kip
Normalized Transverse Distance, T/D	0.7 – 5.8
Vertical Stress, σ_v	304 psf – 1704 psf
Normalized Spacing, S/D	1.3 – 6.3
Reinforcement Length to Total Height Ratio, L/H	0.7 – 1.2
Pile Diameter, D	12.1* in. – 12.75 in.

*Includes the smallest dimension of the pile.

5.3.2 Welded Wire Soil Reinforcement

The same procedure with the same main variables from the ribbed strip reinforcement statistical analysis was carried out for the statistical analysis of the welded wire reinforcement. The data sets used in this analysis consisted of forces measured in the square piles of this study, Budd (2016), Hatch (2014), and Price (2012). A total of 1,058 data observations were used for this analysis. The same main variables were used as above; namely, the pile load, the transverse distance normalized by the pile diameter, the vertical stress, the pile spacing normalized by the pile diameter, and the reinforcement length to the total wall height (including the equivalent surcharge height) ratio. Table 5-6 shows the results from the statistical analysis of the main variables along with the most significant combination of any two variables. Table 5-7 shows each term that was subsequently eliminated from the original equation obtained from Dr. Eggett. The table also shows the R^2 and adjusted R^2 values and by how much they decrease with each term that is eliminated. The last term to remain (not included in the table) was the pile load, P. The first three terms in Table 5-7 were removed for the regression equation, resulting in an R^2 value of 77.4% and an adjusted R^2 value of 77.3%. The R^2 values are according to the common logarithm being applied to the data. The

standard error value was 0.123. Table 5-8 shows the Analysis of Variance (ANOVA) output. The confidence interval used was 95% and Table 5-9 shows those values with their respective parameters. (See Budd (2016) for the statistical analysis on the same data minus the square piles data. This represents all of the data for the welded wire reinforcement for pipe piles only).

Table 5-6. Statistical Analysis of Welded Wire Reinforcement

Parameter	Coefficients	Standard Error	t Stat	P-value
Intercept	-0.0448529546	0.05529	-0.81119	0.41744
Pile Load, P	0.0254355826	0.00096	26.54347	<0.00001
Normalized Transverse Distance, T/D	-0.0773701160	0.00399	-19.37864	<0.00001
Vertical Stress, σ_v	0.0004578021	0.00004	11.02603	<0.00001
Normalized Spacing, S/D	-0.0446780109	0.00317	-14.11065	<0.00001
Length to Height Ratio, L/H	0.6215432267	0.05813	10.69186	<0.00001
$\sigma_v^*(L/H)$	-0.0006453190	0.00004	-14.98365	<0.00001
P^2	-0.0002179049	0.00002	-11.95195	<0.00001

Table 5-7. Term Elimination with the Change of R^2 and Adjusted R^2 for Welded Wire Reinforcement

Term Removed	Adjusted R^2	Decrease in Adjusted R^2	R^2	Decrease in R^2
None	78.13%	-	78.34%	-
$\sigma_v^*(T/D)^+$	77.96%	0.17%	78.15%	0.19%
σ_v^{2+}	77.72%	0.24%	77.89%	0.26%
$P^*(T/D)^+$	77.27%	0.45%	77.42%	0.47%
P^2	74.20%	3.07%	74.35%	3.07%
$\sigma_v^*(L/H)$	68.80%	5.40%	68.95%	5.40%
L/H	66.56%	2.24%	66.69%	2.26%
S/D	63.07%	3.49%	63.17%	3.52%
σ_v	58.15%	4.91%	58.23%	4.94%
T/D	50.38%	7.77%	50.43%	7.80%

⁺ Terms removed for the regression equation.

Table 5-8. ANOVA for Welded Wire Reinforcement

	Degrees of Freedom	Sum-of-Squares	Mean Squares	F Ratio	Significance F
Regression	7	60.45558	8.63651	514.32087	0
Residual	1050	17.63167	0.01679		
Total	1057	78.08725			

Table 5-9. Confidence Interval Values for Welded Wire Reinforcement

Parameter	Lower 95%	Upper 95%
Intercept	-0.15335	0.06364
Pile Load, P	0.02356	0.02732
Normalized Transverse Distance, T/D	-0.08520	-0.06954
Vertical Stress, σ_v	-0.00025	-0.00018
Normalized Spacing, S/D	0.00038	0.00054
Length to Height Ratio, L/H	-0.05089	-0.03847
$\sigma_v^*(L/H)$	0.50747	0.73561
P^2	-0.00073	-0.00056

The number of significant figures in the regression equation was reduced to two for every coefficient, but the R^2 value remained nearly the same at 77.4%. Applying the parameters and the coefficients from Table 5-6, an equation was created to predict the maximum tensile force as shown below:

$$F = 10^{(-0.045 + 0.025P - 2.2 \times 10^{-4} P^2 - 0.077 \frac{T}{D} - 0.045 \frac{S}{D} + 4.6 \times 10^{-4} \sigma_v + 0.62 \frac{L}{H} - 6.5 \times 10^{-4} \sigma_v \frac{L}{H}) - 1} \quad (5-8)$$

Where F = maximum predicted tensile force (kip)

P = pile head load (kip)

T = transverse distance from reinforcement to pile center (in.)

D = pile diameter (in.)

σ_v = vertical stress (psf)

S = spacing from pile center to back face of MSE wall (in.)

L = length of reinforcement (ft.), and

H = total wall height including the equivalent height of surcharge (ft.).

MSE walls with an L/H ratio of 1.0 can be typical for seismic conditions. Equation (5-9) is similar to Equation (5-8), except that the L/H ratio is equal to 1.0, as shown below:

$$F = 10^{\left(0.575 + 0.025P - 2.2 \times 10^{-4} P^2 - 0.077 \frac{T}{D} - 0.045 \frac{S}{D} - 1.9 \times 10^{-4} \sigma_v\right)} - 1 \quad (5-9)$$

MSE walls with an L/H ratio of 0.7 is more typical for static conditions. Equation (5-10) is similar to Equation (5-8), except that the L/H ratio is equal to 0.7, as shown below:

$$F = 10^{\left(0.389 + 0.025P - 2.2 \times 10^{-4} P^2 - 0.077 \frac{T}{D} - 0.045 \frac{S}{D} + 5.0 \times 10^{-6} \sigma_v\right)} - 1 \quad (5-10)$$

Applying Equation (5-8), predicted tensile force was able to be calculated for every data observation. Figure 5-28 shows the measured tensile force versus the predicted tensile force in log-log form. Figure 5-29 shows the same relationship after transforming the data from the logarithm state (taking the measured data to the power of 10, subtracting 1, and applying Equation (5-8) for the predicted data). The red line shows that any point on this line would mean that the measured

force equals the predicted force. Also included in the figure are mean plus and minus one and two standard deviation (σ) lines.

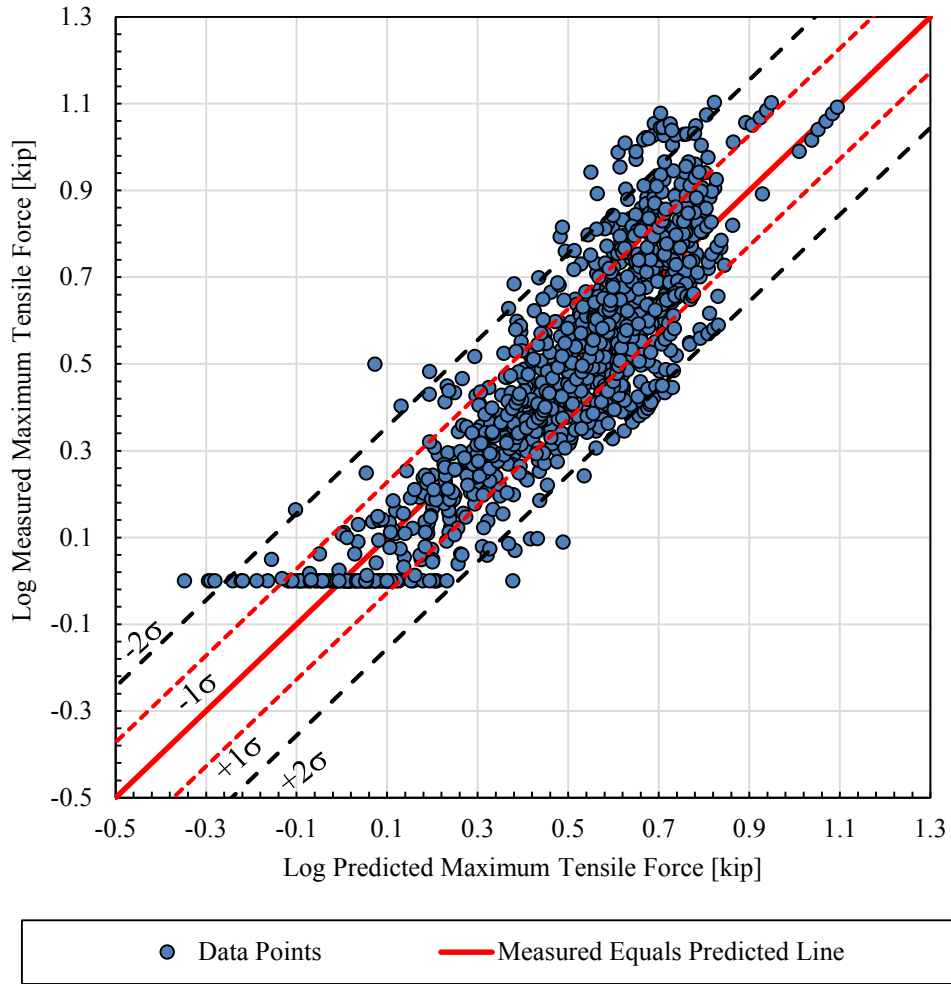


Figure 5-28. Log measured maximum tensile force versus log predicted maximum tensile force, welded wire reinforcement.

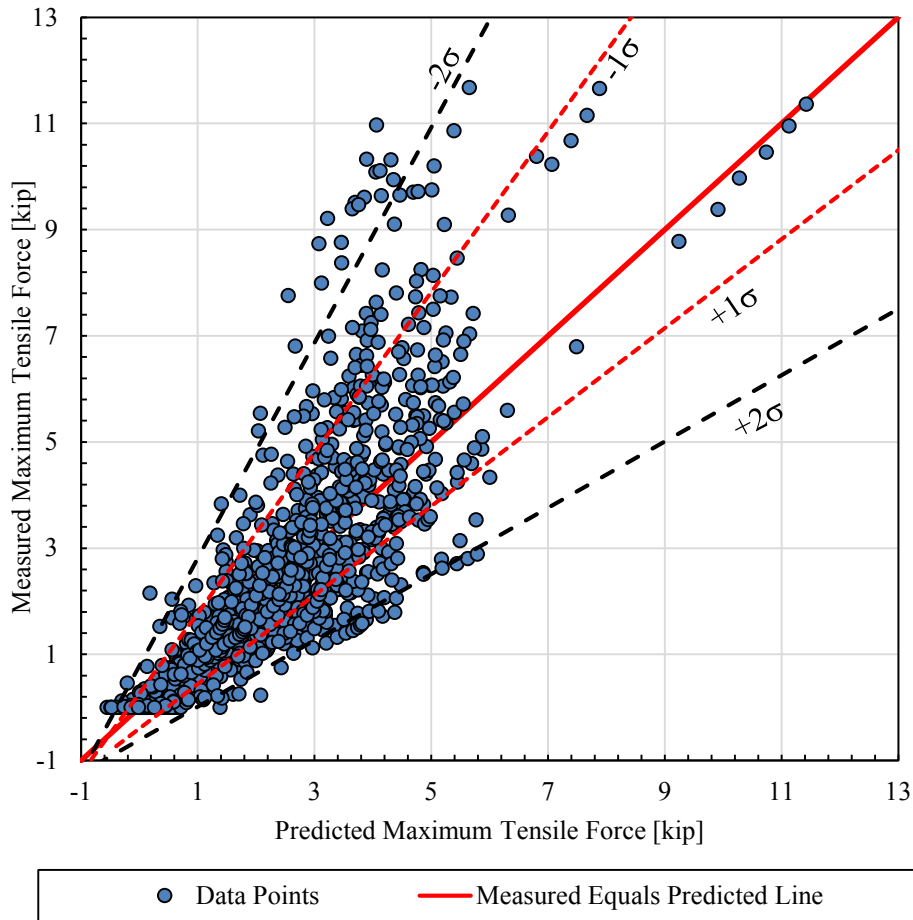


Figure 5-29. Measured maximum tensile force versus predicted maximum tensile force, welded wire reinforcement.

Figure 5-30, Figure 5-31, Figure 5-32, Figure 5-33, and Figure 5-34 show the common logarithm residual (called “log residual”) versus the main parameters. Figure 5-35 shows the logarithm residual versus the logarithm form of the predicted maximum tensile force. The residual, R , for each parameter was calculated using Equation (5-7). This equation provides a measure of the deviation from the best-fit line. Any point on the best-fit line means that there is no difference between the measured tensile force and the predicted tensile force. Most of the residuals fall between -0.2 and 0.2, but there are some in the -0.4 to 0.4 range. The values of the residuals appear

to be uniformly divided with respect to zero indicating that Equation (5-8) is providing an appropriate fit to the data relative to each parameter of interest.

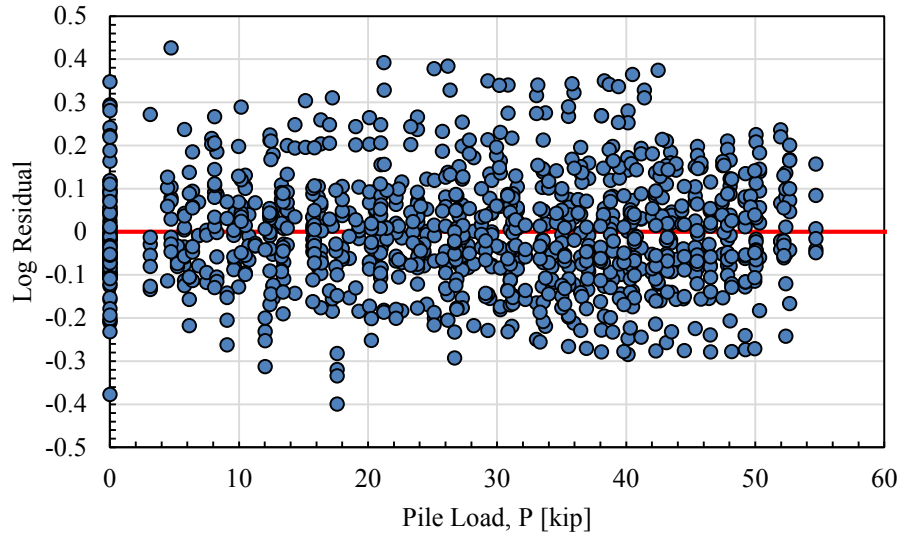


Figure 5-30. Log residual versus pile load, welded wire reinforcement.

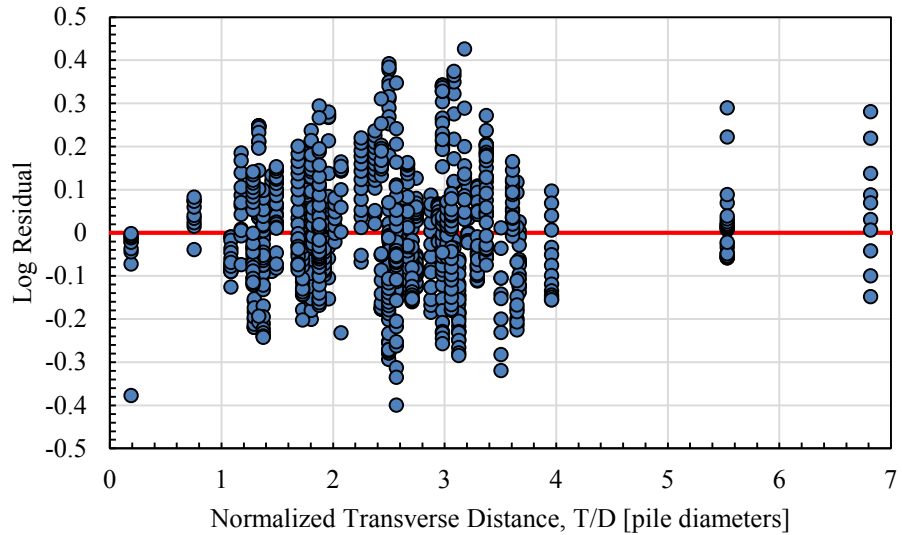


Figure 5-31. Log residual versus normalized transverse distance, welded wire reinforcement.

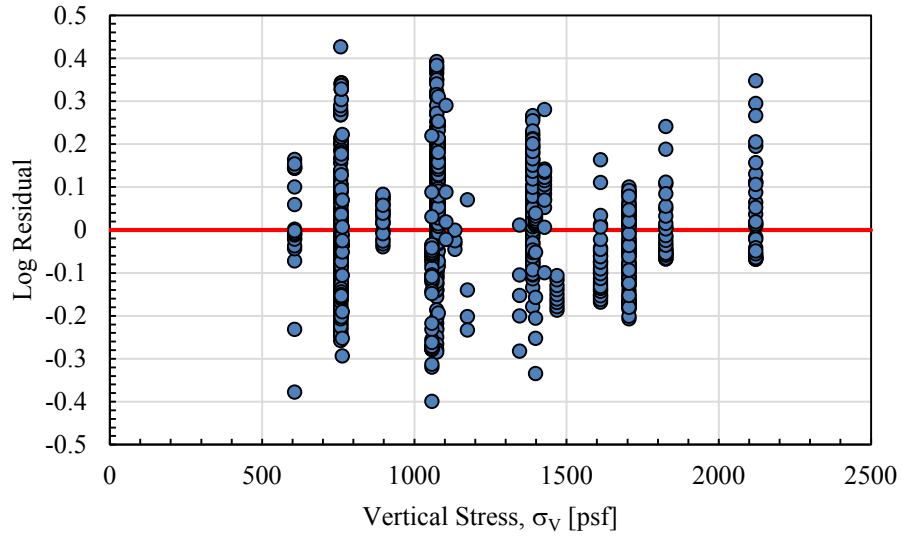


Figure 5-32. Log residual versus vertical stress, welded wire reinforcement.

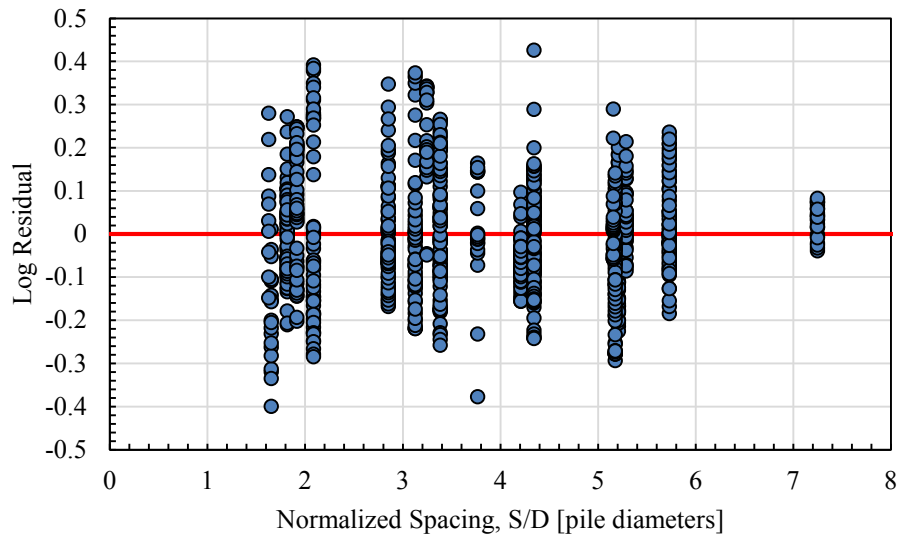


Figure 5-33. Log residual versus normalized spacing, welded wire reinforcement.

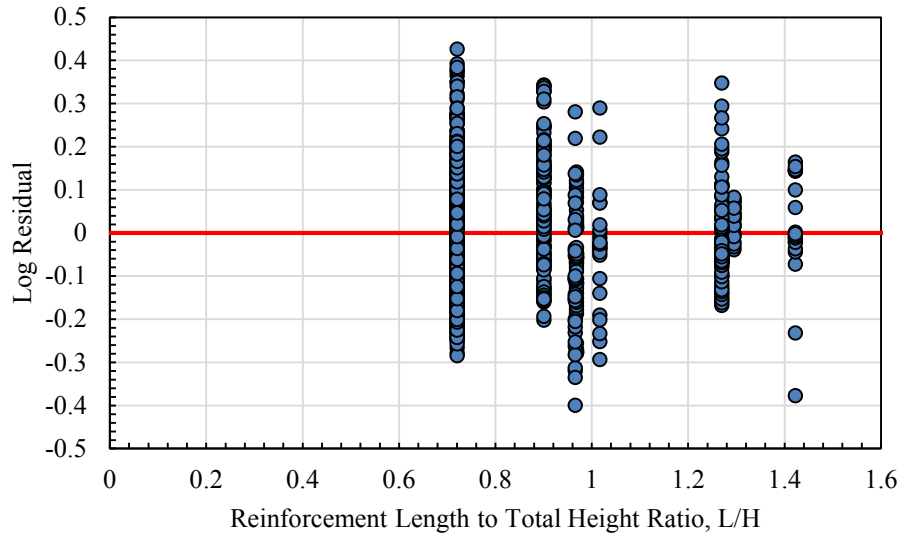


Figure 5-34. Log residual versus L/H ratio, welded wire reinforcement.

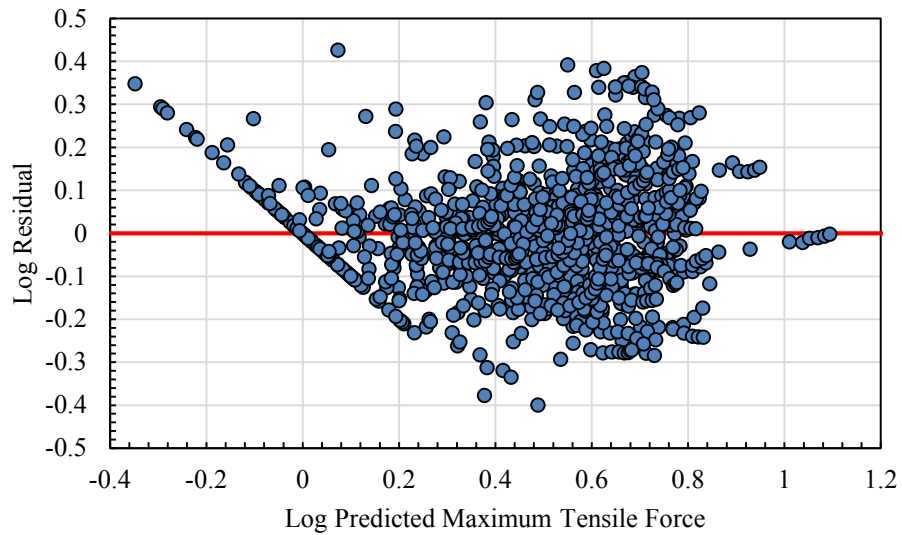


Figure 5-35. Log residual versus log predicted maximum tensile force, welded wire reinforcement.

Table 5-10 shows the minimum and maximum ranges of the main variables used in this statistical analysis. This is given to show that values out of this range may not be as accurate when using the predicted tensile force equation. The highest measured tensile force used to develop the

predicted tensile force equation was 11.7 kips. Pile shape, panel size, and location of the pile behind a panel joint or center was not found to be significant compared to the other parameters. Pile diameter was taken into account at least partially and implicitly through the normalization of the pile and reinforcement spacing, because it was found to be somewhat significant. At this stage, the equations should probably not be used for piles larger than about 18 inches in diameter. Future testing and analysis could better determine the significance of pile diameter and other parameters in predicting the maximum tensile force.

Table 5-10. Numerical Range of Parameters for Welded Wire Reinforcement Statistical Analysis

Parameter	Range
Measured Maximum Tensile Force, F_{measured}	0 kip – 11.7 kip
Pile Load, P	0 kip – 54.7 kip
Normalized Transverse Distance, T/D	0.2 – 6.8
Vertical Stress, σ_v	607 psf – 2121 psf
Normalized Spacing, S/D	1.6 – 7.2
Reinforcement Length to Total Height Ratio, L/H	0.7 – 1.4
Pile Diameter, D	12 in. – 16 in.

5.4 Ground Displacement

5.4.1 H-Piles

Ground displacement was also analyzed using string potentiometers for horizontal displacement and surveying for vertical displacement (see Section 4.2 and Section 4.6, respectively). Figure 5-36, Figure 5-37, Figure 5-38, and Figure 5-39 show the relationship of the horizontal ground displacement versus the distance from the back face of the MSE wall for each of the H-piles (4.5D, 3.2D, 2.5D, 2.2D, respectively). The string potentiometer reading at the pile

center was extrapolated to the ground surface. The stakes closest to the pile face (usually one foot away) generally rotated backwards owing to the ground surface movement. Thus, these points were omitted. However, in Figure 5-40, this data point is not omitted to show how the back rotation of the stake measured lower horizontal displacement for that string potentiometer than for the string potentiometers farther from the pile. The lines shown are only for the load increments corresponding to approximately 0.5, one, two, and three inches of pile head displacement. Generally, the results show that the horizontal displacement decreases rapidly with distance from the pile, as expected. Even for pile head deflections of 2.5 to 3.0 inches, the deflection at the top of the wall was typically less than about 0.3 inches for the H-pile lateral load tests. This result stands in stark contrast to results for tests with extensible geosynthetic reinforcements reported by Pierson (2009) (see Figure 2-18). In that case, wall displacements were almost two inches with a pile head load of three inches.

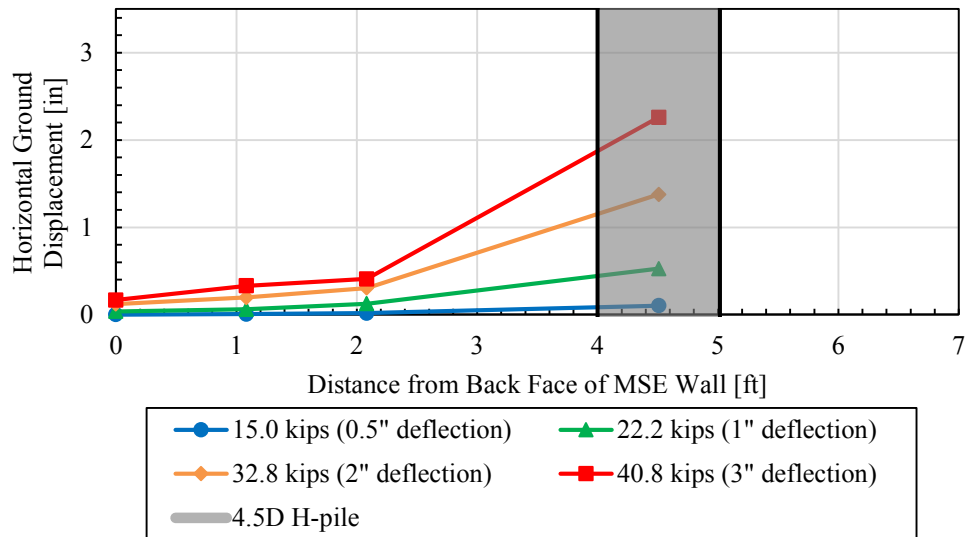


Figure 5-36. Horizontal ground displacement versus distance from the back face of the MSE wall, 4.5D H-pile.

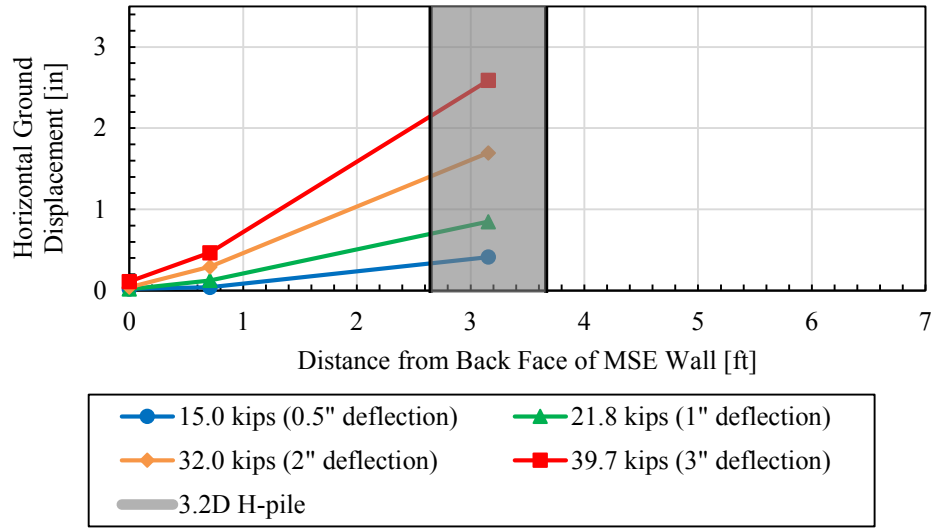


Figure 5-37. Horizontal ground displacement versus distance from the back face of the MSE wall, 3.2D H-pile.

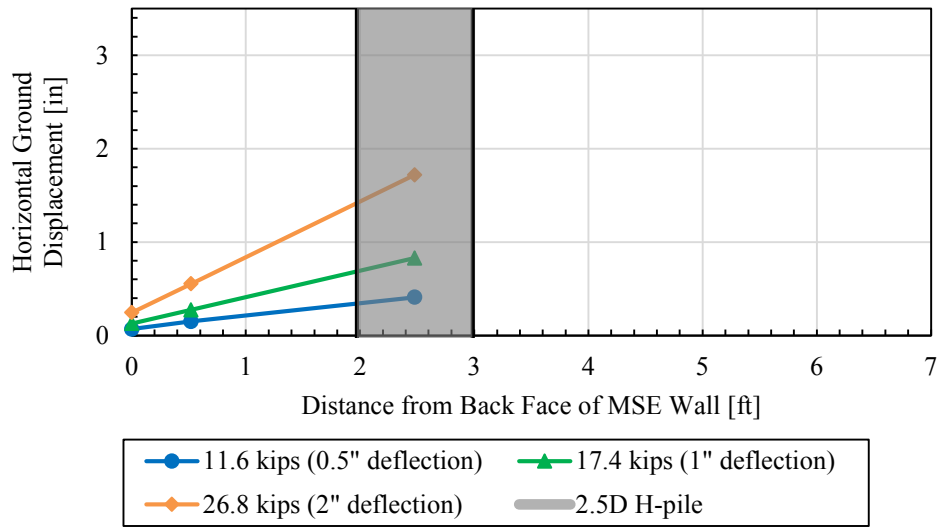


Figure 5-38. Horizontal ground displacement versus distance from the back face of the MSE wall, 2.5D H-pile.

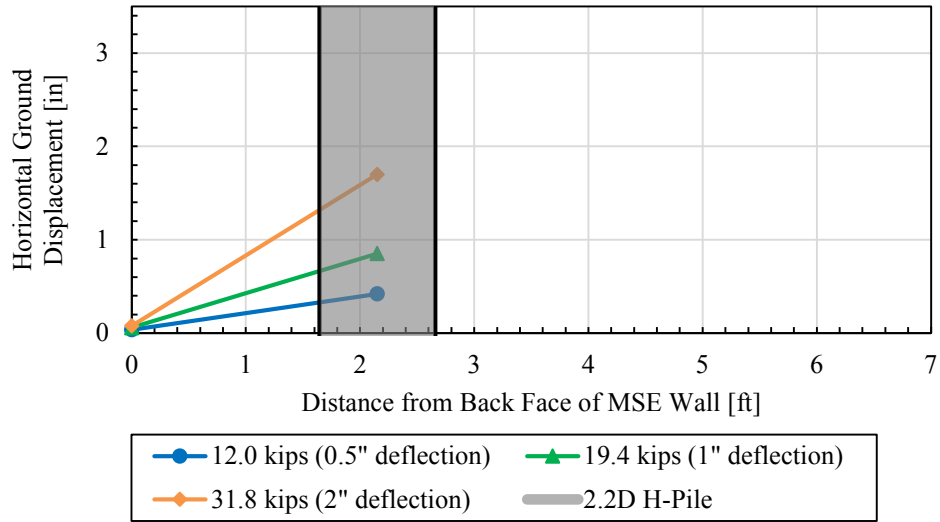


Figure 5-39. Horizontal ground displacement versus distance from the back face of the MSE wall, 2.2D H-pile.

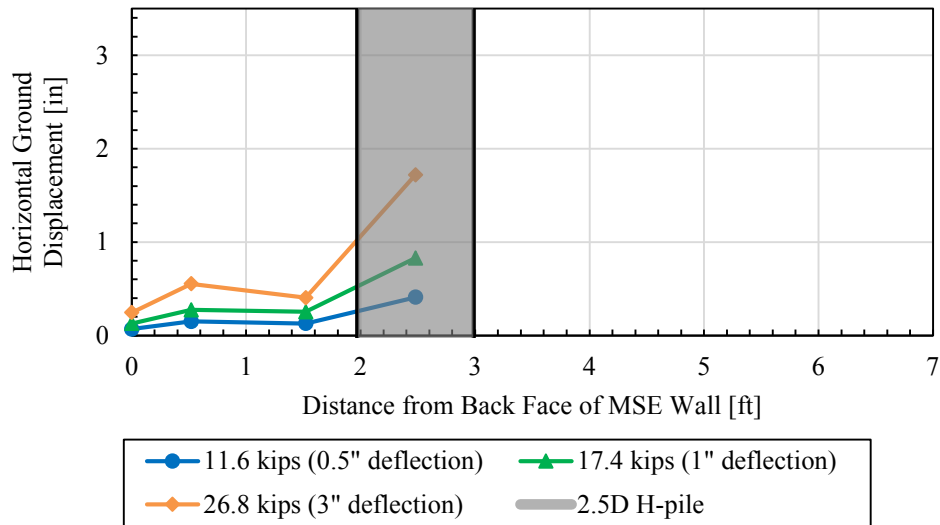


Figure 5-40. Horizontal ground displacement versus distance from the back face of the MSE wall without omitting the data point closest to the pile, 2.5D H-pile.

Figure 5-41 shows the normalized horizontal ground displacement (horizontal ground displacement divided by the displacement at the pile face extrapolated to the ground surface) versus the distance from the pile face divided by the pile diameter (i.e. normalized distance) for the 2” pile load increment. It can be seen that piles spaced farther from the wall develop more horizontal ground displacement. Figure 5-42 shows the best fit line for all of the H-pile data points. This graph shows that the horizontal displacement decreases dramatically from the pile face to a distance of about 2D from the center of the pile, and then gradually decreases beyond this distance. Ground displacement is typically less than 20% and 10% of that at the pile face beyond distances of 1.5 and 4 pile diameters, respectively, within the reinforced soil zone. An equation, shown below, with an R² value of 98.1% was developed using the data from the 0.25-, 0.5-, 1-, 2-, and 3-inch pile load deflection load increment for horizontal ground displacement for H-piles behind an MSE wall:

$$\frac{\delta}{\delta_p} = 1 - 0.97 \tanh\left(0.69 \frac{L}{D}\right) \quad (5-11)$$

where δ = horizontal ground displacement

δ_p = horizontal ground displacement at the pile face at the ground surface

L = distance from point of interest in front of pile to pile face, and

D = pile diameter.

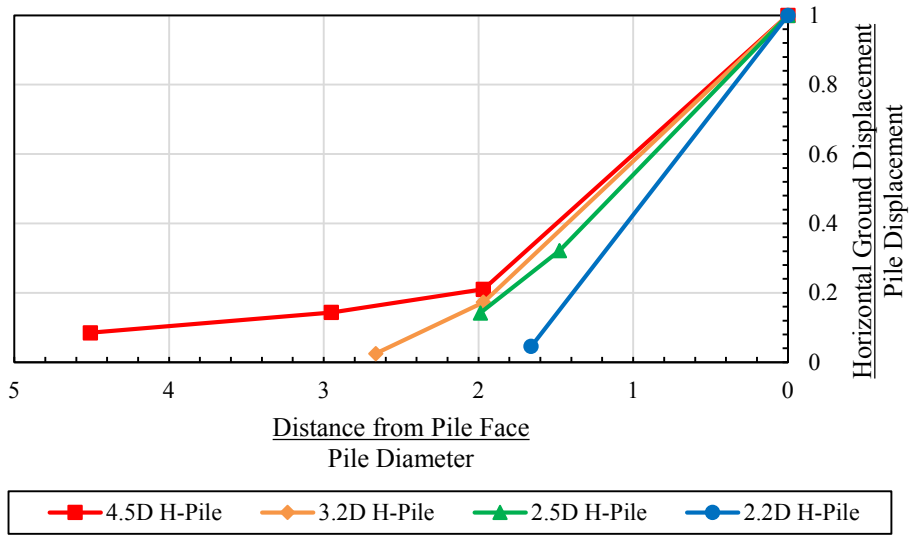


Figure 5-41. Horizontal ground displacement normalized by the displacement at the pile face extrapolated to the ground surface versus normalized distance from pile face for all H-piles for the 2” load increment.

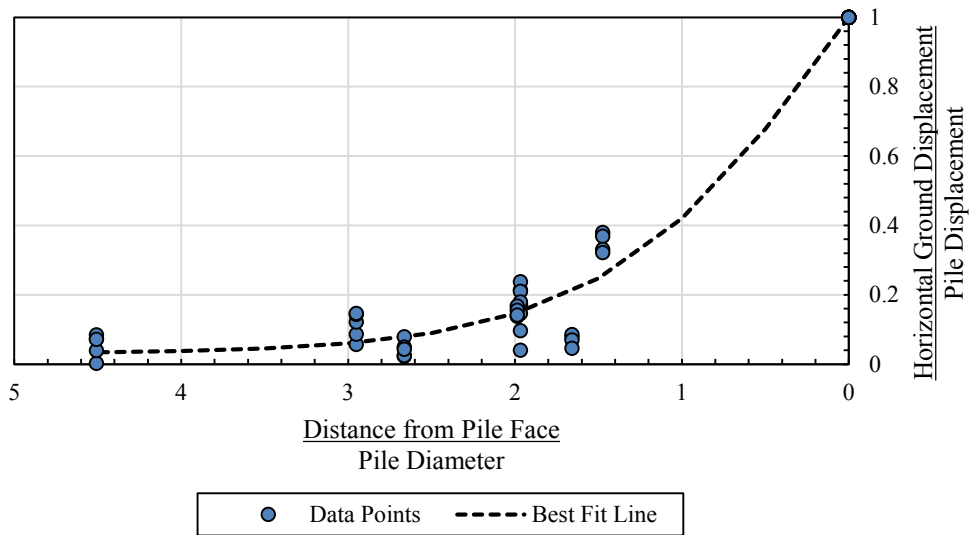


Figure 5-42. Horizontal ground displacement normalized by the displacement at the pile face extrapolated to the ground surface versus normalized distance from pile face for all H-piles for the 0.25”, 0.5”, 1”, 2”, and 3” load increments with the best fit line.

Figure 5-43 shows the vertical ground displacement versus the distance from the back face of the MSE wall (Appendix F has each of the H-piles separated into individual graphs of vertical displacement versus distance from the wall). The locations of the piles are also included. For the 2.5D and 2.2D H-piles, the maximum ground heaving occurs about half of an inch from the pile face and then decreases at the pile face. This may be because space was created when the piles were displaced. For the 4.5D and 3.2D H-piles, the soil heave continues to increase gradually until the face of the pile. The 4.5D pile has a maximum heave of about two inches, while the other piles almost reach three inches.

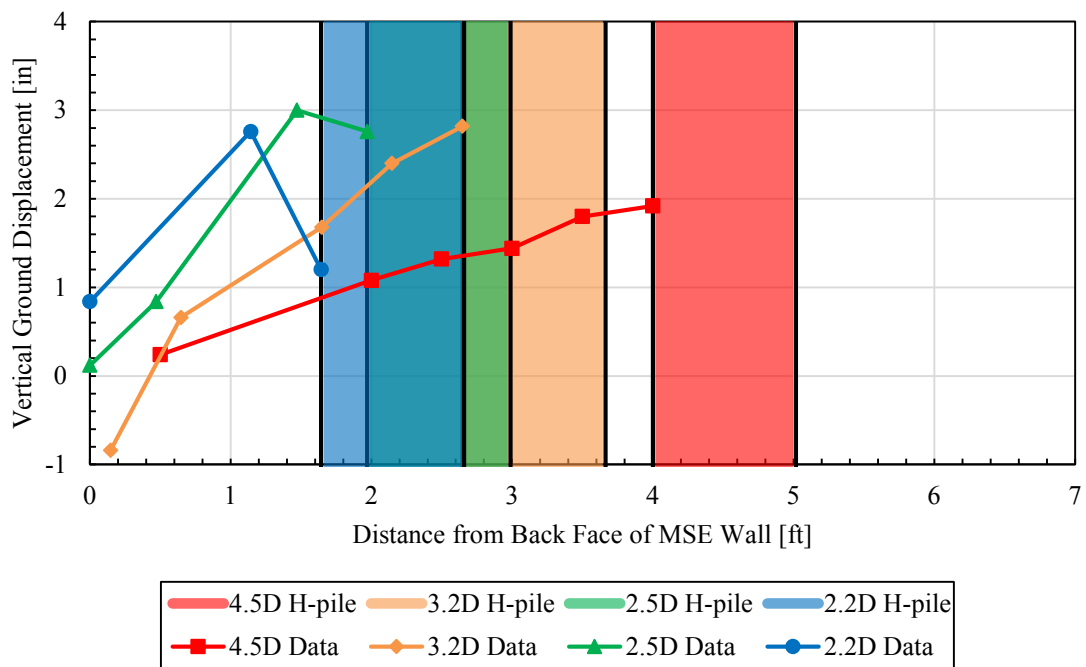


Figure 5-43. Vertical ground displacement versus distance from the back face of the MSE wall for all H-piles.

5.4.2 Square Piles

The same procedure used for the H-piles was used for the square piles to analyze ground displacement. Figure 5-44, Figure 5-45, Figure 5-46, and Figure 5-47 show the relationship of the horizontal ground displacement versus the distance from the back face of the MSE wall for each of the square piles (5.7D, 4.2D, 3.1D, 2.1D, respectively). The string potentiometer reading at the pile center was extrapolated to the ground surface. The stakes closest to the pile face (usually one foot away) generally rotated backwards owing to the ground surface movement. Thus, these points were omitted. However, in Figure 5-48, this data point is not omitted to show how the back rotation of the stake measured lower horizontal displacement for that string potentiometer than for the string potentiometers farther from the pile. The lines shown are only for the load increments corresponding to approximately 0.5, one, two, and three inches of pile head displacement. Generally, the results show that the horizontal displacement decreases rapidly with distance from the pile, as expected. Deflections at the top of the wall ranged from approximately 0.25 to 0.4 inches, with the exception of the 2.1D square pile which showed the string potentiometer at the top of the wall was about 0.7 inches.

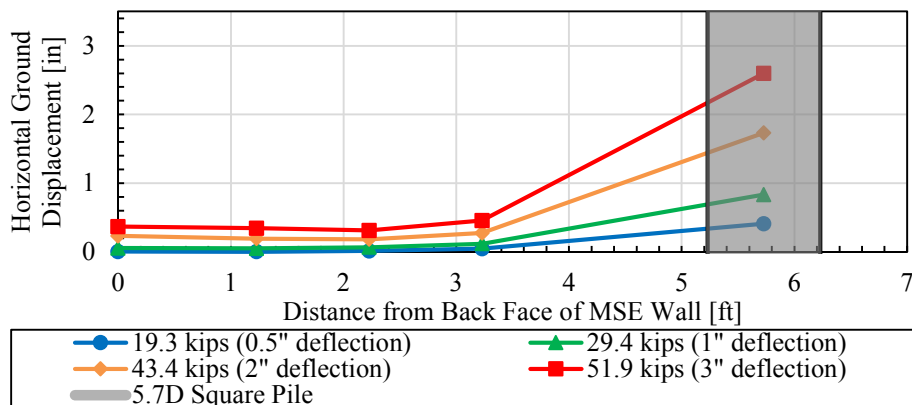


Figure 5-44. Horizontal ground displacement versus distance from the back face of the MSE wall, 5.7D square pile.

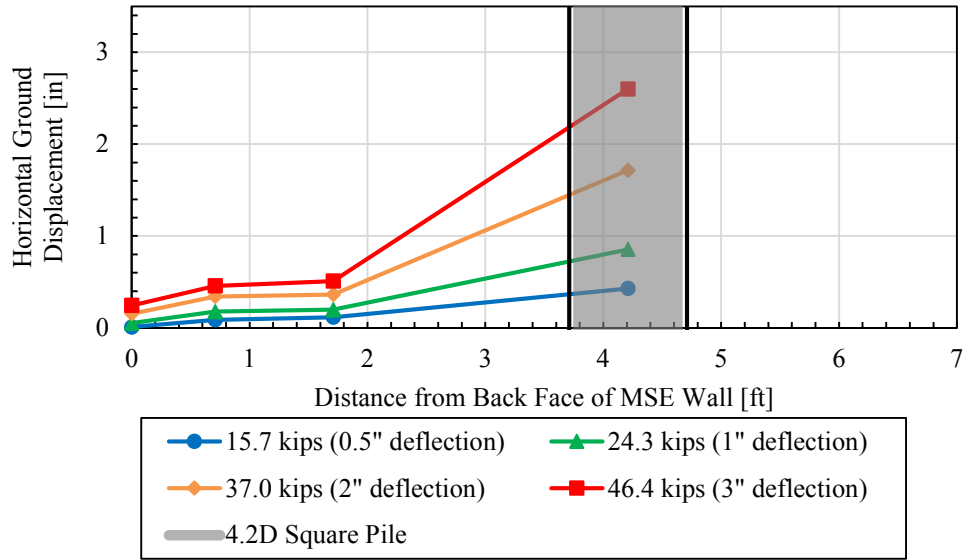


Figure 5-45. Horizontal ground displacement versus distance from the back face of the MSE wall, 4.2D square pile.

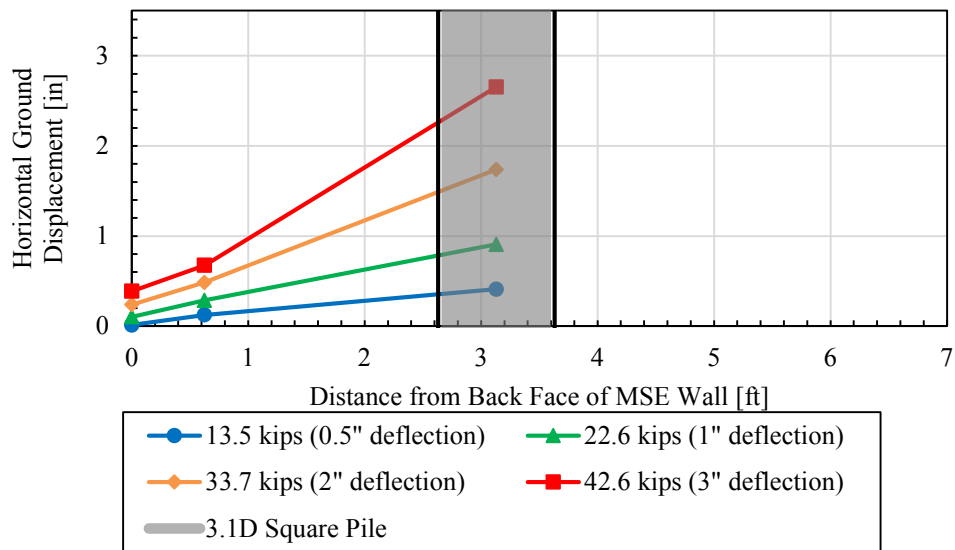


Figure 5-46. Horizontal ground displacement versus distance from the back face of the MSE wall, 3.1D square pile.

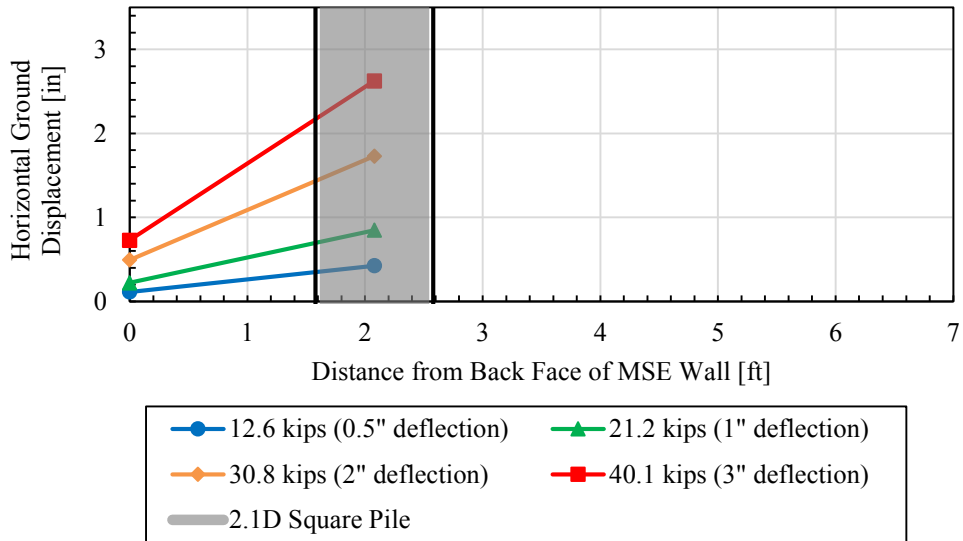


Figure 5-47. Horizontal ground displacement versus distance from the back face of the MSE wall, 2.1D square pile.

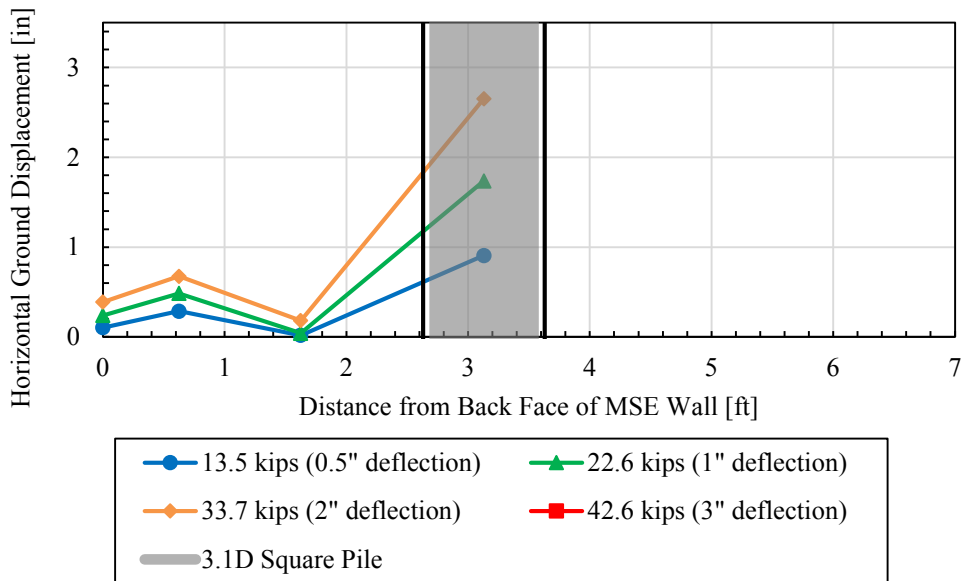


Figure 5-48. Horizontal ground displacement versus distance from the back face of the MSE wall without omitting data the point closest to the pile, 3.1D square pile.

Figure 5-49 shows the normalized horizontal ground displacement (horizontal ground displacement divided by the displacement at the pile face extrapolated to the ground surface) versus the distance from the pile face divided by the pile diameter (i.e. normalized distance) for the 3” pile load increment. It can be seen that piles spaced farther from the wall develop more horizontal ground displacement. Figure 5-50 shows the best fit line for all of the square pile data points. This graph shows that the horizontal displacement decreases dramatically from the pile face to a distance of about 2D from the center of the pile, and then gradually decreases beyond this distance. Ground displacement is typically less than 20% at about 2.0 pile diameters from the pile face.

An equation, shown below, with an R² value of 98.1% was developed using the data from the 0.25-, 0.5-, 1-, 2-, and 3-inch pile load deflection load increments for horizontal ground displacement for square piles behind an MSE wall:

$$\frac{\delta}{\delta_p} = 1 - 0.93 \tanh\left(0.63 \frac{L}{D}\right) \quad (5-12)$$

where δ = horizontal ground displacement

δ_p = horizontal ground displacement at the pile face at the ground surface

L = distance from point of interest in front of pile to pile face, and

D = pile diameter.

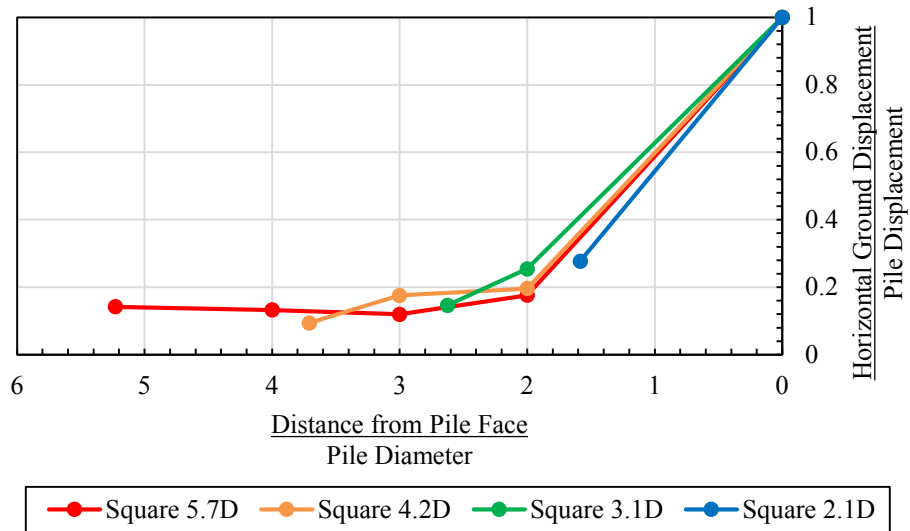


Figure 5-49. Horizontal ground displacement normalized by the displacement at the pile face extrapolated to the ground surface versus normalized distance from pile face for all square piles for the 3” load increment.

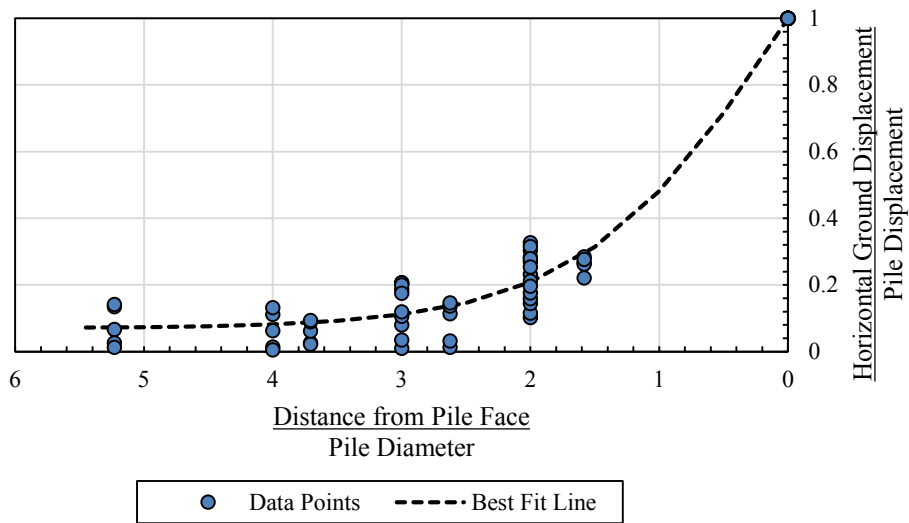


Figure 5-50. Horizontal ground displacement normalized by the displacement at the pile face extrapolated to the ground surface versus normalized distance from pile face for all square piles for the 0.25”, 0.5”, 1”, 2”, and 3” load increments with the best fit line.

Figure 5-51 shows a comparison for the best fit curves from Figure 5-42 and Figure 5-50 of the H-piles and square piles, respectively. The square piles have slightly higher horizontal ground displacement at a given distance than do the H-piles.

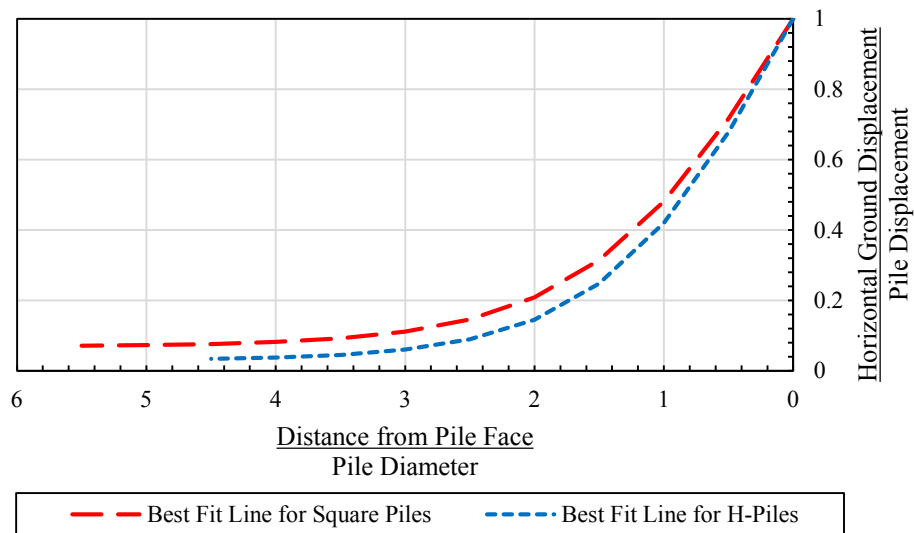


Figure 5-51. Square and H-pile comparison of the best fit lines of the horizontal ground displacement normalized by the displacement at the pile face extrapolated to the ground surface versus normalized distance from pile.

Figure 5-52 shows the vertical ground displacement versus the distance from the back face of the MSE wall (Appendix F has each of the square piles separated into individual graphs of vertical displacement versus distance from the wall). The locations of the piles are also included. Generally, the vertical ground displacement increases closer to the face of the pile, with the only exception being the 3.1D square pile which decreases a fraction of an inch before increasing again. It is interesting to note that for the 5.7D square pile, there is negative displacement at the wall face. This is probably because soil dropped into the extra space created owing to the wall deflecting

outward. The maximum vertical ground displacement for the three closest piles to the wall do not surpass two inches, while the 5.7D square pile does.

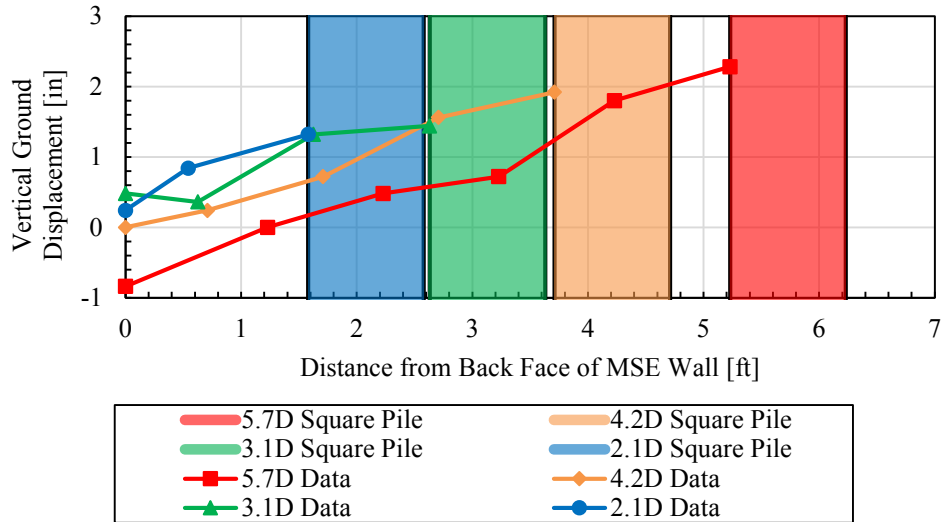


Figure 5-52. Vertical ground displacement versus distance from the back face of the MSE wall for all square piles.

5.5 Wall Panel Displacement

5.5.1 H-Piles

Wall displacement was recorded by the use of DIC, shape arrays, and the string potentiometers located nearest the top of the wall. Table 5-11 shows which string potentiometers were used with their respective piles during lateral loading. Even though the string potentiometers were used to measure pile displacement, the string potentiometer reading right on top of the wall was also used to measure wall displacement for the top of the wall. This value was used as a reference when comparing the DIC and shape array data. The maximum pile head displacement and associated wall displacement are summarized for each pile in Table 5-11. Peak values were

used in Table 5-11 instead of the one-minute hold values to compare with DIC, which only took measurements at the peak and five-minute hold of the load increments. Table 5-12 shows the distance from the panel joint to the center of the pile. Four shape arrays were placed for each pile test to record wall displacement. Table 5-13 shows the transverse distance of the shape arrays from the pile center for their respective piles. The direction of left or right of the pile is taken from looking at the front side of the MSE wall (North).

Figure 5-53 and Figure 5-54 show color fringe contours of longitudinal displacement overlain across a graphic image of the MSE wall obtained from DIC for the 3” pile displacement for the 4.5D H-pile and the 3.2D H-pile, respectively. Figure 5-55 shows the 2.25” pile displacement for the 2.5D H-pile, and Figure 5-56 shows the 2” displacement for the 2.2D H-pile. The DIC images show the peak wall displacements at the specified pile head displacements. Knowing that the nominal wall panel size is 5 ft high x 10 ft wide, the field of view for the DIC images is typically about 10 to 12 feet in each dimension. The scales range from -0.1 to 0.3 inches, except that for the 2.2D H-pile, the scale ranges from -0.3 to 0.3 inches.

Table 5-11. H-Pile String Potentiometers for Wall Displacement at Peak Loads

H-Pile	String Potentiometer	Wall Displacement [in]	Pile Head Deflection [in]
4.5D	SP 34	0.18	2.84
3.2D	SP 34	0.11	2.95
2.5D	SP 34	0.27	2.19
2.2D	SP 34	0.08	1.98

Table 5-12. Transverse Distance from Nearest Panel Joint to Center of H-Pile

H-pile	Pile Behind Joint or Panel Center?	Transverse Distance from Nearest Panel Joint to Pile Center (looking at front of wall)
4.5D	Joint	5" Right
3.2D	Panel Center	52" Left
2.5D	Joint	5" Right
2.2D	Panel Center	52" Left

Table 5-13. H-Pile Shape Array Transverse Distances

	Shape Array #	Transverse Distance [in]	Direction
4.5D H-pile	45104	6	Right
	45112	25	Right
	45134	53	Right
	45115	93.5	Right
3.2D H-pile	45134	11	Left
	45115	29.5	Right
	45112	67.5	Right
	45104	98.5	Left
2.5D H-pile	45112	0	Center
	45104	31	Right
	45134	56	Right
	45115	94.5	Right
2.2D H-pile	45134	0	Center
	45104	25	Left
	45112	56	Left
	45115	83	Left

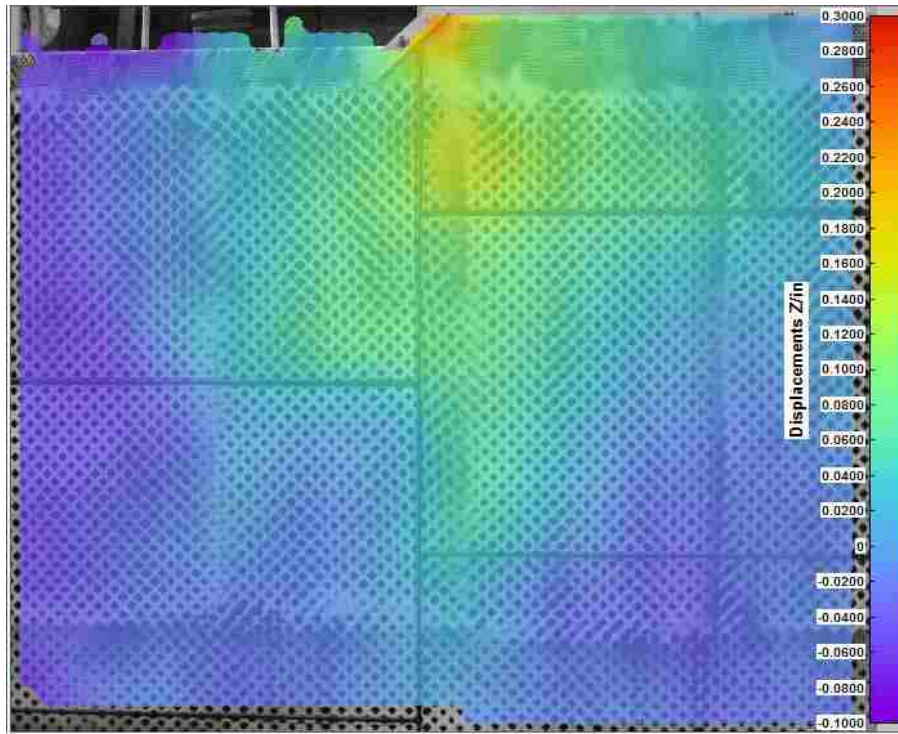


Figure 5-53. DIC wall displacement for the 4.5D H-pile at the 44.1 kip and 3" load increment.

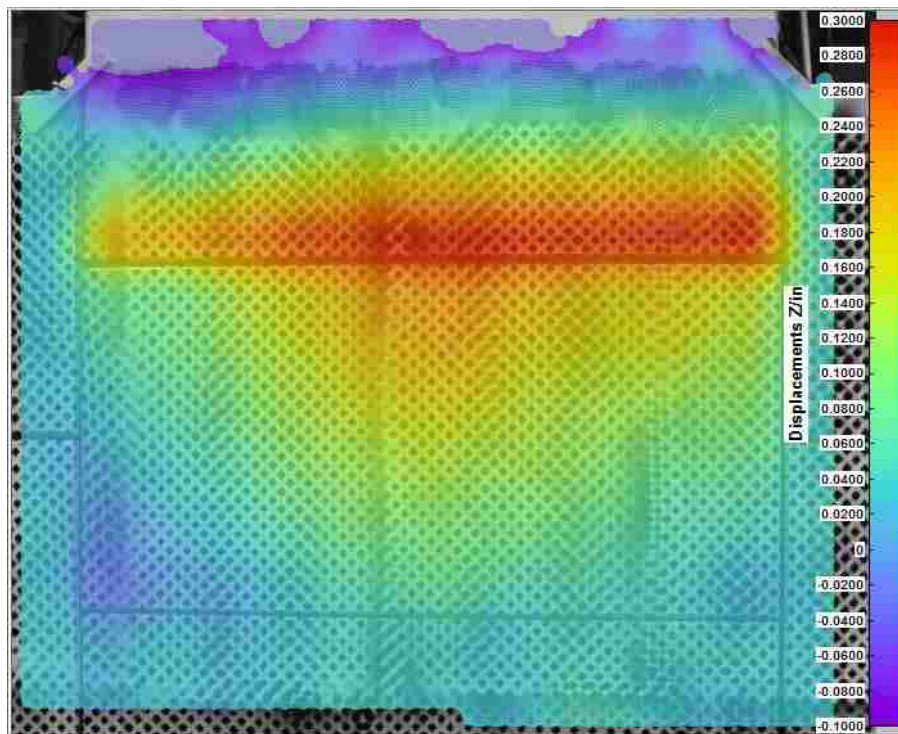


Figure 5-54. DIC wall displacement for the 3.2D H-pile at the 43.8 kip and 3" load increment.

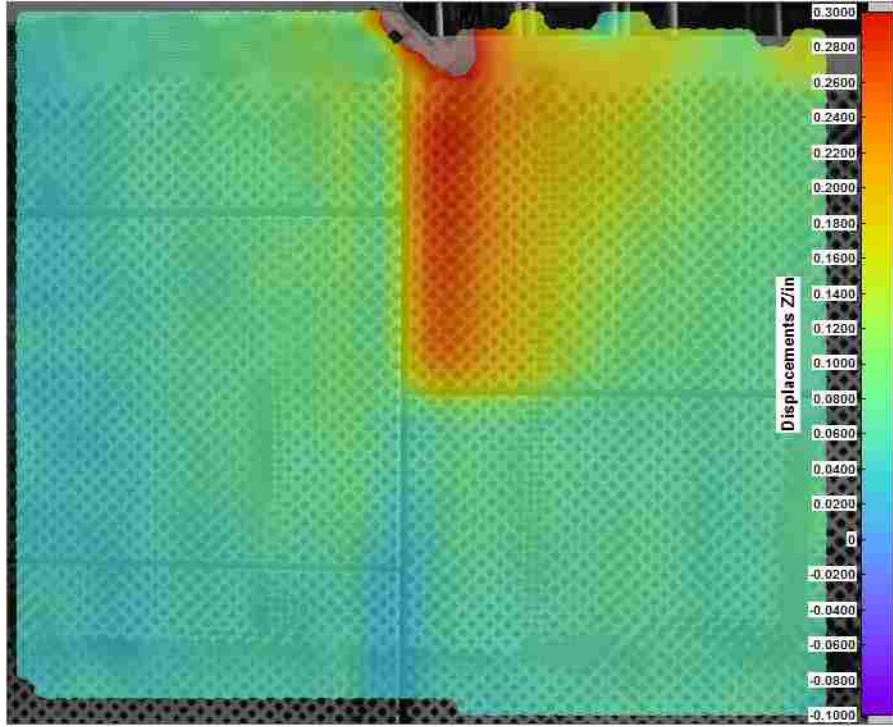


Figure 5-55. DIC wall displacement for the 2.5D H-pile at the 30.4 kip and 2.25" load increment.

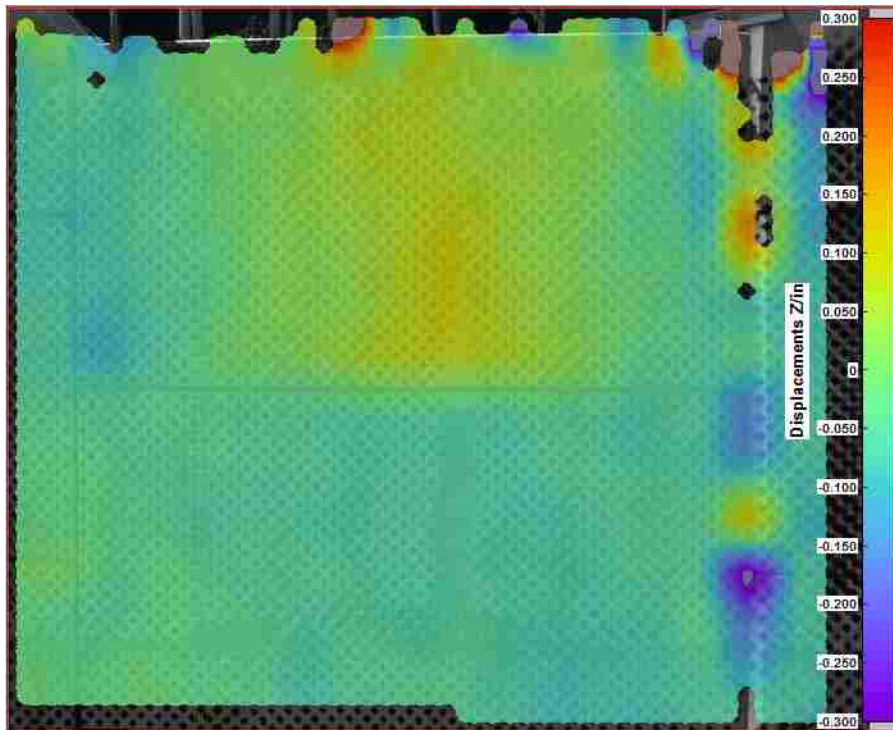


Figure 5-56. DIC wall displacement for the 2.2D H-pile at the 37.8 kip and 2" load increment.

The DIC images show the total z displacement (movement normal in a direction parallel to the ground). To ensure accurate readings, two data points were measured at the bottom left and bottom right of the DIC images where assumptions are made that wall displacements are zero. This is because of the minimal effect of the pile loading the farther the point of interest is from the top of the wall where the pile is located. The points were not zero, but the average of these points was taken and subtracted from all of the other points as a way to zero out the displacements.

The wall displacement is generally greatest along the length of the pile. The 4.5D H-pile and 2.5D H-pile are located roughly along vertical joints of the wall panels. The other H-piles are in the middle of their respective wall panels, however the top wall panel for the 3.2D H-pile test only has one level of reinforcements (two strips total on this panel) because the soil only extended to the mid-height of the wall panel and the panel extend about 2.5 feet above the top of the backfill soil. This is because the H-piles were tested during Phase 1 of the project when the soil only extended to a height of 15 ft.

Lower wall displacements are shown for the tests on the 4.5D and 2.2D H-piles; the wall deflected about 0.10-0.15 inches. However, the 2.2D H-pile is showing the 2" pile displacement. The higher wall displacements occur in the 3.2D and 2.5D H-piles; where the wall deflects about 0.30 inches. For the 2.5 H-pile, the high wall displacement occurs along the length of the pile, but only in the upper panel and on one side of the joint. Displacement does not always transfer smoothly across the joint, particularly if a pile is slightly offset from the joint. Nonetheless, wall displacements are still within acceptable ranges. Generally, the wall displacements are higher on the upper panels until there is a break from the panel joints.

Displacement patterns for the test on 3.2D H-pile are interesting in that the maximum wall deflection occurs along the horizontal joint at the base of the top wall panel. This is likely a result

of the fact that the top wall panel is only restrained by one level of reinforcements and the wall begins to rotate outward at the base. In this case, better performance would have been achieved if wall panels had been cast to a height of 7.5 feet so that three levels of reinforcement were present near the top of the wall preventing wall rotation. In general, the DIC images show that the closer the pile is to the wall, the more wall deflection will occur. Also, the maximum wall deflections occur along the joints of the concrete wall panels that were in front of the pile being loaded laterally.

Using the DIC data, wall deflections were obtained throughout the duration of the pile loading at the ribbed strip locations identified in Table 4-3. These reinforcements were the same reinforcements instrumented for the analysis described in Section 5.2, and the explanation of the layers and the transverse distance location in relation to the center of the pile is explained in Section 4.3.1. Figure 5-57, Figure 5-58, Figure 5-59, and Figure 5-60 show the wall deflections at the reinforcement locations versus the one-minute pile head load for H-piles 4.5D, 3.2D, 2.5D, and 2.2D respectively. Also shown in the figures is the displacement at the top of the wall obtained from the string potentiometers nearest the edge of the wall. Generally, the highest wall displacement occurred at the top of the wall and decreased as the depth increased.

Generally, wall displacement is more affected by transverse distance from the center of the pile as opposed to proximity to the top of the wall (at least for approximately the first 4-5 feet). The 3.2D H-pile shows the highest reinforcement displacement and the 2.2D H-pile shows the lowest. Again, the lower values of the 2.2D H-pile may be explained by the data not being analyzed beyond two inches of pile displacement.

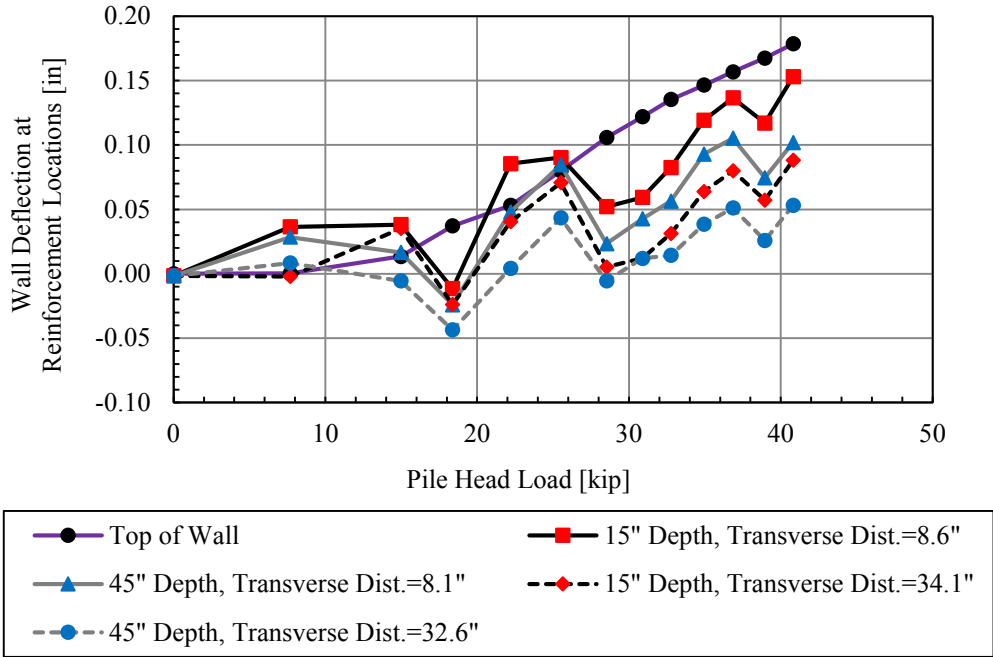


Figure 5-57. Wall deflection at reinforcement locations and top of wall versus pile head load, 4.5D H-pile.

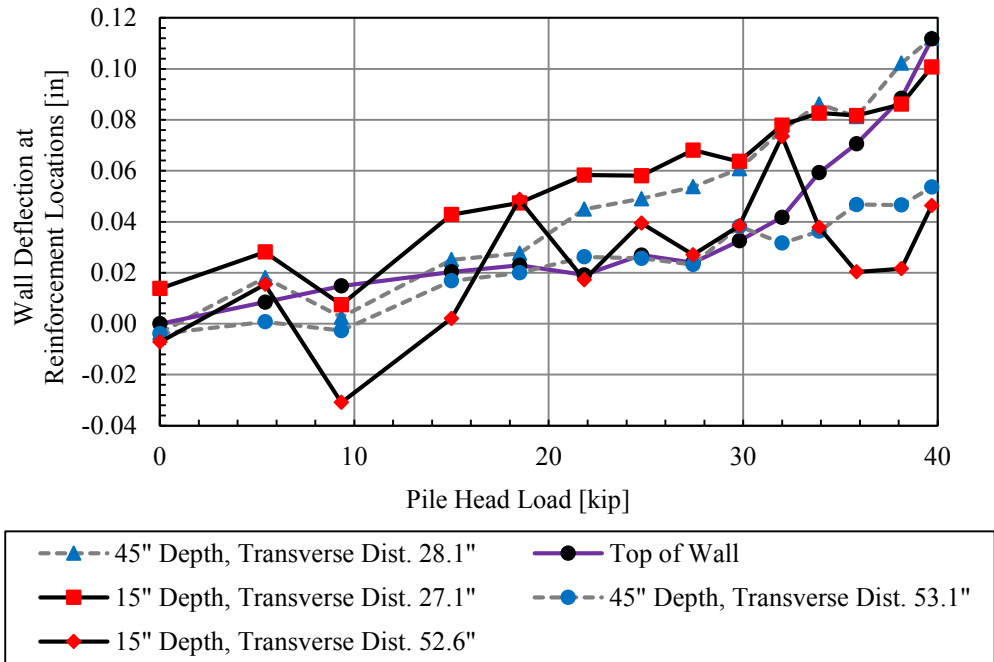


Figure 5-58. Wall deflection at reinforcement locations and top of wall versus pile head load , 3.2D H-pile.

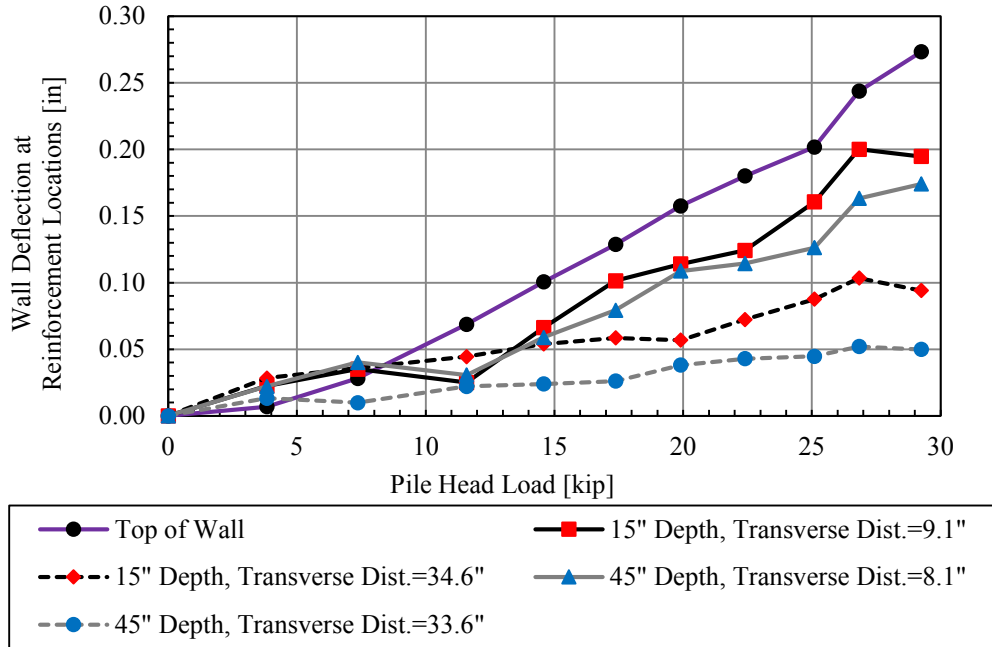


Figure 5-59. Wall deflection at reinforcement locations and top of wall versus pile head load , 2.5D H-pile.

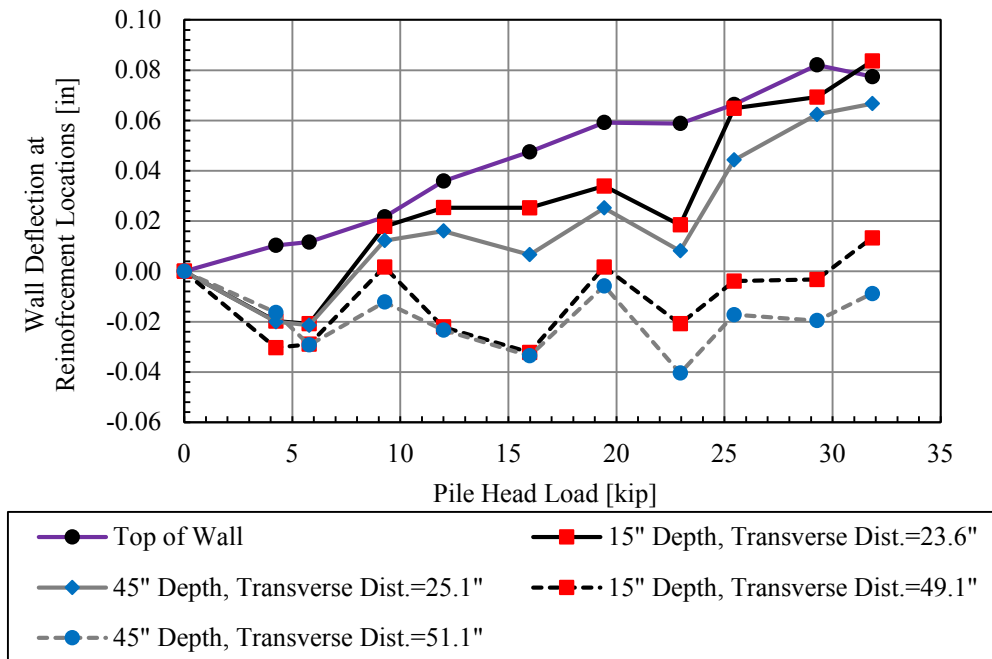


Figure 5-60. Wall deflection at reinforcement locations and top of wall versus pile head load, 2.2D H-pile.

The string potentiometer measurements from Table 5-11 were plotted against the shape array (SAA) wall deflections instrumented closest to the pile along the depth of the wall. The shape array identifications are in Table 5-13. When the shape array closest to the pile was not in front of the pile, DIC wall displacements were obtained both directly in front of the pile and directly in front of the shape array for comparison. These comparisons are shown in Figure 5-61, Figure 5-62, Figure 5-63, and Figure 5-64. The DIC data does not always go to a depth of 0 feet owing to the difficulty of obtaining data near the boundary of the DIC images. Typically, the shape arrays yielded the higher displacements, and the highest shape array wall displacement occurred for the H-pile located closest to the wall. Although the DIC and shape array readings at similar spacing were not aligned, the DIC reading directly in front of the pile near the top of the wall lines up close to the string potentiometer readings, with the exception of the 3.2D H-pile. This may be because the panel rotated backwards for that pile, and thus gave low and even negative values for the DIC data. There seems to be agreement with what was stated previously, in that below the first panel joint the wall displacements decrease.

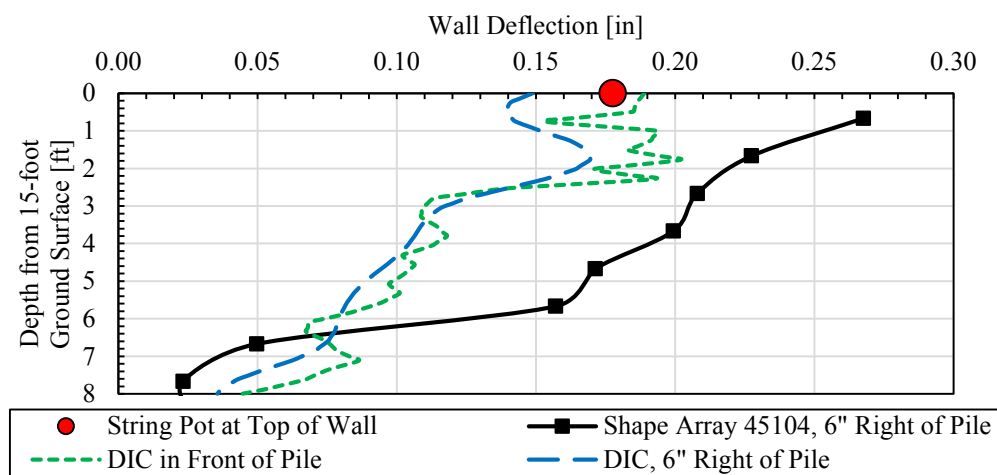


Figure 5-61. Depth from the 15-foot ground surface versus peak wall displacement at the 3” load increment for 4.5D H-pile.

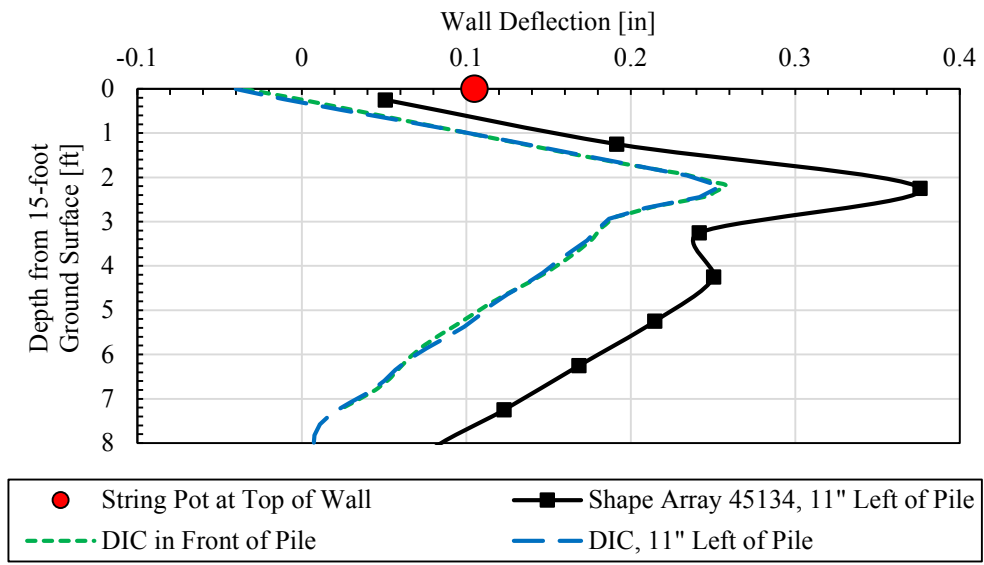


Figure 5-62. Depth from the 15-foot ground surface versus peak wall displacement at the 3” load increment for 3.2D H-pile.

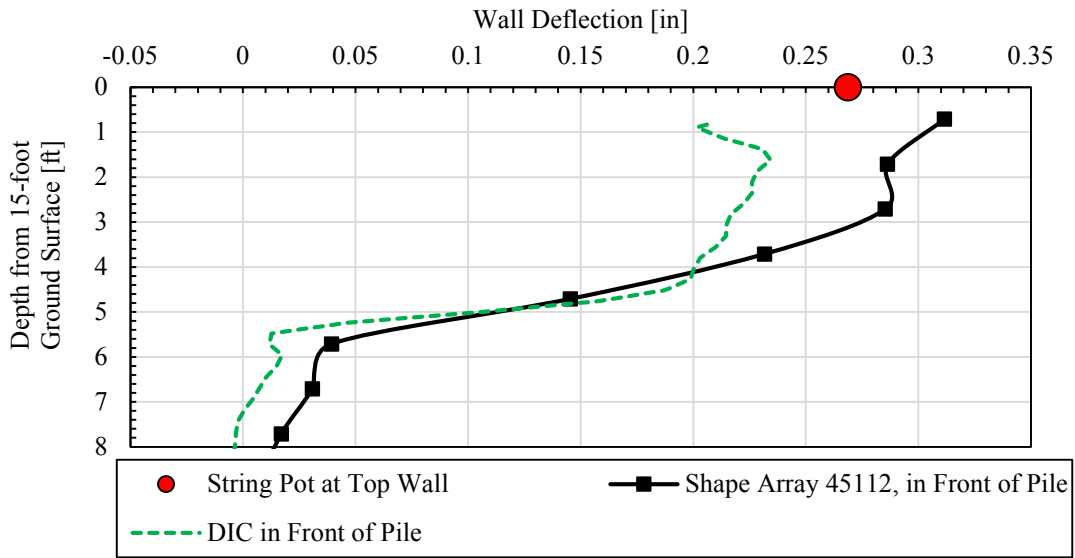


Figure 5-63. Depth from the 15-foot ground surface versus peak wall displacement at the 2.25” load increment for 2.5D H-pile.

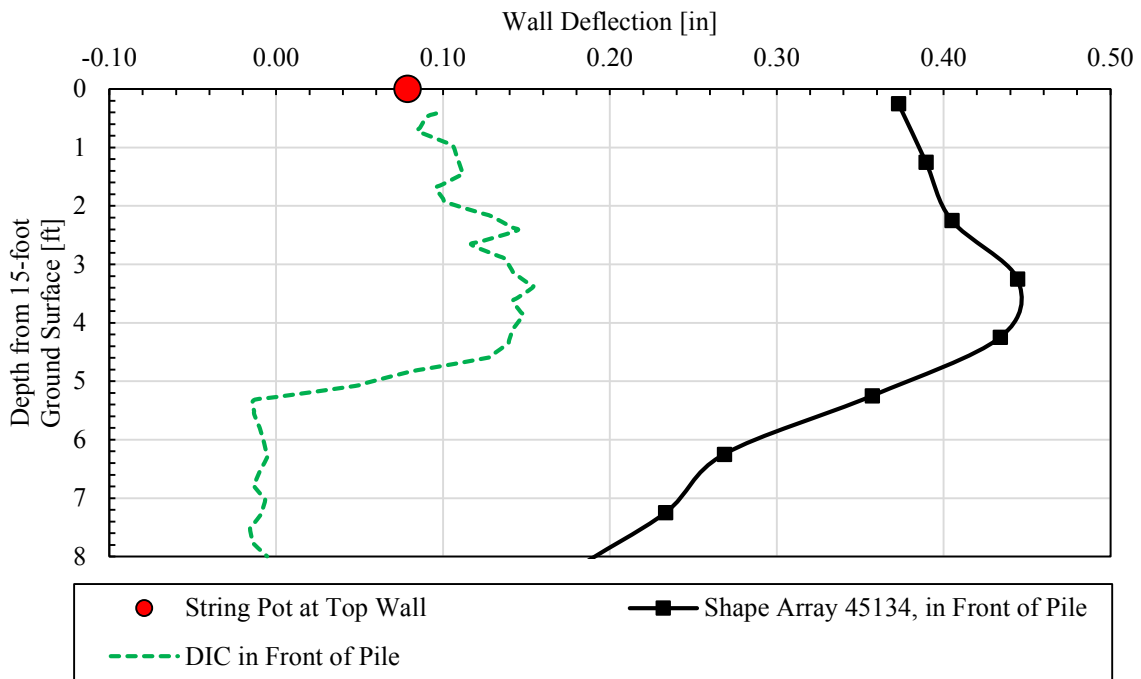


Figure 5-64. Depth from the 15-foot ground surface versus peak wall displacement at the 2” load increment for 2.2D H-pile.

Figure 5-65, Figure 5-66, Figure 5-67, and Figure 5-68 are the wall displacements of all of the shape arrays with their respective H-piles. For the most part, the farther the shape array is located transversely from the pile, the lower the wall displacements are. It is interesting to note that shape arrays 45104 and 45112 for H-piles 3.2D and 2.2D show very low displacements probably owing to the fact that these shape arrays were behind different concrete panels at the time of testing.

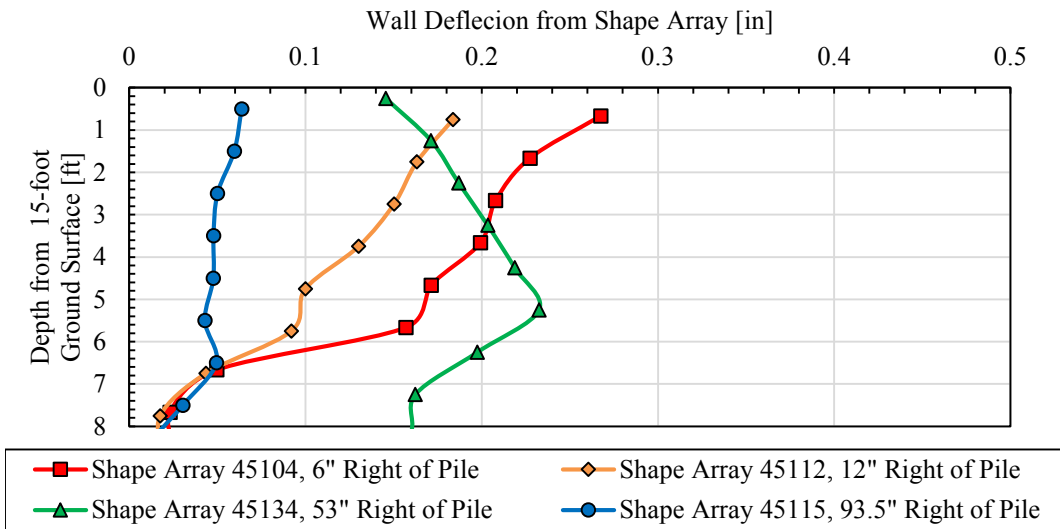


Figure 5-65. Depth from the 15-foot ground surface versus wall deflection from shape array for 3" load increment, 4.5D H-pile.

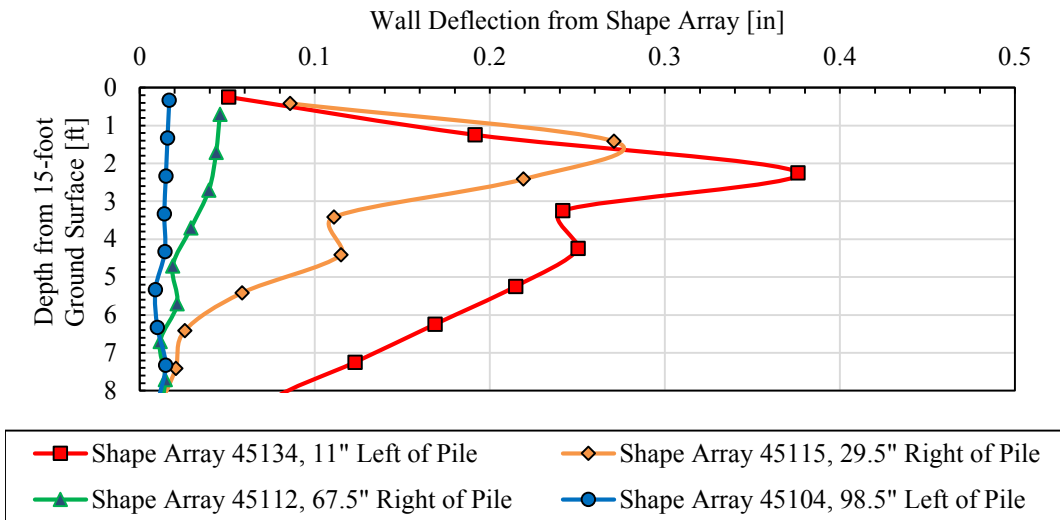


Figure 5-66. Depth from the 15-foot ground surface versus wall deflection from shape array for 3" load increment, 3.2D H-pile.

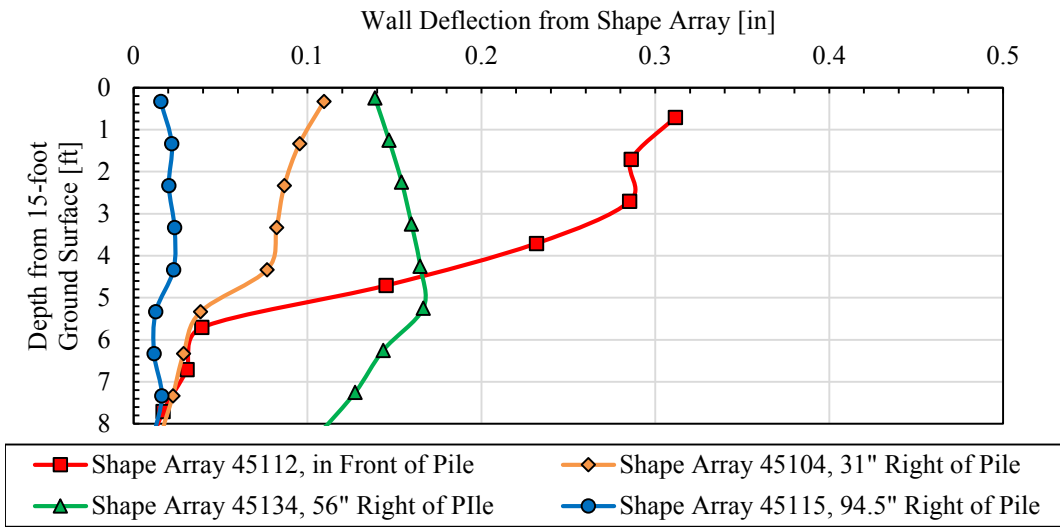


Figure 5-67. Depth from the 15-foot ground surface versus wall deflection from shape array for 2.25" load increment, 2.5D H-pile.

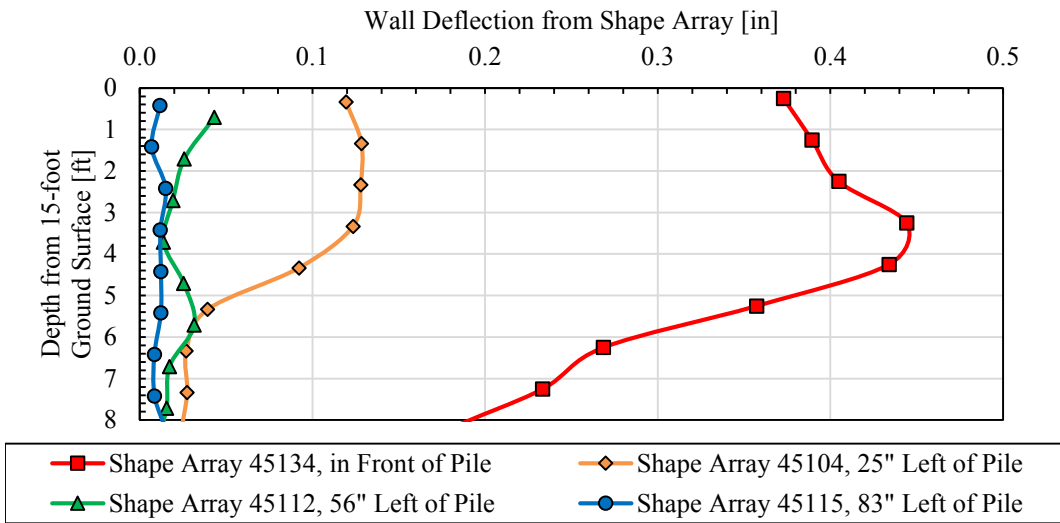


Figure 5-68. Depth from the 15-foot ground surface versus wall deflection from shape array for 2" load increment, 2.2D H-pile.

5.5.2 Square Piles

Wall displacement was also recorded by the use of DIC, shape arrays, and the string potentiometers located nearest the top of the wall for the square piles similar to that of the H-piles. Table 5-14 shows which string potentiometers were used with their respective piles during lateral loading, along with the associated peak pile head displacement and wall displacement. Table 5-15 shows the distance from the panel joint to the center of the pile. Table 5-16 shows the transverse distance of the shape arrays from the pile center for their respective piles. However, much of the shape array data for the peak displacement was not able to be obtained and the table makes mention of which shape arrays that pertained to. The direction of left or right of the pile is taken from looking at the front side of the MSE wall (North).

Figure 5-69, Figure 5-70, Figure 5-71, and Figure 5-72 show color fringe contours of longitudinal displacement overlain across a graphic image of the MSE wall obtained from DIC for the 3" pile displacement for all of the square piles. The scales range from -0.1 to 0.6 inches, except that for the 2.1D square pile, it ranges from -0.2 to 0.8 inches.

Table 5-14. Square Pile String Potentiometers for Wall Displacement at Peak Loads

Square Pile	String Potentiometer	Wall Displacement [in]	Pile Head Deflection [in]
5.7D	SP 35	0.36	3.00
4.2D	SP 34	0.24	2.98
3.1D	SP 38	0.38	3.02
2.1D	SP 32	0.73	2.98

Table 5-15. Transverse Distance from Nearest Panel Joint to Center of Square Pile

Square pile	Pile Behind Joint or Panel Center?	Transverse Distance from Nearest Panel Joint to Pile Center (looking at front of wall)
5.7D	Joint	3" Left
4.2D	Panel Center	53" Left
3.1D	Joint	3" Right
2.1D	Panel Center	57" Right

Table 5-16. Square Pile Shape Array Transverse Distances

	Shape Array #	Transverse Distance [in]	Direction	Valid Data Obtained for Peak?
5.7D Square	45134	4	Right	Yes
	45104	29.5	Left	No
	45115	65.5	Left	No
	45112	88	Left	Yes
4.2D Square	45115	10	Left	No
	45112	32.5	Left	Yes
	45134	64	Left	Yes
	45104	94	Left	No
3.1D Square	45134	4	Left	No
	45104	34	Left	No
	45115	56	Left	No
	45112	98	Left	No
2. 1D Square	45115	13.5	Right	Yes
	45112	28.5	Left	Yes
	45104	35.5	Right	No
	45134	65.5	Right	Yes

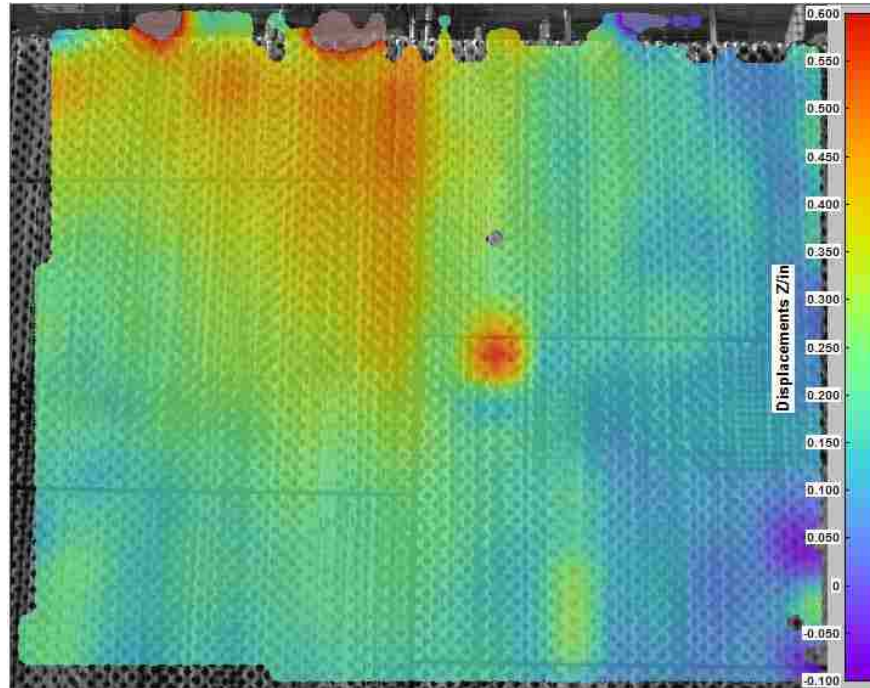


Figure 5-69. DIC wall displacement for the 5.7D square pile at the 51.9 kip and 3" load increment.

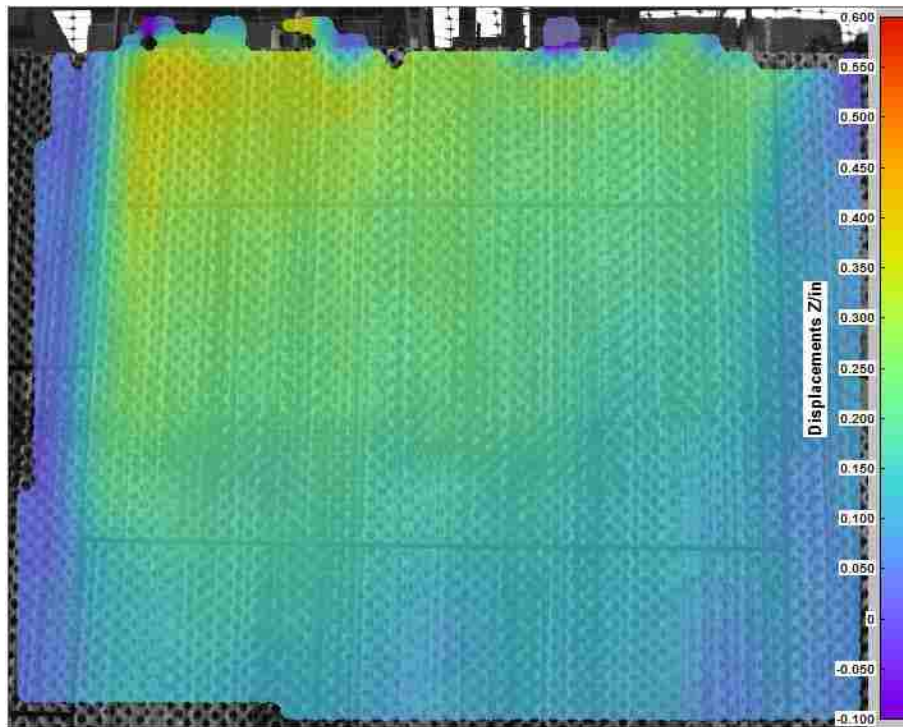


Figure 5-70. DIC wall displacement for the 4.2D square pile at the 46.4 kip and 3" load increment.

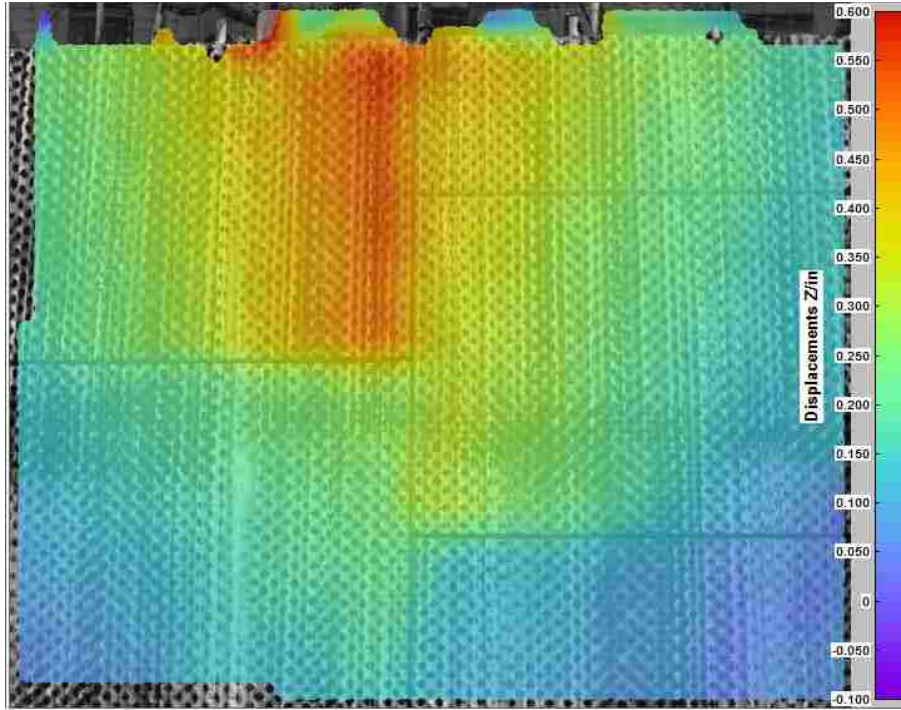


Figure 5-71. DIC wall displacement for the 3.1D square pile at the 42.6 kip and 3" load increment.

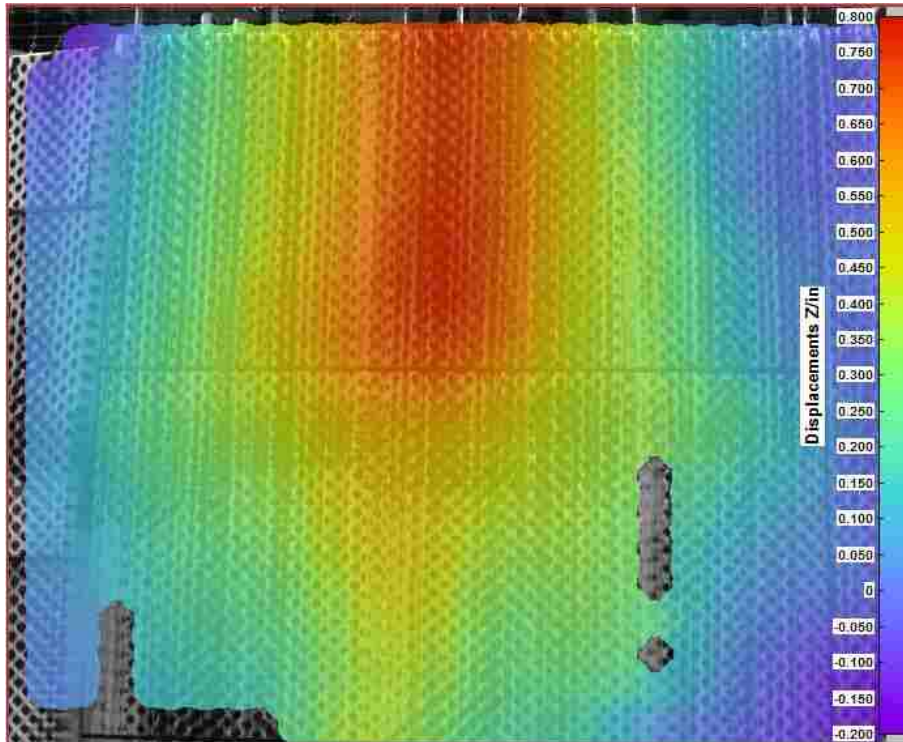


Figure 5-72. DIC wall displacement for the 2.1D square pile at the 40.1 kip and 3" load increment.

The DIC images show the total z displacement (movement normal in a direction parallel to the ground). To ensure accurate readings, two data points were measured at the bottom left and bottom right of the DIC images where assumptions are made that wall displacements are zero. This is because of the minimal effect of the pile loading the farther the point of interest is from the top of the wall where the pile is located. The points were not zero, but the average of these points was taken and subtracted from all of the other points as a way to zero out the displacements.

As expected, the highest wall displacements occur closer to the top of the wall and also along the length of the pile. The 5.7D square pile lateral load test displaces the wall over 0.5 inches while the 4.2D square pile lateral load test displaces the wall about 0.4 inches. The 3.1D square pile test displaces the wall the most at 0.6 inches. This is expected, owing to this pile being closer to the wall than the other two piles. It is interesting to note that for the 4.2D square pile test, the displacement spreads out thinner than the other load tests. This might be because the concrete wall panel is actually about 7.5 feet in height and thus there are no panel joints to keep the wall displacement from being more concentrated. The high displacement spot in the 5.7D square pile test seems to be erroneous.

Using the DIC data, wall deflections were obtained during the duration of the pile loading at the welded wire reinforcement locations using Table 4-4. These reinforcements were the same reinforcements instrumented for the analysis described in Section 5.2, and the explanation of the layers and the transverse distance location in relation to the center of the pile is explained in Section 4.3.1. Figure 5-73, Figure 5-74, Figure 5-75, and Figure 5-76 show the wall deflection at the reinforcement locations versus the one-minute pile head load for square piles 5.7D, 4.2D, 3.1D, and 2.1D respectively. The figures also include the wall deflection at the top of the wall obtained from the string potentiometers nearest the edge of the wall during the lateral load test. This is

included in the other square pile load tests as well. Generally, the highest wall displacement happened at the top of the wall and decreases as the depth increases. The displacements are also generally higher for the reinforcements closer to the pile as well as for when the pile is closer to the wall. The 5.7D square pile has extra reinforcement data in the third and fourth layers. The reinforcement in the third layer has the lowest wall displacement as expected, but the fourth layer displacement is an exception and has relatively higher displacement. This may be due to the fact that there is an erroneous high displacement spot around that reinforcement location.

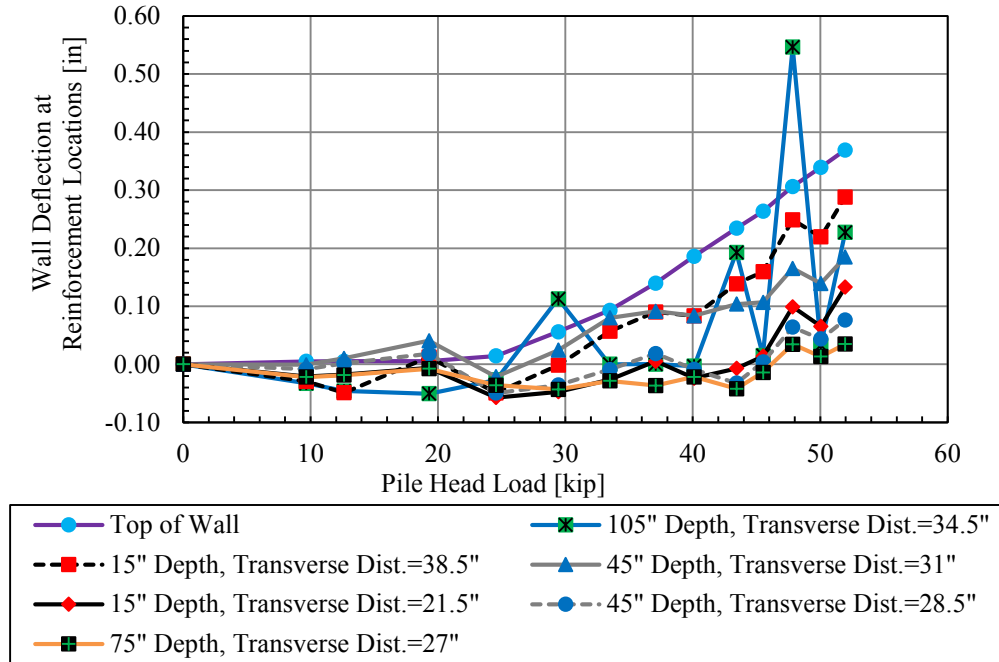


Figure 5-73. Wall deflection at reinforcement locations and top of wall versus pile head load, 5.7D square pile.

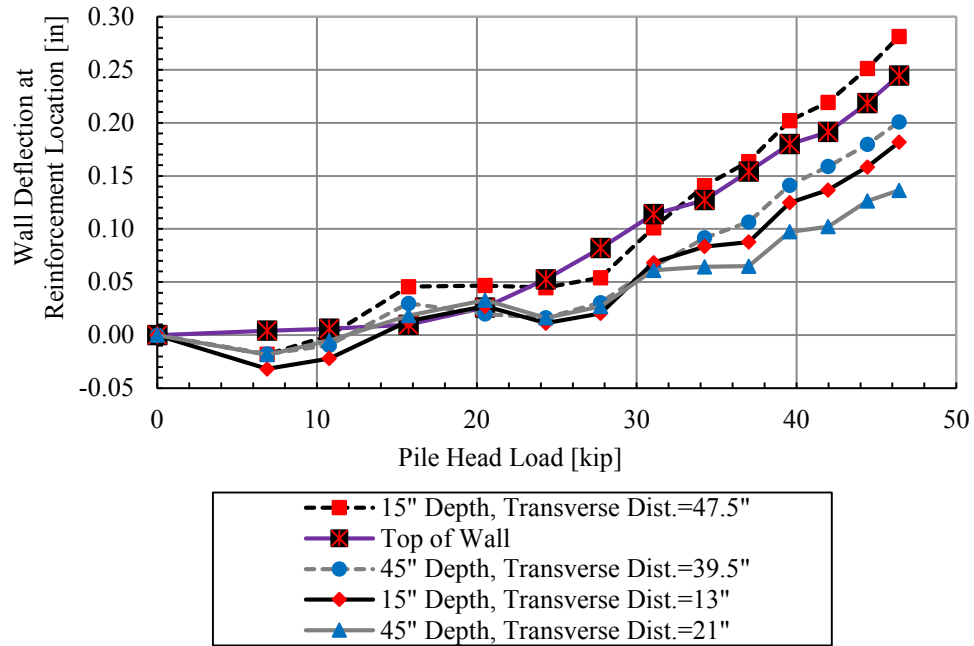


Figure 5-74. Wall deflection at reinforcement locations and top of wall versus pile head load, 4.2D square pile.

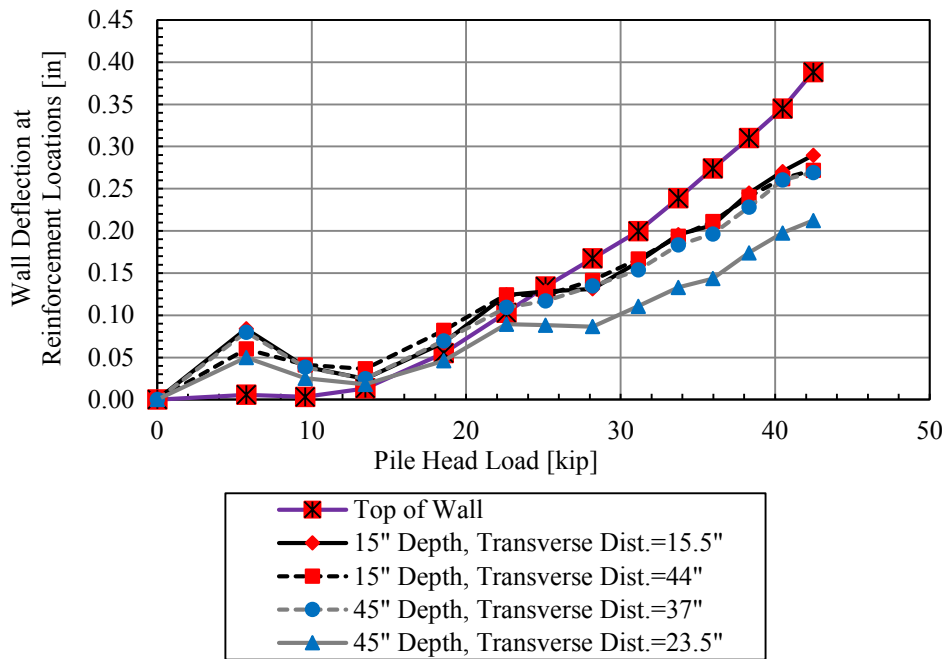


Figure 5-75. Wall deflection at reinforcement locations and top of wall versus pile head load, 3.1D square pile.

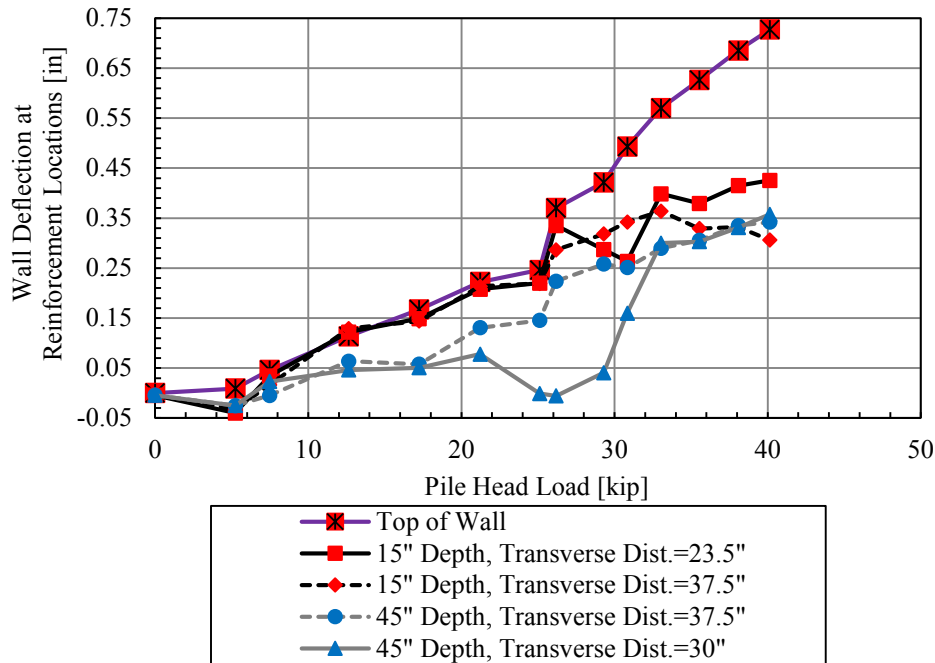


Figure 5-76. Wall deflection at top of wall versus pile head load, 2.1D square pile.

The string potentiometer measurements from Table 5-14 were plotted against the shape array (SAA) wall deflections instrumented closest to the pile along the depth of the wall. The shape array identifications are in Table 5-16. DIC peak wall displacements were obtained for both directly in front of the pile and directly in front of the shape array for comparison, since the shape array was not directly in front of the pile. Figure 5-77 shows the data for the 5.7D square pile. The shape array data was invalid for square pile 4.2D, and thus no shape array data is used for comparison, which is shown in Figure 5-78. For square pile 3.1D in Figure 5-79, the shape array data for the five-minute load hold was used because the peak shape array data was unavailable. Figure 5-80 shows the data for the 2.1D square pile.

It can be seen that the DIC data increases in wall deflection towards the top of the wall. The DIC data does not always go to a depth of 0 feet owing to the difficulty of obtaining data near the boundary of the DIC images. However, the curves generally line up with the string potentiometer

reading at the top of the wall. The shape array curve for the 3.1D square pile is unusually high. The string potentiometer reading for the 2.1D square pile is very high comparatively (around 0.7 inches). The string potentiometer at this pile is also not agreeable with the shape array curve, however the DIC curve does line up with the string potentiometer. DIC curves did not line up with the shape array curves. Shape array data did not always yield consistent results, and thus there could have been a problem in instrumentation or in their operation.

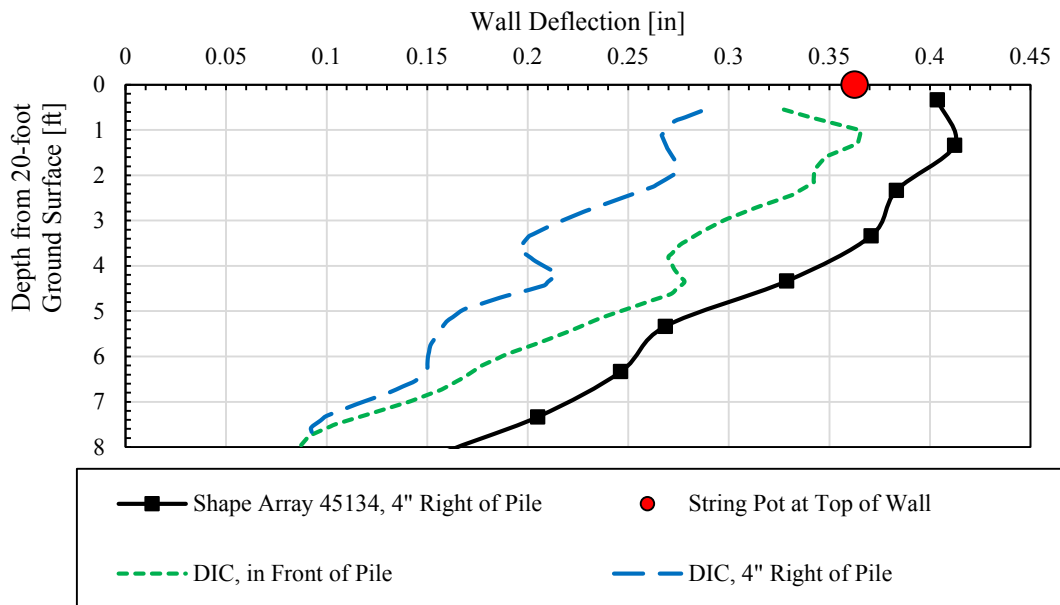


Figure 5-77. Depth from the 20-foot ground surface versus wall deflection from shape array for 3" load increment, 5.7D square pile.

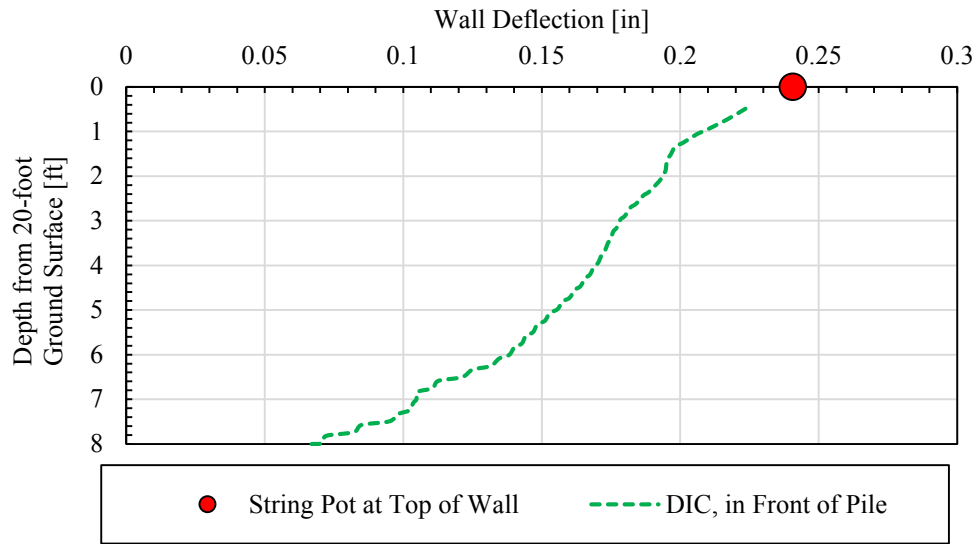


Figure 5-78. Depth from the 20-foot ground surface versus wall deflection from shape array for 3" load increment, 4.2D square pile.

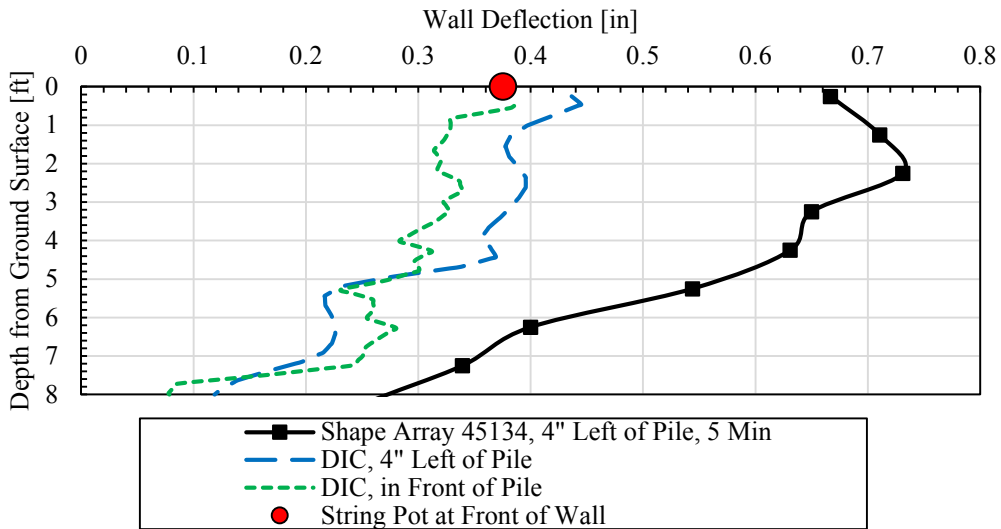


Figure 5-79. Depth from the 20-foot ground surface versus wall deflection from shape array for 3" load increment, 3.1D square pile

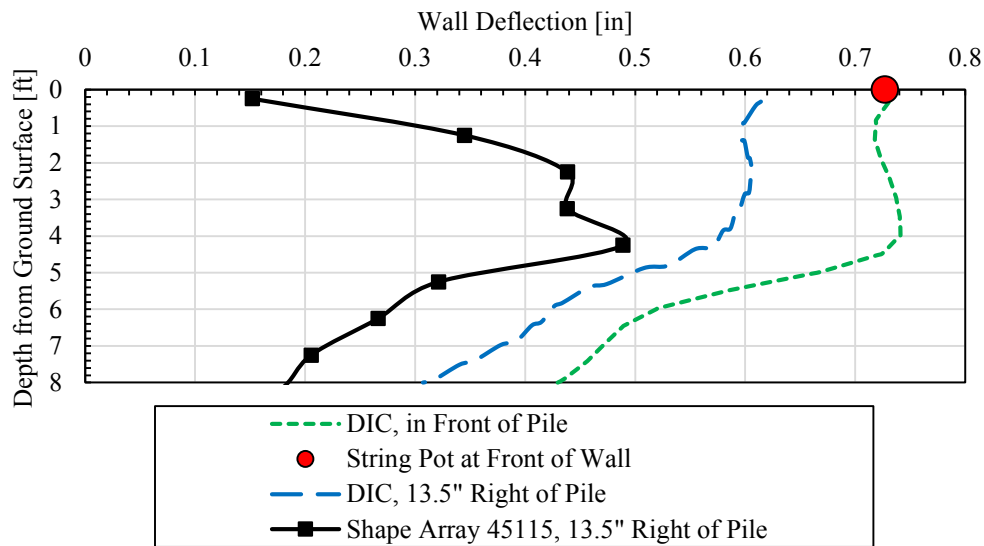


Figure 5-80. Depth from the 20-foot ground surface versus wall deflection from shape array for 3” load increment, 2.1D square pile.

Figure 5-81, Figure 5-82, Figure 5-83, and Figure 5-84 are the wall displacements of all of the shape arrays that were able to yield valid data. The shape arrays shown for the 4.2D square pile yielded very low displacements. Accurate results were not able to be obtained from the shape array data for the peak wall displacements, and thus for the 3.1D square pile, the five-minute load hold shape array wall displacements were used. For this square pile load, Shape Array 45112 yielded results similar to that of the DIC and string potentiometer (about 0.4 inches). This shape array was about 98” to the left of the pile. During construction, shape arrays did not always stay up tight against the wall, and thus soil often fell in between the cracks. This in turn would not give reasonable data. For the 2.1D square pile loading, Shape Array 45112 (28.5” left of the pile) yielded closer results to the string potentiometer (0.7 inches).

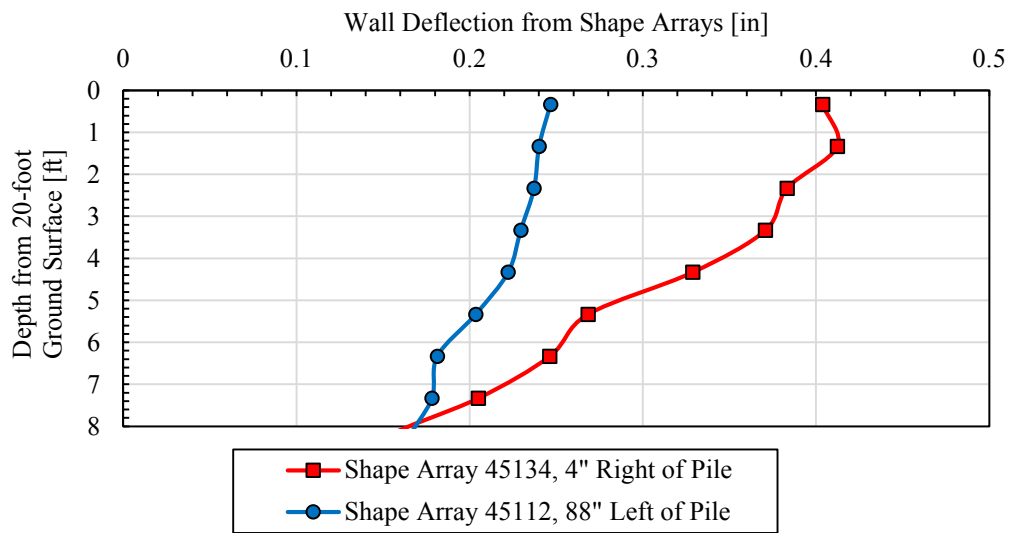


Figure 5-81. Depth from the 20-foot ground surface versus wall deflection from shape array for 3" load increment, 5.7D square pile.

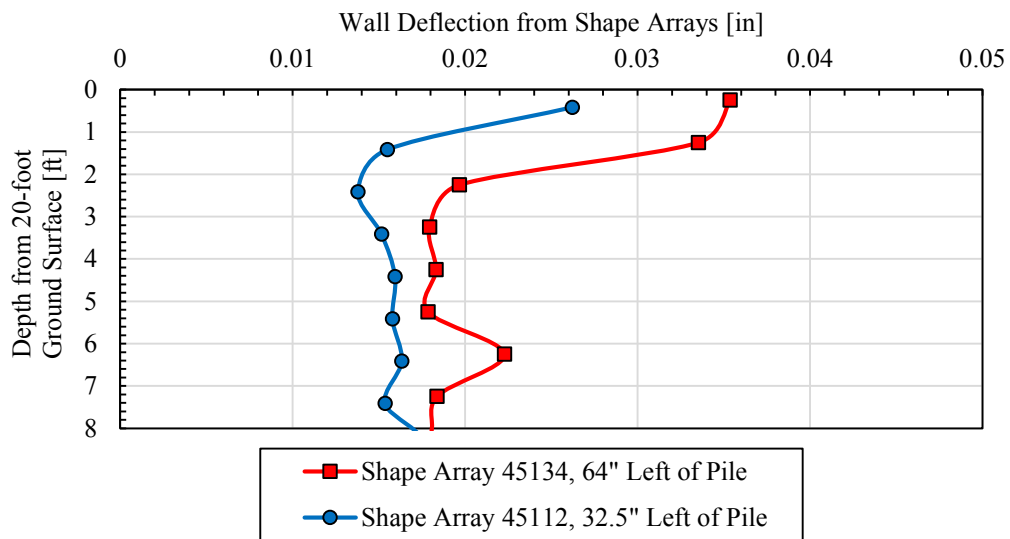


Figure 5-82. Depth from the 20-foot ground surface versus wall deflection from shape array for 3" load increment, 4.2 square pile.

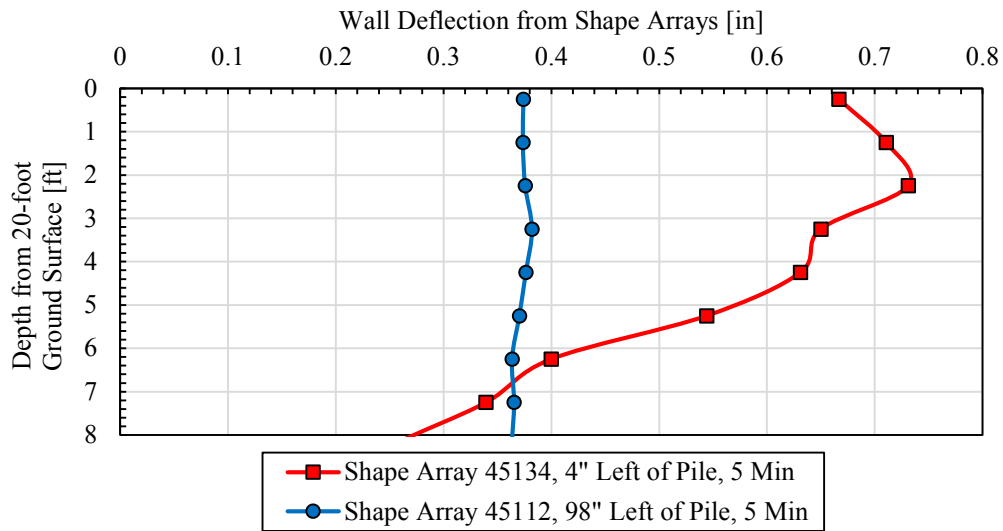


Figure 5-83. Depth from the 20-foot ground surface versus wall deflection from shape array for 3” load increment at 5-minute hold, 3.1D square pile.

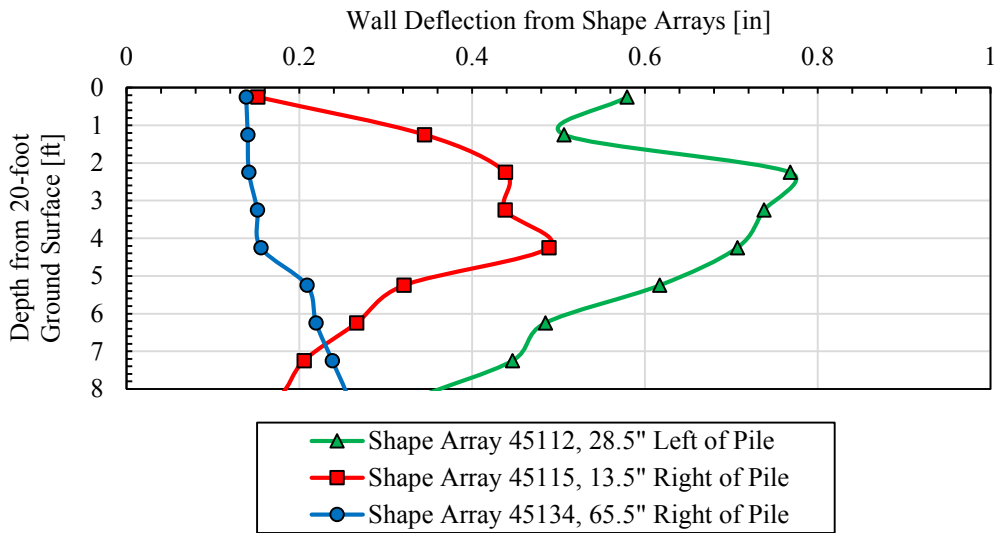


Figure 5-84. Depth from the 20-foot ground surface versus wall deflection from shape array for 3” load increment, 2.1D square pile.

5.6 Bending Moment versus Depth Curves

5.6.1 H-Piles

Plots of bending moment versus depth along the length of the piles were obtained by calculating the bending moment at several depths along the pile; namely 2, 4, 6, 9, 12, 15, and 18 feet relative to the top of the 20-foot backfill (as explained in Section 4.3.2). Thus, relative to the 15-foot ground surface during the testing of the H-piles, these depths correspond to 1, 4, 7, 10, and 13 feet. As also explained previously, the strain gauges were applied to two sides of the pile; one side was where the pile was being loaded, and the other side was directly opposite of the loading. Occasionally some of the strain gauges were damaged and thus the data needed to be omitted from the calculations. The bending moment, M , in kip-inches at any depth was computed using the equation:

$$M = EI\phi = \frac{EI(\mu\varepsilon_t - \mu\varepsilon_c)}{2y} * 10^{-6} \quad (5-13)$$

where M = pile bending moment at the depth of interest (kip-in.)

E = modulus of elasticity (29,000 ksi)

I = moment of inertia of the pile and the angle irons combined (187 in⁴ for H-piles about weak axis, 335 in⁴ for square piles)

ϕ = curvature

$\mu\varepsilon_t$ = micro strain reading of the strain gauge on the tension side

$\mu\epsilon_c$ = micro strain reading of the strain gauge on the compression side, and

y = distance from the neutral axis to the strain gauge (in.).

As shown in Equation (5-13), the small angle approximation method was used. Whenever data from a damaged or malfunctioning strain gauge on the tension side needed to be omitted, the compression side was multiplied by -1 and then that value was subtracted by the actual compression side value. If the compression side needed to be omitted, the tension side value was subtracted by the tension side value multiplied by -1. Owing to the strain gauges being installed with the wrong side of the waterproof wafer against the pile, all of the bending moment values were multiplied by a factor of 3 to obtain the correct value. Strain gauges were laboratory tested (ten tests were conducted) and it was concluded that the incorrect installation underestimated the correct bending moment by a factor of 3. On some of the other piles tested, rotation occurred when the piles were installed. However, for the H-piles, the rotation of the piles was negligible and thus no rotation correction was needed when calculating the moment and the distance between the neutral axis and the strain gauges.

Figure 5-85, Figure 5-86, Figure 5-87, and Figure 5-88 show curves of the bending moment versus depth below the 20-foot ground surface. Although data was taken for all of the load increments, these figures only show the data corresponding to pile deflections of approximately 0.5, one, two, and three inches (three inches only applied to H-piles 4.5D and 3.2D). The maximum moment occurs for the 3.2D H-pile at over 2,600 kip-inches. The maximum measured moment occurs between four feet and seven feet from the ground surface for curves corresponding with the two- to three-inch deflections. Figure 5-89 displays the maximum moment for the 0.5-, 1-, 2-, and 3- inch pile load increments normalized by the respective pile head loads versus the spacing from

the MSE wall normalized by the pile diameter for each of the H-piles. This figure seems to show that piles spaced closer to the wall develop slightly greater bending moment. This is because the closer proximity to the wall weakens the soil resistance for the pile, and thus there is greater induced pile bending moment to some extent.

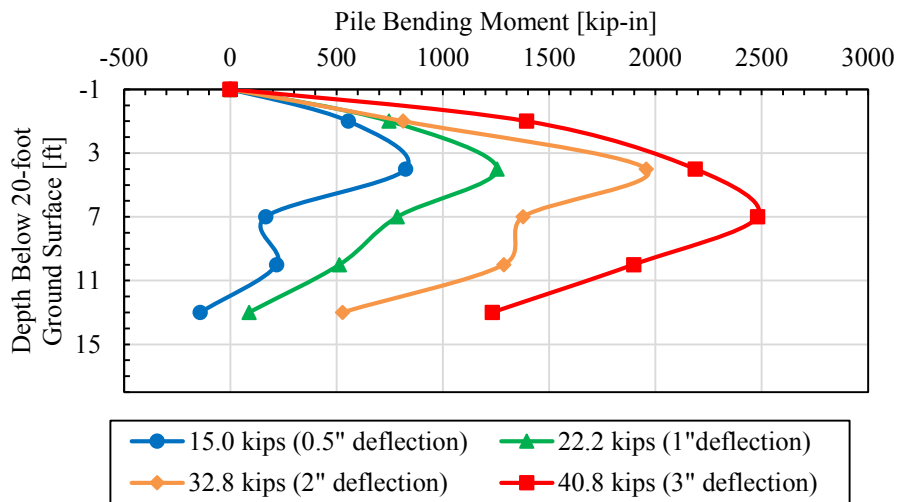


Figure 5-85. Bending moment versus depth curves for four load levels during test of 4.5D H-pile.

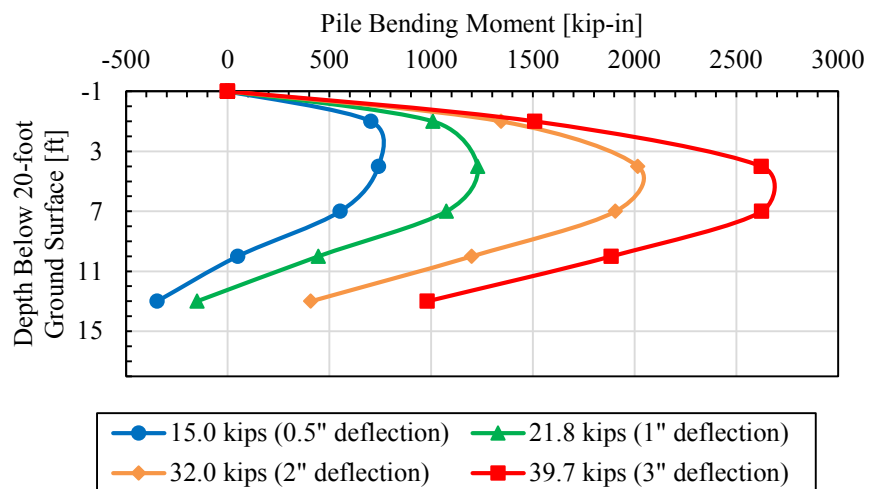


Figure 5-86. Bending moment versus depth curves for four load levels during test of 3.2D H-pile.

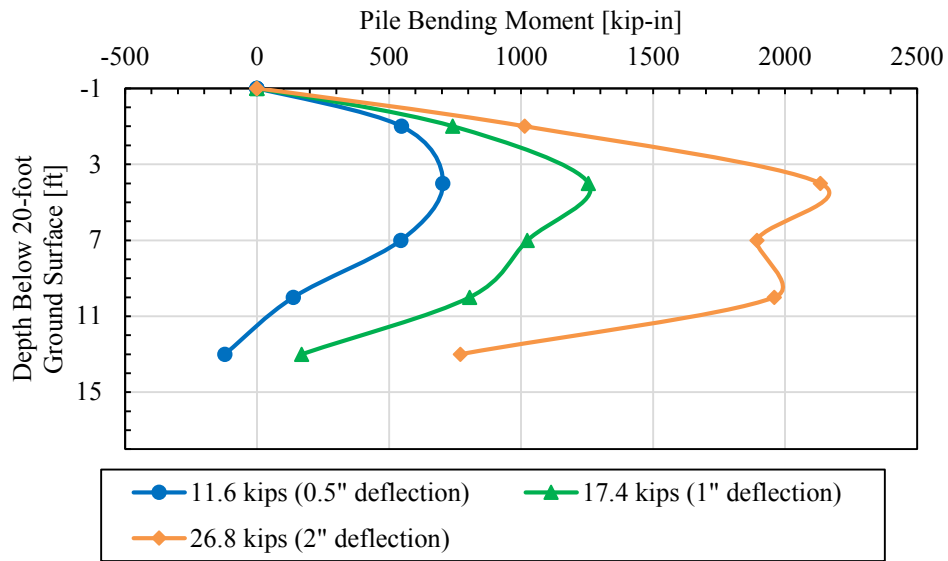


Figure 5-87. Bending moment versus depth curves for three load levels during test of 2.5D H-pile.

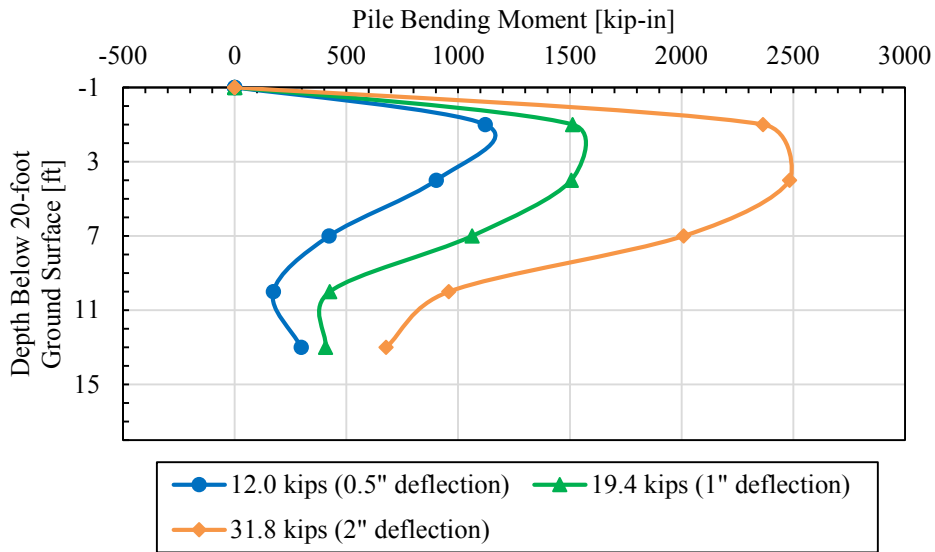


Figure 5-88. Bending moment versus depth curves for three load levels during test of 2.2D H-pile.

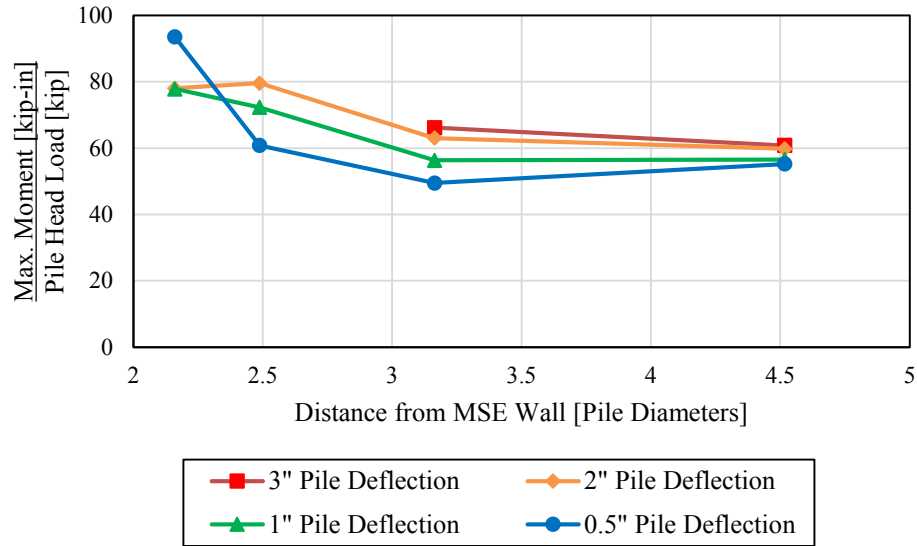


Figure 5-89. Maximum moment corresponding to the 0.5-, 1-, 2-, and 3-inch pile displacement normalized by pile head load versus distance from MSE wall normalized by pile diameter for H-piles.

5.6.2 Square Piles

The performance of the square piles was measured by calculating the bending moment at several depths along the pile; namely 2, 4, 6, 9, 12, 15, and 18 feet from the top of the soil (as explained in section 4.3.2). The strain gauges were instrumented the same as the H-piles, and thus Equation (5-13) also applies to the square piles for calculating bending moment.

Owing to the strain gauges being installed with the wrong side of the waterproof wafer against the pile, all of the bending moment values were multiplied by a factor of 3 to obtain the correct value. Strain gauges were laboratory tested (ten tests were conducted) and it was concluded that the incorrect installation underestimated the correct bending moment by a factor of 3. During installation, the square piles horizontally rotated a few degrees and thus correction was addressed to account for the shortened distance of the neutral axis y by multiplying it by the cosine of the angle of rotation. The angles of rotation were 0, 4, 5, and 5 degrees for the 5.7D, 4.2D, 3.1D, and

2.1D square piles, respectively. Thus, the increase in moment was almost negligible. Figure 5-90 below illustrates a rotated square pile.

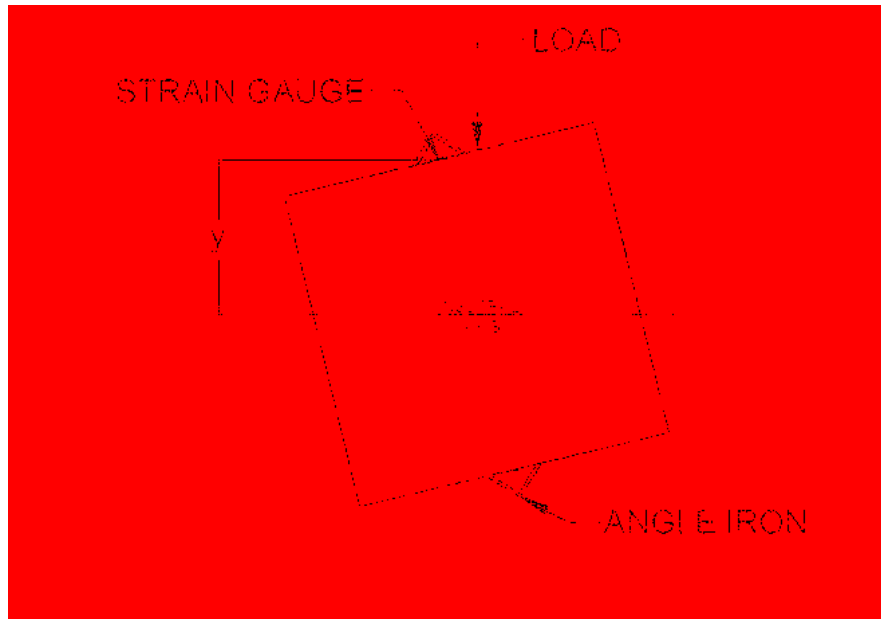


Figure 5-90. Square pile rotation needing correction for calculating pile bending moments.

Figure 5-91, Figure 5-92, Figure 5-93, and Figure 5-94 show the depth below the ground surface versus the pile bending moment deflection. Although data was taken for all the load cycles, the following figures only show the data corresponding to pile deflections of approximately 0.5, one, two, and three inches. The maximum moment occurs for the 3.1D square pile at over 3,400 kip-inches. The maximum measured moment occurs between four feet and six feet from the ground surface for curves corresponding with all of the shown pile deflection curves for all of the square piles except for the 5.7D square pile. This pile's maximum moment occurs at around nine feet below the ground surface. Figure 5-95 displays the maximum moment for the 0.5-, 1-, 2-, and 3-inch pile load increments normalized by the respective pile head loads versus the spacing from the MSE wall normalized by the pile diameter for each of the square piles. With the exception of the

2.1D square pile spacing, this figure shows that piles spaced closer to the wall develop slightly greater bending moment. This is because the closer proximity to the wall weakens the soil resistance for the pile, and thus there is greater induced pile bending moment.

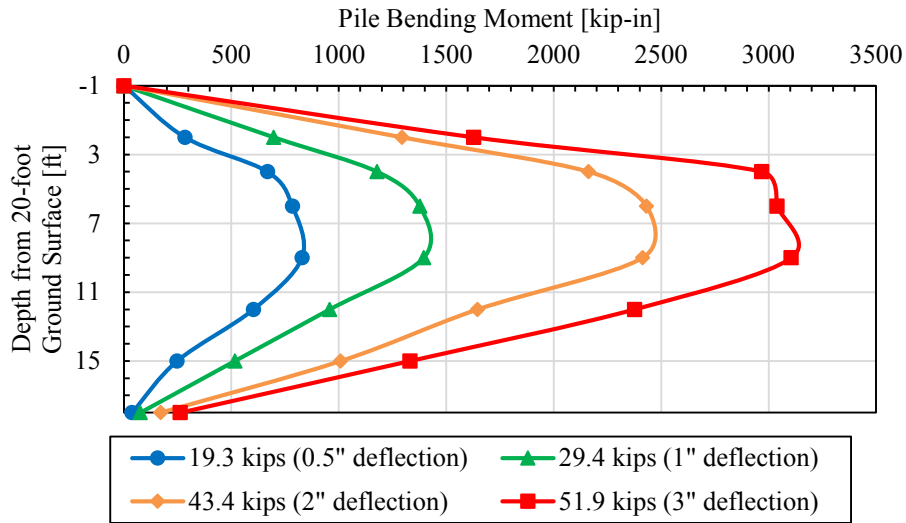


Figure 5-91. Bending moment versus depth curves for four load levels during test of 5.7D square pile.

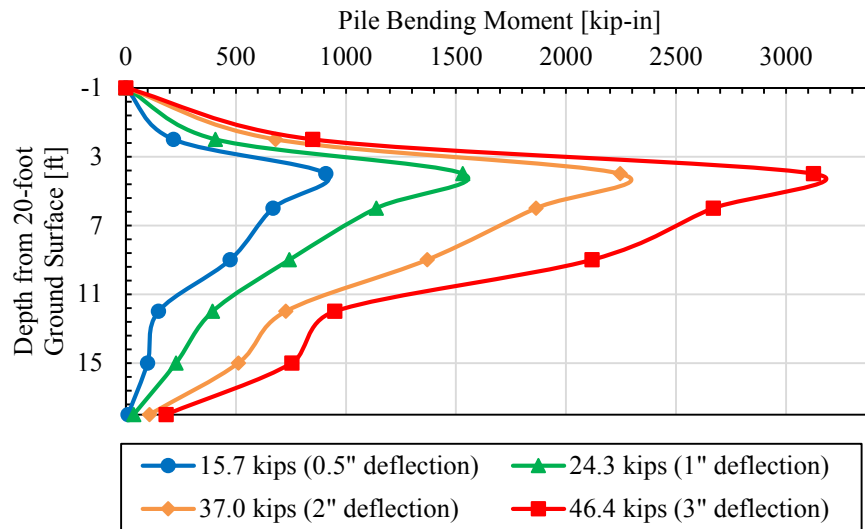


Figure 5-92. Bending moment versus depth curves for four load levels during test of 4.2D square pile.

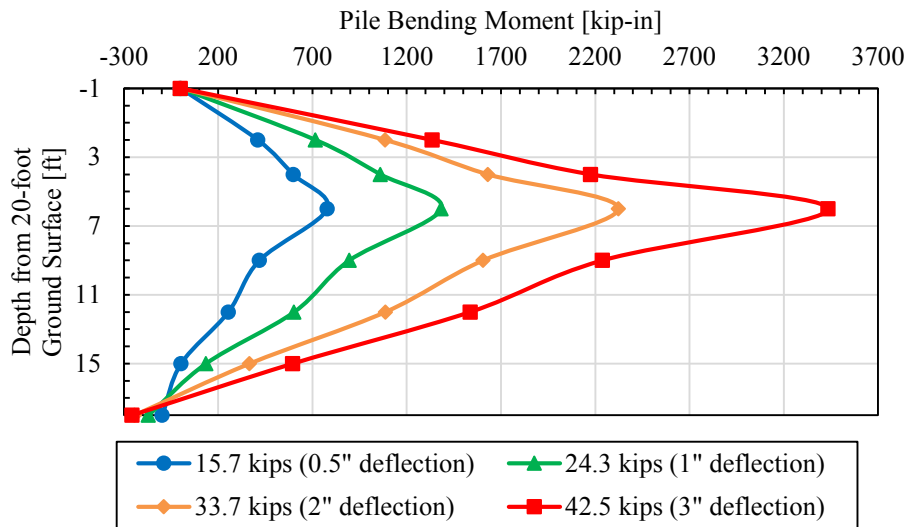


Figure 5-93. Bending moment versus depth curves for four load levels during test of 3.1D square pile.

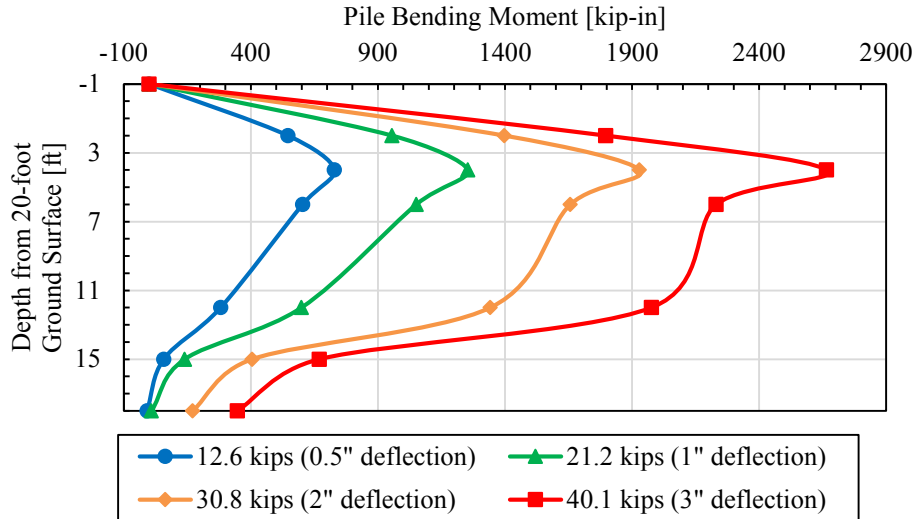


Figure 5-94. Bending moment versus depth curves for four load levels during test of 2.1D square pile.

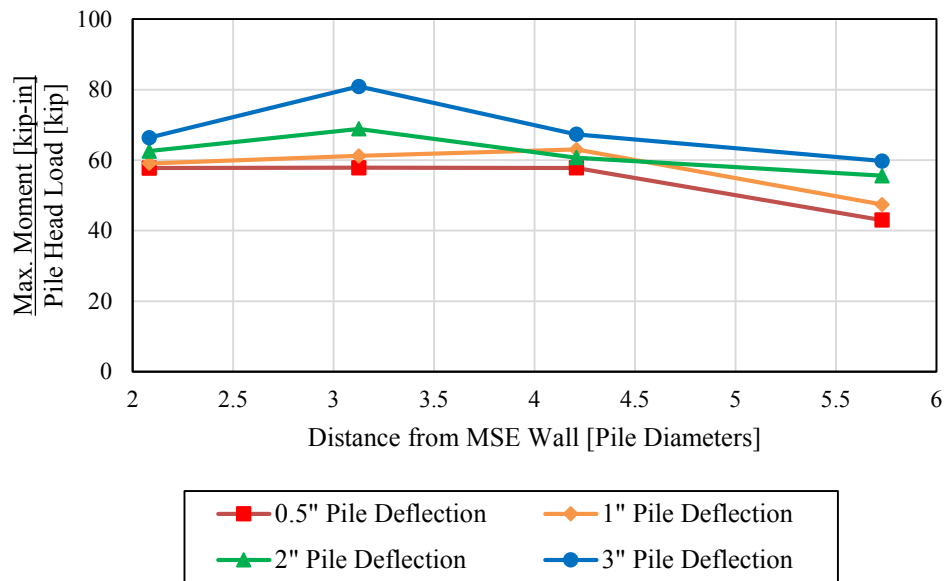


Figure 5-95. Maximum moment corresponding to the 0.5-, 1-, 2-, and 3-inch pile displacement normalized by pile head load versus distance from MSE wall normalized by pile diameter for square piles.

6 LATERAL PILE LOAD ANALYSIS

LPILE, a computer program used to analyze piles loaded laterally, was used to compare computed response with actual results. The soil resistance p per length versus the pile deflection y is nonlinear, and thus the model in LPILE replaces the soil with nonlinear springs (Isenhower et al., 2015). The conventional analysis mode was used with the option to use modification factors for p - y curves. Static loading was the loading type, with 100 pile increments, 500 maximum iterations, and with the convergence tolerance on deflection being 10^{-5} inches.

LPILE requires certain input parameters for the soil and the pile to perform an analysis. Some of these parameters include the pile material properties, the effective soil unit weight (γ), the soil friction angle (ϕ), the initial soil modulus of subgrade reaction (k), the depths of the layers, and the actual pile lateral loads obtained from the field for each specific pile. The pile load for each increment was the average load between 1 and 1.5 minutes after each load increment was applied. A discussion of soil and pile properties used in the analysis is provided subsequently.

Based on the LPILE analysis, curves for pile head load versus pile deflection, pile moment versus depth, and pile load versus pile rotation were produced for comparison with the actual results. P -multipliers were also back-calculated to define the reduction in soil resistance as piles were located closer to the MSE wall face. The use of LPILE in this study is consistent with the similar research reported by Price (2012), Nelson (2013), Hatch (2014), Han (2014), Besendorfer (2015), and Budd (2016).

6.1 Material Properties

The following section describes the material properties and parameters used for the modeling of LPILE.

6.1.1 H-Piles

The section type used for the H-piles was elastic section (non-yielding). Table 6-1 shows the pile properties used for the H-piles. The pile moment of inertia and cross-sectional area for an HP12X74 pile reported in the Steel Construction Manual are 21.8 in² and 186 in⁴, respectively. However, owing to the angle irons attached to the pile (running along the length of the pile in the middle of the pile web), the area and moment of inertia slightly increased. AutoCAD was used to model the HP12X74 pile shape with angle irons, and an appropriate cross-sectional area and moment of inertia were calculated. Table 6-1 shows material properties for the HP12x74 pile accounting for the angle irons.

Table 6-1. LPILE Pile Materials for H-Piles

Structural Shape	Total Length [ft]	Flange Width [in]	Shape Depth [in]	Flange Thickness [in]	Web Thickness [in]	Cross-sectional Area [in ²]	Moment of Inertia [in ⁴]	Modulus of Elasticity [psi]
H-Pile Weak Axis	35	12.2	12.1	0.61	0.605	22.6	187	29,000,000

In LPILE the load was applied at the top of the pile model one foot above the ground surface to match field loading conditions. Since the H-piles were tested at Phase 1, the top layer representing the reinforced fill is 15' thick while the underlying 20-foot thick layer is the native

silty sand extending below the base of the pile at 18 feet of embedment. Assumptions were made for the effective unit weight and the friction angle for the native soil; however, subsequent parametric studies indicate that these values had negligible effect on the response of the pile under lateral loads.

The type of sand modeled in LPILE was American Petroleum Institute (API) sand (2010) with modifications adopted from O’Neill and Murchison (1983). For the reinforced fill, the effective unit weight was the average moist unit weight measured for Phase 1. The friction angle was back-calculated as explained subsequently in section 6.2.1. The initial modulus of subgrade reaction was then obtained as a function of the friction angle using the correlation shown in Figure 2-15. Table 6-2 shows the soil profile modeled in LPILE without a surcharge ($q=0$ psf).

Since a partial surcharge of 600 psf was applied immediately behind the test pile in the field, an effort was made to investigate the effect of a surcharge on the computed pile behavior. Unfortunately, a surcharge can only be modeled in LPILE by applying a thin uniform soil layer producing the same additional pressure both in front and behind the pile.

Table 6-2. LPILE Soil Profile for H-Piles with no Surcharge

Depth Below Load Point [ft]	Description	Soil Type (p-y) Model	Effective Unit Weight, γ [pcf]	Friction Angle, ϕ [deg]	Modulus of Subgrade, k [pci]
1-16	Reinforced Fill	API Sand (O’Neill)	127.5	39.5	245
16-36	Underlying Native Soil	API Sand (O’Neill)	125	34	115

In LPILE the dead load surcharge of 600 psf was modeled by converting the surcharge into a layer with a unit weight of 2400 pcf with a 3-inch thickness. To eliminate any contribution of lateral resistance in the “surcharge” layer, a gap of 10 inches was specified between the pile and soil in this layer before lateral resistance would develop. This effectively reduced the ϕ and k in this layer to zero. Table 6-3 shows the soil profile in LPILE with a surcharge.

Table 6-3. LPILE Soil Profile for H-Piles with Surcharge

Depth Below Load Point [ft]	Description	Soil Type (p-y) Model	Effective Unit Weight, ϕ [pcf]	Friction angle, ϕ [deg]	Modulus of Subgrade, k [pci]
0.75-1	Surcharge	User Input	2400	-	-
1-16	Reinforced Fill	API Sand (O'Neill)	127.5	30.5	60
16-36	Underlying Native Soil	API Sand (O'Neill)	125	34	115

6.1.2 Square Piles

The section type used for the square piles was also an elastic section (non-yielding). Table 6-4 shows the pile properties used for the square piles. The pile moment of inertia and cross-sectional area for the HSSX12X12X5/16 steel shape are 13.4 in² and 304 in⁴, respectively, in the Steel Construction Manual. However, owing to the angle irons attached to the pile and running along the length of the pile, the area and moment of inertia slightly increased. AutoCAD was used to model the square piles first without angle irons to check against the actual values in the Steel Construction Manual. Once the values were found to be in agreement, AutoCAD was used to add

the angle irons and then calculate the increased cross-sectional area and moment of inertia. Table 6-4 shows these values.

Table 6-4. LPILE Pile Materials for Square Piles

Structural Shape	Total Length [ft]	Pile Section Width [in]	Pile Section Depth [in]	Cross-sectional Area [in²]	Moment of Inertia [in⁴]	Modulus of Elasticity [psi]
Rectangular	40	12	12	14.1	335	29,000,000

In LPILE the load was applied at the top of the pile model one foot above the ground surface to match field loading conditions. Since the square piles were tested in Phase 2, the top layer is 5 ft thick, and then the next layer is 15 ft for the reinforced fill while the rest of the underlying soil is the native silty sand which was modeled as a 20-foot thick layer extending below the pile tip as described previously. Material properties in this layer had relatively little effect on pile performance. Once again, all soil layers were modeled in LPILE using the API Sand (O'Neill et al., 1983) p-y curve model. For the reinforced fill, the effective unit weight was the average moist unit weight measured for Phase 2 for the top layer, and the average moist unit weight measured for Phase 1 for the next layer. The friction angle was back-calculated as explained subsequently in section 6.2.2, and the modulus k was based on the correlation with the friction angle shown in Figure 2-15.

Table 6-5 summarizes the soil profile modeled in LPILE without a surcharge ($q=0$ psf). Surcharge was modeled using the same procedure as described previously for the H-piles and Table 6-6 shows the soil profile in LPILE with a surcharge. Table 6-7 shows the different friction

angles for the different studies involved in this project (Hatch, 2014; Han, 2014; Besendorfer, 2015; and Budd, 2016).

Table 6-5. LPILE Soil Profile for Square Piles

Depth [ft]	Description	Soil Type (p-y) Model	Eff. Unit Weight, γ [pcf]	Friction angle, ϕ [deg]	Modulus of Subgrade, k [pci]
1-6	Reinforced Fill	API Sand (O'Neill)	126.2	38	205
6-21	Reinforced Fill	API Sand (O'Neill)	127.5	38	205
21-41	Underlying Native Soil	API Sand (O'Neill)	125	34	115

Table 6-6. LPILE Soil Profile for Square Piles with Surcharge

Depth [ft]	Description	Soil Type (p-y) Model	Eff. Unit Weight, γ [pcf]	Friction angle, ϕ [deg]	Modulus of Subgrade, k [pci]
0.75-1	Surcharge	User Input	2400	-	-
1-6	Reinforced Fill	API Sand (O'Neill)	126.2	30.5	60
6-21	Reinforced Fill	API Sand (O'Neill)	127.5	30.5	60
16-36	Underlying Native Soil	API Sand (O'Neill)	125	34	115

Table 6-7. Comparison of Friction Angles from LPILE of Different Studies

Study	Friction Angle in LPILE Modeled without a Surcharge	Friction Angle in LPILE Modeled with a Surcharge
Hatch (2014)	39	-
Han (2014)	39	-
Besendorfer (2015)	39	30
Budd (2016)	38	30
This Study, H-piles	38	30.5
This Study, Square Piles	39.5	30.5

6.2 Results of LPILE Analysis

As mentioned previously, LPILE was used to back-calculate appropriate p-multipliers for each pile load test. Initially, the square and H-piles farthest from the wall were analyzed, and the soil properties necessary to match the measured load-deflection curves were determined. Based on the assumption that the pile farthest from the MSE wall (4.5 to 5.7 pile diameters away) would be relatively unaffected by the presence of the wall, a p-multiplier of 1.0 was assumed for this case, indicating no wall interaction. For piles located closer to the wall, these back-calculated soil parameters were then held constant for each pile and a constant p-multiplier was back-calculated to produce agreement with the measured load-deflection curve for that pile. As explained previously, p-multipliers are factors that are multiplied by the normal lateral soil resistance to account for the reduced lateral soil resistance for piles near an MSE wall. Separate analyses were performed in LPILE using both the no-surcharge and surcharge models.

Once the appropriate soil parameters and p-multipliers had been determined, computed pile load versus pile rotation and pile bending moment versus depth curves were also compared with measured curves.

6.2.1 H-Piles

The H-pile farthest from the wall was located 4.5 pile widths behind the wall. In calibrating the soil model, both ϕ and k affect the computed load-deflection curve; however, k has more effect on the curve at small deflection levels while ϕ has a greater effect at larger deflections as the soil layers begin to reach failure. Neglecting any surcharge pressure for the H-piles, the best agreement with the measured curve was produced with a friction angle of 39.5° and a k of 245 pci (see Table 6-2 above) with a p-multiplier of 1.0. For the LPILE model with a surcharge, best agreement was

produced with a friction angle of 30.5° and a k of 60 pci (see Table 6-3). The surcharge has the effect of increasing the confining pressure and reducing the friction angle necessary to produce agreement as would be expected. In reality, the friction angle is likely somewhere between these two cases. A comparison of the measured load-deflection curve with curves computed by LPILE with and without surcharge is provided in Figure 6-1. The curve computed with no surcharge provides better agreement with the measured curve than the curve with surcharge; particularly at deflections less than about one inch. This result suggests that the model without surcharge is more realistic which is likely due to the fact that no surcharge was placed between the pile and the wall where most of the lateral resistance was developed. For subsequent LPILE analyses of piles located closer to the wall, ϕ and k were kept constant for the respective model types (surcharge or no surcharge) and the p -multiplier was changed until the load-deflection curve computed by LPILE matched the measured curve.

Table 6-8 shows the back-calculated p -multipliers for the H-piles for with and without surcharge included in the model. The LPILE model with a surcharge increased the back-calculated p -multipliers for the H-piles. The closer the normalized spacing for the pile was, the more the p -multiplier increased. The 3.2D pile only increased by 0.02, 2.5D increased by 0.07, and 2.2D increased by 0.11.

Figure 6-2, Figure 6-3, and Figure 6-4 show the pile head load versus the pile head deflection for each of the H-piles located 3.2D, 2.5D, and 2.2 from the wall, respectively. The figures show both models of LPILE (with and without surcharge) and the measured data. The comparison between each pile separately shows little difference between the LPILE models and the measured data at large deflections; however, the model without surcharge generally provides much better agreement at deflections less than one inch and is the preferred model. When the

surcharge q equals 600 psf; it signifies the LPILE modeled with a surcharge. When q equals 0, it means there was no surcharge modeled in LPILE.

Table 6-8. P-multipliers for H-Piles from LPILE

Pile	P-multiplier	
	No Surcharge	Surcharge
4.5D	1.00	1.00
3.2D	0.85	0.87
2.5D	0.60	0.67
2.2D	0.73	0.84

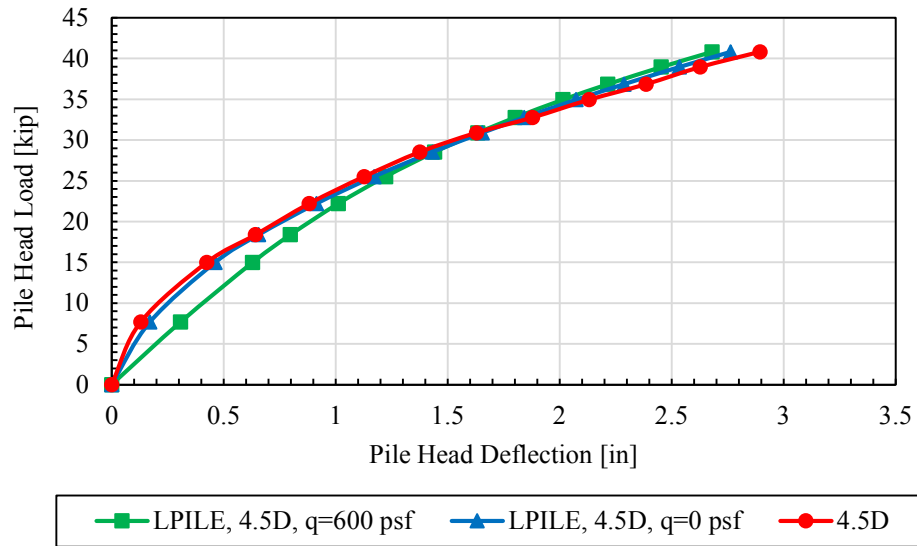


Figure 6-1. Comparison of measured pile head load versus deflection curve for the 4.5D H-pile with curves computed using LPILE assuming no surcharge and 600 psf surcharge.

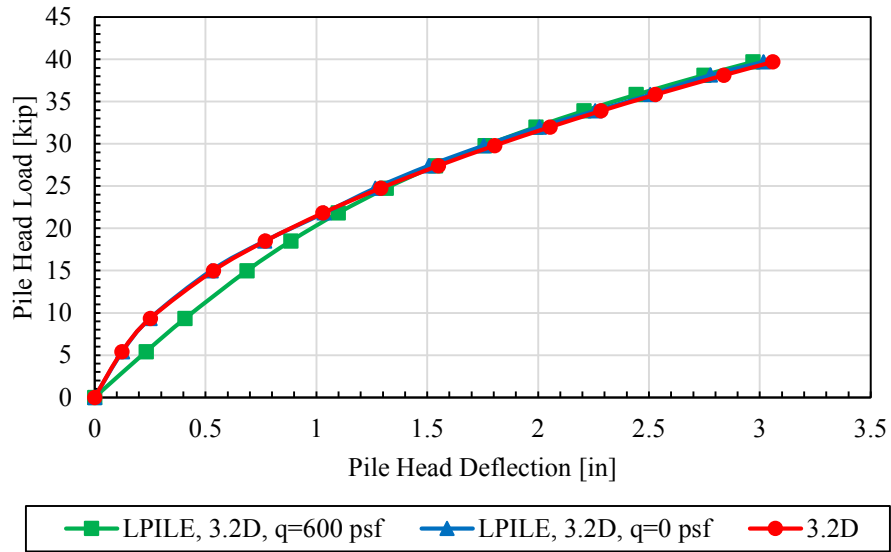


Figure 6-2. Comparison of measured pile head load versus deflection curve for the 3.2D H-pile with curves computed using LPILE assuming no surcharge and 600 psf surcharge.

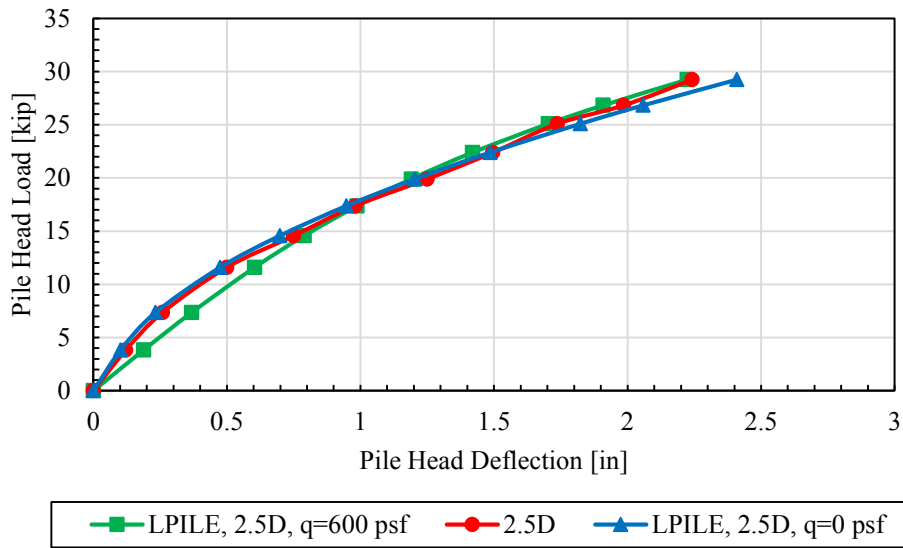


Figure 6-3. Comparison of measured pile head load versus deflection curve for the 2.5D H-pile with curves computed using LPILE assuming no surcharge and 600 psf surcharge.

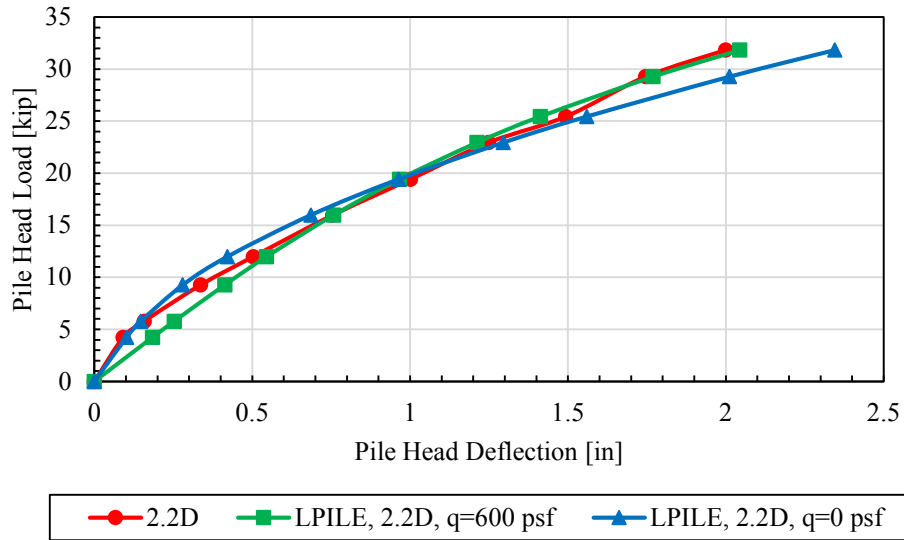


Figure 6-4. Comparison of measured pile head load versus deflection curve for the 2.2D H-pile with curves computed using LPILE assuming no surcharge and 600 psf surcharge.

The p-multipliers for 3.2D and 2.5D seem to fit previous data and Equation (2-20a) reasonably well. However, the H-pile spaced at 2.2D has a higher p-multiplier than would be expected, especially since it has a higher p-multiplier than the 2.5D H-pile which should not be the case since the 2.5D pile is farther away from the wall. This does not make sense and goes against previous research which has found that the p-multiplier decreases as the distance to the wall decreases (Pierson, 2009; Rollins et al., 2013; Han, 2014; Hatch, 2014; Besendorfer, 2015; and Budd, 2016). This is most likely because of a difference in compaction.

This research study differs from the other related research on lateral pile resistance near MSE walls in that the other tests all involved pipe piles. In contrast, this study involved tests with square and H shapes. Figure 6-5 shows a comparison of the load-deflection curves for H-piles spaced at 4.5D and the pipe piles spaced at similar distances at this same MSE wall location. Figure 6-6, Figure 6-7, and Figure 6-8 also show the same comparisons of load-deflection curves for the H-piles spaced at 3.2D, 2.5D, and 2.2D, respectively with curves for pipe piles at similar spacing,

respectively. For a given nominal spacing, the actual spacing differed between the different pile tests by at least as large as a whole pile diameter for some of the comparisons, thus Figure 6-9 shows the comparison of the most comparable spacing for the 3.2D H-pile. Data for the mentioned pipe piles are found in Hatch (2014), Han (2014), Besendorfer (2015), and Budd (2016). Generally, the H-pile develops significantly lower lateral resistance in comparison with all of the comparable pipe piles except for the case with the H-pile closest to the wall. Lower lateral resistance would be expected for the H-pile relative to the pipe pile because the moment of inertia for the H-pile loaded about its weak axis is only 71% of the moment of inertia for the pipe pile (without considering the angle irons). However, the 2.2D H-pile is higher than the respective pipe piles most likely because of a greater compaction effort in the soil adjacent to this pile.

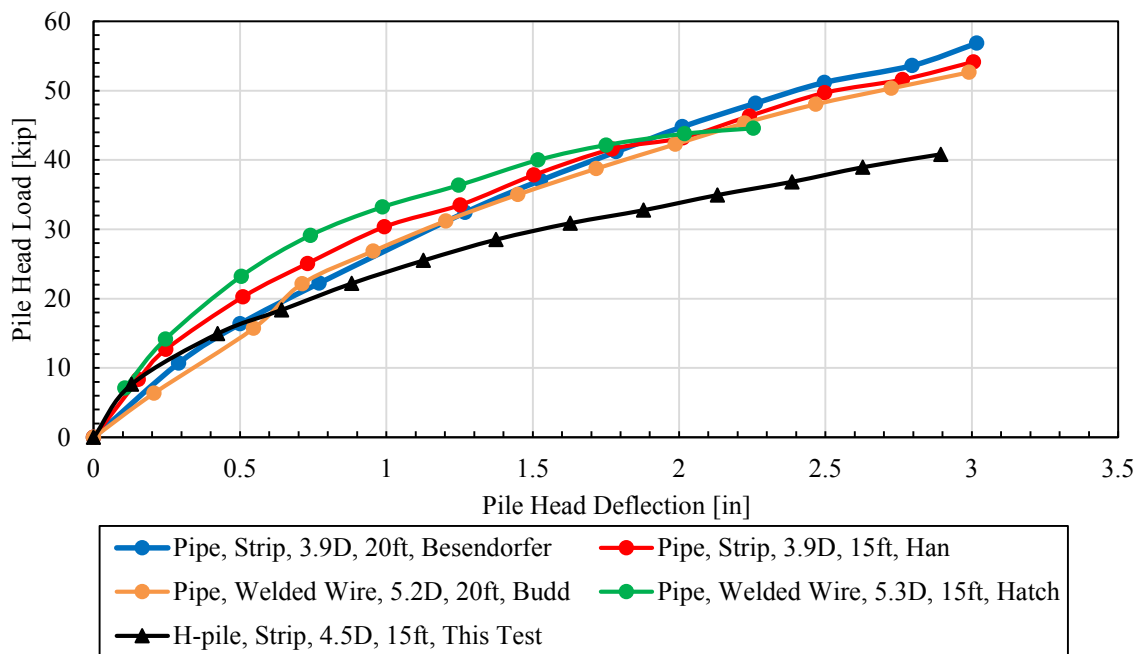


Figure 6-5. Comparison of load-deflection curve for 4.5D H-pile with curves for pipe piles at the similar spacing of the nominal 5D distance.

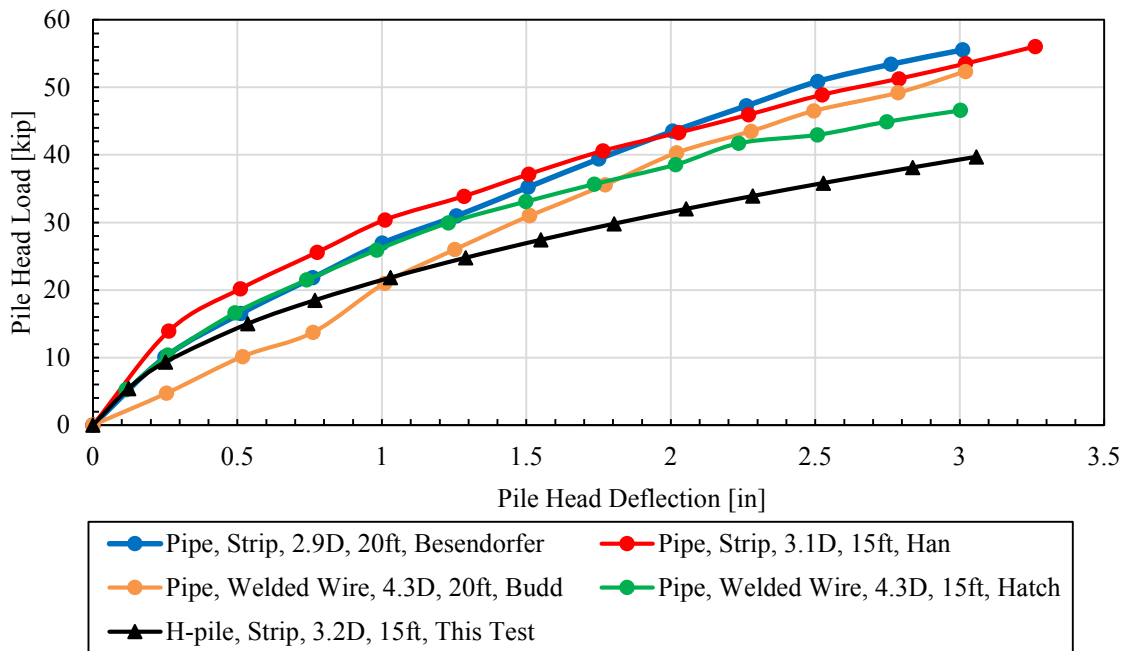


Figure 6-6. Comparison of load-deflection curve for 3.2D H-pile with curves for pipe piles at the similar spacing of the nominal 4D distance.

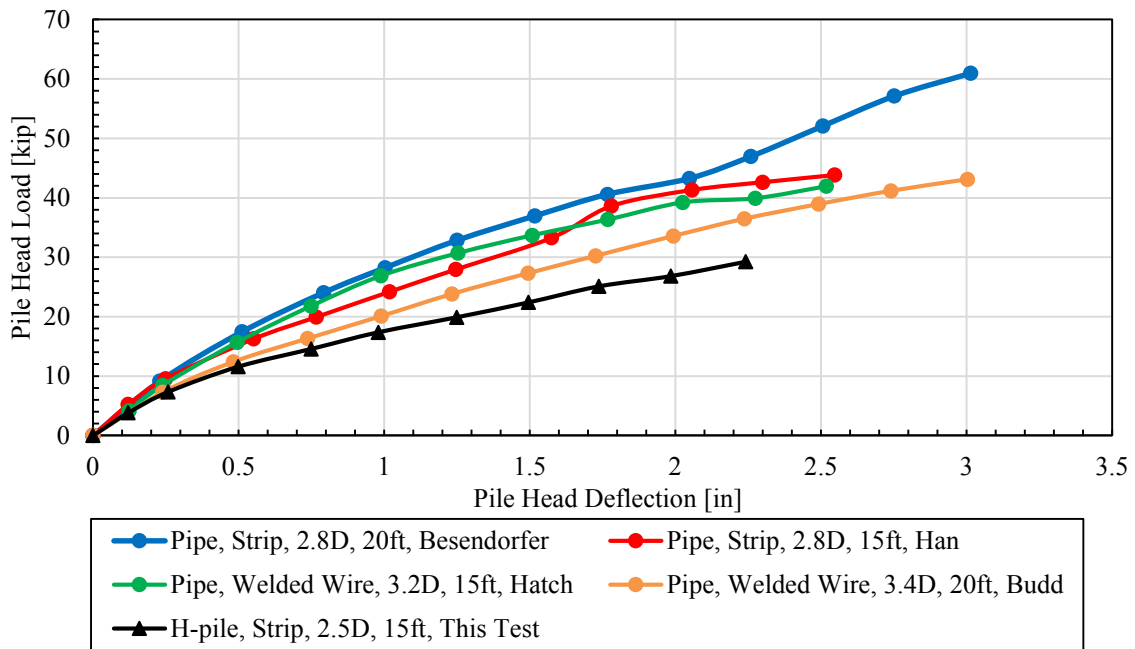


Figure 6-7. Comparison of load-deflection curve for 2.5D H-pile with curves for pipe piles at the similar spacing of the nominal 3D distance.

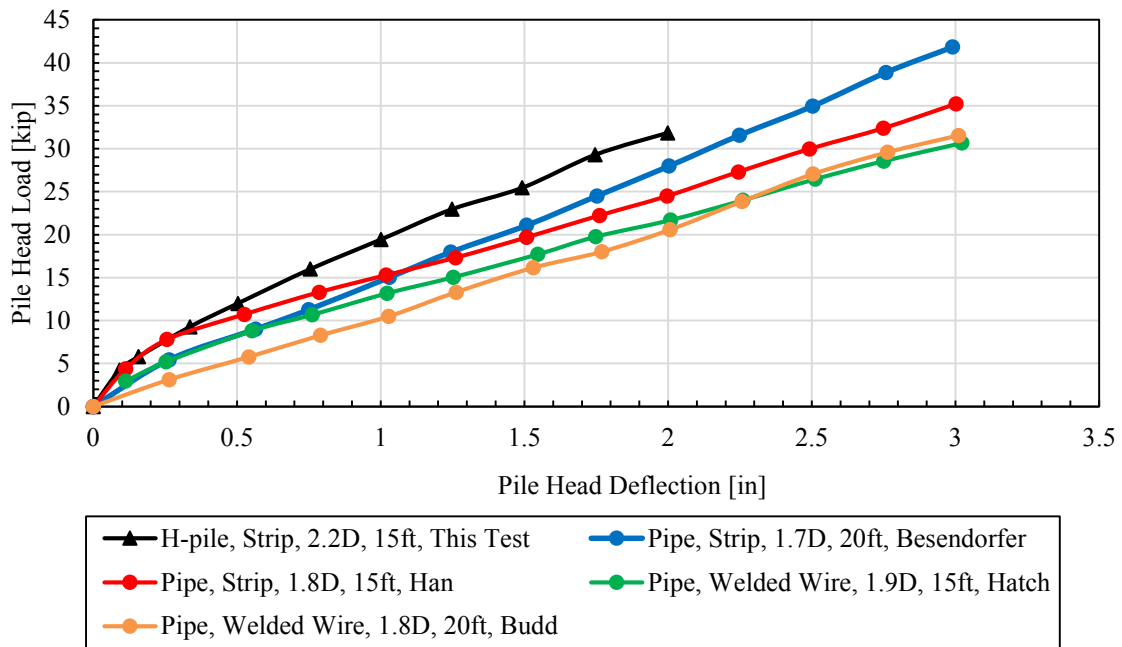


Figure 6-8. Comparison of load-deflection curve for 2.2D H-pile with curves for pipe piles at the similar spacing of the nominal 2D distance.

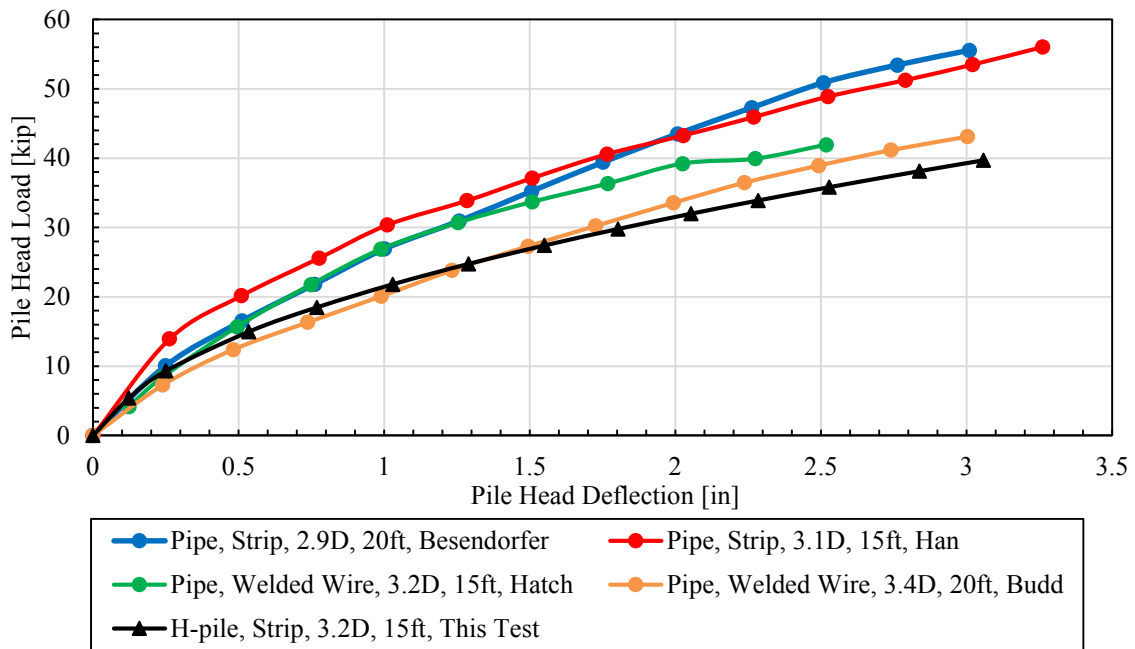


Figure 6-9. Comparison of the most comparable spacing for 3.2D H-pile and curves for pipe piles.

6.2.2 Square Piles

Similar LPILE analyses and comparisons were performed for the square piles as for the H-piles. The square pile farthest from the wall was located 5.7 pile widths behind the wall. Neglecting any surcharge pressure for the square piles, the best agreement with the measured curve was produced with a friction angle of 38° and a k of 205 pci (see Table 6-5 above) for a p-multiplier of 1.0. For the LPILE model with a surcharge, best agreement was produced with a friction angle of 30.5° and a k of 60 pci (see Table 6-6).

A comparison of the measured load-deflection curve with curves computed by LPILE with and without surcharge is provided in Figure 6-10. As was the case with the H-piles, the overall agreement is better assuming no surcharge than with a surcharge. Table 6-9 shows the back-calculated p-multipliers for the square piles for with and without surcharge included in the model. The p-multipliers for the LPILE model with a surcharge stayed the same for all of the cases, except for the 3.1D square pile, which only decreased by 0.02.

Figure 6-11, Figure 6-12, and Figure 6-13 show the pile head load versus the pile head deflection for each of the square piles spaced at 4.2D, 3.1D, and 2.1D, respectively. The figures show both models of LPILE (with and without surcharge) and the measured data. The comparison between each pile separately shows little difference between the measured and computed curves at deflections greater than 0.75 inches. However, at small deflections the curve computed without surcharge generally produces better overall agreement. This observation suggests that pile behavior is better modeled without a surcharge. In addition, the non-surcharge model has a more accurate soil friction angle.

Table 6-9. P-multipliers for Square Piles from LPILE

Pile	P-multiplier	
	No Surcharge	Surcharge
5.7D	1.00	1.00
4.2D	0.77	0.75
3.1D	0.63	0.63
2.1D	0.57	0.57

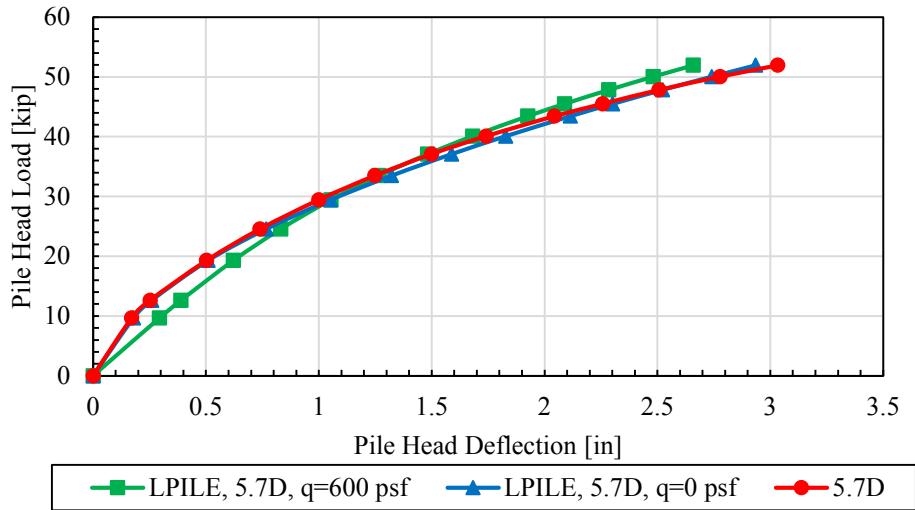


Figure 6-10. Comparison of measured pile head load versus deflection curve for the 5.7D square pile with curves computed using LPILE assuming no surcharge and 600 psf surcharge.

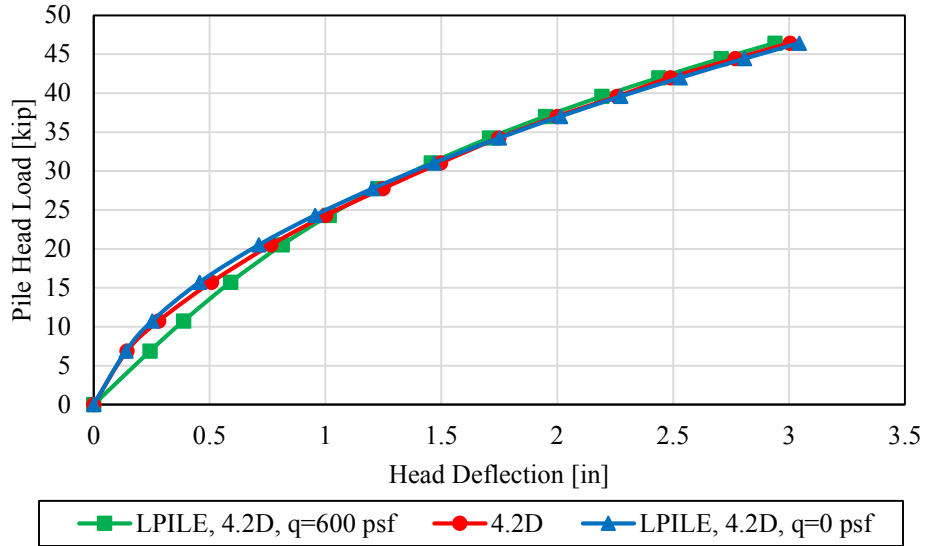


Figure 6-11. Comparison of measured pile head load versus deflection curve for the 4.2D square pile with curves computed using LPILE assuming no surcharge and 600 psf surcharge.

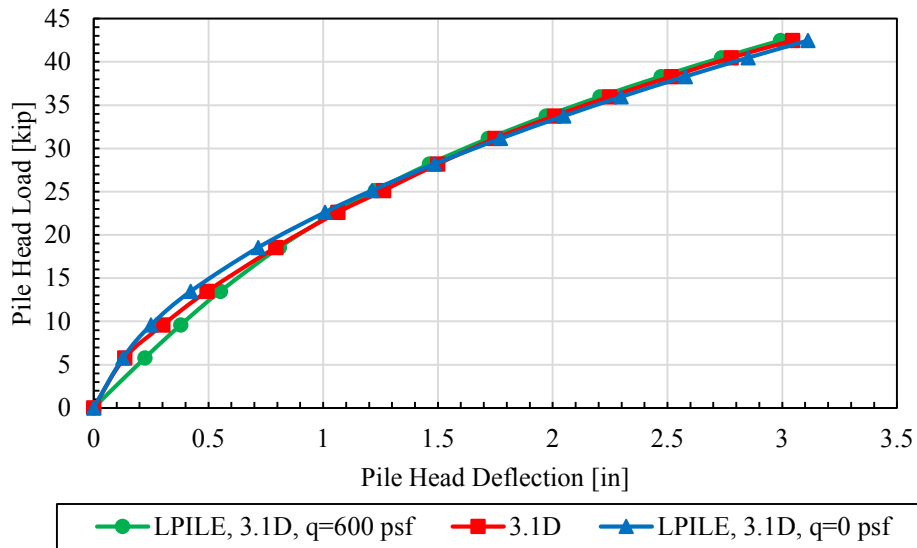


Figure 6-12. Comparison of measured pile head load versus deflection curve for the 3.1D square pile with curves computed using LPILE assuming no surcharge and 600 psf surcharge.

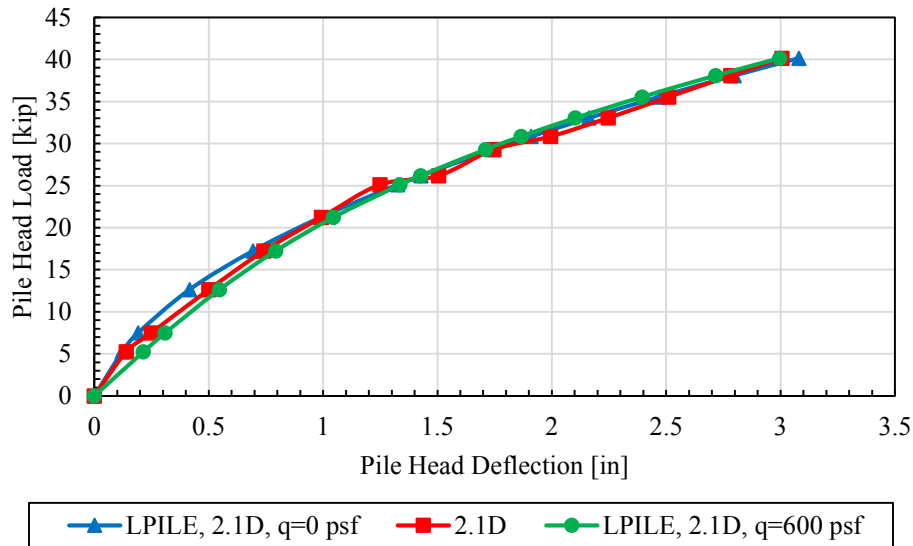


Figure 6-13. Comparison of measured pile head load versus deflection curve for the 2.1D square pile with curves computed using LPILE assuming no surcharge and 600 psf surcharge.

The p-multipliers decrease as the spacing from the wall decreases, which seem to fit previous data and Equation (2-20a) reasonably well. Figure 6-14 shows a comparison of the load-deflection curves for the square pile spaced at 5.7D and the pipe piles spaced at similar distances as mentioned in Section 6.2.1. Figure 6-15, Figure 6-16, and Figure 6-17 also show the same comparisons of load-deflection curves for the square piles spaced at 4.2D, 3.1D, and 2.1D, respectively with curves for pipe piles at similar spacing, respectively. The square pile is generally lower among the other pipe piles except for the 2.1D square pile. It was expected that the square pile be the highest as compared to the pipe piles owing to the geometry of the front flat face and higher passive resistance (Reese & Van Impe, 2011) and this is the case for the 2.1D square pile. Also, the moment of inertia for the pipe pile is about 86% of that of the square pile. A possible reason for the exception of the 2.1D square pile is that the compaction between the piles and MSE wall may have been greater.

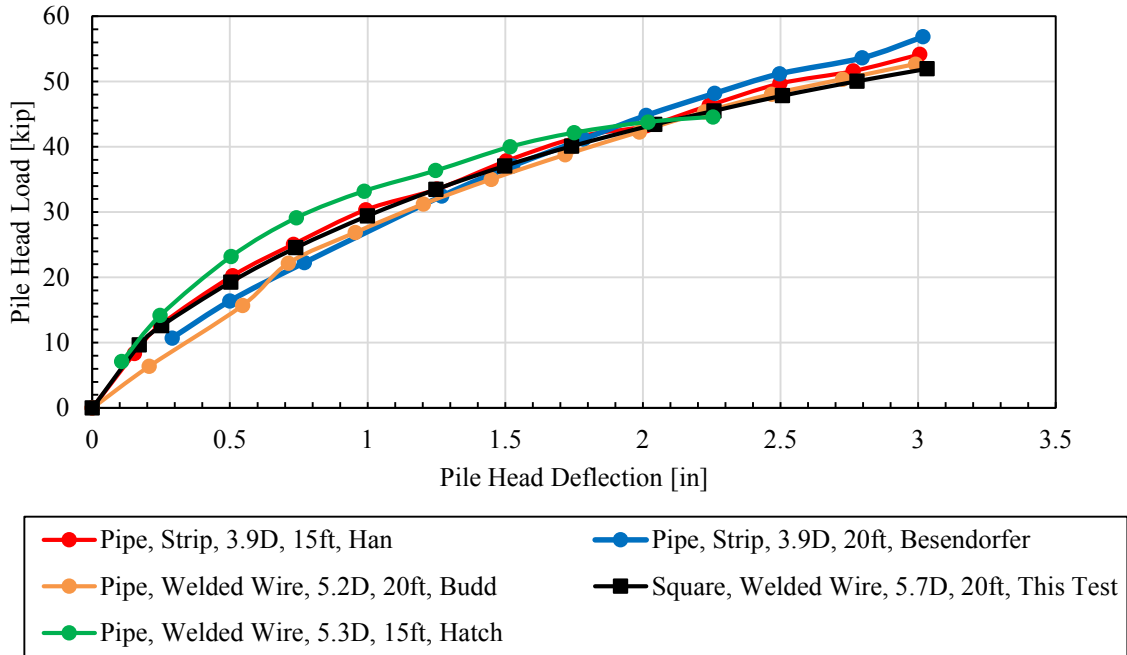


Figure 6-14. Comparison of load-deflection curve for 5.7D square pile with curves for pipe piles at the similar spacing of the nominal 5D distance.

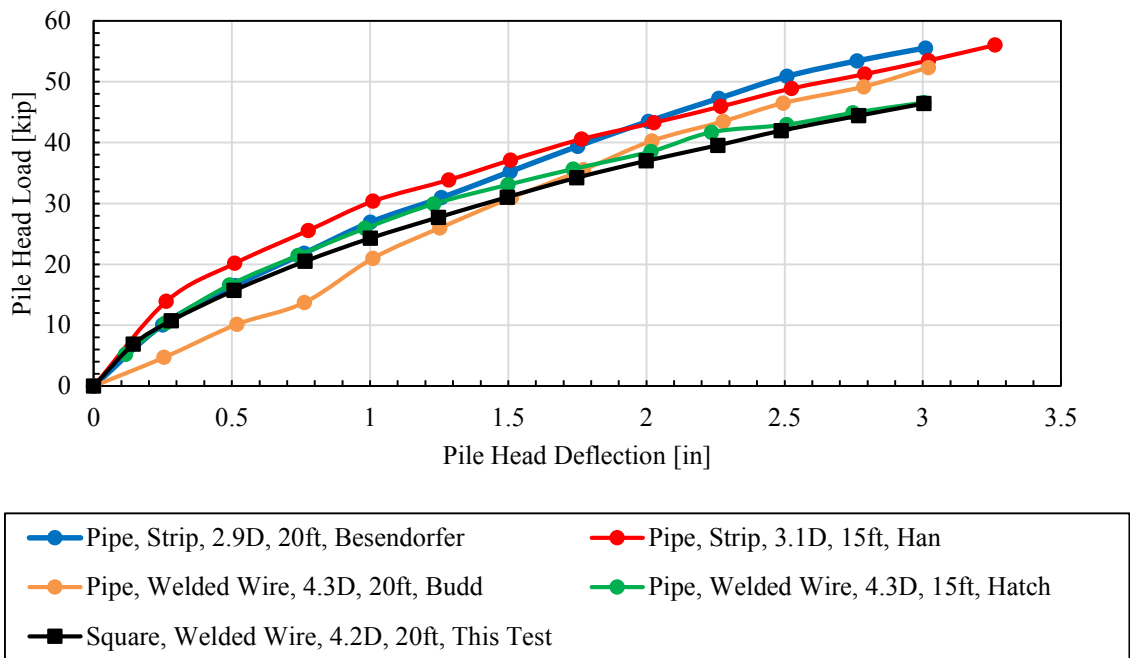


Figure 6-15. Comparison of load-deflection curve for 4.2D square pile with curves for pipe piles at the similar spacing of the nominal 4D distance.

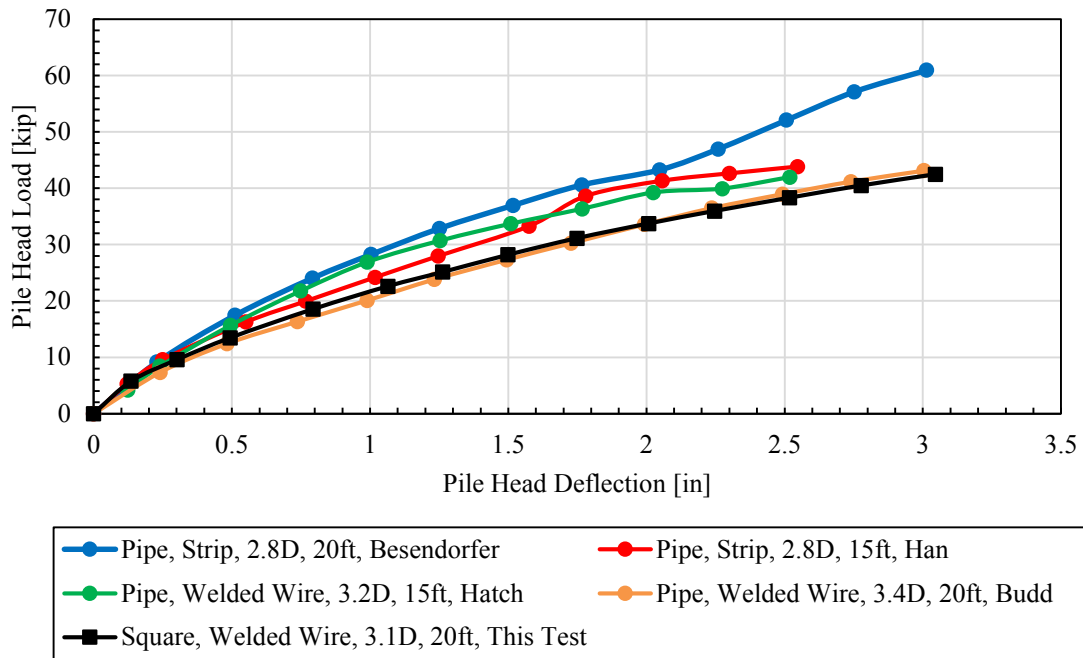


Figure 6-16. Comparison of load-deflection curve for 3.1D square pile with curves for pipe piles at the similar spacing of the nominal 3D distance.

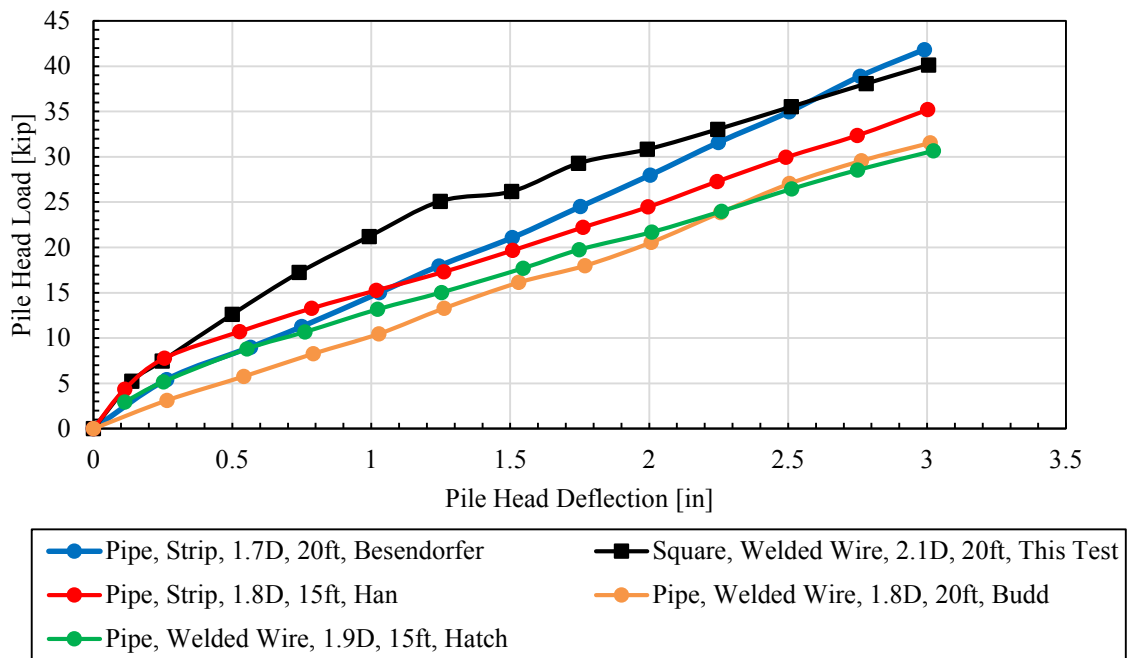


Figure 6-17. Comparison of load-deflection curve for 2.1D square pile with curves for pipe piles at the similar spacing of the nominal 2D distance.

6.2.3 P-Multipliers versus Pile Spacing Curves

Figure 6-18 provides a plot of the back-calculated p-multipliers versus the normalized distance from the wall. Data points include p-multipliers for this study and all of the other tests for this MSE wall project (Hatch, 2014; Han, 2014; Besendorfer, 2015; and Budd, 2016) and other p-multipliers from similar projects (Price, 2012; and Nelson, 2013) as shown in Table 6-10. As indicated previously, the normalized distance is defined to be the spacing from the center of the pile to the back face of the MSE wall divided by the outside diameter or width of the pile. The p-multipliers used are from the LPILE model using no surcharge. P-multipliers are plotted assuming no surcharge to be consistent with previous studies (as those mentioned above) that did not include the surcharge in their LPILE model. Generally, the analyses without surcharge produced somewhat better agreement than the surcharge model, although the differences are relatively small.

There were ten observations that were at least four pile diameters from the wall. Though three observations did not have a p-multiplier of 1.0, the average p-multiplier for these piles was about 0.94. One of these observations had a p-multiplier of 0.95. Price (2012) had two piles tested from the same wall with p-multipliers of 1.0 for piles spaced at 7.2D and 3.8D. Thus, a conclusion is drawn that piles with a normalized distance of 4D or greater have a p-multiplier approximately equal to 1.0. Observations that did not have a p-multiplier of 1.0 are considered aberrations from the general trend.

A linear regression analysis was then performed using all data points referenced previously for all piles spaced closer than four pile diameters from the wall. There were 22 observations that were included in the linear regression analysis as shown in Equation (6-1a). The equation below, also known as the best fit line, calculates a p-multiplier as follows:

$$\text{If } \frac{S}{D} \leq 3.8, \text{ then } P_{mult} = 0.31 \frac{S}{D} - 0.16 \leq 1.0 \quad (6-1a)$$

$$\text{If } \frac{S}{D} > 3.8, \text{ then } P_{mult} = 1.0 \quad (6-1b)$$

where P_{mult} = p-multiplier

S = distance from the center of the pile to the back face of the MSE wall, and

D = outside diameter of the pile.

This equation shows that any normalized distance greater than about 3.8D will have a p-multiplier of 1.0. The coefficient of determination is about 0.736, or 73.6%.

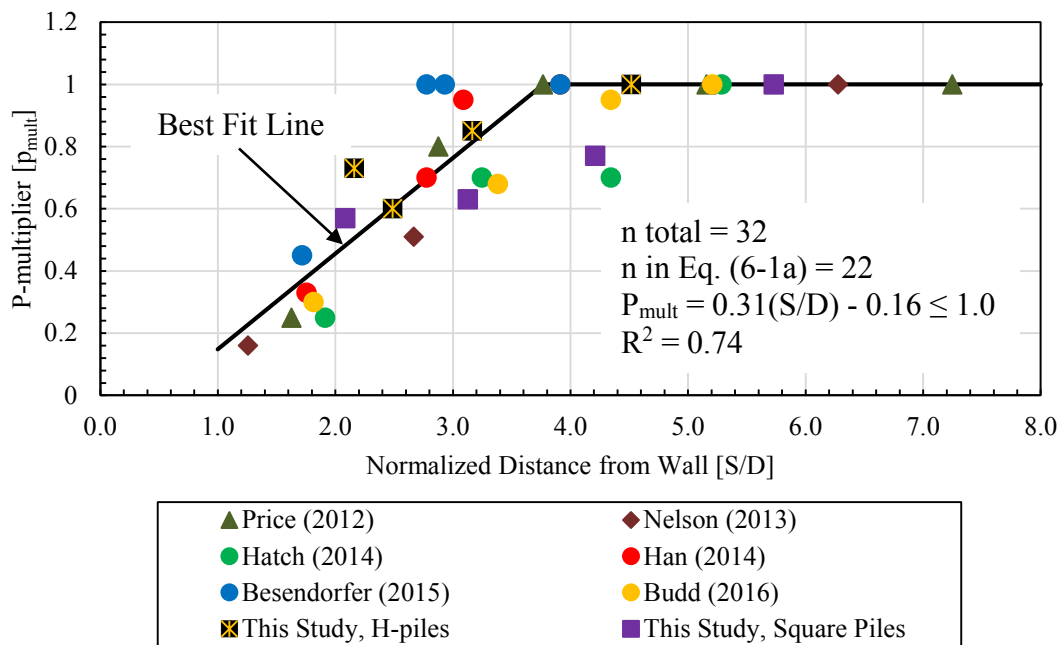


Figure 6-18. Comparison of p-multiplier versus normalized distance from MSE wall from data from Price (2012), Nelson (2013), Hatch (2014), Han (2014), Besendorfer (2015), Budd (2016), and this study with the best fit line with data points used for Equation (6-1a) and within the bounds of Equation (6-1b).

There are three aberrations from the observations used for Equation (6-1a). Two of these points are the 2.9D and 2.8D pipe piles from Besendorfer (2015). These piles have a p-multiplier of 1.0, whereas other piles spaced at similar distances from the wall have lower p-multipliers. The third aberration was from the H-piles of this study. H-pile 2.2D was higher than the H-pile 2.5D. These aberrations are likely owing to differences in compaction that are inherent in the lower compactive effort used near an MSE wall. If these observations are removed, a linear regression analysis (with 19 observations) yields a coefficient of determination of 0.862, or 86.2% (using two significant figures). This shows that there is fairly good correlation between the data. Using this analysis without the three aberrations explained above, the equation below calculates a p-multiplier as follows:

$$\text{If } \frac{S}{D} \leq 3.9, \text{ then } P_{mult} = 0.31 \frac{S}{D} - 0.20 \leq 1.0 \quad (6-2a)$$

$$\text{If } \frac{S}{D} > 3.9, \text{ then } P_{mult} = 1.0 \quad (6-2b)$$

This equation shows that any normalized distance greater than about 3.9D will have a p-multiplier of 1.0. The best fit line of Equation (6-1a) has the same slope as that of Equation (6-2a). The drop in the coefficient of determination when including the three aberrations is only because there are more data points where variability is unexplained. Figure 6-19 provides a plot of the p-multipliers versus the normalized distance from the wall with the best fit line from Equation (6-2a) and Equation (6-2b) excluding the three aberrations explained above.

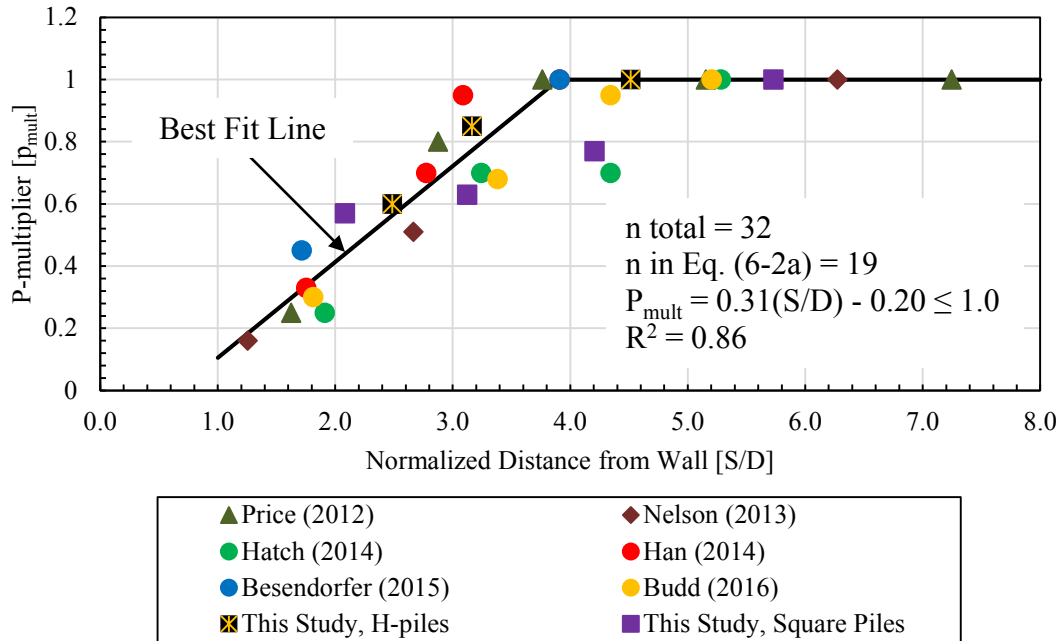


Figure 6-19. Comparison of p-multiplier versus normalized distance from MSE wall from data from Price (2012), Nelson (2013), Hatch (2014), Han (2014), Besendorfer (2015), Budd (2016), and this study without the aberrations with the best fit line with data points used for Equation (6-2a) and within the bounds of Equation (6-2b).

Equation (6-2a) and Equation (6-2b) are the research team’s recommended equations for application. Figure 6-18 and Figure 6-19 show that normalized spacing from the wall strongly effects the p-multipliers.

Figure 6-20 is similar to Figure 6-18, however, it is different in that it compares the L/H ratio (the length of the reinforcement to the height of the wall including surcharge). The surcharge is included in the height calculation because this is the approach that AASHTO takes. The L/H ratio of 0.9 for this study corresponds to the H-piles, and the L/H ratio of 0.7 for this study corresponds to the square piles. The L/H ratio does not seem to affect the p-multipliers significantly. Figure 6-21 compares the effect of reinforcement types (welded wire versus ribbed strip), Figure 6-22 compares the effect of wall systems (single-stage or two-stage), Figure 6-23 compares the effect of pile shapes, Figure 6-24 compares the effect of pile diameters, and Figure

6-25 compares the effect of pile locations behind the panel center or joint on p-multipliers. These figures show that the reinforcement type, wall system, pile shape, pile diameter, and pile location behind the panel center or joint do not seem to strongly effect the p-multiplier versus normalized distance from the wall curve. The pile diameter range was small, with 12 inches being the smallest diameter and 16 inches being the largest diameter. Thus, piles larger than about 18 inches should probably not be used with the equations given above.

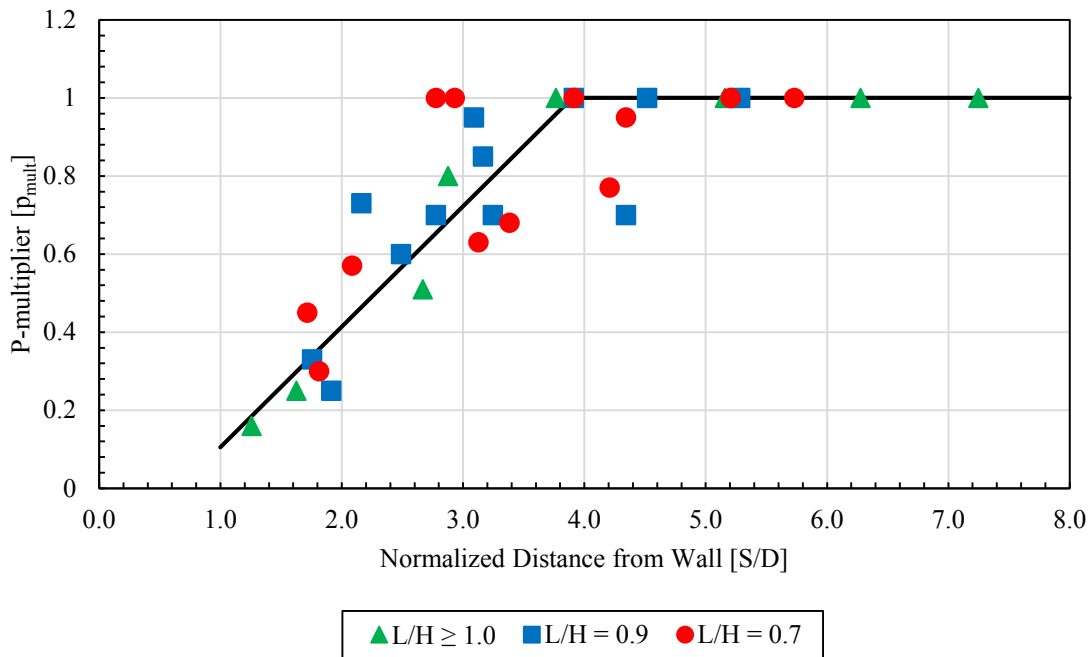


Figure 6-20. P-multiplier versus normalized distance from wall comparing L/H ratios from data from Price (2012), Nelson (2013), Hatch (2014), Han (2014), Besendorfer (2015), Budd (2016), and this study.

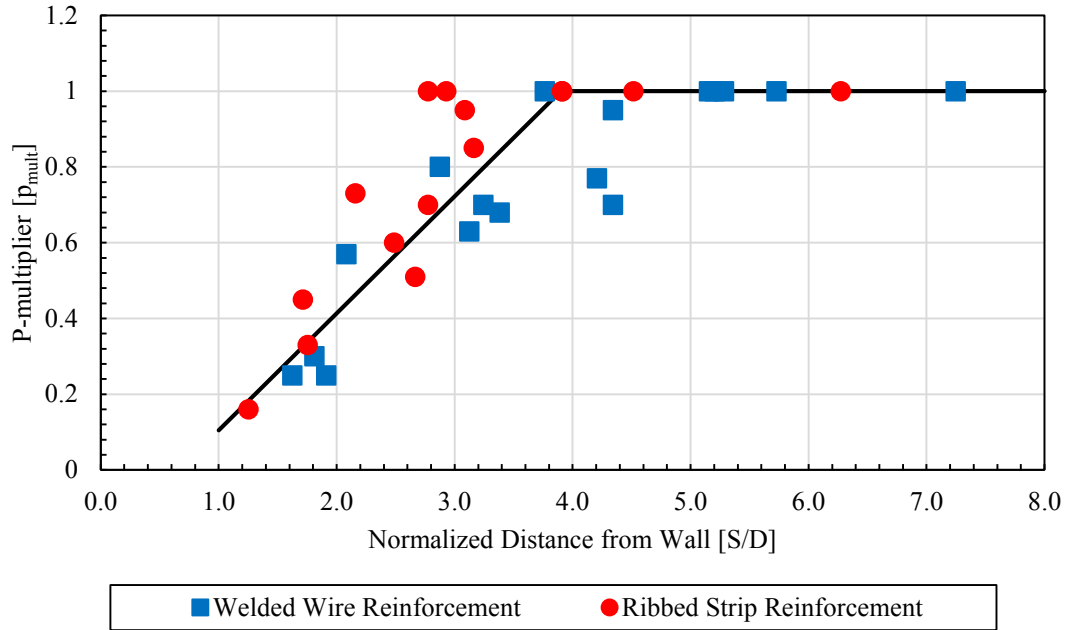


Figure 6-21. P-multiplier versus normalized distance from wall comparing reinforcement types from data from Price (2012), Nelson (2013), Hatch (2014), Han (2014), Besendorfer (2015), Budd (2016), and this study.

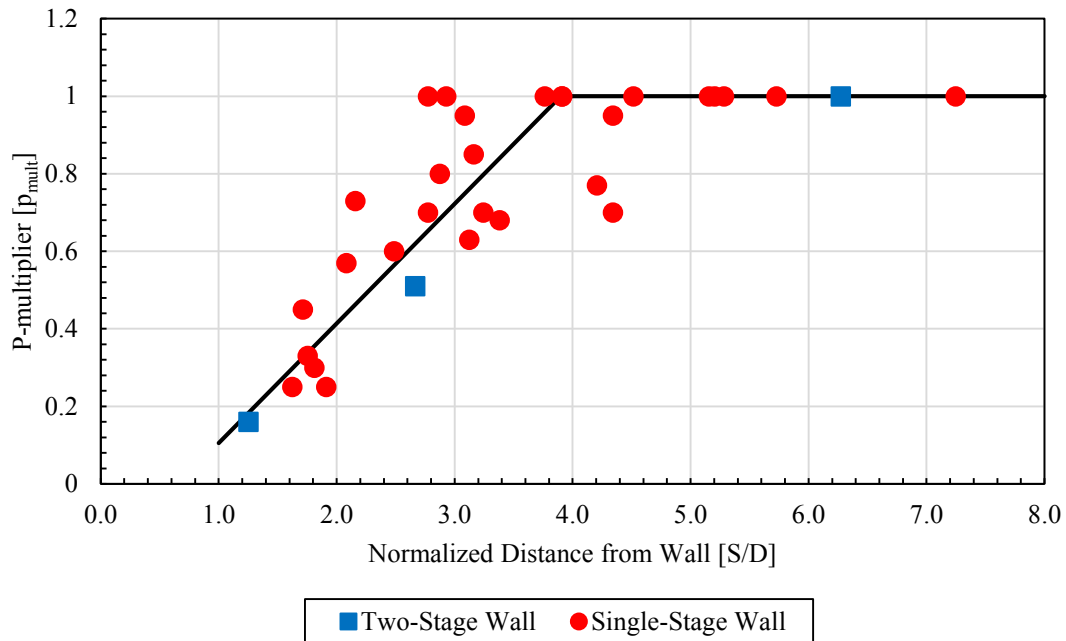


Figure 6-22. P-multiplier versus normalized distance from wall comparing wall systems from data from Price (2012), Nelson (2013), Hatch (2014), Han (2014), Besendorfer (2015), Budd (2016), and this study.

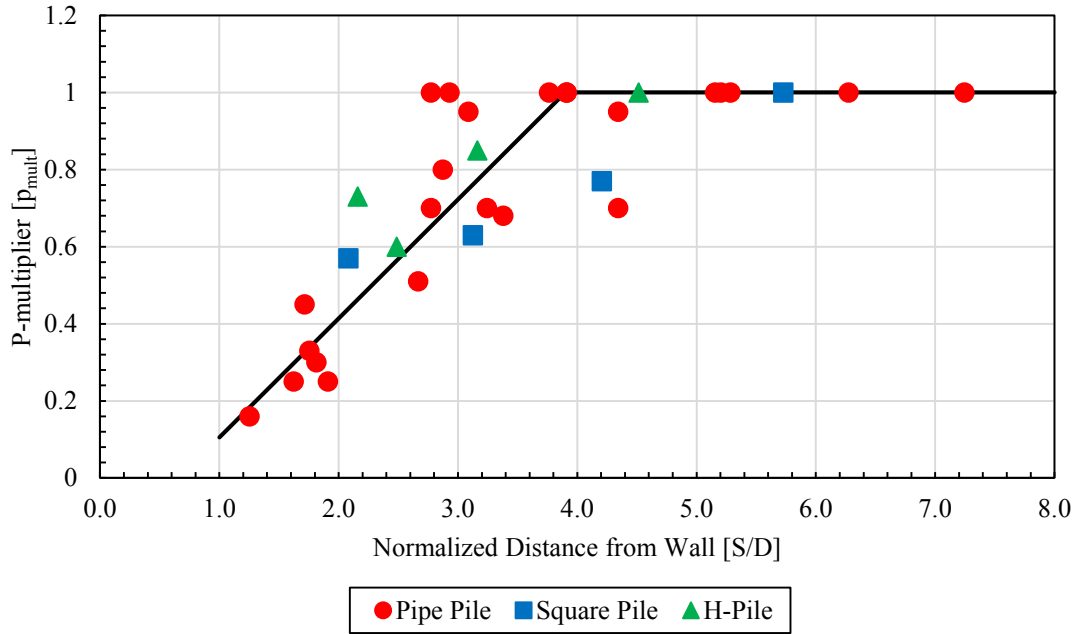


Figure 6-23. P-multiplier versus normalized distance from wall comparing pile shapes from data from Price (2012), Nelson (2013), Hatch (2014), Han (2014), Besendorfer (2015), Budd (2016), and this study.

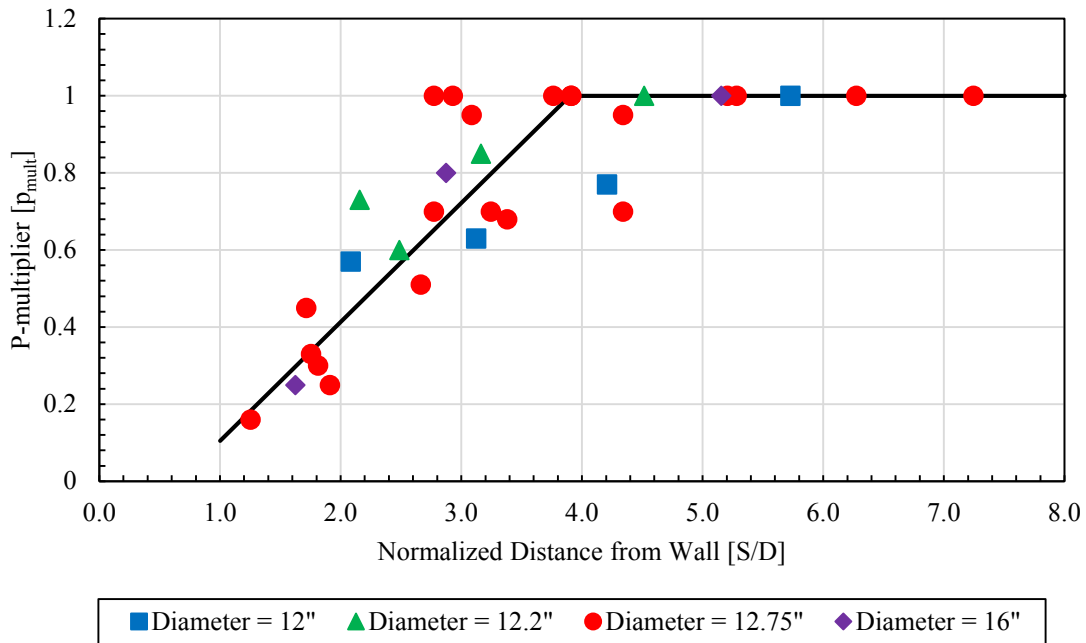


Figure 6-24. P-multiplier versus normalized distance from wall comparing pile diameters from data from Price (2012), Nelson (2013), Hatch (2014), Han (2014), Besendorfer (2015), Budd (2016), and this study.

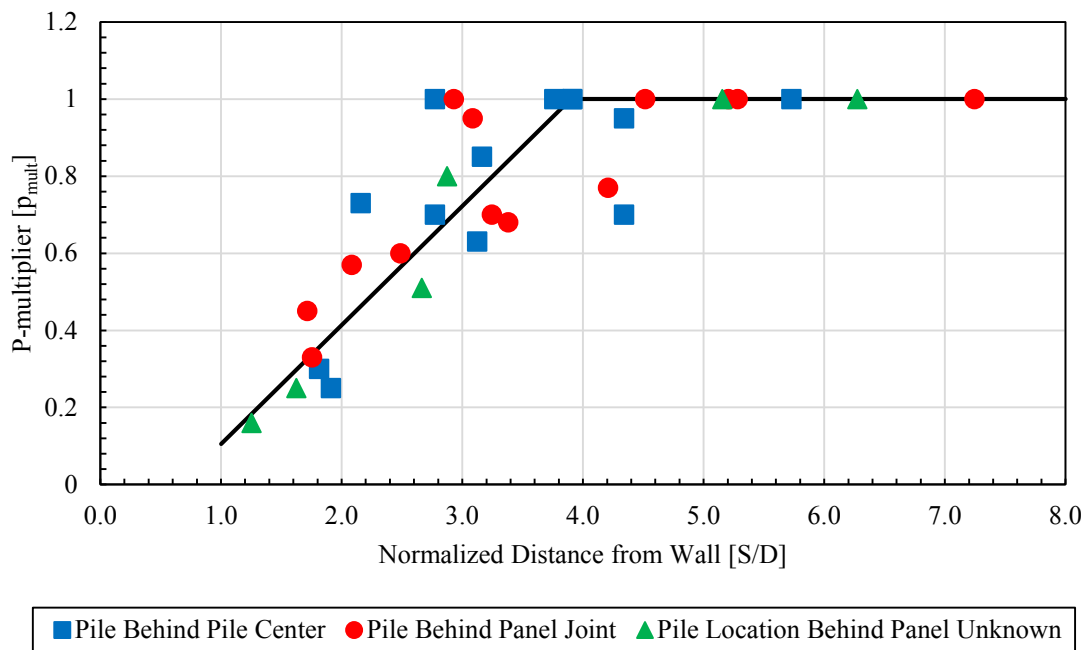


Figure 6-25. P-multiplier versus normalized distance from wall comparing pile locations behind the panel center or joint from data from Price (2012), Nelson (2013), Hatch (2014), Han (2014), Besendorfer (2015), Budd (2016), and this study.

Table 6-10. Summary of P-multipliers

Study	Pile Shape	Normalized Distance from Wall	P-multiplier	L/H Ratio	Reinforcement Type
Price	Pipe	7.2	1	1.29	Welded Wire
	Pipe (16" dia. with HDPE wrapping)	5.2	1	0.98	
	Pipe	3.8	1	1.42	
	Pipe (16" dia. with HDPE wrapping)	2.9	0.8	1.27	
	Pipe (16" dia. with HDPE wrapping)	1.6	0.25	0.97	
Nelson*	Pipe	6.3	1	1.03	Ribbed Strip
		2.7	0.51	1.2	
		1.3	0.16	1.03	
Hatch	Pipe	5.3	1	0.90	Welded Wire
		4.3	0.70		
		3.2	0.70		
		1.9	0.25		
Han	Pipe	3.9	1	0.90	Ribbed Strip
		3.1	0.95		
		2.8	0.70		
		1.8	0.33		
Besendorfer	Pipe	3.9	1	0.72	Ribbed Strip
		2.9 ⁺	1		
		2.8 ⁺	1		
		1.7	0.45		
Budd	Pipe	5.2	1	0.72	Welded Wire
		4.3	0.95		
		3.4	0.68		
		1.8	0.30		
This Study	H-Pile	4.5	1	0.90	Ribbed Strip
		3.2	0.85		
		2.5	0.60		
		2.2 ⁺	0.73		
This Study	Square	5.7	1	0.72	Welded Wire
		4.2	0.77		
		3.1	0.63		
		2.1	0.57		

⁺Piles not included in the linear regression analysis for the p-multiplier Equation 6-2a.

*Two-stage MSE wall facing type.

6.2.4 Pile Head Load versus Rotation Curves

Rotation curves were computed for both the H-piles in Figure 5-4 and for the square piles in Figure 5-8. For each pile, rotation curves are compared with the curves from the LPILE models with and without a surcharge.

6.2.4.1 H-Piles

Measured pile head load versus pile head rotation curves were compared to the computed curves using the LPILE models with and without surcharge included. Figure 6-26, Figure 6-27, Figure 6-28, and Figure 6-29 show the rotation curves for H-piles at 4.5D, 3.2D, 2.5D, and 2.2D behind the wall, respectively.

The data all yielded very similar results. Generally, the computed load-rotation curves are in reasonably good agreement with the measured curve. However, the computed rotations begin to exceed the measured rotation for pile rotations greater than about one degree. In addition, the error in the computed rotation tends to increase as the piles are located closer to the MSE wall, presumably owing to the reduced lateral resistance.

It is interesting to note that the LPILE model with a surcharge computes somewhat smaller rotations than the LPILE model without a surcharge for every H-pile. This suggests that surcharge provides more rotational resistance for a given lateral load, which makes sense, because the surcharge induces greater vertical stress near the surface.

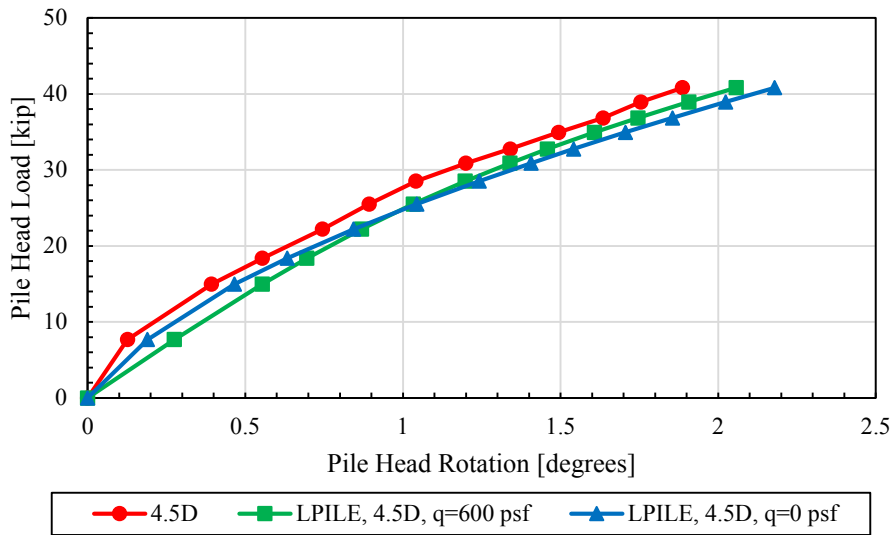


Figure 6-26. Comparison of measured pile head load versus pile head rotation curve for the 4.5D H-pile with curves computed using LPILE assuming no surcharge and 600 psf surcharge.

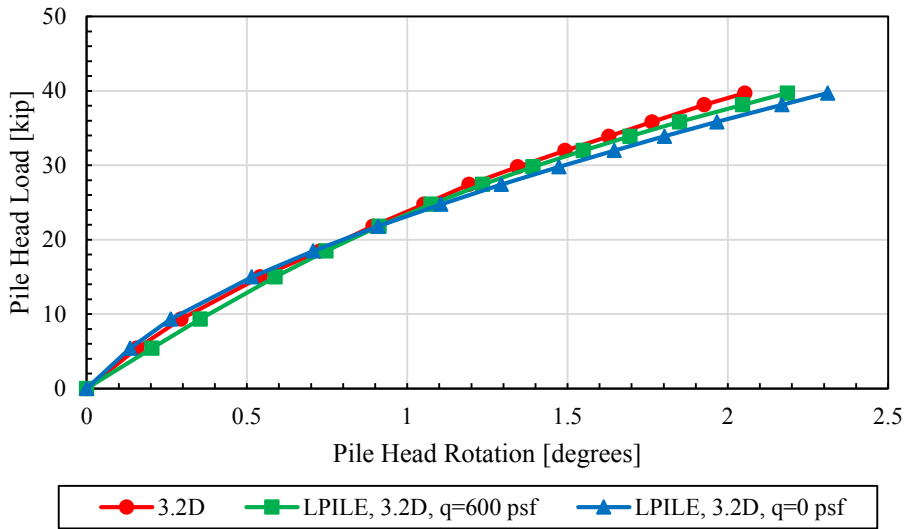


Figure 6-27. Comparison of measured pile head load versus pile head rotation curve for the 3.2D H-pile with curves computed using LPILE assuming no surcharge and 600 psf surcharge.

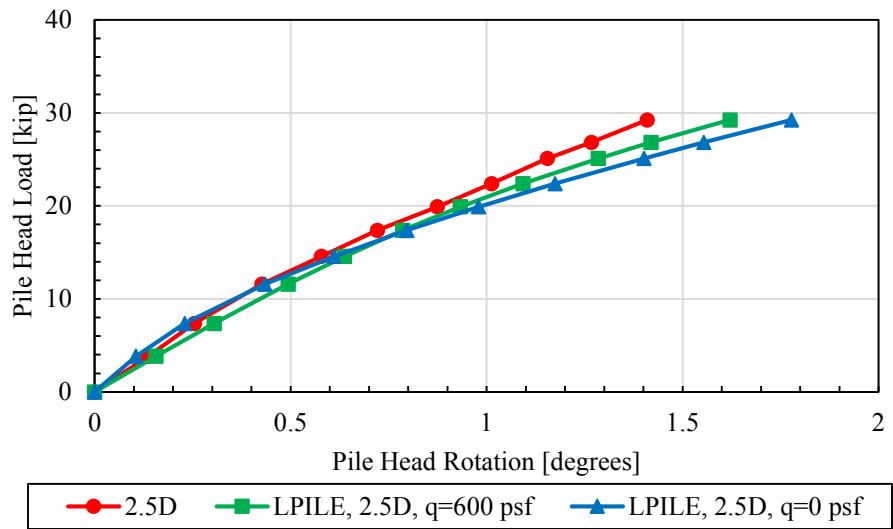


Figure 6-28. Comparison of measured pile head load versus pile head rotation curve for the 2.5D H-pile with curves computed using LPILE assuming no surcharge and 600 psf surcharge.

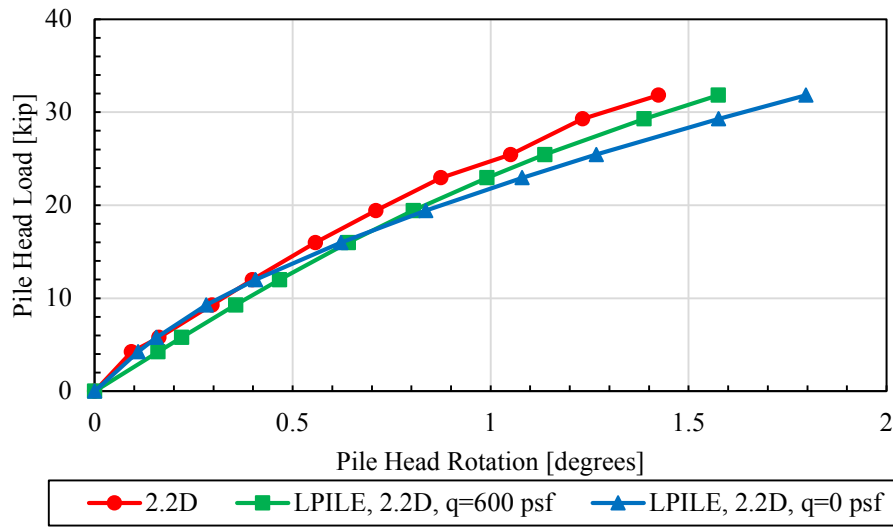


Figure 6-29. Comparison of measured pile head load versus pile head rotation curve for the 2.2D H-pile with curves computed using LPILE assuming no surcharge and 600 psf surcharge.

6.2.4.2 Square Piles

Pile head load versus pile rotation of the test data was also compared to the LPILE models of both the surcharge included and not included. Using the same parameters as shown above, Figure 6-30, Figure 6-31, Figure 6-32, and Figure 6-33 show the rotation curves for square piles 5.7D, 4.2D, 3.1D, and 2.1D respectively. The data all yielded very similar results. The 5.7D LPILE surcharge model had somewhat higher resistance to rotation. The rotation angle peaks at about 2 degrees for all of the piles. As mentioned above, these square piles were displaced to three inches during lateral loading.

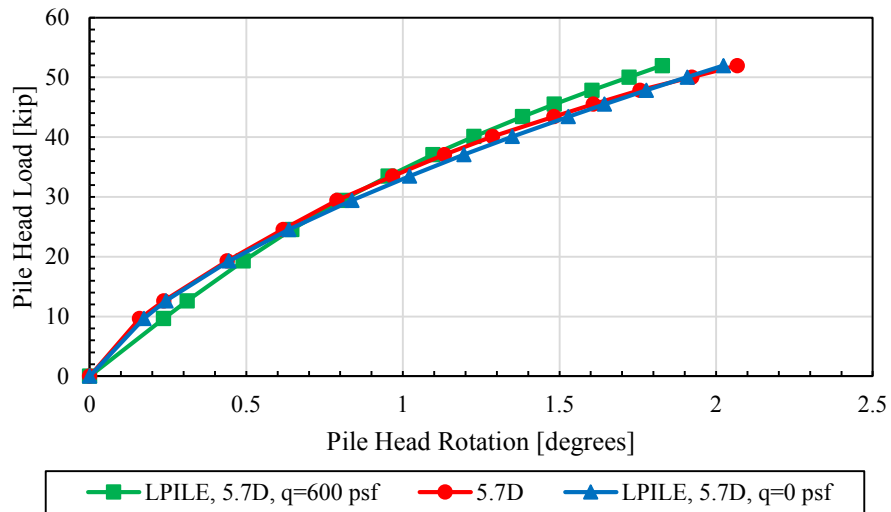


Figure 6-30. Comparison of measured pile head load versus pile head rotation curve for the 5.7D square pile with curves computed using LPILE assuming no surcharge and 600 psf surcharge.

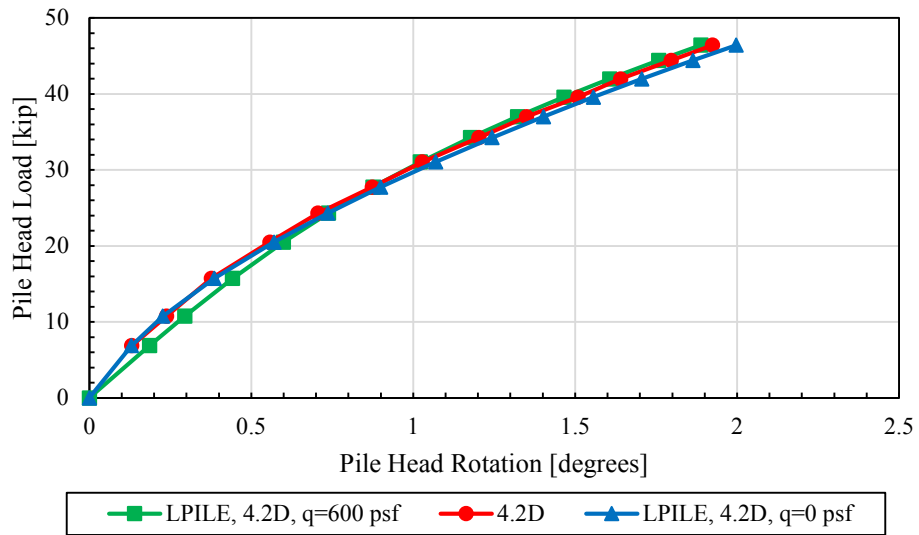


Figure 6-31. Comparison of measured pile head load versus pile head rotation curve for the 4.2D square pile with curves computed using LPILE assuming no surcharge and 600 psf surcharge.

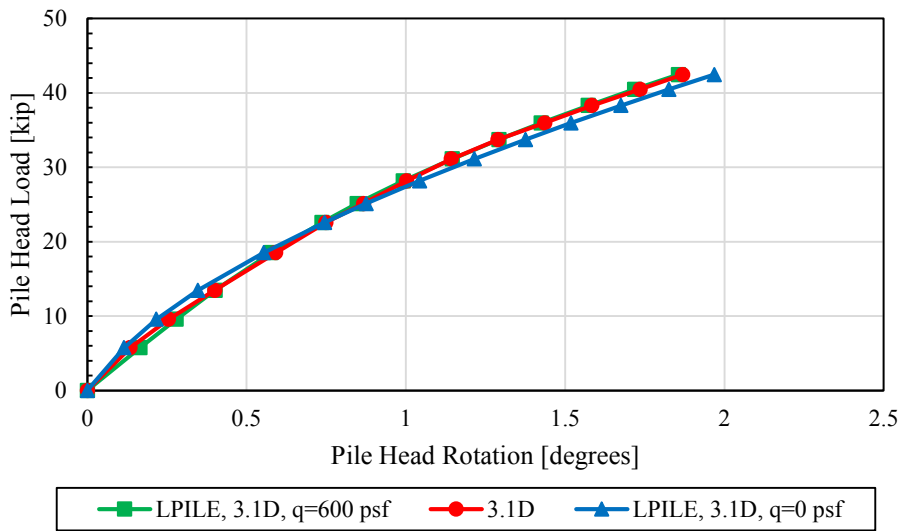


Figure 6-32. Comparison of measured pile head load versus pile head rotation curve for the 3.1D square pile with curves computed using LPILE assuming no surcharge and 600 psf surcharge.

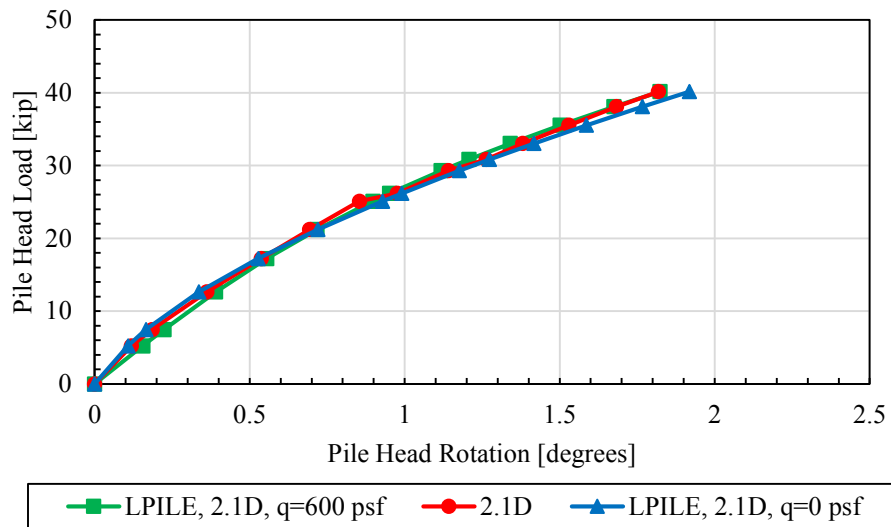


Figure 6-33. Comparison of measured pile head load versus pile head rotation curve for the 2.1D square pile with curves computed using LPILE assuming no surcharge and 600 psf surcharge.

6.2.5 Bending Moment versus Depth Curves

Moment curves were computed for both the H-piles and square piles to be compared with the LPILE models with and without a surcharge.

6.2.5.1 H-Piles

Pile bending moment versus depth curves were also computed using both of the LPILE models with and without surcharge along with appropriate p-multipliers for each pile. Figure 6-34, Figure 6-35, Figure 6-36, and Figure 6-37 show comparisons of measured and computed curves for piles located at 4.5D, 3.2D, 2.5D, and 2.2D, respectively. The figures correspond with the three-inch deflection for H-piles 4.5D and 3.2D, and with the two-inch deflection for H-piles 2.5D and 2.2D. All of the said figures also have curves corresponding to the 0.5-inch deflection. Generally, the moment increases until a certain depth, after which it decreases steadily. For all of the H-piles, the measured bending moment curve is larger than either LPILE model for both the

0.5-inch and three-inch deflections. This shows that LPILE underestimates the bending stress of an H-pile loaded about the weak axis. For the two to three-inch deflection curves, the LPILE curve modeled without a surcharge yields a higher maximum moment than the LPILE curve modeled with a surcharge, with the exception of the 4.5D H-pile. As explained, this suggests that a surcharge provides more resistance for a given lateral load. LPILE underestimates the actual bending moment of the piles by at least a couple of hundred kip-inches. For the 0.5-inch deflection curves, there is little difference between both LPILE models. The maximum measured moment occurs between 4 and 7 feet from the ground surface for curves corresponding with the two- to three-inch deflections. This is also true for both LPILE model curves.

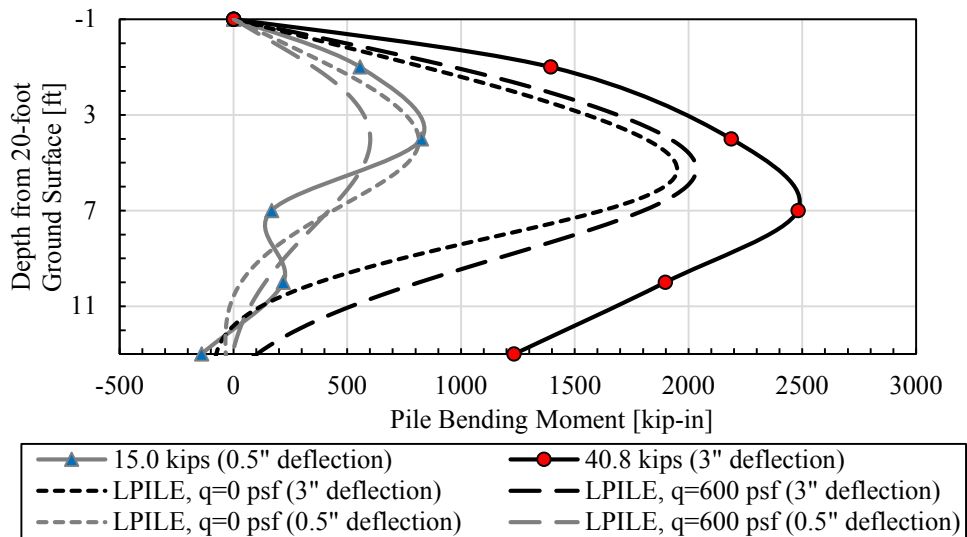


Figure 6-34. Comparison of depth from the ground surface versus pile bending moment curve and LPILE curves of both with the surcharge model and without the surcharge model for the 4.5D H-pile.

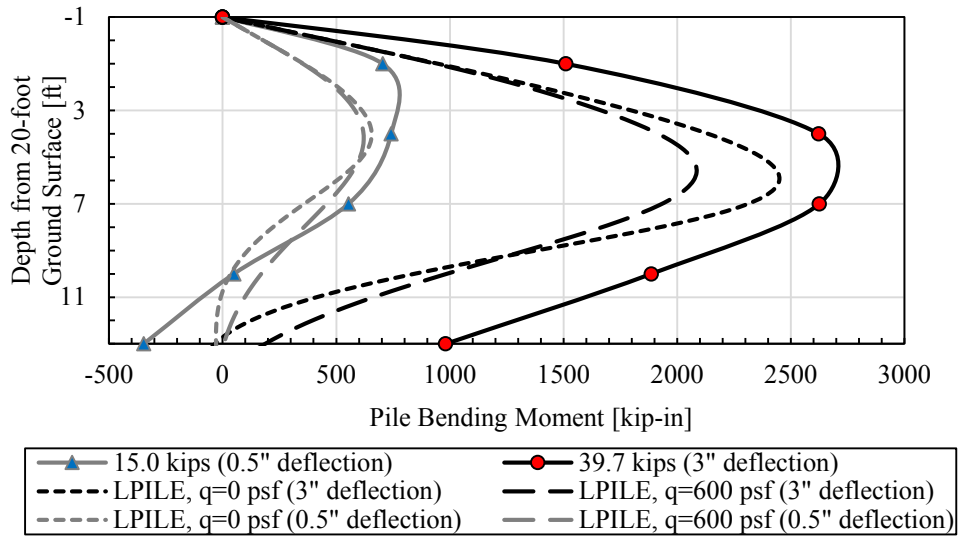


Figure 6-35. Comparison of depth from the ground surface versus pile bending moment curve and LPILE curves of both with the surcharge model and without the surcharge model for the 3.2D H-pile.

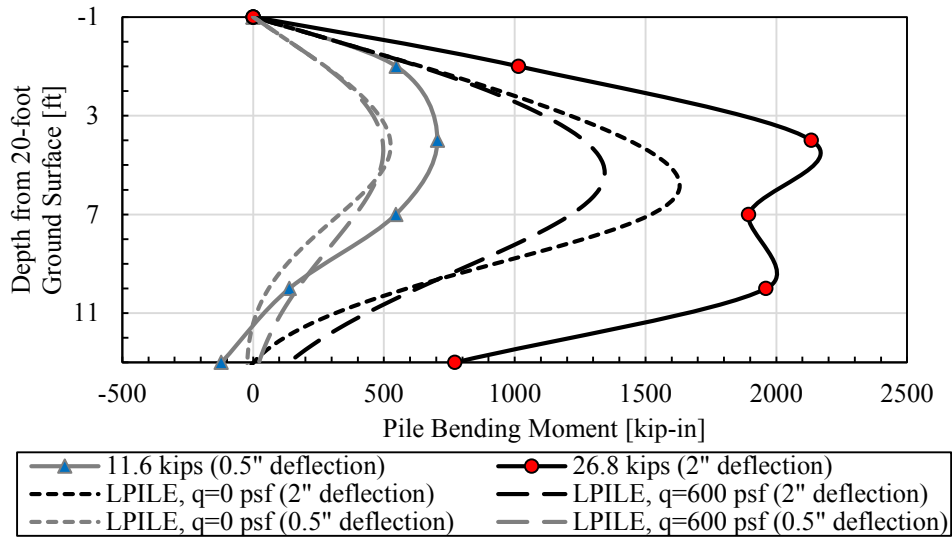


Figure 6-36. Comparison of depth from the ground surface versus pile bending moment curve and LPILE curves of both with the surcharge model and without the surcharge model for the 2.5D H-pile.

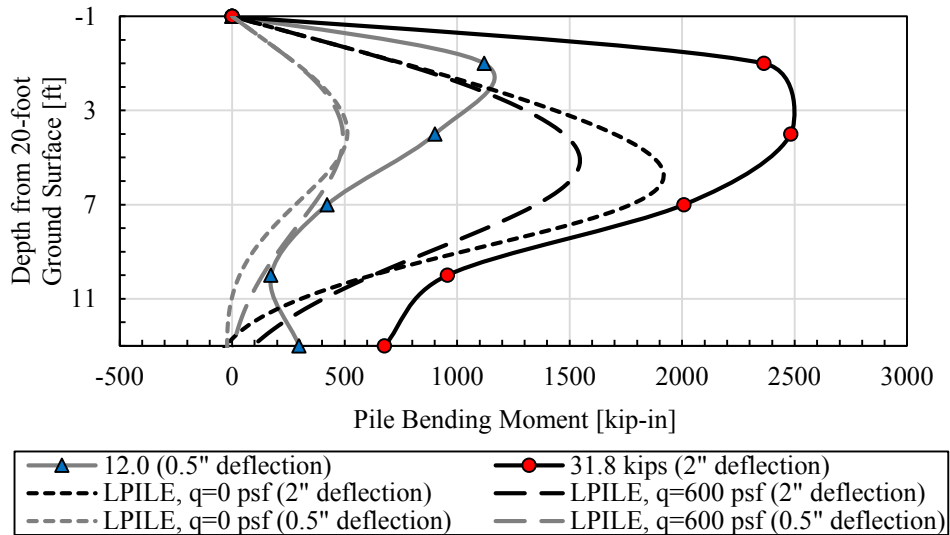


Figure 6-37. Comparison of depth from the ground surface versus pile bending moment curve and LPILE curves of both with the surcharge model and without the surcharge model for the 2.2D H-pile.

6.2.5.2 Square Piles

Pile bending moment versus depth curves were also computed for the square piles using both of the LPILE models with and without surcharge along with appropriate p-multipliers for each pile. Figure 6-38, Figure 6-39, Figure 6-40, and Figure 6-41 show comparisons of measured and computed curves for piles located at 5.7D, 4.2D, 3.1D, and 2.1D, respectively. The figures correspond with the three-inch deflection (the largest pile load) and the 0.5-inch deflection.

For the curves corresponding with the three-inch deflection, the LPILE curve modeled without a surcharge has a higher maximum moment than does the actual moment computed, with the exception of the 3.1D square pile. This suggests that LPILE gives conservative values for the bending stress of a square pile. However, for all of the square piles, the maximum moment of the measured moment curve is larger than the LPILE curve modeled with a surcharge. The overall shape of the curve is reasonably well captured. In all of the cases for the curves corresponding with the three-inch deflection, the LPILE model without a surcharge computes a higher maximum

moment than the LPILE model with a surcharge. This is likely because the surcharge increases the vertical stress and therefore the lateral resistance, producing more restraint on bending. The depth of the measured and computed LPILE maximum moments occurs 4 to 7 feet below the ground surface for most of the curves corresponding to the three-inch deflection. In all cases except for the 5.7D pile, the LPILE models have the maximum moment occur a few feet deeper than the measured moment curves.

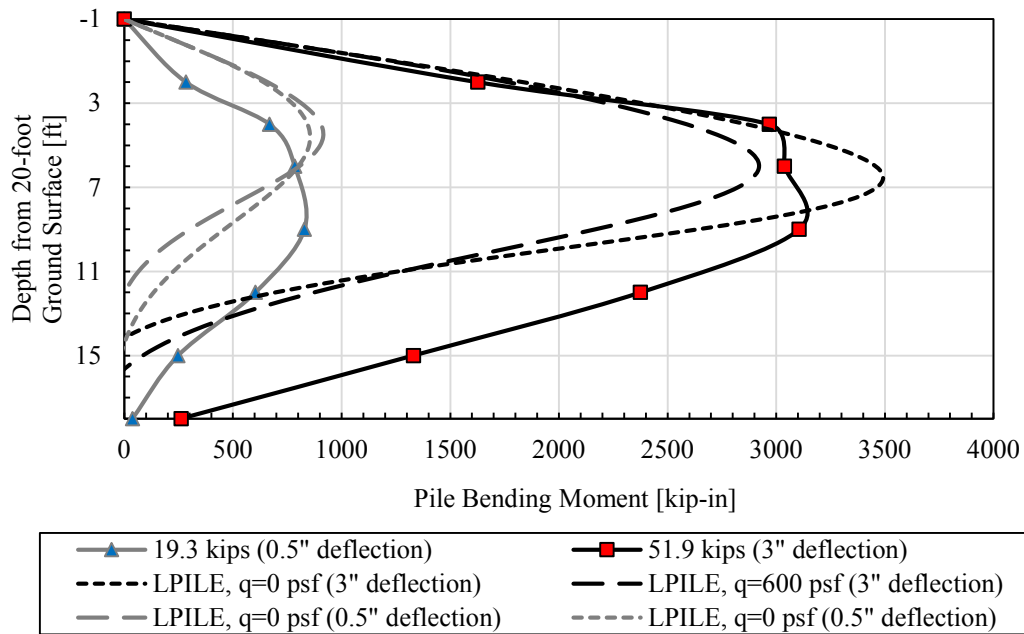


Figure 6-38. Comparison of depth from the ground surface versus pile bending moment curve and LPILE curves of both with the surcharge model and without the surcharge model for the 5.7D square pile.

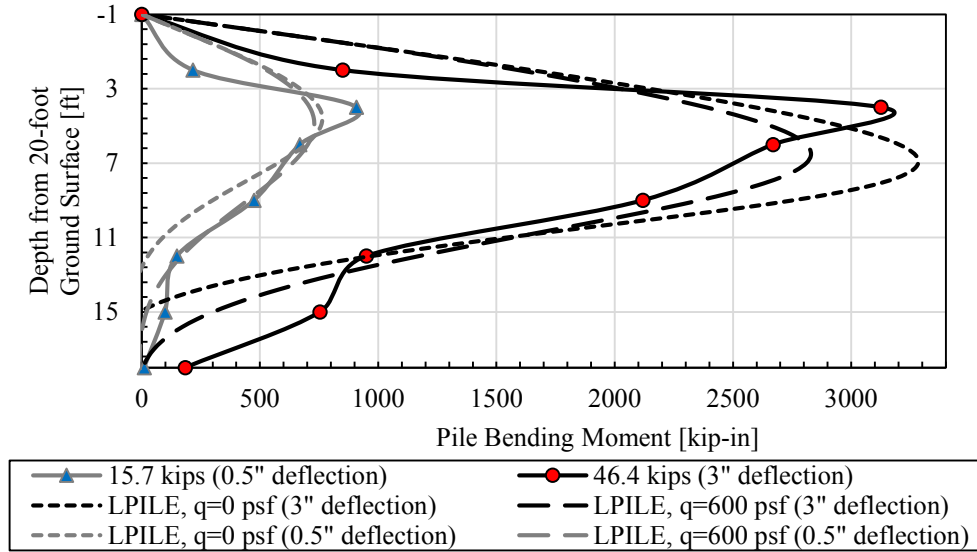


Figure 6-39. Comparison of depth from the ground surface versus pile bending moment curve and LPILE curves of both with the surcharge model and without the surcharge model for the 4.2D square pile.

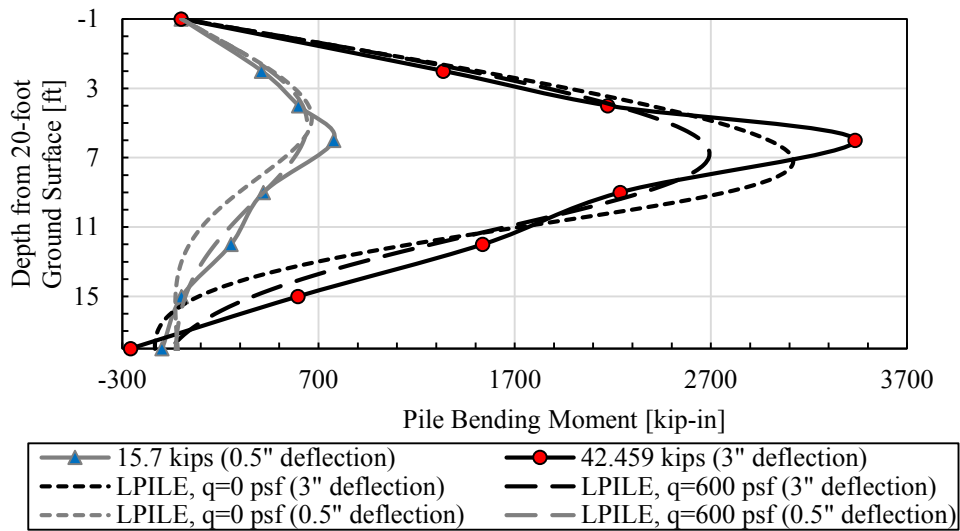


Figure 6-40. Comparison of depth from the ground surface versus pile bending moment curve and LPILE curves of both with the surcharge model and without the surcharge model for the 3.1D square pile.

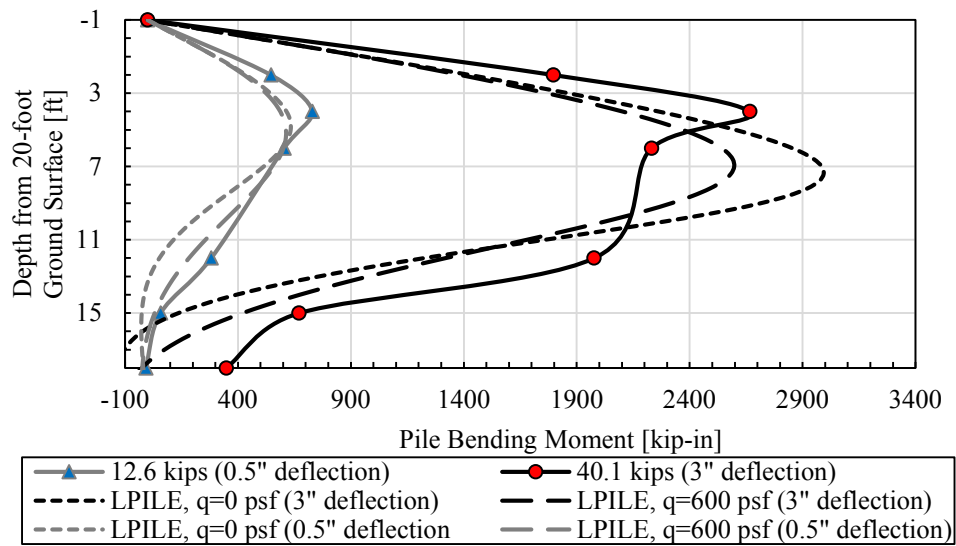


Figure 6-41. Comparison of depth from the ground surface versus pile bending moment curve and LPILE curves of both with the surcharge model and without the surcharge model for the 2.1D square pile.

7 CONCLUSION

Full scale lateral load tests were conducted on four H-piles spaced at 4.5, 3.2, 2.5, and 2.2 pile diameters behind an MSE wall, as well as four square piles spaced at 5.7, 4.2, 3.1, and 2.1 pile diameters from the wall. Ribbed strip soil reinforcement was used on the side of the MSE wall with the H-piles, and welded wire soil reinforcement was used on the side of the MSE wall with the square piles. The following sections are conclusions that were obtained relative to the lateral pile resistance, and relative to the force induced in the reinforcements. Recommendations for further research is then given.

7.1 Conclusions Relative to Lateral Pile Resistance

1. Piles placed closer to an MSE wall experience a reduction in lateral resistance. The 2.2D and 2.5D H-piles experienced about 81% and 73% of the lateral resistance of the 4.5D H-pile, respectively. The 2.1D square pile experienced about 66% of the lateral resistance of the 5.7D square pile. However, it was generally found that piles placed more than 3.9 pile diameters from the wall did not experience any significant decrease in lateral load resistance.
2. P-multipliers were obtained by back-analysis with LPILE for each test. The simple p-multiplier approach was generally successful in matching the measured load-deflection curve. For the model in LPILE without a surcharge, the p-multipliers for the H-piles spaced at 4.5D, 3.2D, 2.5D, and 2.2D were 1.0, 0.85, 0.60, and 0.73, respectively. The p-

multiplier for the 2.2D H-pile was higher than expected, which may be a result of greater compaction between the wall and pile. For the square piles spaced at 5.7D, 4.2D, 3.1D, and 2.1D, the p-multipliers were 1.0, 0.77, 0.63, and 0.57, respectively. When the surcharge behind the pile was approximated by a uniform surcharge over the entire surface, the p-multipliers for the H-piles tended to decrease slightly. There was almost no change for the p-multipliers for the square piles.

3. Based on all of the tests reported in this and previous related theses, the p-multiplier was 1.0 for normalized distances of 3.9D and decreased linearly for piles placed closer than 3.9 pile diameters. The best-fit equation (Equation 6-1a) for predicting the p-multipliers based on the spacing of the pile behind the wall had an R^2 value of about 74% for all data involving piles spaced closer than four pile widths, but increased to 86% with the exclusion of a few aberrations (Equation 6-2a).
4. For the pile loads and widths involved in this study, the p-multiplier versus distance curve was not significantly affected by the reinforcement length to wall height (L/H) ratio or the reinforcement type. It is conceivable that the pile shape or type of wall system may influence the p-multipliers.
5. Despite the relatively large pile head loads and displacements, the maximum wall deflections in front of the H-piles generally ranged from about 0.3 to 0.4 inches, and there was little distress to the wall. The maximum wall deflections in front of the square piles generally ranged from about 0.4 inches to 0.75 inches. Larger deflections occurred along the joints of the concrete panels in front of the piles loaded laterally. Wall displacements were generally largest a few feet below the top of the wall.

7.2 Conclusions Relative to Force Induced in the Reinforcements

1. Tensile force in the reinforcements generally increases from the wall to the pile, and then decreases along the rest of the reinforcement length. The maximum force typically occurs near the pile.
2. The maximum reinforcement force increases with an increase in applied lateral loading and when the pile spacing behind the wall decreases. The maximum reinforcement force also decreases as the transverse distance from the pile center to the reinforcement increases. Generally, within the top two layers, the reinforcement with higher vertical stress did not always produce higher induced force.
3. Statistical regression equations were produced to predict the maximum reinforcement force. The main effects used in the equations were the lateral pile load, transverse distance from the reinforcement to the pile center normalized by the pile diameter, spacing from the pile center to the wall normalized by the pile diameter, vertical stress, and reinforcement length to height ratio where the height includes the equivalent height of the surcharge. Equation (5-4) was obtained for ribbed strip reinforcement, and accounts for 76.2% variation. Equation (5-8) was obtained for welded wire reinforcement, and accounts for 77.4% variation.

7.3 Recommendations for Further Research

Compaction of the soil between the piles and MSE wall was a governing factor in the results of the lateral load testing. Further research could involve the lateral testing of piles with different levels of compaction for the soil between the piles and wall, and the soil properties could be correlated with relative compaction. In this case, it would be recommended that the piles be kept at the same distance from the wall, possibly far enough behind the wall where the p-multiplier

would not be a variable. In addition, wall displacements seemed to be affected most when the piles were behind a panel joint configuration. This suggests that further reductions might need to be made to laterally loaded piles depending on their location behind an MSE wall panel joint or center, and thus further research could be performed based on panel configurations.

The displacement control method was used to load the piles laterally in increments. This type of loading was most representative of static loading. However, like all structures, piles are susceptible to seismic loading. Thus, it is recommended that further research be performed for piles loaded cyclically to be most representative of this and other type of cyclic loading. Also, the pile loading was modeled as a pinned-head connection, but pile caps would be better represented as a fixed-end connection. Thus, future research could also include laterally loaded piles modeled with a fixed-end connection. Finally, all tests in this study have involved piles with a diameter of about 12 inches, and normalization by pile diameter had been assumed to be appropriate. Additional tests with larger pile diameters could be useful to determine if this is actually the case.

REFERENCES

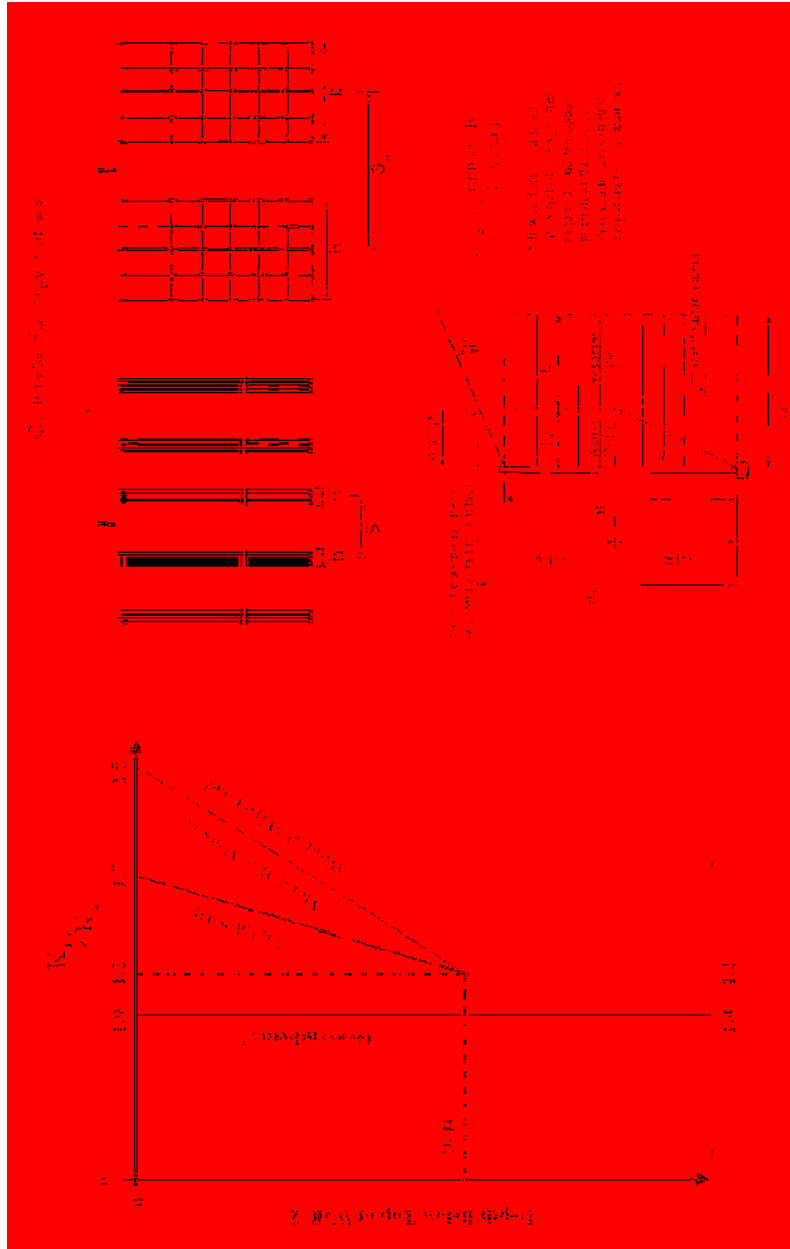
- AASHTO LRFD Bridge Design Specifications*. (2012). 6th Ed., Washington, DC.
- American Petroleum Institute, 2010. *Recommended Practice for Planning, Designing and Constructing Fixed Offshore Platforms - Working Stress Design, API RP 2A-WSD*, 21st Edition, Errata and Supplement, 2010.
- Berg, R.R., Christopher, B.R., and Samtani, N.C. (2009). “Design of Mechanically Stabilized Earth Walls and Reinforced Soil Slopes” *FHWA, Washington, D.C., Report No. FHWA-NHI-10-024*.
- Besendorfer, J. J. (2015). “Lateral Resistance of Pipe Piles Near 20-ft Tall MSE Abutment Wall with Strip Reinforcements” MS Thesis, Department of Civil and Environmental Engineering, Brigham Young University, Provo, UT.
- Budd, R. T. (2016). “Lateral Resistance of Pipe Piles Behind a 20-ft Tall MSE Wall with Welded-Wire Reinforcements” MS Thesis, Department of Civil and Environmental Engineering, Brigham Young University, Provo, UT.
- Bustamante, G. X. (2014). “Influence of Pile Shape on Resistance to Lateral Loading” MS Thesis, Department of Civil and Environmental Engineering, Brigham Young University, Provo, UT.
- Han, J. J. C. (2014). “Lateral Resistance of Piles Near 15 Foot Vertical MSE Abutment Walls Reinforced with Ribbed Steel Strips” MS Thesis, Department of Civil and Environmental Engineering, Brigham Young University, Provo, UT.
- Hatch, C. K. (2014). “Lateral Resistance of Piles Near Vertical MSE Abutment Walls” MS Thesis, Department of Civil and Environmental Engineering, Brigham Young University, Provo, UT.
- Isenhower, W.M., Wang S. (2015). *Technical Manual for LPile 2015 (Using Data Format Version 8)*. Ensoft Inc., Austin, TX.

- Jayawickrama, P. W., Lawson, W. D., Wood, T. A., and Surles, J. G. (2015). "Pullout Resistance Factors for Steel MSE Reinforcements Embedded in Gravelly Backfill." *J. Geotech. Geoenviron. Eng. Journal of Geotechnical and Geoenvironmental Engineering*, 141(2), 04014090.
- Lawson, W., Jayawickrama, P., Wood, T., and Surles, J. (2013). "Pullout Resistance Factors for Inextensible Mechanically Stabilized Earth Reinforcements in Sandy Backfill." *Transportation Research Record: Journal of the Transportation Research Board*, 2362, 21-29.
- "Measurement Principles of (DIC)." *Digital Image Correlation (DIC) Measurement Principles*, <<http://www.dantecdynamics.com/measurement-principles-of-dic>> (Aug. 11, 2015).
- Nelson, K. R. (2013). "Lateral Resistance of Piles Near Vertical MSE Abutment Walls at Provo Center Street" MS Thesis, Department of Civil and Environmental Engineering, Brigham Young University, Provo, UT.
- O'Neill, M. W., and Murchison, J. M., 1983. "An Evaluation of p-y Relationships in Sands," *Report to the American Petroleum Institute, PRAC 82-41-1*, The University of Houston-University Park, Houston.
- Pierson, M., Parsons, R.L., Han, J., Brown, D.A. and Thompson, W.R. (2009). "Capacity of Laterally Loaded Shafts Constructed Behind the Face of a Mechanically Stabilized Earth Block Wall", *Kansas Department of Transportation, Report No. K-TRAN: KU-07-6*.
- Price, J. S. (2012). "Lateral Resistance of Piles Near Vertical MSE Abutment Walls" MS Thesis, Department of Civil and Environmental Engineering, Brigham Young University, Provo, UT.
- Reese, L. C., and Van Impe, W. F. (2011), *Single Piles and Pile Group under Lateral Loading*. 2nd Ed., A. A. Balkema, Rotterdam, Netherlands.
- Rollins, K. M., Price, J. S., and Nelson, K. R. (2013). "Lateral Resistance of Piles Near Vertical MSE Abutment Walls", *Utah Department of Transportation, Report No. UT-IX.13*.
- Russell, D. N. (2016). "The Influence of Pile Shape and Pile Sleeves on Lateral Load Resistance" MS Thesis, Department of Civil and Environmental Engineering, Brigham Young University, Provo, UT.

Source: “Test Site”. 40°27’11.23” N and 111°53’57.99” W. GOOGLE EARTH. April 9, 2013.
February 6, 201

APPENDIX A.

CAPACITY TO DEMAND RATIO AGAINST PULLOUT CALCULATIONS



Ribbed Strip Reinforcement

MSE Wall- Ribbed Strip Side

MSE Wall Properties

H	20
H ₁	24.8
w _p	3.84
h _p	4.32
4	4

$$H_1 = H + H_{q3}$$

Reinforcement Properties

γ _r	126.2
φ _r	38
K _r	0.66
C _u	0.238
D ₁₀	60.0
D ₃₀	3
D ₆₀	0.05

$$K_r = \tan^2(45 - \frac{\phi_r}{2})$$

[Eqn. 4-25]

$$= D_{60}/D_{10}$$

Strip Reinforcement Properties

S _v	2.5
S _h	2.5
L ₁	18
a	1
C	2
b	50
t	1.968
τ	4
R _c	0.157
	0.066

$$L_1 = L_2 + L_3$$

[Fig. 3-3]

[pp. 3-16, 4-43]

[Eqn. 4-32a]

[Eqn. 4-30]

Surcharge

γ _{sur}	126
H _{sur}	4.8
q	600
γ _{sur} (kN/m ³)	1.36
γ _{sur} (pcf)	0.9

Load Factor for Maximum Permanent Loads

Resistance Factor for Pullout

Depth, Z [ft]	Resistance Length in Resistance Zone, L _r [ft]
at Z = 0	0
at Z = H ₁ /2	12.38
at Z = H ₁	24.8

$$L_r = 0.3H$$

Top of Structure

$$F^* = 1.2 + \log C_u \leq 2.0$$

$$F^* = \tan \phi_r$$

Depth Below Top of Wall, Z	K _r , K _s	F*
0	1.7	2
20	1.2	0.781

Boundaries for Pullout Friction Factor, F*

[Sim. to Eqn. 4-35]

[Fig. 4-9 and Eqns. 4-37, 4-40]

[Eqn. 4-32a] [Eqns. 3-6, 3-7]

[Fig. 4-10]

[Table 4-2]

[Table 4-7]

Reinforcement Level	Depth to Layer, Z [ft]	K _r /K _s	Horizontal Earth Pressure Coefficient, K _e	Vertical Stress, σ _v = γ _{sur} (Z+H _{sur}) [psf]	Factored Horizontal Stress, σ _h = K _e (γ _{sur} (Z+H _{sur})) [psf]	Reinforcement Demand, T _{req} = σ _h (50) [kN]	Strip Reinforcement Pullout Friction Factor, F*	Length of Reinforcement in Resistance Zone, L _r [ft]	Length of Reinforcement in Active Zone, L _a [ft]	Factored Pullout Resistance, P _{pr} = F* F _{req} L _a CR _c [kN]	Capacity to Demand Ratio, COB = P _{pr} /T _{req}
1	1.25	1.67	0.397	758	406	102	1.924	10.57	7.43	182	1.79
2	3.75	1.61	0.362	1073	554	138	1.771	10.57	7.43	237	1.72
3	6.25	1.54	0.367	1389	688	172	1.619	10.57	7.43	281	1.63
4	8.75	1.48	0.352	1704	811	2.03	1.467	10.57	7.43	312	1.54
5	11.25	1.42	0.337	2020	920	2.30	1.314	10.57	7.43	332	1.44
6	13.75	1.36	0.323	2335	1017	2.54	1.162	11.40	6.60	3.65	1.44
7	16.25	1.29	0.308	2651	1101	2.75	1.010	12.90	5.10	4.08	1.48
8	18.75	1.23	0.293	2966	1173	2.93	0.857	14.40	3.60	4.33	1.48

Average COB: 1.56

Welded Wire Reinforcement

MSE Wall- Phase 2

MSE Wall Properties

Wall Height	H	20	ft
Total Height	H _t	24.8	ft
Panel Width	w _p	3.94	ft
Panel Height	h _p	4.94	ft
Reinforcements per Panel Along Wall Length		2	

$$H_1 = H + H_{eq}$$

Soil Properties

Reinforced Backfill Moist Unit Weight	γ ₁	125.2	pcf
Friction Angle	φ ₁	38	deg
Active Earth Pressure Coefficient	K _a	0.186	rad
		0.238	(Eqn. 4-25)

$$K_a = \tan^2 \left(45 - \frac{\phi_1}{2} \right)$$

Top of Structure Depth of 20 ft +

$$F^* = 20(r/S_2) \quad F^* = 10(t/S_2)$$

Grid Reinforcement Properties

Approximate Vertical Spacing	S _v	2.5	ft
Approximate Horizontal Spacing	S _h	5	ft
Length of Reinforcement	L	18	ft
Longitudinal Grid Spacing	S _l	8	in
Scale Effect Correction Factor	α	1	(p. 3-18)
Reinforcement Effective Unit Perimeter	C	2	(pp. 3-16, 4-43)
Nominal Transverse Wire Thickness, w/T1	τ	0.374	in

$$L_r = 0.311$$

$$L = L_r + L_s$$

Surcharge

Unit Weight of Surcharge	γ _{1s}	125.2	pcf
Equivalent Surcharge Height	H _{1s}	4.8	ft
Surcharge (Dead Load)	q	600	psf

Depth Below Top of Wall, Z	K _a /K _o	F* (Top Layer)	F* (Other Layers)
0	2.5	1.247	0.623
20	1.2	0.623	0.312

Depth, Z [ft]	Reinforcement Length in Resistance Zone, l
at Z = 0	10.57
at Z = H ₁ /2	10.57
at Z = H ₁	18


Depth Below Top of Wall, Z	K _a /K _o	F* (Top Layer)	F* (Other Layers)
0	2.5	1.247	0.623
20	1.2	0.623	0.312

Reinforcement Layer	Wire Type	Depth to Layer, z [ft]	K _a /K _o	Horizontal Earth Pressure Coefficient, K _a	Vertical Stress, σ _v = (Z+H _{1s})γ ₁ [psf]	Horizontal Stress, σ _h = K _a (Z+H _{1s})γ ₁ [psf]	Reinforcement Demand, T _{req} = w _s (S _v) [lb/ft]	Transverse Grid Spacing, S _t [in]	Reinforcement Pullout Friction Factor, F*	Length of Reinforcement in Resistance Zone, L _r [ft]	Length of Reinforcement in Active Zone, L _a [ft]	Grid Reinforcement Width, b [ft]	Grid Reinforcement Coverage Ratio, R _c = b/S _l	Nominal Pullout Resistance, P _n = F* _{av} LC [lb/ft]	Capacity to Demand Ratio, CDR = P _n /T _{req}
1	6W1TX1.00W11	1.25	2.42	0.58	758	436	109	6	1.208	10.57	7.43	3.33	0.667	12.90	11.84
2	6W1TX1.00W11	3.75	2.26	0.54	1073	576	144	12	0.565	10.57	7.43	2.87	0.533	6.84	4.75
3	5W1TX1.00W11	6.25	2.09	0.50	1389	692	173	12	0.526	10.57	7.43	2.87	0.533	8.24	4.76
4	5W1TX1.00W11	8.75	1.93	0.46	1704	783	196	12	0.487	10.57	7.43	2.87	0.533	9.36	4.78
5	5W1TX1.00W11	11.25	1.77	0.42	2020	850	212	12	0.448	10.57	7.43	2.67	0.533	10.21	4.80
6	6W1TX1.00W11	13.75	1.61	0.38	2335	892	223	12	0.409	11.40	6.60	3.33	0.667	14.52	6.51
7	6W1TX1.00W11	16.25	1.44	0.34	2651	910	228	12	0.370	12.90	5.10	3.33	0.667	18.87	7.41
8	6W1TX1.00W11	18.75	1.28	0.30	2966	904	226	12	0.331	14.40	3.60	3.33	0.667	18.86	8.34

Average CDR: 6.65

APPENDIX B. GENEVA ROCK LABORATORY TEST REPORTS


Phase 1

 GENEVA ROCK PRODUCTS, INC. 1565 West 400 North • P.O. Box 538 • Oram, UT 84059 • (801) 765-7800 • Fax (801) 765-7830 • www.genevareck.com		AGGREGATE SUBMITTAL	
		Report of Physical Properties	
GRP Material Description: <u>Fill - 3/8" HARDPAC</u>		Report Date: <u>April 15, 2014</u>	
GRP Material Code: <u>FINE</u>		Reviewed by: <u>Victor Johnson</u>	
Source Location/Code: <u>North Hansen / S27</u>		Report No. <u>S27FINE00114</u>	

TEST RESULTS				
Standard	PHYSICAL PROPERTIES		Result	Test Source
ASTM C 29 AASHTO T 19	Unit Weight	Unit Weight, lbs./cu.ft. =	112.0	
		Voids, % = <input type="checkbox"/> Jigged <input type="checkbox"/> Loose <input checked="" type="checkbox"/> Rodded	30	
ASTM D 1557 AASHTO T 160	Modified Proctor	Max. density, lbs./cu.ft. = Optimum Moisture, % =	133.0 7	
ASTM D 698 AASHTO T 99	Standard Proctor	Max. density, lbs./cu.ft. = Optimum Moisture, % =	128.0 7.8	
ASTM D 4318 AASHTO T 89/90	Liquid Limit Plastic Limit Plasticity Index	Liquid Limit = Plastic Limit = Plasticity Index =	0 0 NP	
ASTM C 131 AASHTO T 96	L.A. Abrasion	Small Coarse Loss, % = Grading Revolutions, =		
ASTM C 695	L.A. Abrasion	Large Coarse Loss, % = Grading Revolutions, =		
ASTM C 128 AASHTO T 84	Fine Specific Gravity & Absorption	Bulk Specific Gravity (dry) = Bulk Specific Gravity, SSD = Apparent Specific Gravity = Absorption, % =	2.581 2.599 2.628 0.7	
ASTM C 127 AASHTO T 85	Coarse Specific Gravity & Absorption	Bulk Specific Gravity (dry) = Bulk Specific Gravity, SSD = Apparent Specific Gravity = Absorption, % =		
ASTM D 2419 AASHTO T 176	Sand Equivalent	Sand Equivalent, % =	34	
ASTM C 88 AASHTO T 104	Soundness	Coarse Soundness Loss, % = Magnesium No. of Cycles =		
	Soundness	Fine Soundness Loss, % = Sodium Sulfate No. of Cycles =	1.0	
ASTM C 1252 AASHTO T 304	Fine Aggregate Angularity	Uncompacted Voids, % = Method C (as received material)	48.3	
ASTM C 40 AASHTO T 21	Organic Impurities	Coarse Aggregate, % = Fine Aggregate, % =	Lighter Plate # 1	
ASTM C 142 AASHTO T 112	Clay / Friable Particles	Coarse Aggregate, % = Fine Aggregate, % =	0.0	
ASTM C 129 AASHTO T 113	Lightweight Pieces	Coarse Aggregate, % = Fine Aggregate, % =		
ASTM D 1983 AASHTO T 193	CBR	Surcharge = 10 lbs. CBR @ 0.1% Swell% = 0.0% CBR @ 0.2% =	50 99	
ASTM D 5821	Fractured Face	1 or 2 Faces = Fractured Face, % =		
ASTM D 2487	Soil Classification	Group Symbol = Group Name =		Well-graded gravel with silt and sand
ASTM D 2488	Soil Description & Identification	Group Symbol = Group Name =		Cu=66.7 Cc=1.8

SIEVE ANALYSIS		
ASTM C 136	AASHTO T 27	
Sieve Size	% Passing	Spec.
450 mm (18")		
375 mm (15")		
300 mm (12")		
250 mm (10")		
225 mm (9")		
200 mm (8")		
150 mm (6")		
125 mm (5")		
100 mm (4")		
75.0 mm (3")		
63.0 mm (2-1/2")		
50.0 mm (2")		
37.5 mm (1-1/2")		
25.0 mm (1")		
19.0 mm (3/4")		
12.5 mm (1/2")	100	
9.5 mm (3/8")	100	
6.3 mm (1/4")		
4.75 mm (No.4)	77	
2.36 mm (No.8)	52	
2.00 mm (No.10)		
1.18 mm (No.16)	37	
0.600 mm (No.30)	30	
0.425 mm (No.40)		
0.300 mm (No.50)	25	
0.180 mm (No.80)		
0.150 mm (No.100)	20	
0.075 mm (No.200)	14	
ASTM D 422		
Hydrometer =		
ASTM C 566 AASHTO T 255		
Moisture Content, % =		
ASTM C 136 AASHTO T 27		
Fineness Modulus (FM) =		
AASHTO M 145		
Classification of Soils =	A1B	
ASTM D 4791 Ratio =		
Flat & Elongated =		

Phase 2

 UNIVERSITY OF MANITOBA Faculty of Forestry and Environmental Science Department of Forest Management Forestry Engineering and Technology Forestry Engineering and Technology Forestry Engineering and Technology		REPORT NO. 1014 REPORT OF FIELD PRODUCTION FOREST ENGINEERING AND TECHNOLOGY FOREST ENGINEERING AND TECHNOLOGY FOREST ENGINEERING AND TECHNOLOGY	
Project Name	Client	Project No.	Project Date
Project Location	Project Description	Project Status	Project Type
1. PROJECT NAME	2. CLIENT	3. PROJECT NO.	4. PROJECT DATE
5. PROJECT LOCATION	6. PROJECT DESCRIPTION	7. PROJECT STATUS	8. PROJECT TYPE
9. PROJECT LOCATION	10. PROJECT DESCRIPTION	11. PROJECT STATUS	12. PROJECT TYPE
13. PROJECT LOCATION	14. PROJECT DESCRIPTION	15. PROJECT STATUS	16. PROJECT TYPE
17. PROJECT LOCATION	18. PROJECT DESCRIPTION	19. PROJECT STATUS	20. PROJECT TYPE
21. PROJECT LOCATION	22. PROJECT DESCRIPTION	23. PROJECT STATUS	24. PROJECT TYPE
25. PROJECT LOCATION	26. PROJECT DESCRIPTION	27. PROJECT STATUS	28. PROJECT TYPE
29. PROJECT LOCATION	30. PROJECT DESCRIPTION	31. PROJECT STATUS	32. PROJECT TYPE
33. PROJECT LOCATION	34. PROJECT DESCRIPTION	35. PROJECT STATUS	36. PROJECT TYPE
37. PROJECT LOCATION	38. PROJECT DESCRIPTION	39. PROJECT STATUS	40. PROJECT TYPE
41. PROJECT LOCATION	42. PROJECT DESCRIPTION	43. PROJECT STATUS	44. PROJECT TYPE
45. PROJECT LOCATION	46. PROJECT DESCRIPTION	47. PROJECT STATUS	48. PROJECT TYPE
49. PROJECT LOCATION	50. PROJECT DESCRIPTION	51. PROJECT STATUS	52. PROJECT TYPE
53. PROJECT LOCATION	54. PROJECT DESCRIPTION	55. PROJECT STATUS	56. PROJECT TYPE
57. PROJECT LOCATION	58. PROJECT DESCRIPTION	59. PROJECT STATUS	60. PROJECT TYPE
61. PROJECT LOCATION	62. PROJECT DESCRIPTION	63. PROJECT STATUS	64. PROJECT TYPE
65. PROJECT LOCATION	66. PROJECT DESCRIPTION	67. PROJECT STATUS	68. PROJECT TYPE
69. PROJECT LOCATION	70. PROJECT DESCRIPTION	71. PROJECT STATUS	72. PROJECT TYPE
73. PROJECT LOCATION	74. PROJECT DESCRIPTION	75. PROJECT STATUS	76. PROJECT TYPE
77. PROJECT LOCATION	78. PROJECT DESCRIPTION	79. PROJECT STATUS	80. PROJECT TYPE
81. PROJECT LOCATION	82. PROJECT DESCRIPTION	83. PROJECT STATUS	84. PROJECT TYPE
85. PROJECT LOCATION	86. PROJECT DESCRIPTION	87. PROJECT STATUS	88. PROJECT TYPE
89. PROJECT LOCATION	90. PROJECT DESCRIPTION	91. PROJECT STATUS	92. PROJECT TYPE
93. PROJECT LOCATION	94. PROJECT DESCRIPTION	95. PROJECT STATUS	96. PROJECT TYPE
97. PROJECT LOCATION	98. PROJECT DESCRIPTION	99. PROJECT STATUS	100. PROJECT TYPE

APPENDIX C. LOAD DISPLACEMENT CURVES

H-Piles

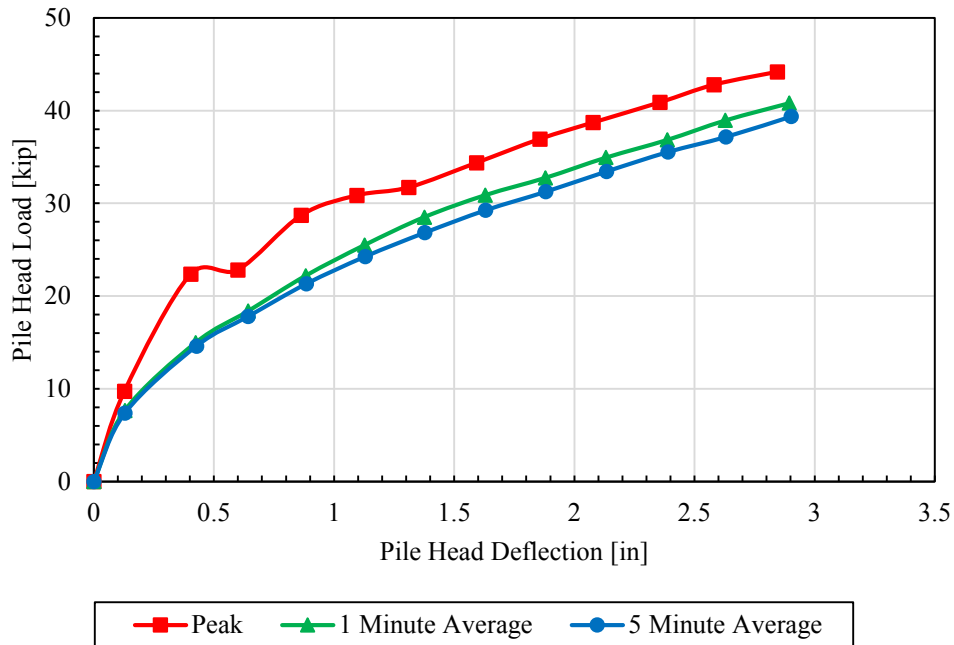


Figure C-1. Pile head load versus pile head deflection comparing peak, 1-minute hold, and 5-minute hold for 4.5D H-pile.

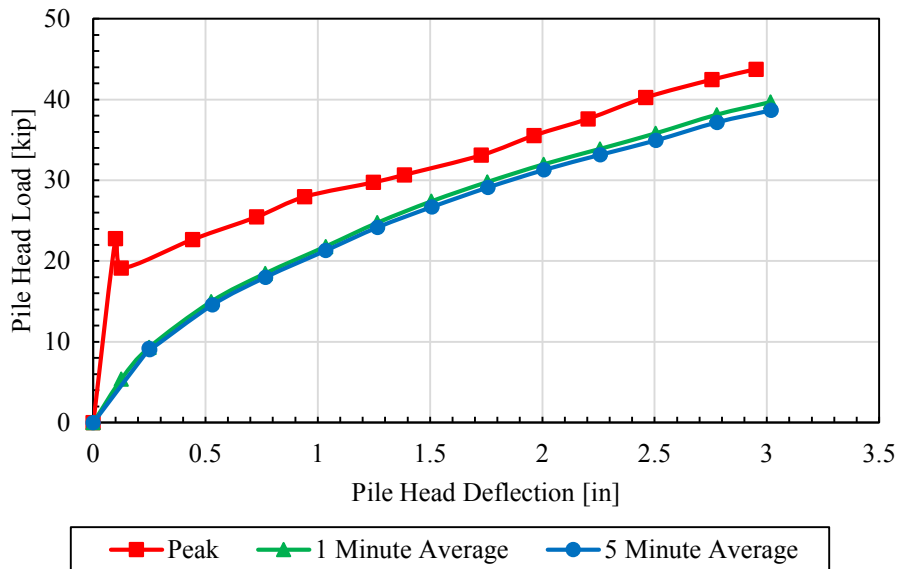


Figure C-2. Pile head load versus pile head deflection comparing peak, 1-minute hold, and 5-minute hold for 3.2D H-pile.

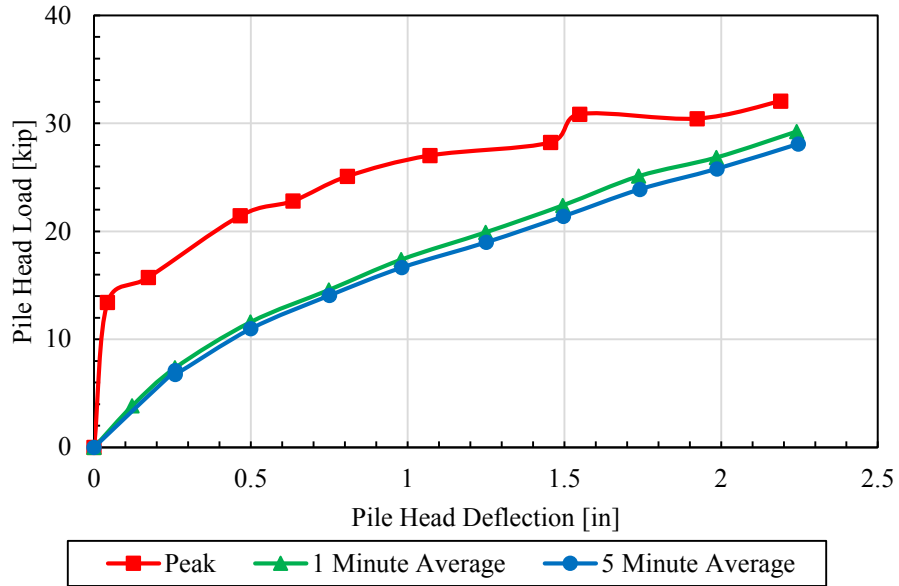


Figure C-3. Pile head load versus pile head deflection comparing peak, 1-minute hold, and 5-minute hold for 2.5D H-pile.

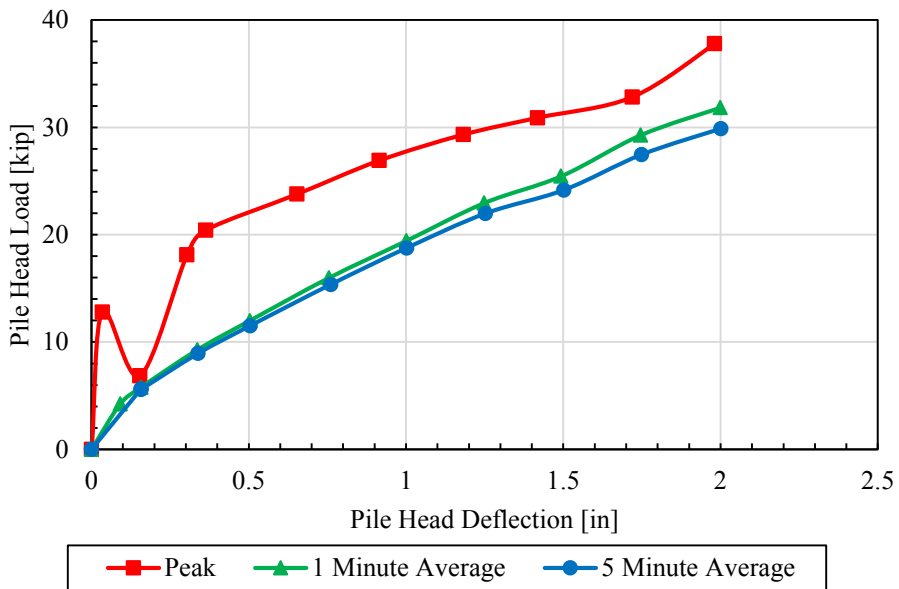


Figure C-4. Pile head load versus pile head deflection comparing peak, 1-minute hold, and 5-minute hold for 2.2D H-pile.

Square Piles

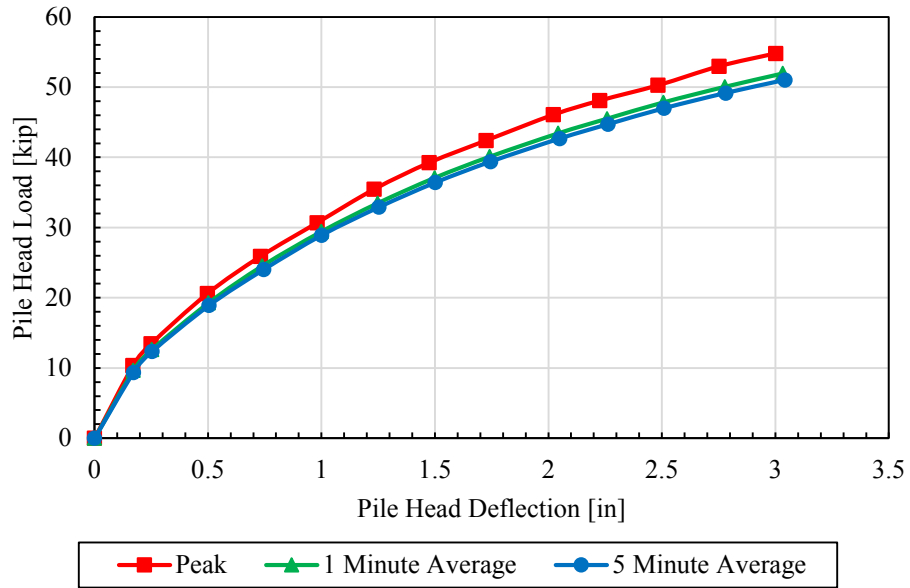


Figure C-5. Pile head load versus pile head deflection comparing peak, 1-minute hold, and 5-minute hold for 5.7D square pile.

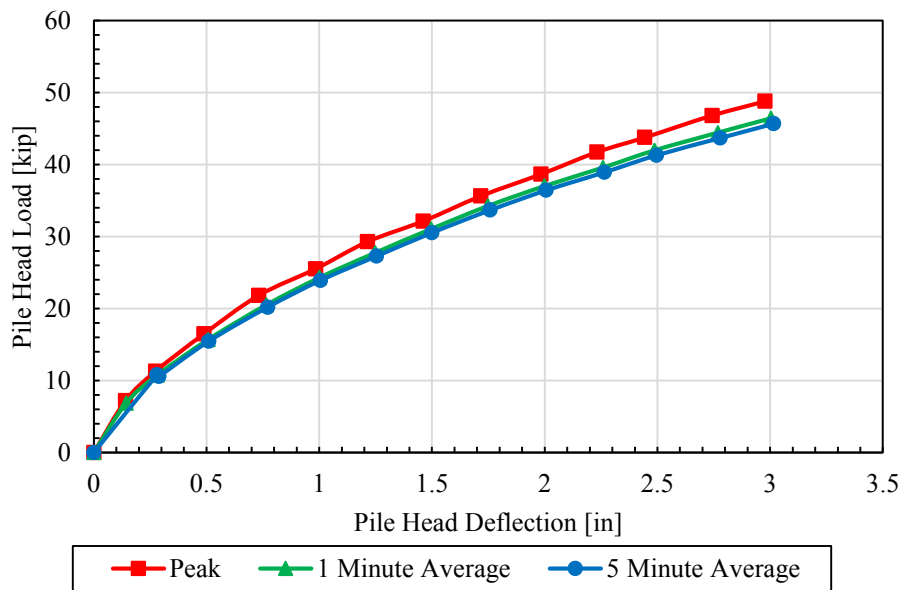


Figure C-6. Pile head load versus pile head deflection comparing peak, 1-minute hold, and 5-minute hold for 4.2D square pile.

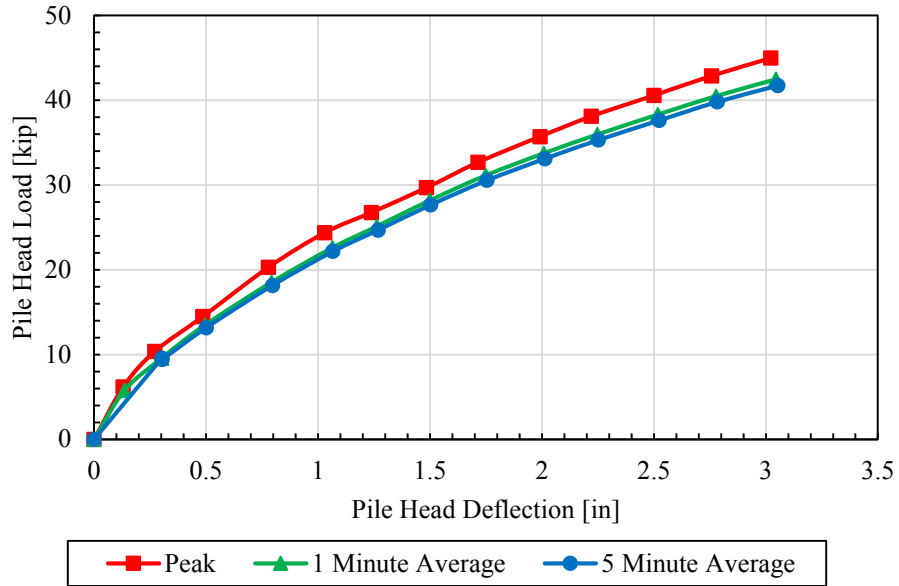


Figure C-7. Pile head load versus pile head deflection comparing peak, 1-minute hold, and 5-minute hold for 3.1D square pile.

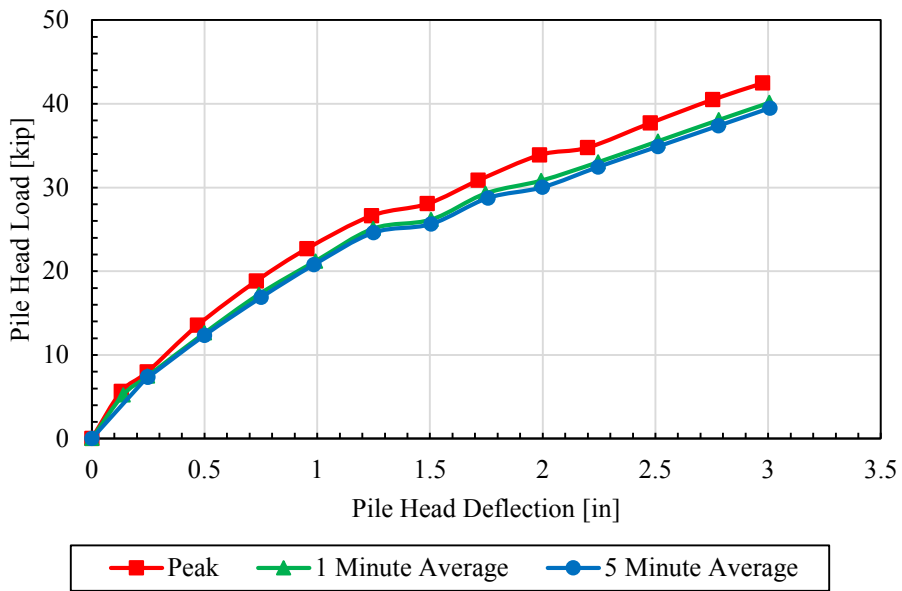


Figure C-8. Pile head load versus pile head deflection comparing peak, 1-minute hold, and 5-minute hold for 2.1D square pile.

APPENDIX D. INDUCED FORCE IN THE REINFORCEMENT CURVES

H-Piles

4.5D Soil Reinforcement Curves

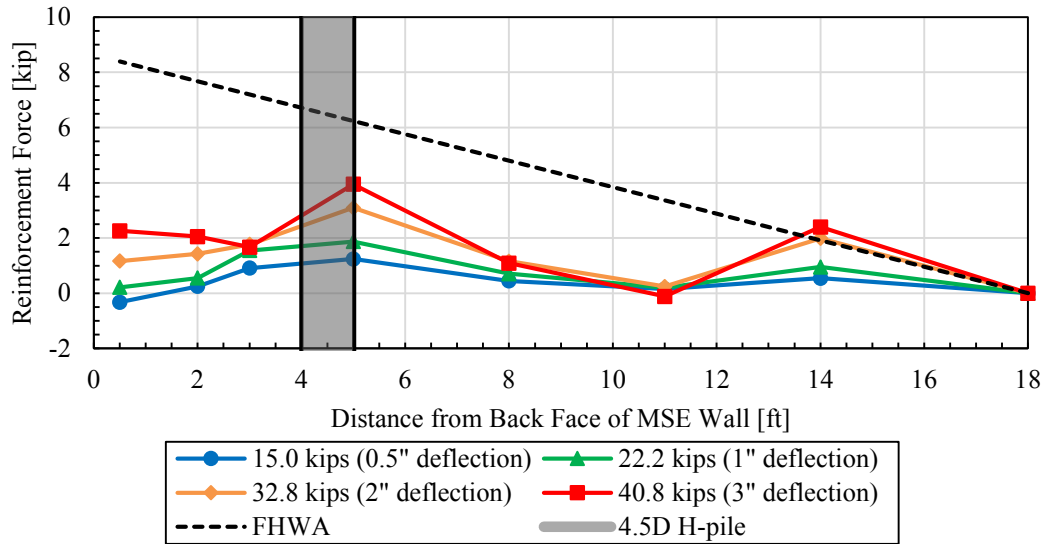


Figure D-1. Reinforcement force versus distance from back face of MSE wall (H-pile 4.5D, 15-inch depth, strip #3, transverse spacing 34.1 inches).

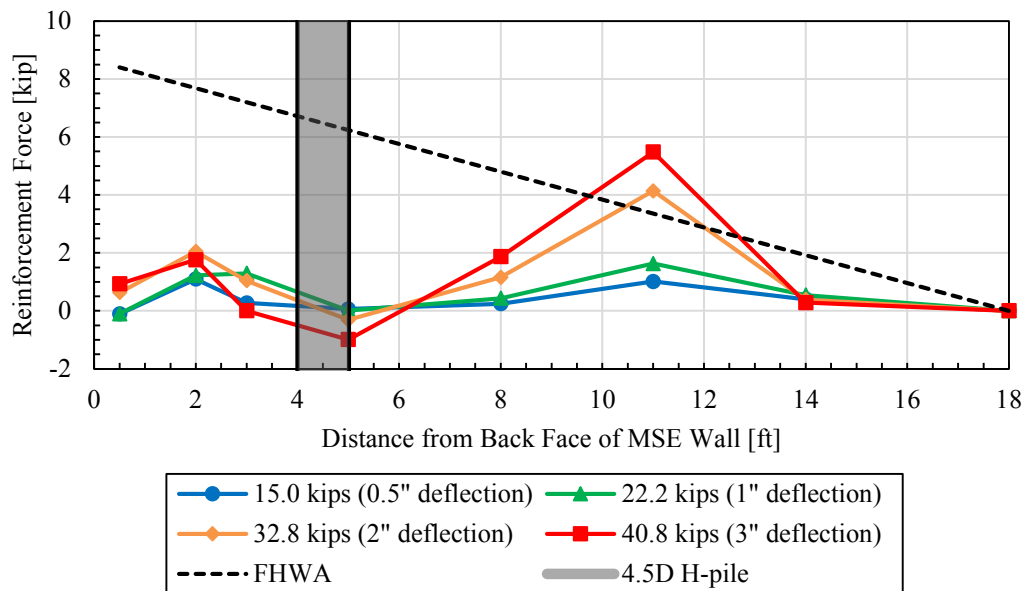


Figure D-2. Reinforcement force versus distance from back face of MSE wall (H-pile 4.5D, 15-inch depth, strip #4, transverse spacing 8.6 inches).

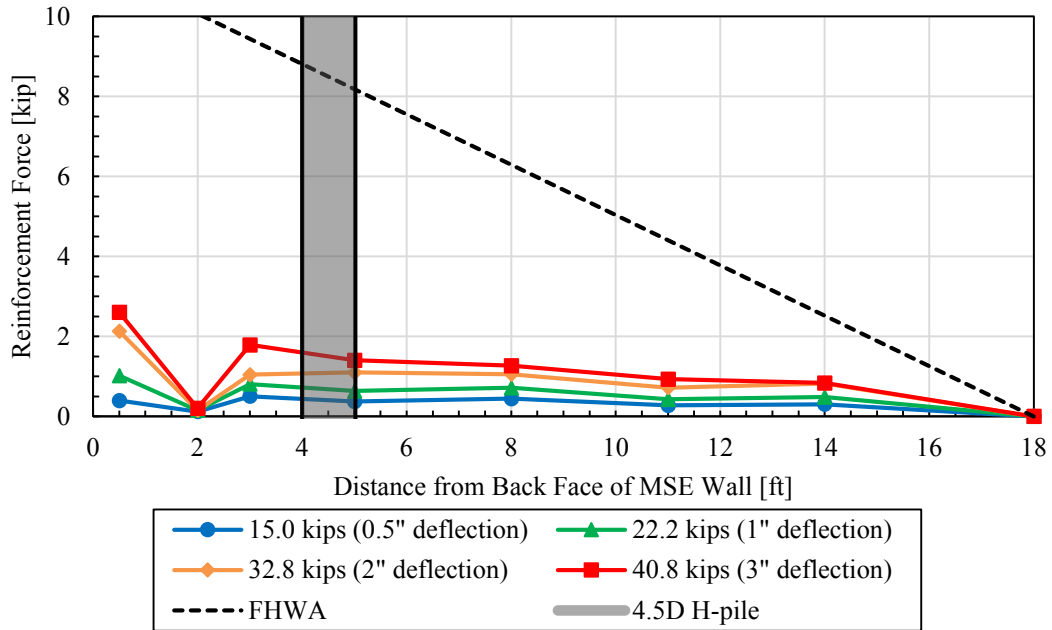


Figure D-3. Reinforcement force versus distance from back face of MSE wall (H-pile 4.5D, 45-inch depth, strip #16, transverse spacing 32.6 inches).

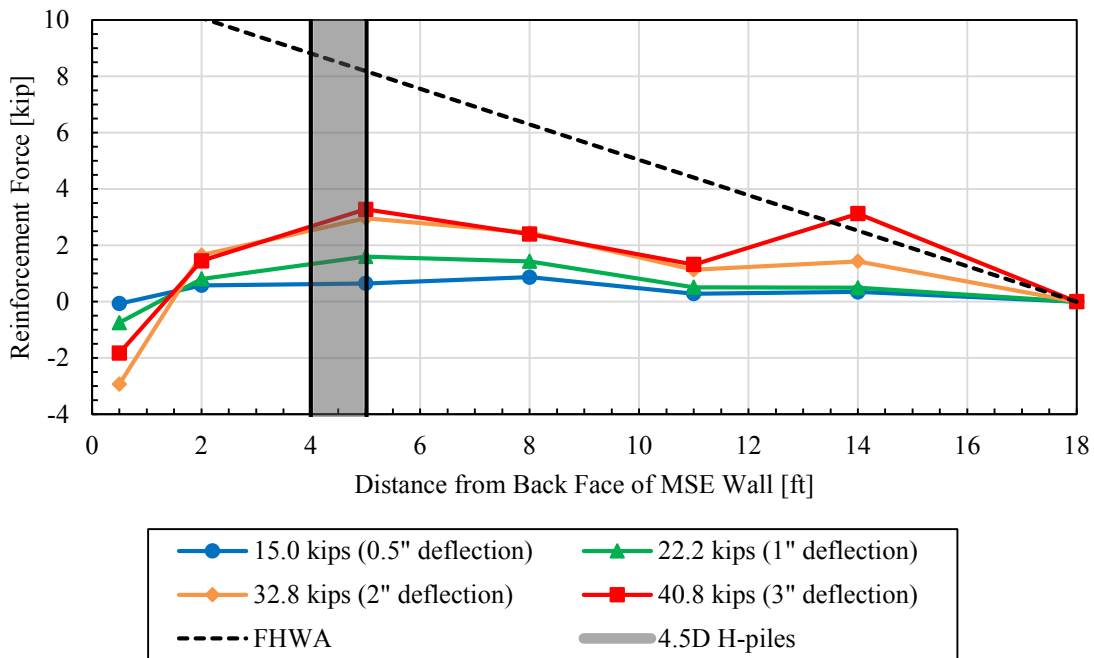


Figure D-4. Reinforcement force versus distance from back face of MSE wall (H-pile 4.5D, 45-inch depth, strip #11, transverse spacing 8.1 inches).

3.2D Soil Reinforcement Curves

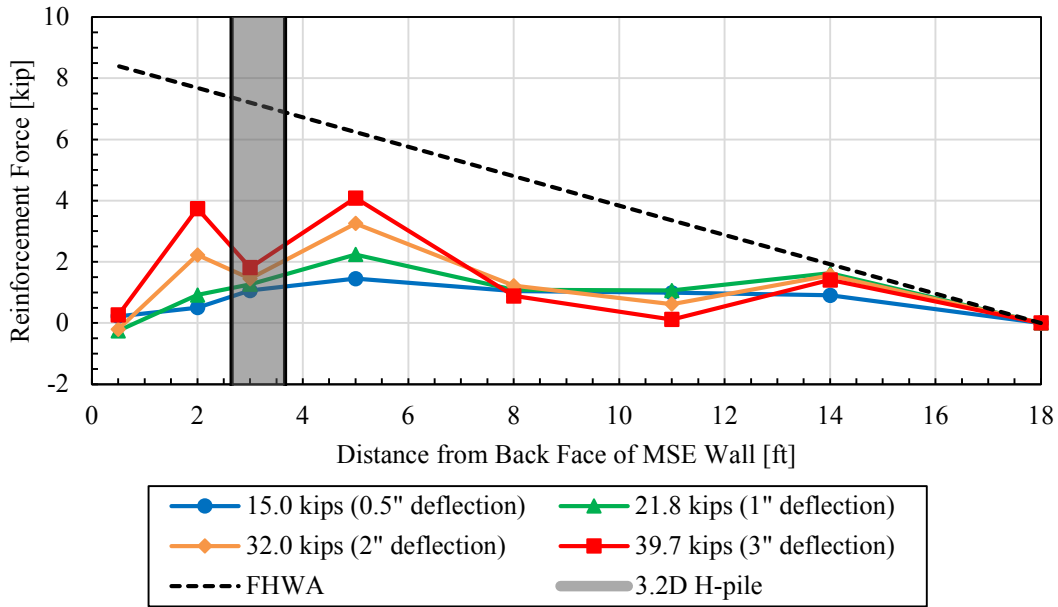


Figure D-5. Reinforcement force versus distance from back face of MSE wall (H-pile 3.2D, 15-inch depth, strip #3, transverse spacing 27.1 inches).

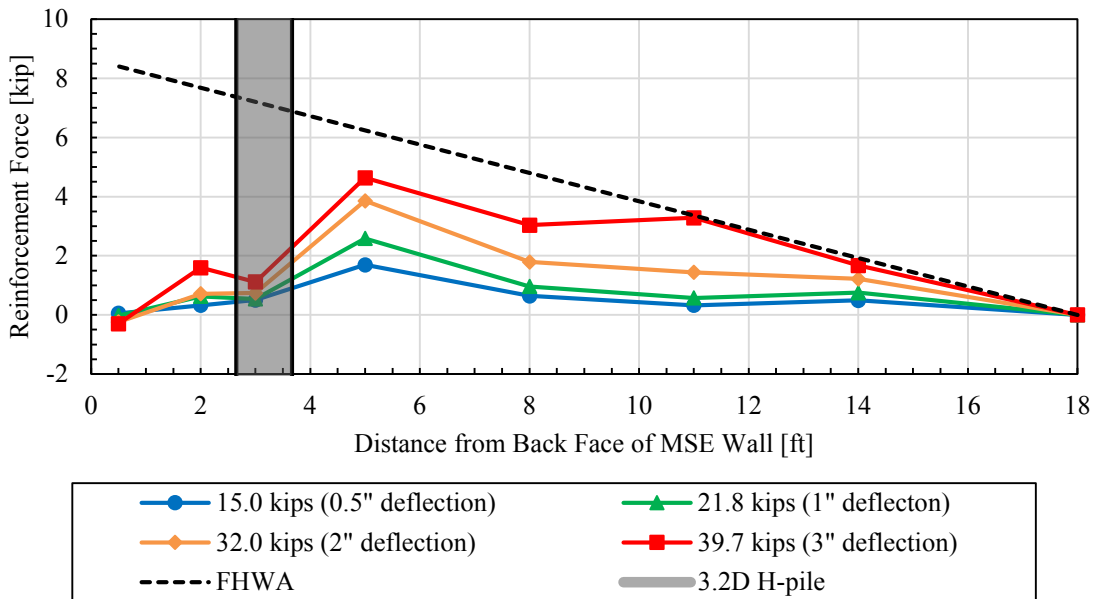


Figure D-6. Reinforcement force versus distance from back face of MSE wall (H-pile 3.2D, 15-inch depth, strip #4, transverse spacing 52.6 inches).

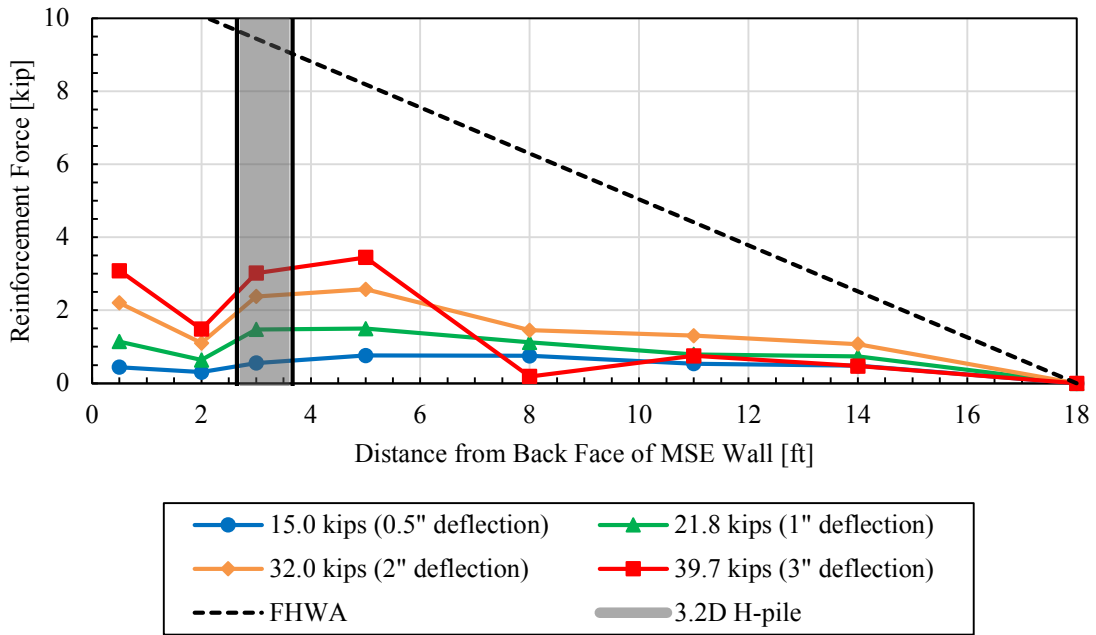


Figure D-7. Reinforcement force versus distance from back face of MSE wall (H-pile 3.2D, 45-inch depth, strip #16, transverse spacing 28.1 inches).

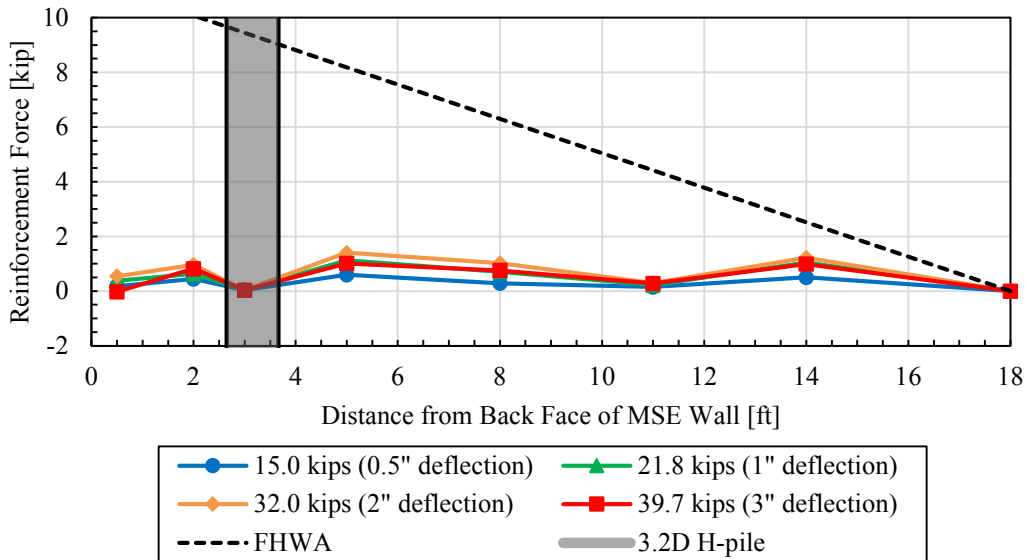


Figure D-8. Reinforcement force versus distance from back face of MSE wall (H-pile 3.2D, 45-inch depth, strip #11, transverse spacing 53.1 inches).

2.5D Soil Reinforcement Curves

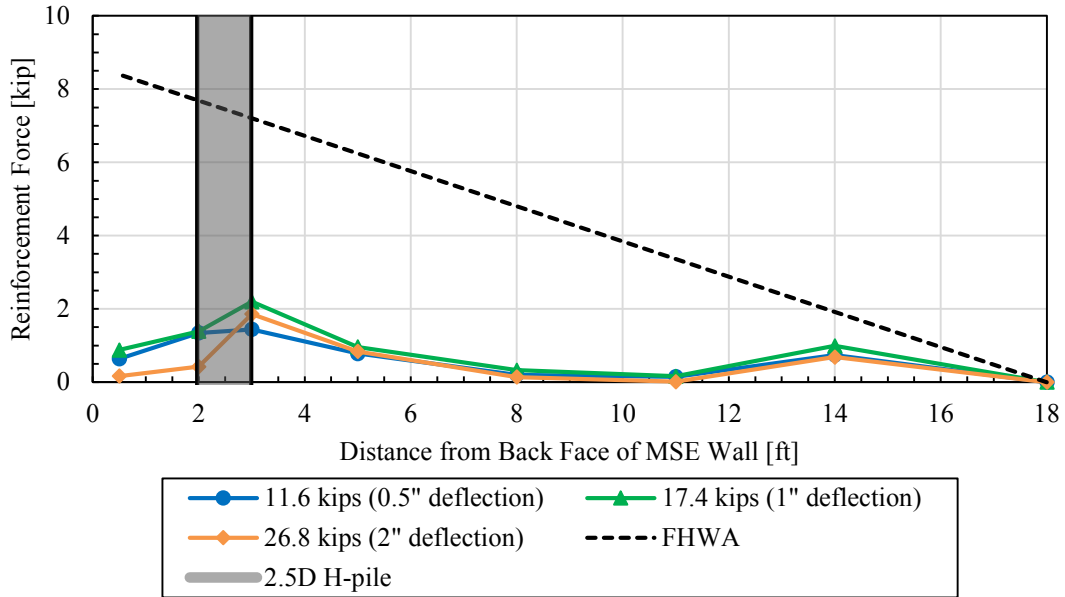


Figure D-9. Reinforcement force versus distance from back face of MSE wall (H-pile 2.5D, 15-inch depth, strip #8, transverse spacing 34.6 inches).

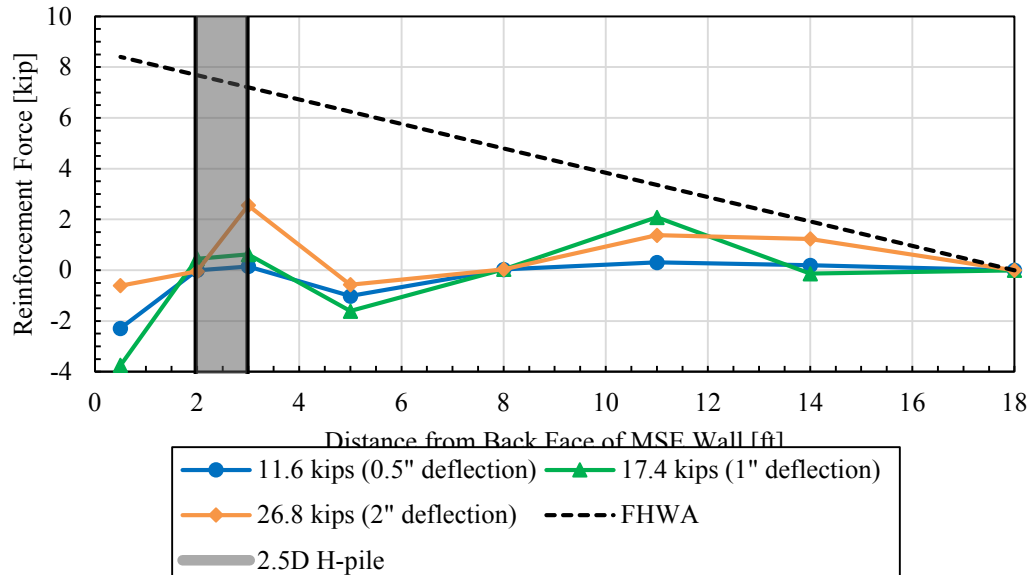


Figure D-10. Reinforcement force versus distance from back face of MSE wall (H-pile 2.5D, 15-inch depth, strip #7, transverse spacing 9.1 inches).

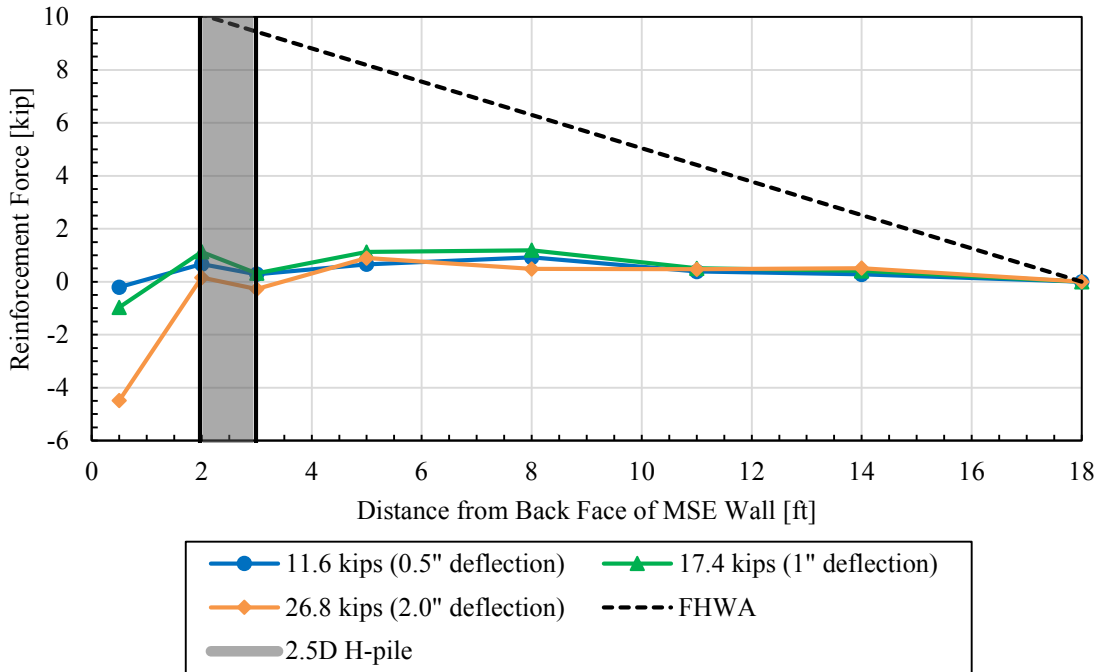


Figure D-11. Reinforcement force versus distance from back face of MSE wall (H-pile 2.5D, 45-inch depth, strip #14, transverse spacing 33.6 inches).

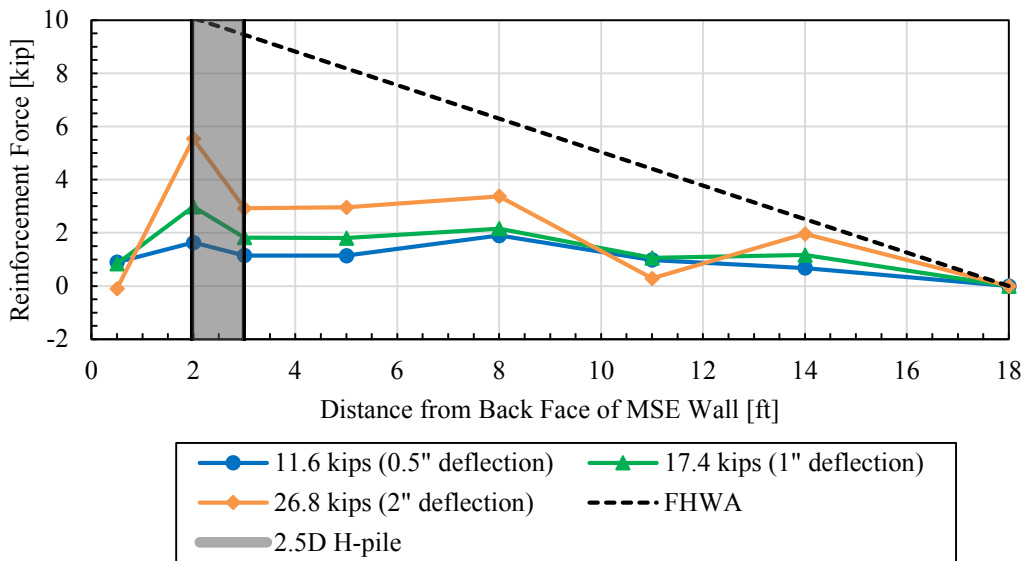


Figure D-12. Reinforcement force versus distance from back face of MSE wall (H-pile 2.5D, 45-inch depth, strip #15, transverse spacing 8.1 inches).

2.2D Soil Reinforcement Curves

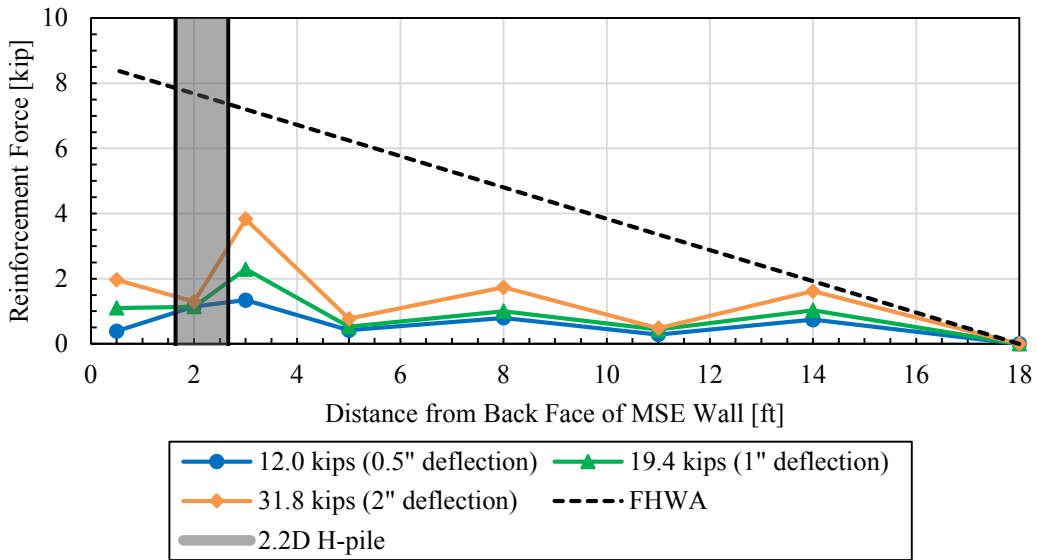


Figure D-13. Reinforcement force versus distance from back face of MSE wall (H-pile 2.2D, 15-inch depth, strip #8, transverse spacing 23.6 inches).

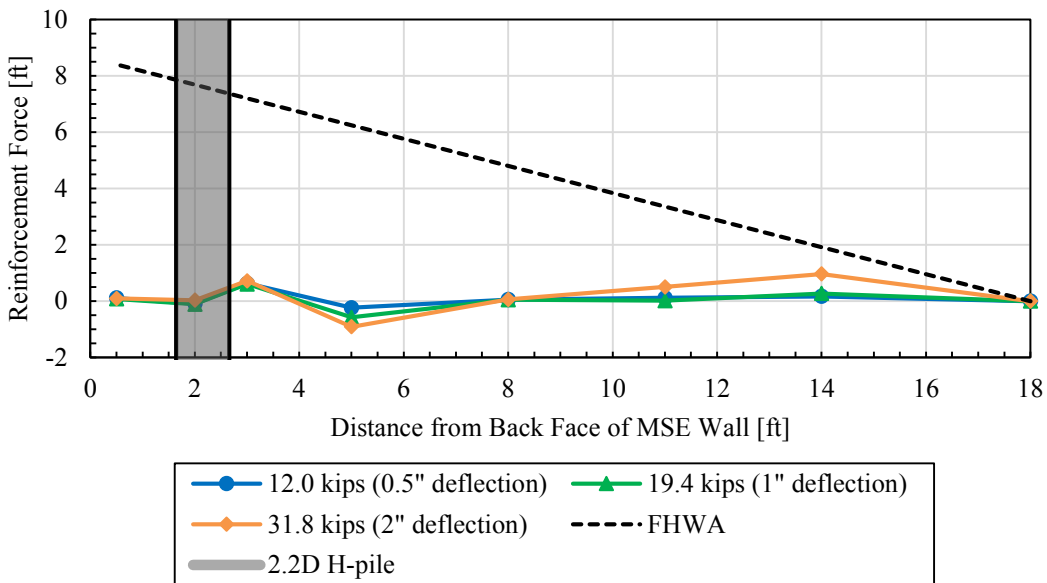


Figure D-14. Reinforcement force versus distance from back face of MSE wall (H-pile 2.2D, 15-inch depth, strip #7, transverse spacing 49.1 inches).

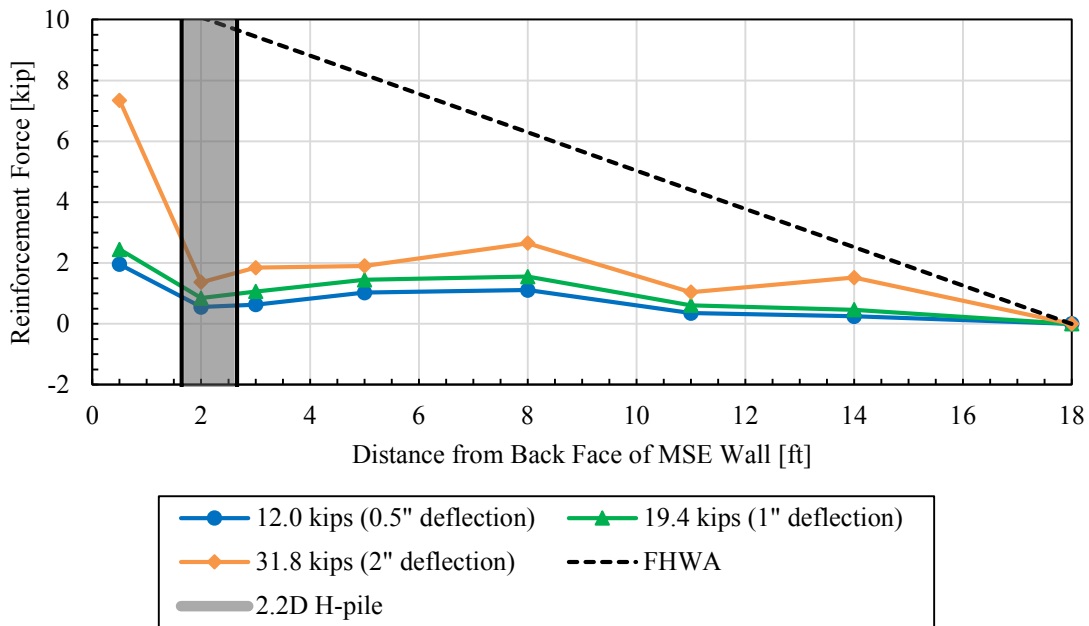


Figure D-15. Reinforcement force versus distance from back face of MSE wall (H-pile 2.2D, 45-inch depth, strip #14, transverse spacing 25.1 inches).

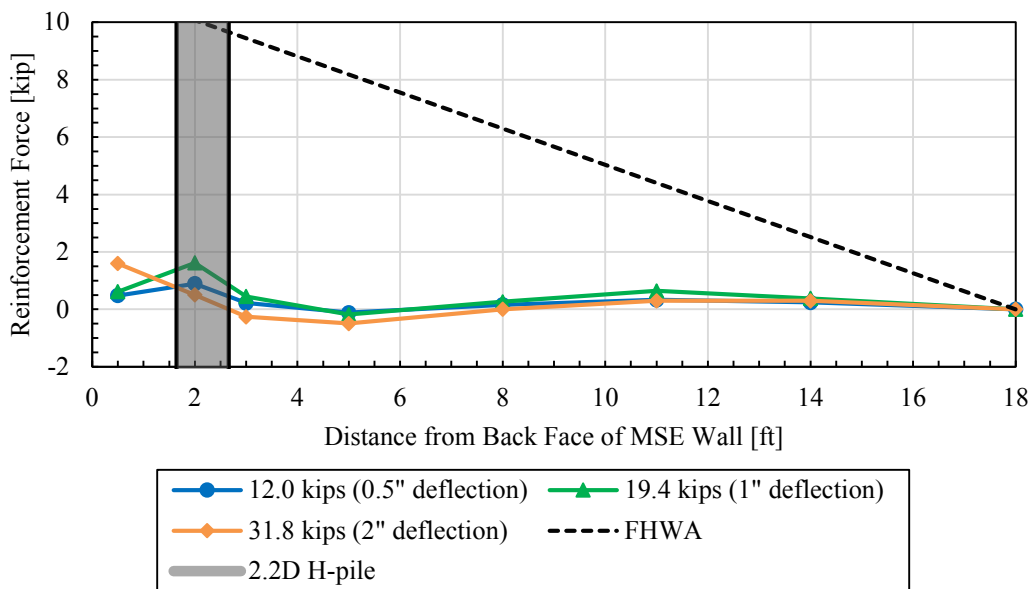


Figure D-16. Reinforcement force versus distance from back face of MSE wall (H-pile 2.2D, 45-inch depth, strip #15, transverse spacing 51.1 inches).

Square Piles

5.7D Soil Reinforcement Curves

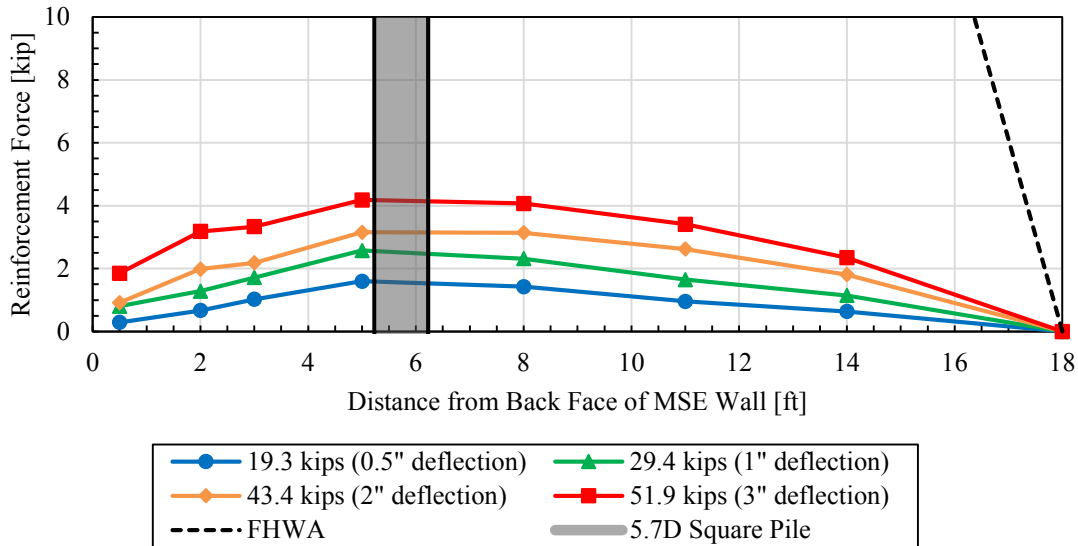


Figure D-17. Reinforcement force versus distance from back face of MSE wall (square pile 5.7D, 15-inch depth, welded wire #5, transverse spacing 21.5 inches).

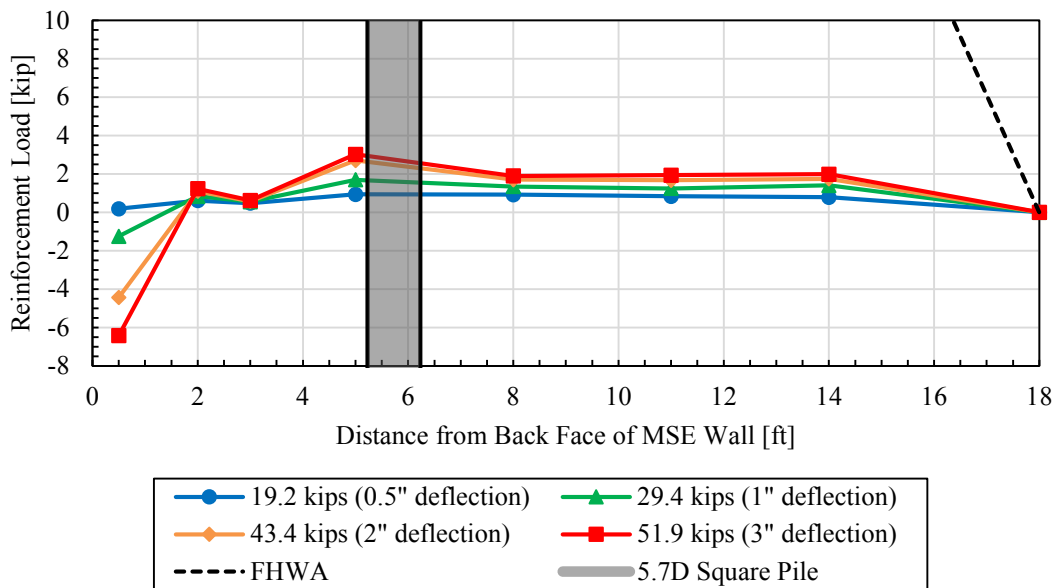


Figure D-18. Reinforcement force versus distance from back face of MSE wall (square pile 5.7D, 15-inch depth, welded wire #4, transverse spacing 38.5 inches).

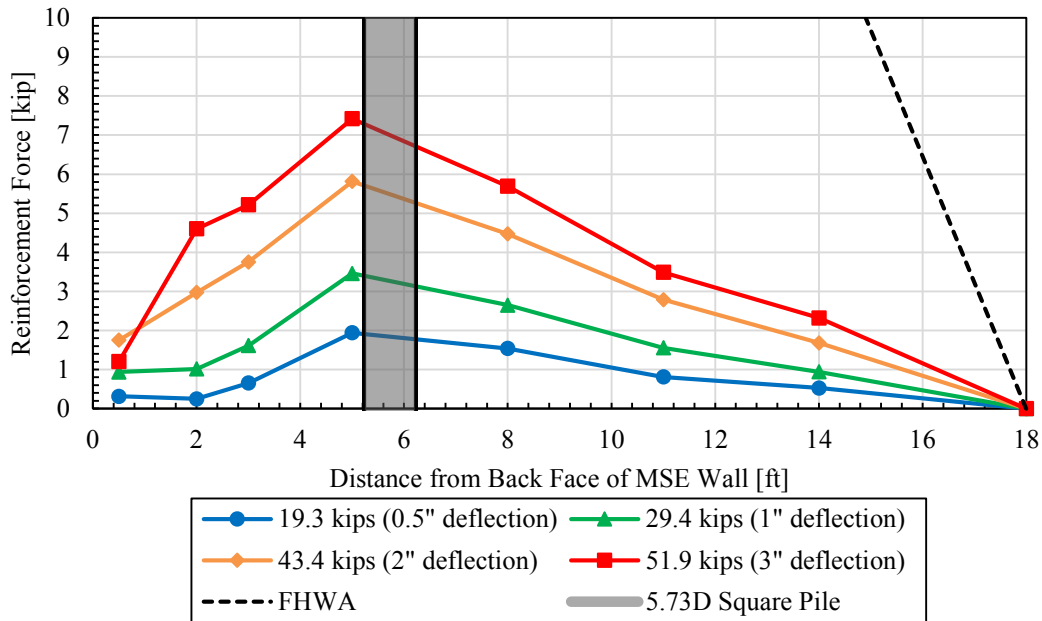


Figure D-19. Reinforcement force versus distance from back face of MSE wall (square pile 5.7D, 45-inch depth, welded wire #26, transverse spacing 28.5 inches).

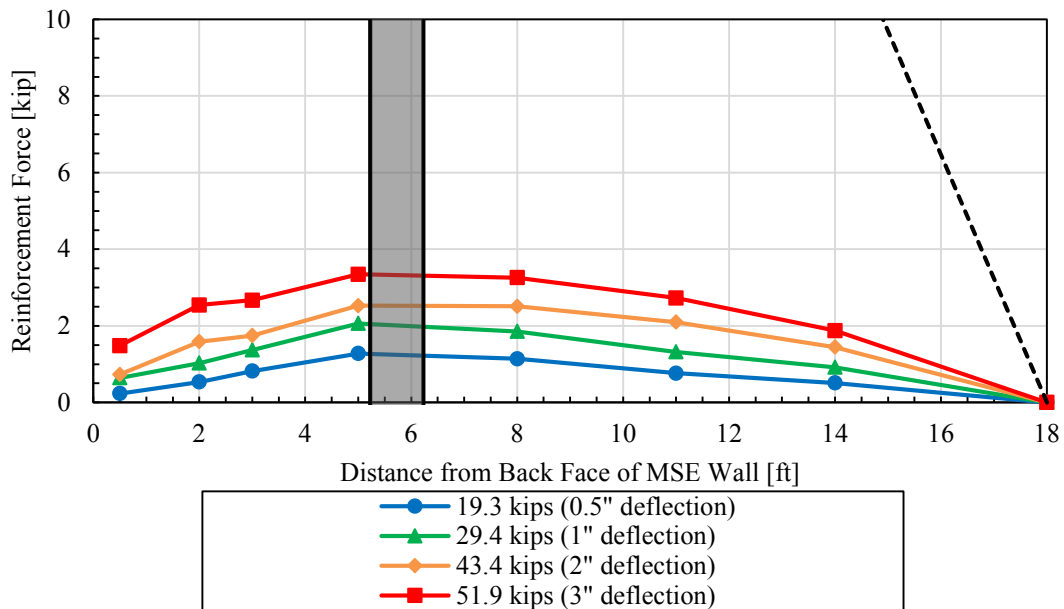


Figure D-20. Reinforcement force versus distance from back face of MSE wall (square pile 5.7D, 45-inch depth, welded wire #27, transverse spacing 31 inches).

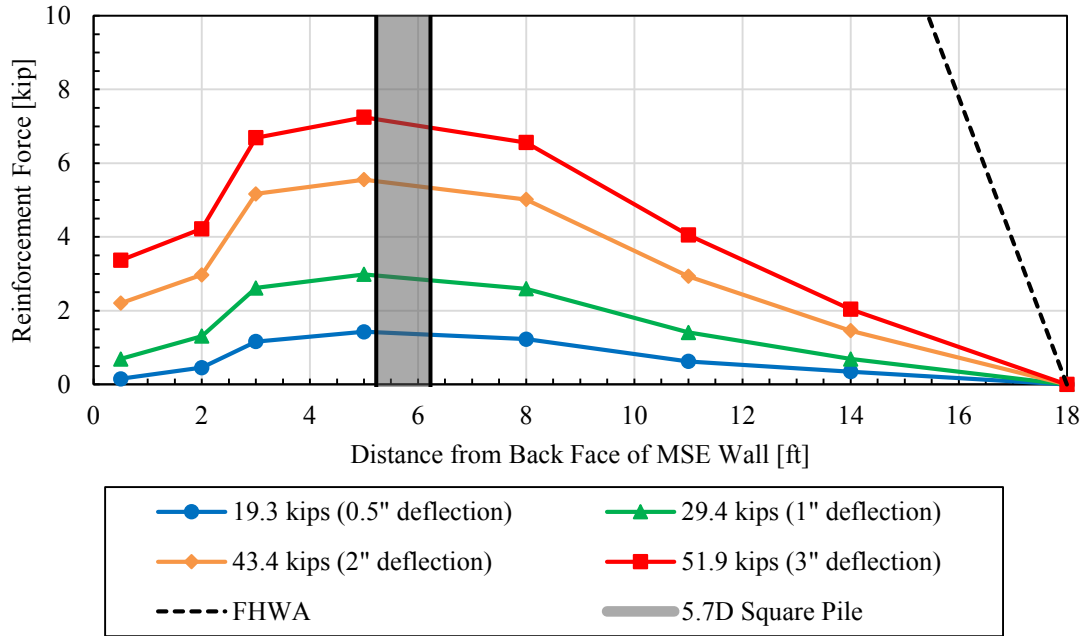


Figure D-21. Reinforcement force versus distance from back face of MSE wall (square pile 5.7D, 75-inch depth, welded wire #21, transverse spacing 27 inches).

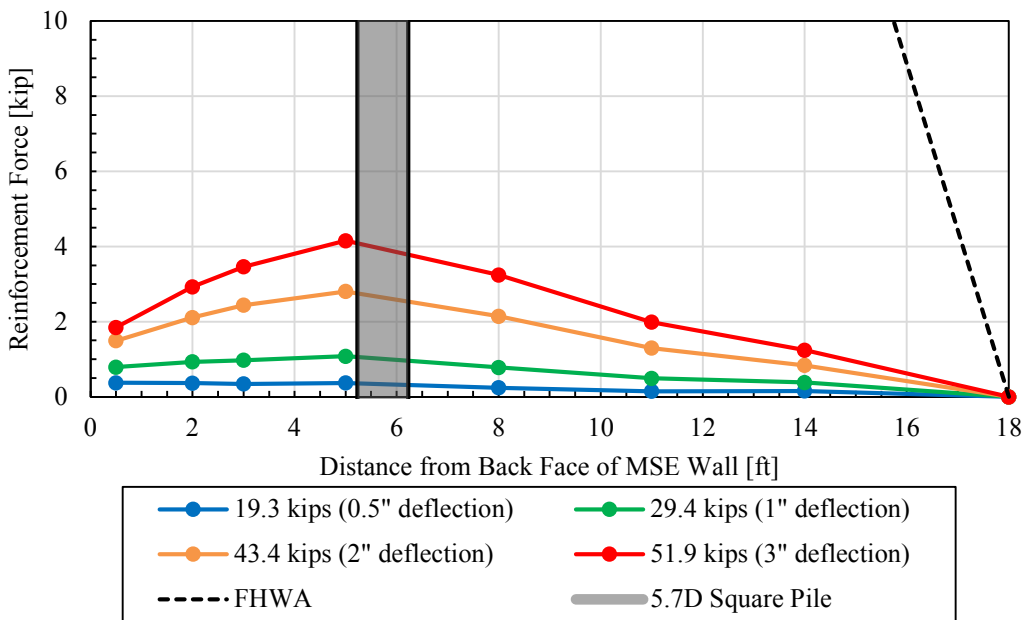


Figure D-22. Reinforcement force versus distance from back face of MSE wall (square pile 5.7D, 105-inch depth, welded wire #17, transverse spacing 34.5 inches).

4.2D Soil Reinforcement Curves

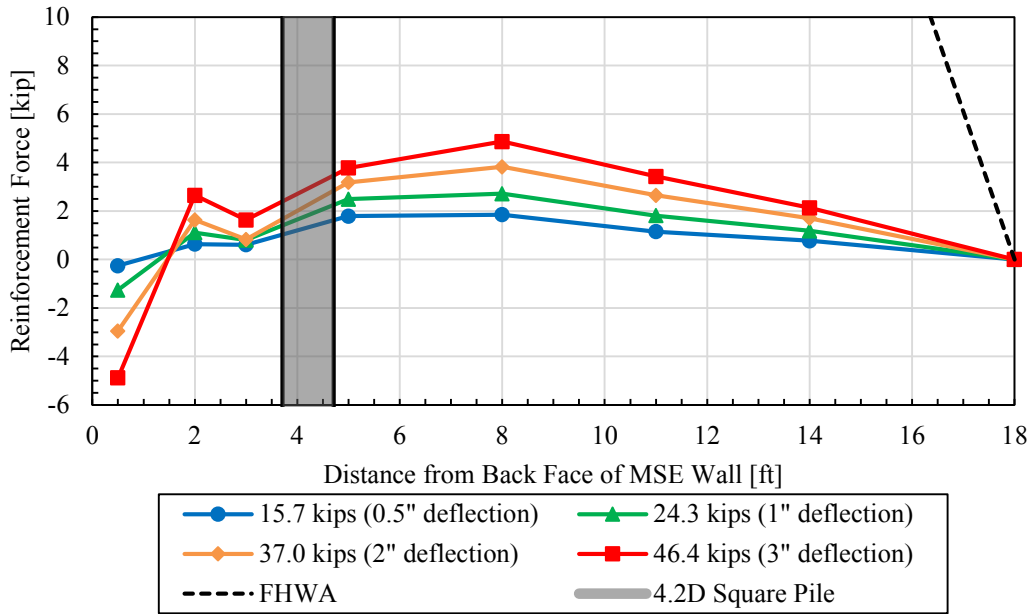


Figure D-23. Reinforcement force versus distance from back face of MSE wall (square pile 4.2D, 15-inch depth, welded wire #4, transverse spacing 13 inches).

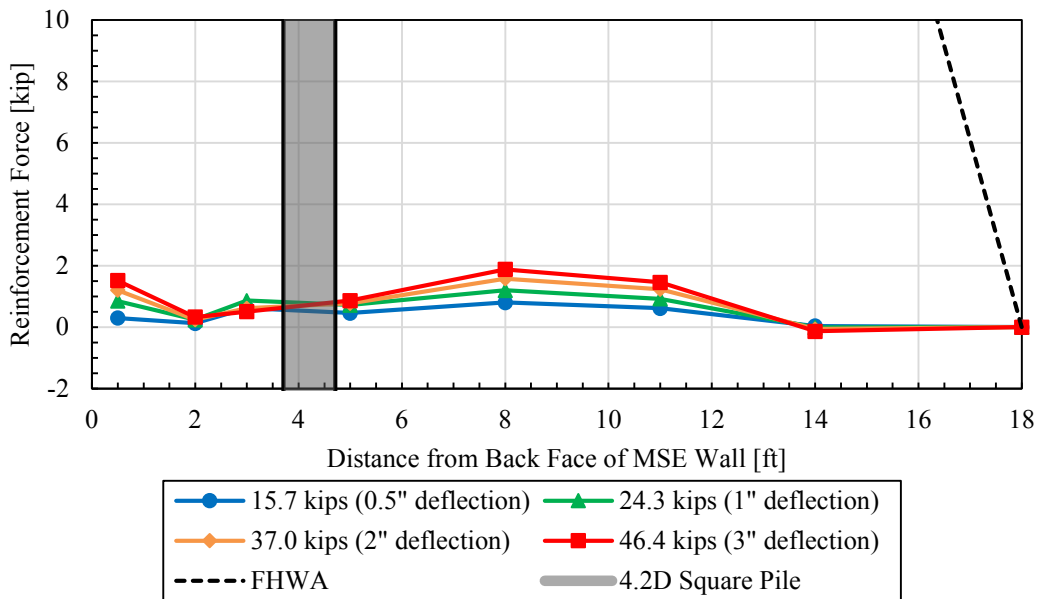


Figure D-24. Reinforcement force versus distance from back face of MSE wall (square pile 4.2D, 15-inch depth, welded wire #3, transverse spacing 47.5 inches).

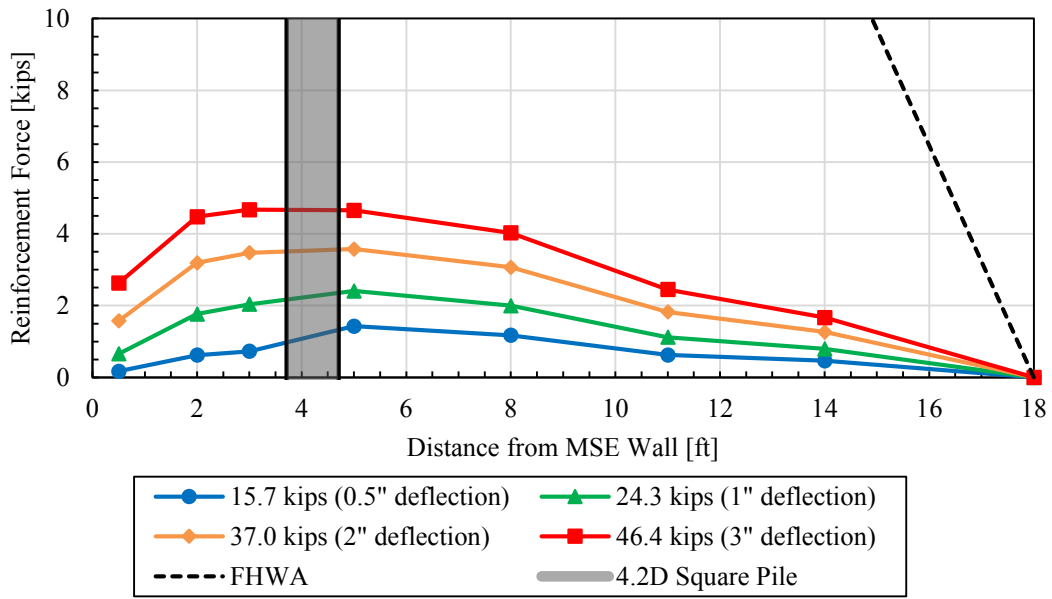


Figure D-25. Reinforcement force versus distance from back face of MSE wall (square pile 4.2D, 45-inch depth, welded wire #27, transverse spacing 21 inches).

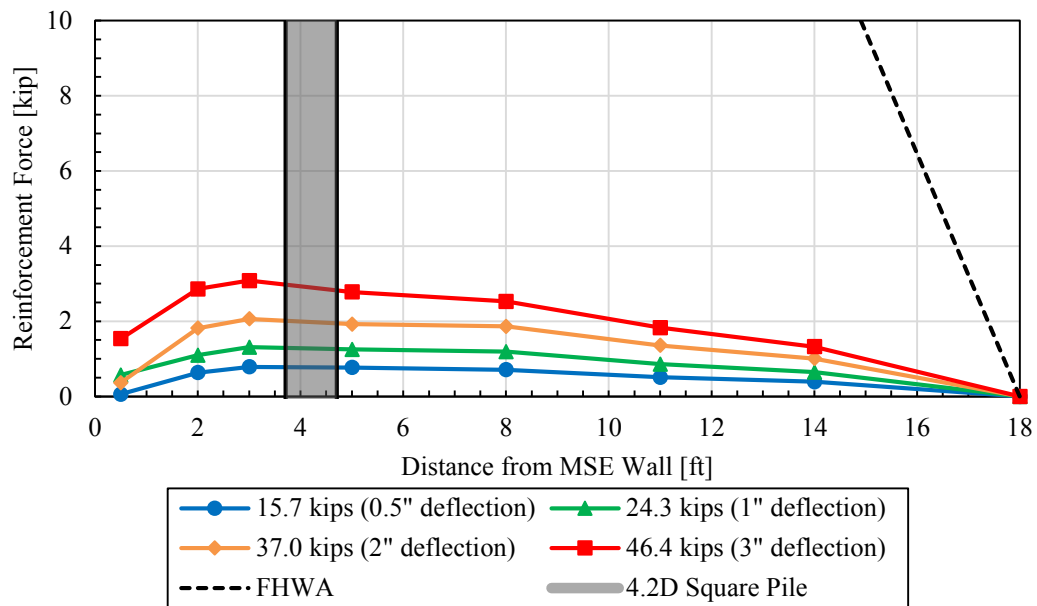


Figure D-26. Reinforcement force versus distance from back face of MSE wall (square pile 4.2D, 45-inch depth, welded wire #28, transverse spacing 39.5 inches).

3.1D Soil Reinforcement Curves

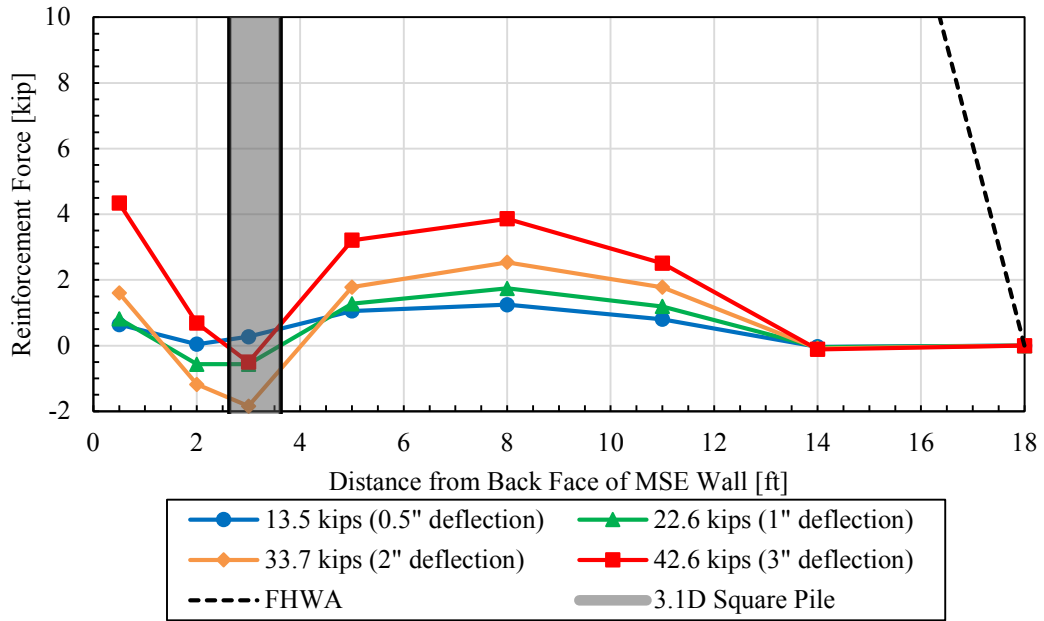


Figure D-27. Reinforcement force versus distance from back face of MSE wall (square pile 3.1D, 15-inch depth, welded wire #3, transverse spacing 15.5 inches).

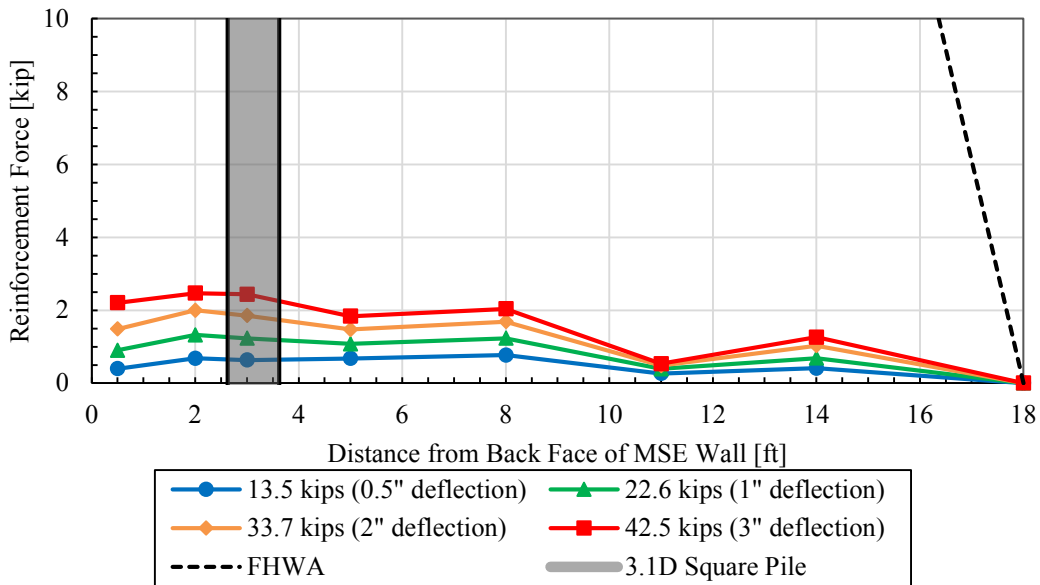


Figure D-28. Reinforcement force versus distance from back face of MSE wall (square pile 3.1D, 15-inch depth, welded wire #2, transverse spacing 44 inches).

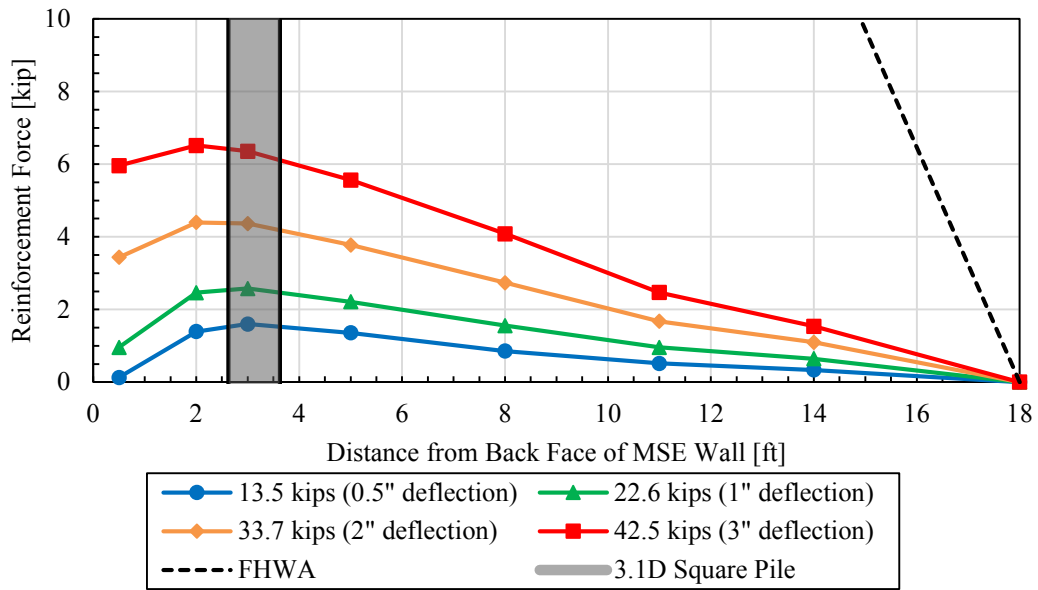


Figure D-29. Reinforcement force versus distance from back face of MSE wall (square pile 3.1D, 45-inch depth, welded wire #28, transverse spacing 23.5 inches).

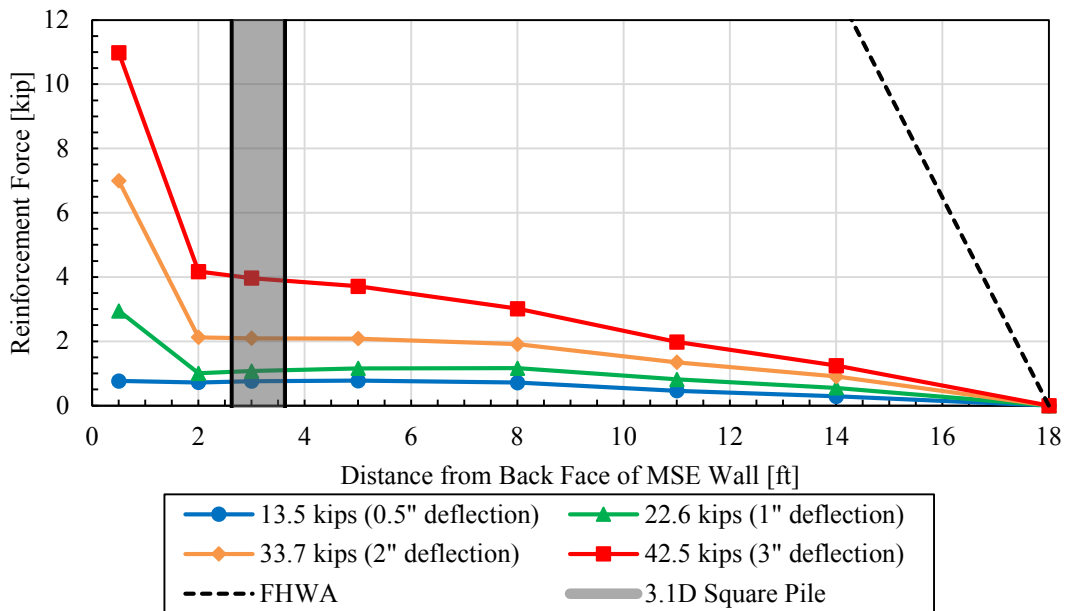


Figure D-30. Reinforcement force versus distance from back face of MSE wall (square pile 3.1D, 45-inch depth, welded wire #29, transverse spacing 37 inches).

2.1D Soil Reinforcement Curves

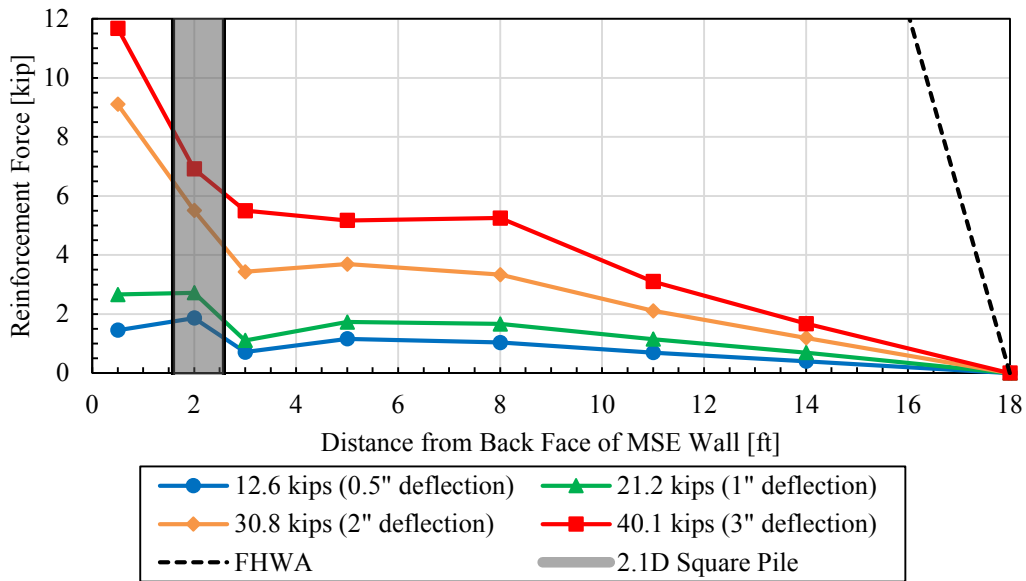


Figure D-31. Reinforcement force versus distance from back face of MSE wall (square pile 2.1D, 15-inch depth, welded wire #2, transverse spacing 23.5 inches).

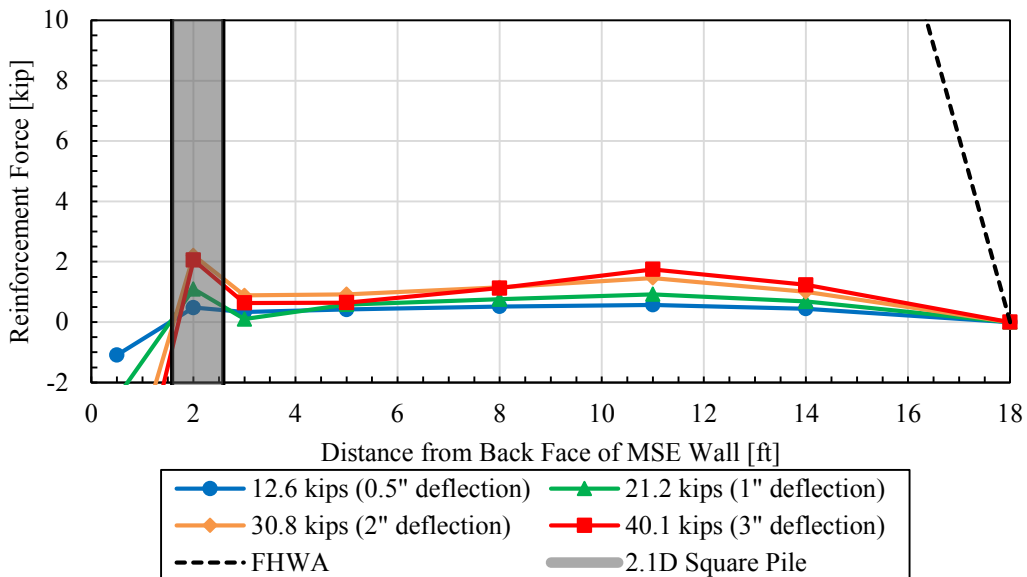


Figure D-32. Reinforcement force versus distance from back face of MSE wall (square pile 2.1D, 15-inch depth, welded wire #1, transverse spacing 37.5 inches).

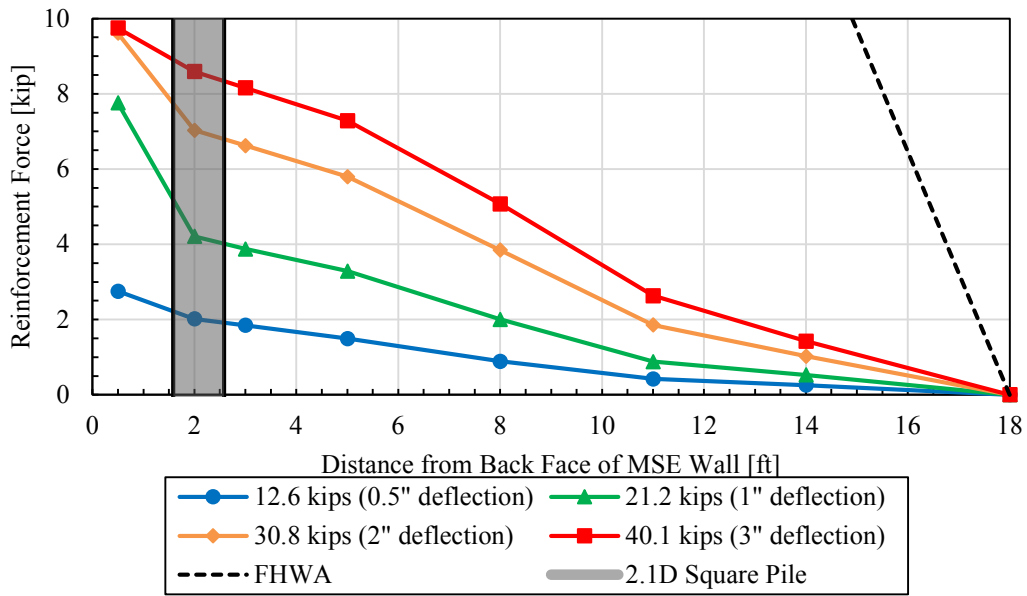


Figure D-33. Reinforcement force versus distance from back face of MSE wall (square pile 2.1D, 45-inch depth, welded wire #29, transverse spacing 30 inches).

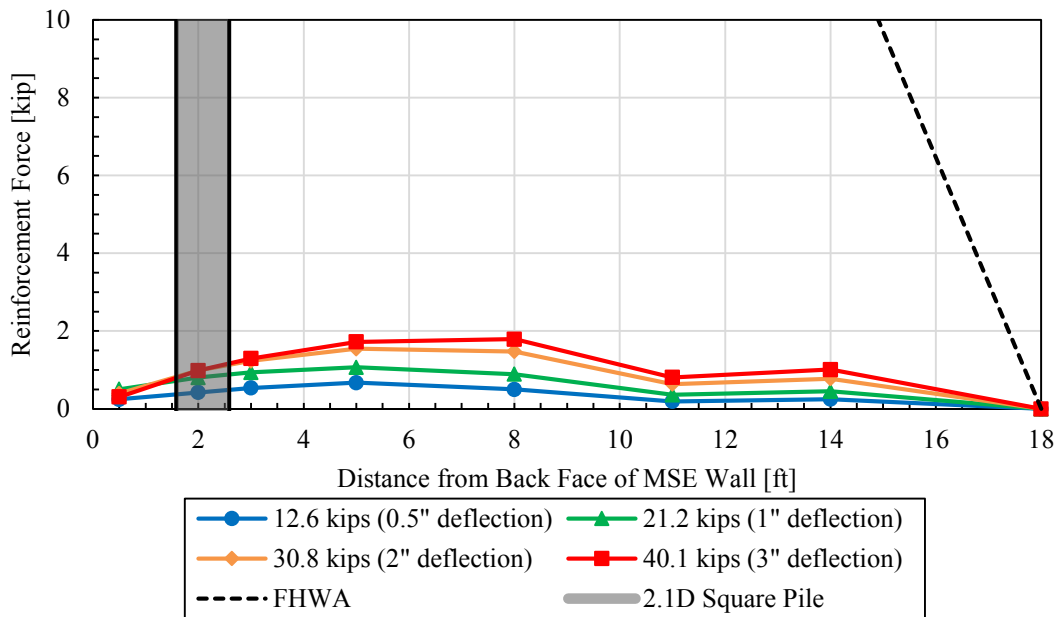


Figure D-34. Reinforcement force versus distance from back face of MSE wall (square pile 2.1D, 45-inch depth, welded wire #30, transverse spacing 37.5 inches).

APPENDIX E. STATISTICAL ANALYSIS DATA OF PIPE PILES WITHIN RIBBED STRIP REINFORCEMENT

Table E-1. Statistical Analysis Data of Ribbed Strip Reinforcement of Pipe Piles

Parameter	Coefficients	Standard Error	t Stat	P-value
Intercept	-1.8959204180	0.20553	-9.22469	<0.00001
Pile Load, P	0.0284582504	0.00115	24.68453	<0.00001
Normalized Transverse Distance, T/D	-0.0232492106	0.00707	-3.28707	0.00106
Vertical Stress, σ_v	0.0025190053	0.00028	8.93580	<0.00001
Normalized Spacing, S/D	-0.0343075454	0.00396	-8.66478	<0.00001
Length to Height Ratio, L/H	1.4642771789	0.16072	9.11065	<0.00001
$\sigma_v^*(L/H)$	-0.0012644575	0.00018	-7.04195	<0.00001
σ_v^2	-0.0000006085	<0.00001	-9.32383	<0.00001
$P^*(T/D)$	-0.0020748413	0.00024	-8.78667	<0.00001
P^2	-0.0002084736	0.00002	-11.44068	<0.00001

Table E-2. Term Elimination with the Change of R^2 and Adjusted R^2 of Pipe Piles Data

Term Removed	Adjusted R^2	Decrease in Adjusted R^2	R^2	Decrease in R^2
None	80.67%	None	81.03%	None
$(T/D)^*(S/D)^+$	80.42%	0.25%	80.76%	0.27%
$\sigma_v^*(T/D)^+$	80.13%	0.29%	80.45%	0.31%
$(L/H)^{2+}$	79.62%	0.51%	79.92%	0.53%
$P^*(S/D)^+$	78.71%	0.91%	78.99%	0.93%
$P^*(L/H)^+$	77.35%	1.36%	77.62%	1.37%
$\sigma_v^*(L/H)$	75.86%	1.49%	76.12%	1.51%
σ_v^2	74.59%	1.27%	74.83%	1.29%
L/H	73.18%	1.41%	73.39%	1.43%
σ_v	72.61%	0.57%	72.79%	0.60%
S/D	70.96%	1.65%	71.11%	1.68%
$P^*(T/D)$	68.53%	2.43%	68.65%	2.46%
P^2	64.78%	3.74%	64.88%	3.77%
T/D	51.45%	13.33%	51.52%	13.36%

⁺Terms removed for the prediction equation.

Table E-3. ANOVA for Ribbed Strip Reinforcement Data of Pipe Piles

	Degrees of Freedom	Sum-of-Squares	Mean Squares	F Ratio	Significance F
Regression	9	43.03714	4.78190	283.69859	<0.00001
Residual	736	12.40571	0.01686		
Total	745	55.44285			

Table E-4. Confidence Interval Values for Ribbed Strip Reinforcement Data of Pipe Piles

Parameter	Lower 95%	Upper 95%
Intercept	-2.29941	-1.49243
Pile Load, P	0.02619	0.03072
Normalized Transverse Distance, T/D	-0.03713	-0.00936
Vertical Stress, σ_v	0.00197	0.00307
Normalized Spacing, S/D	-0.04208	-0.02653
Length to Height Ratio, L/H	1.14875	1.77980
$\sigma_v^*(L/H)$	-0.00162	-0.00091
σ_v^2	<0.00001	<0.00001
$P^*(T/D)$	-0.00254	-0.00161
P^2	-0.00024	-0.00017

The R^2 value is 77.6%, the adjusted R^2 value is 77.4%, and the R^2 value of the equation below is 77.1%. That standard error value was 0.130. There were a total of 726 observations. The highest measured tensile force used to develop the predicted tensile force equation was 10.4 kips.

$$F = 10^{(-1.9 + 0.028P - 0.0023\frac{T}{D} - 2.1 \times 10^{-4} P^2 - 0.0021P\frac{T}{D} - 0.034\frac{S}{D} + 0.0025\sigma_v + 1.5\frac{L}{H} - 6.1 \times 10^{-7} \sigma_v^2 - 0.0013\sigma_v\frac{L}{H}) - 1} \quad (E-1)$$

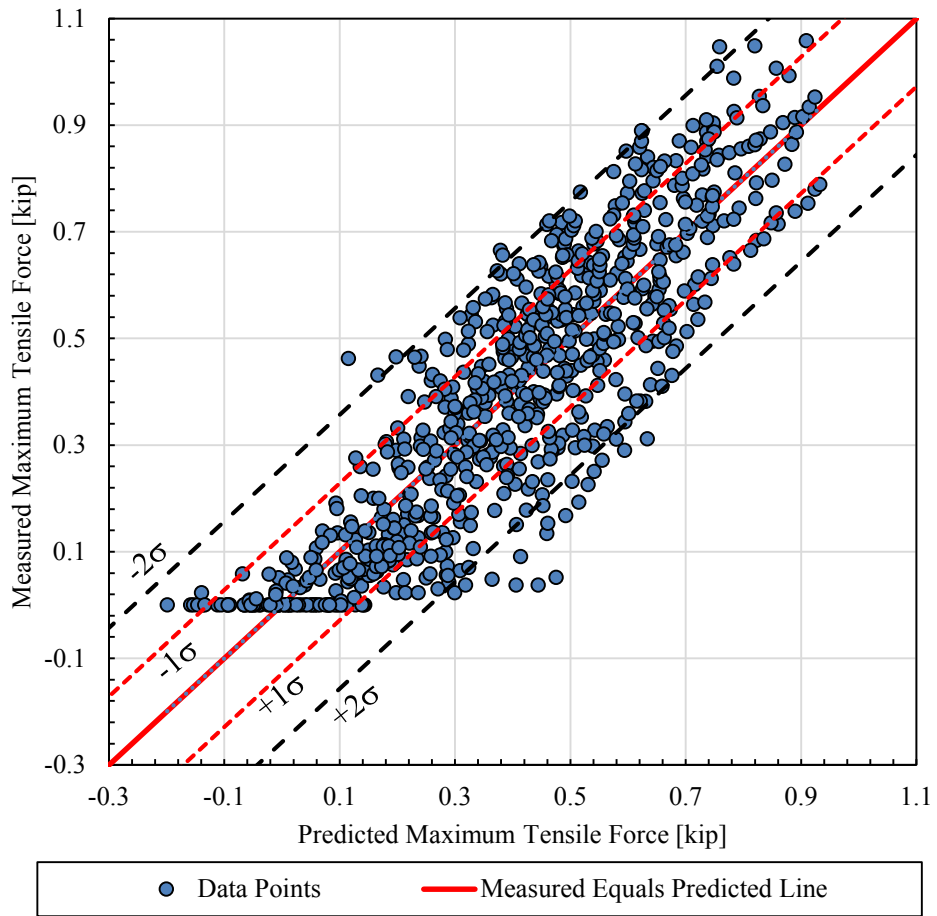


Figure E-1. Log measured maximum tensile force versus log predicted maximum tensile force, ribbed strip reinforcement of pipe piles.

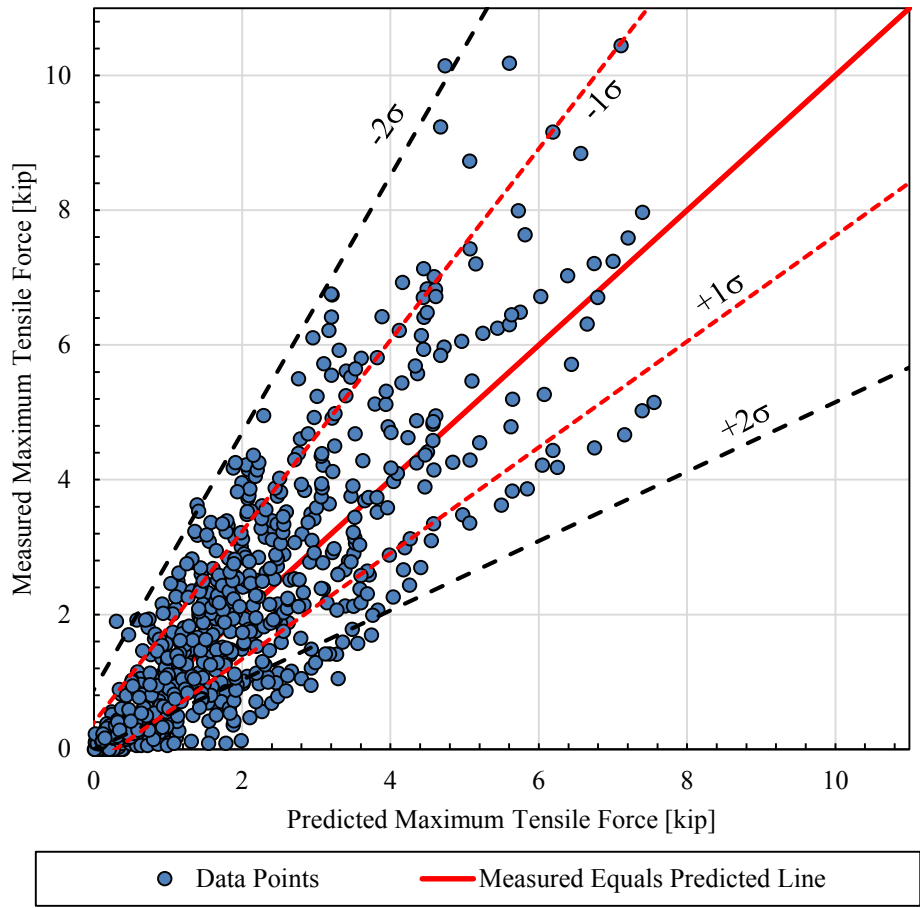


Figure E-2. Measured maximum tensile force versus predicted maximum tensile force, ribbed strip reinforcement of pipe piles.

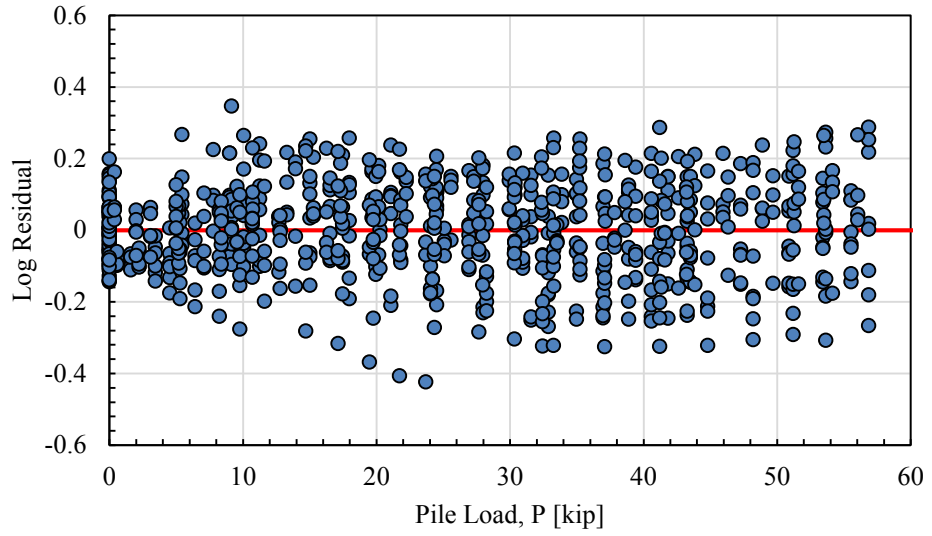


Figure E-3. Log residual versus pile load, ribbed strip reinforcement of pipe piles.

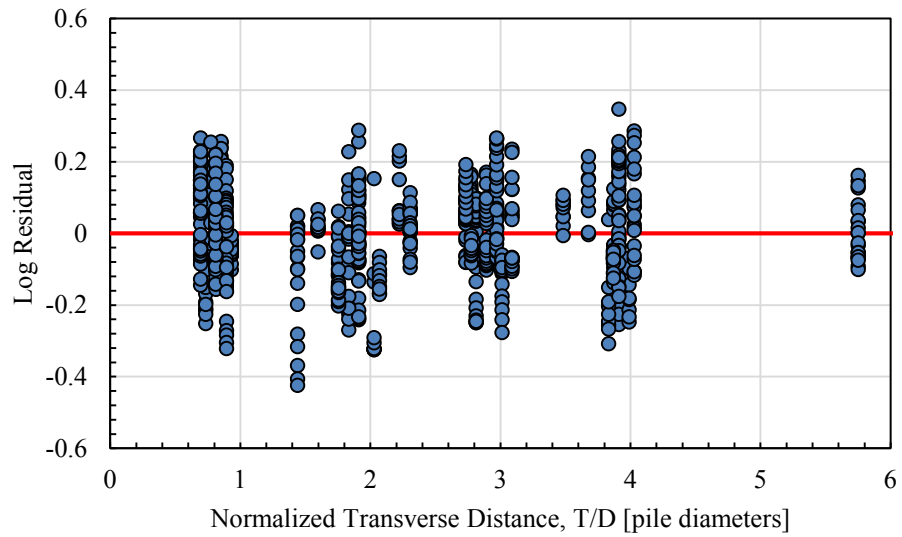


Figure E-4. Log residual versus normalized transverse distance, ribbed strip reinforcement of pipe piles.

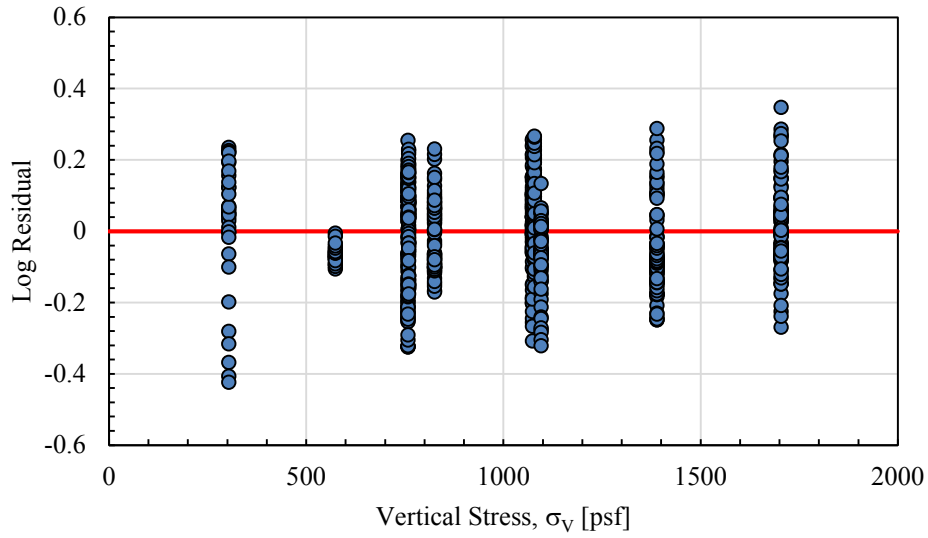


Figure E-5. Log residual versus vertical stress, ribbed strip reinforcement of pipe piles.

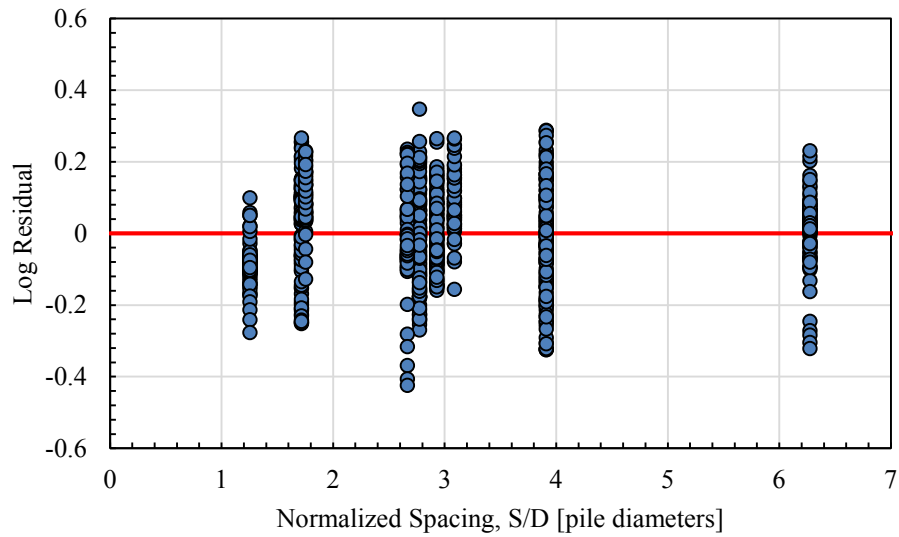


Figure E-6. Log residual versus normalized spacing, ribbed strip reinforcement of pipe piles.

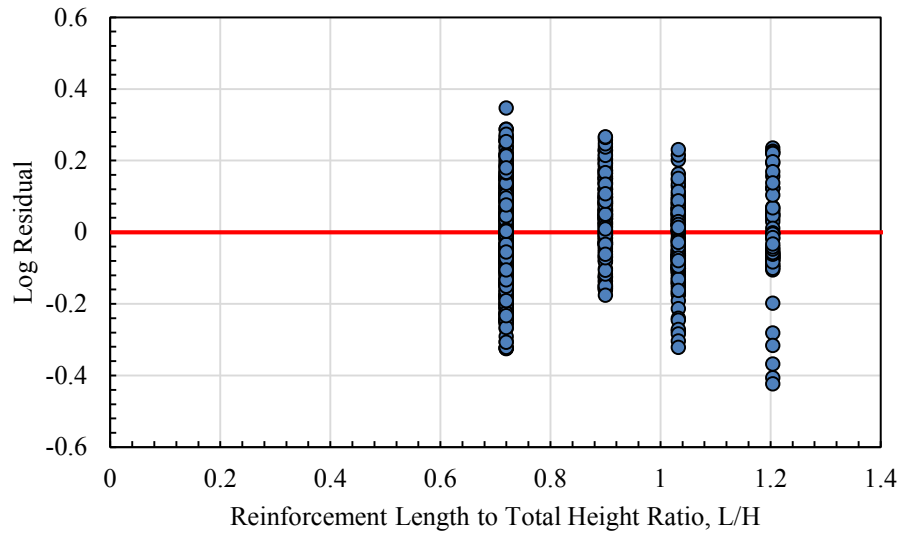


Figure E-7. Log residual versus L/H ratio, ribbed strip reinforcement of pipe piles.

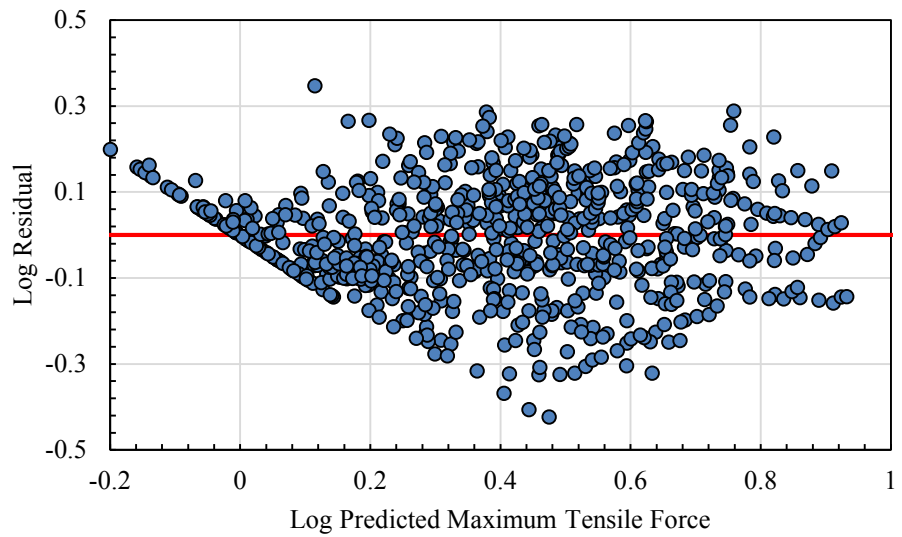


Figure E-8. Log residual versus log predicted maximum tensile force, ribbed strip reinforcement of pipe piles.

**Table E-5. Numerical Range of Parameters for Ribbed Strip Reinforcement
Statistical Analysis for Pipe Piles**

Parameter	Range
Measured Maximum Tensile Force, F_{measured}	0 kip – 10.4 kip
Pile Load, P	0 kip - 56.9 kip
Normalized Transverse Distance, T/D	0.7 - 5.8
Vertical Stress, σ_v	304 psf - 1704 psf
Normalized Spacing, S/D	1.3 - 6.3
Reinforcement Length to Total Height Ratio, L/H	0.7 - 1.2
Pile Diameter, D	12.75

APPENDIX F. VERTICAL GROUND DISPLACEMENT CURVES

H-Piles

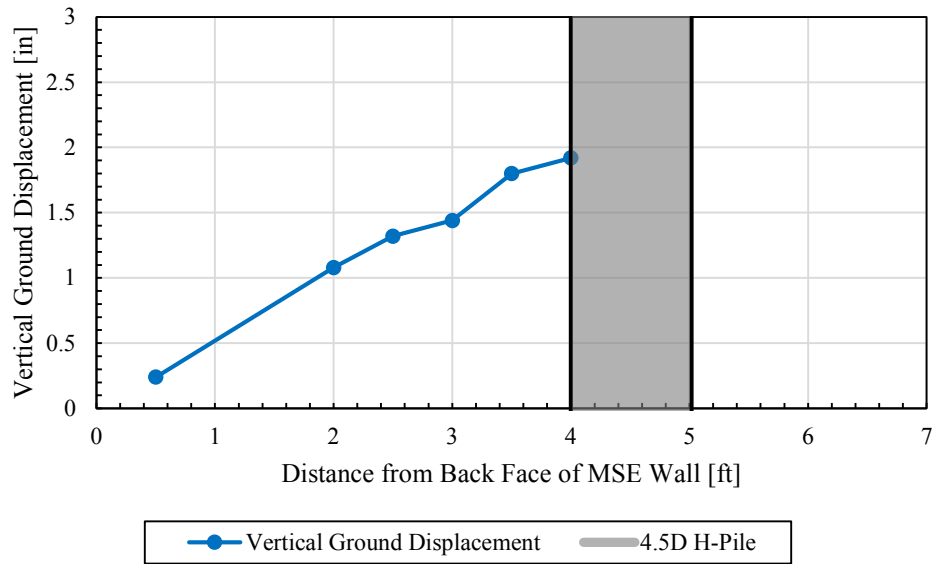


Figure F-1. Vertical ground displacement versus distance from back face of MSE wall, H-pile 4.5D.

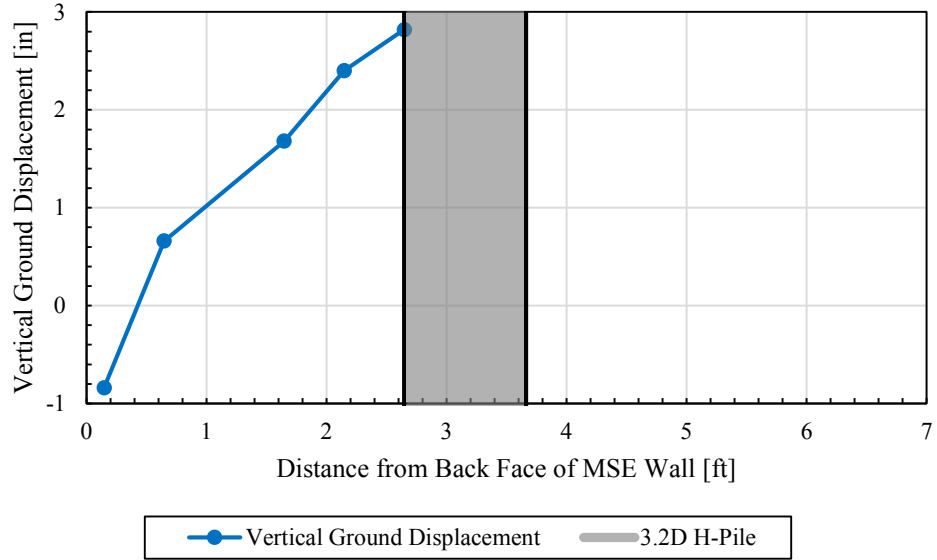


Figure F-2. Vertical ground displacement versus distance from back face of MSE wall, H-pile 3.2D.

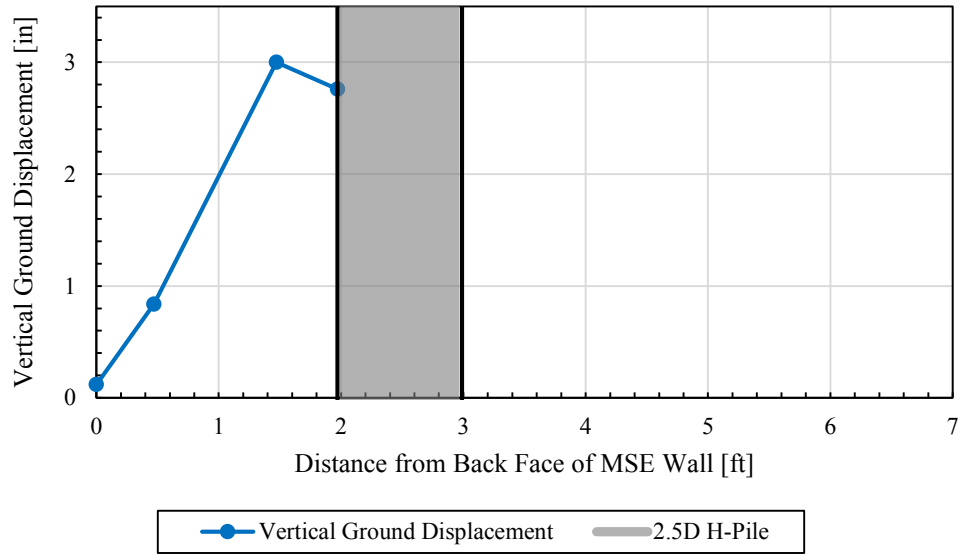


Figure F-3. Vertical ground displacement versus distance from back face of MSE wall, H-pile 2.5D.

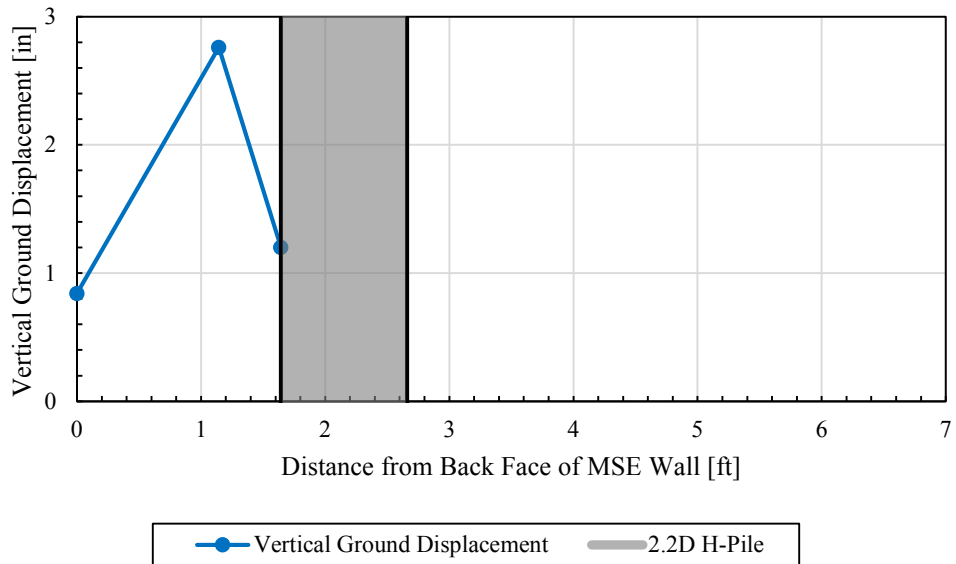


Figure F-4. Vertical ground displacement versus distance from back face of MSE wall, H-pile 2.2D.

Square Piles

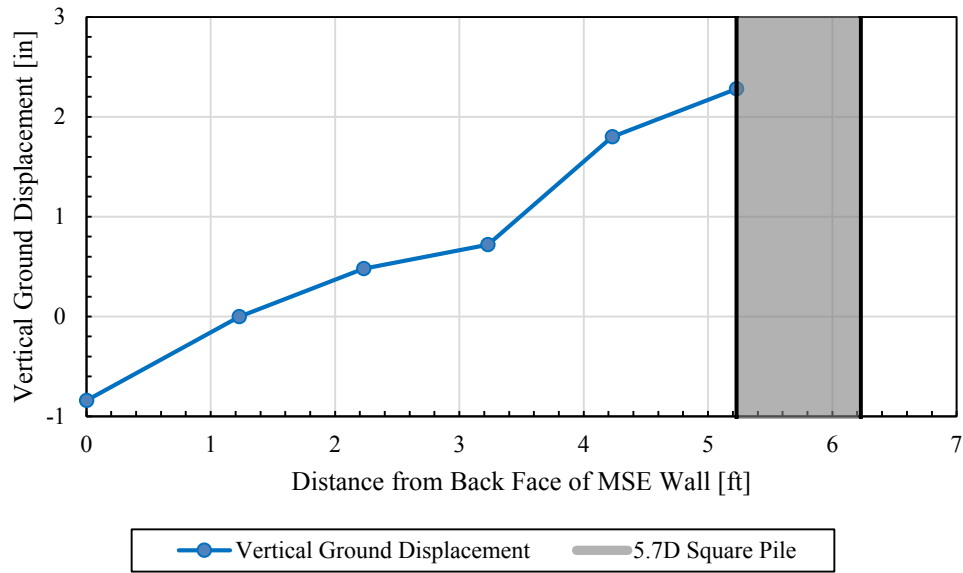


Figure F-5. Vertical ground displacement versus distance from back face of MSE wall, square pile 5.7D.

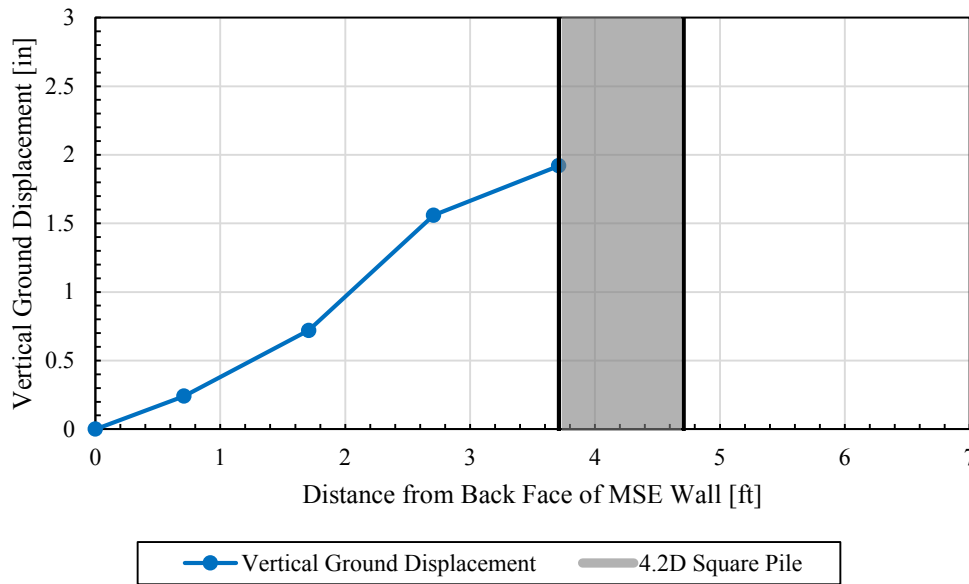


Figure F-6. Vertical ground displacement versus distance from back face of MSE wall, square pile 4.2D.

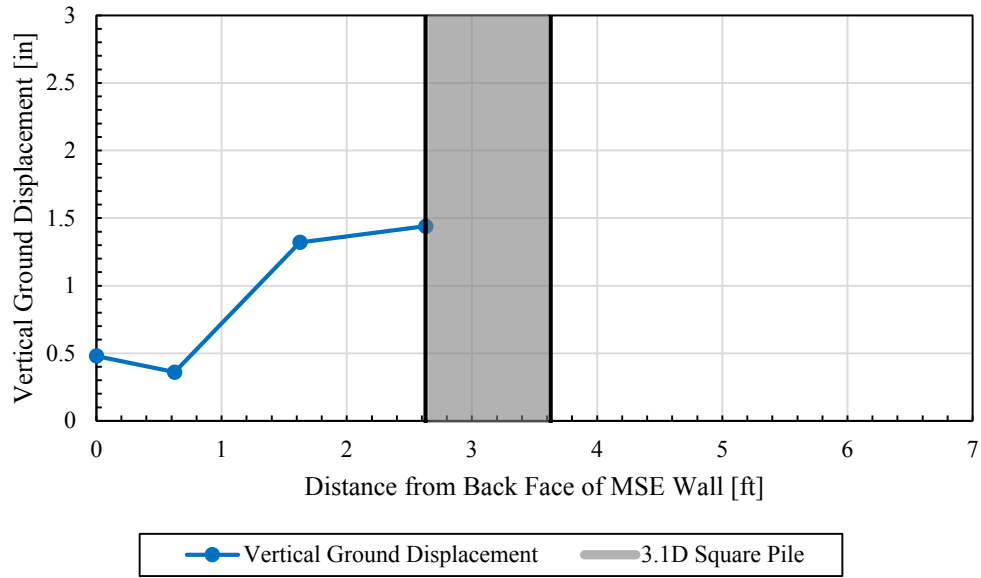


Figure F-7. Vertical ground displacement versus distance from back face of MSE wall, square pile 3.1D.

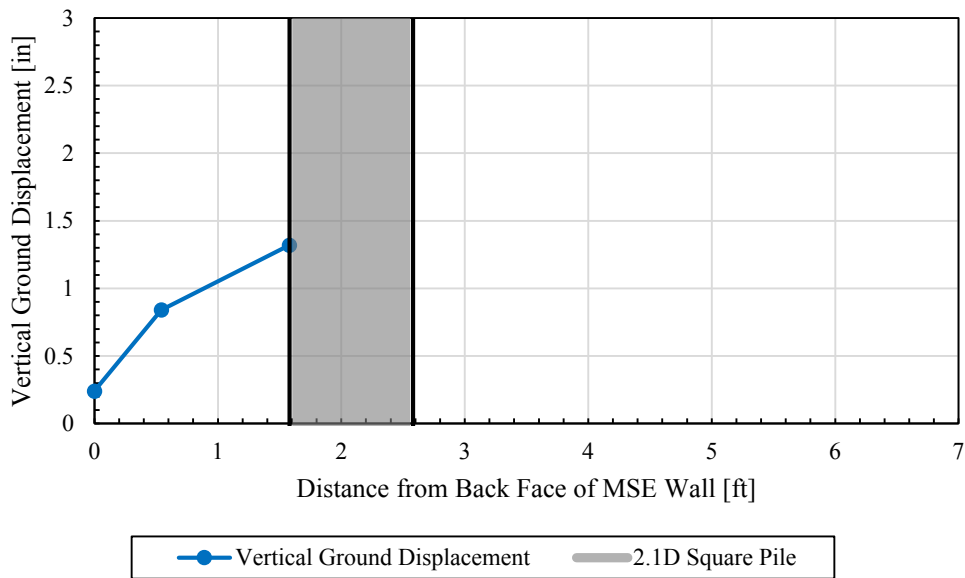


Figure F-8. Vertical ground displacement versus distance from back face of MSE wall, square pile 2.1D.

**APPENDIX G. MAXIMUM REINFORCEMENT FORCE AGAINST H-PILE AND
SQUARE PILE HEAD DISPLACEMENT CURVES**

H-Piles

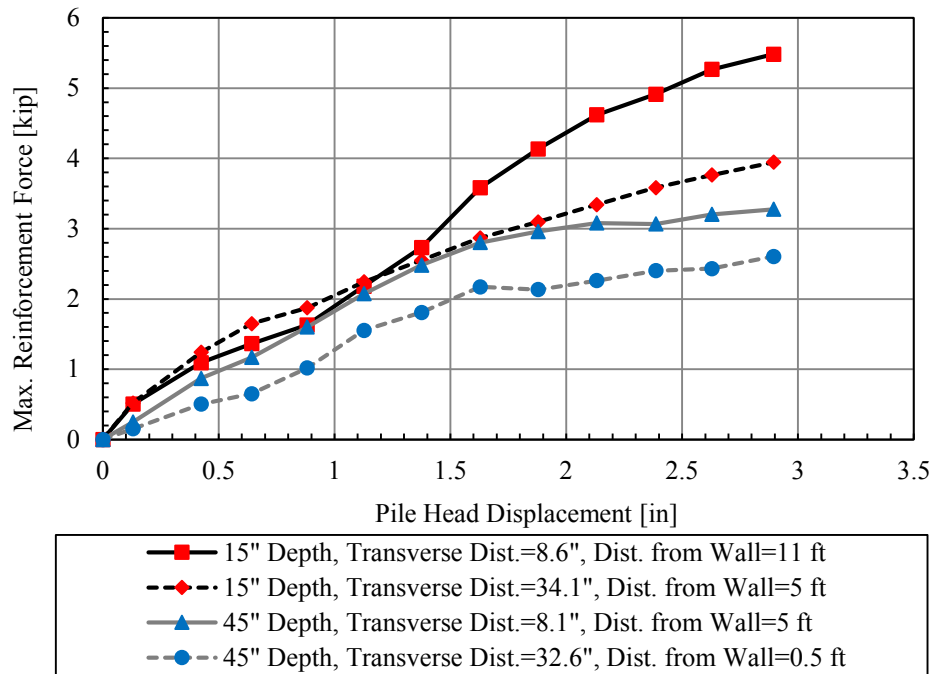


Figure G-1. Maximum reinforcement force for each instrumented ribbed strip versus pile head displacement for H-pile 4.5D.

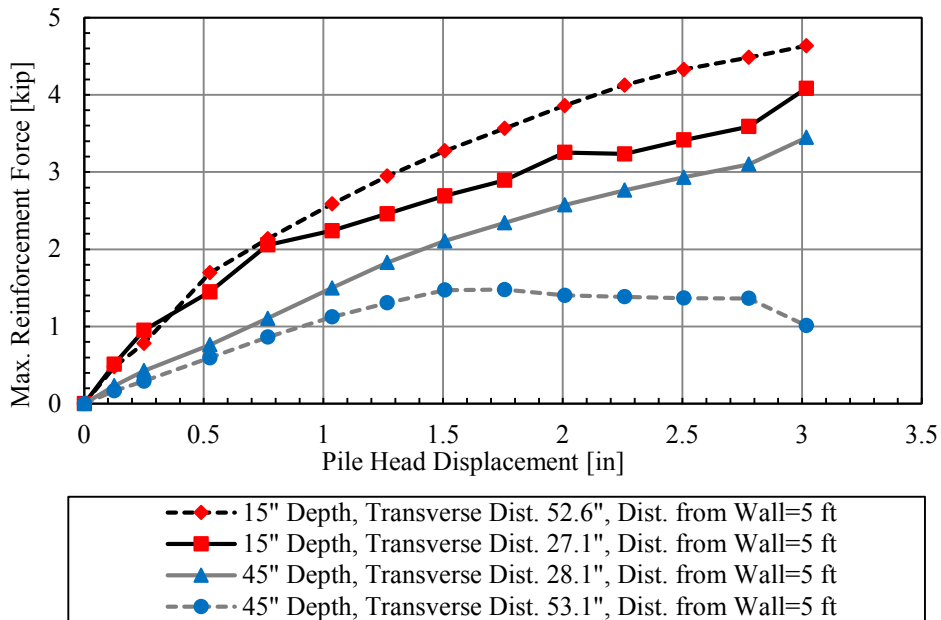


Figure G-2. Maximum reinforcement force for each instrumented ribbed strip versus pile head displacement for H-pile 3.2D.

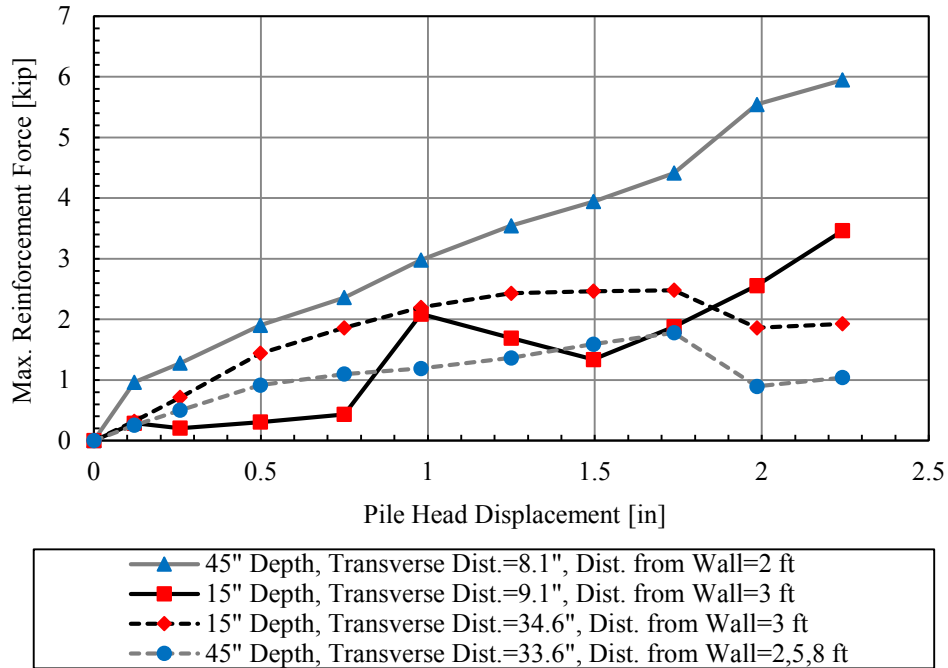


Figure G-3. Maximum reinforcement force for each instrumented ribbed strip versus pile head displacement for H-pile 2.5D.

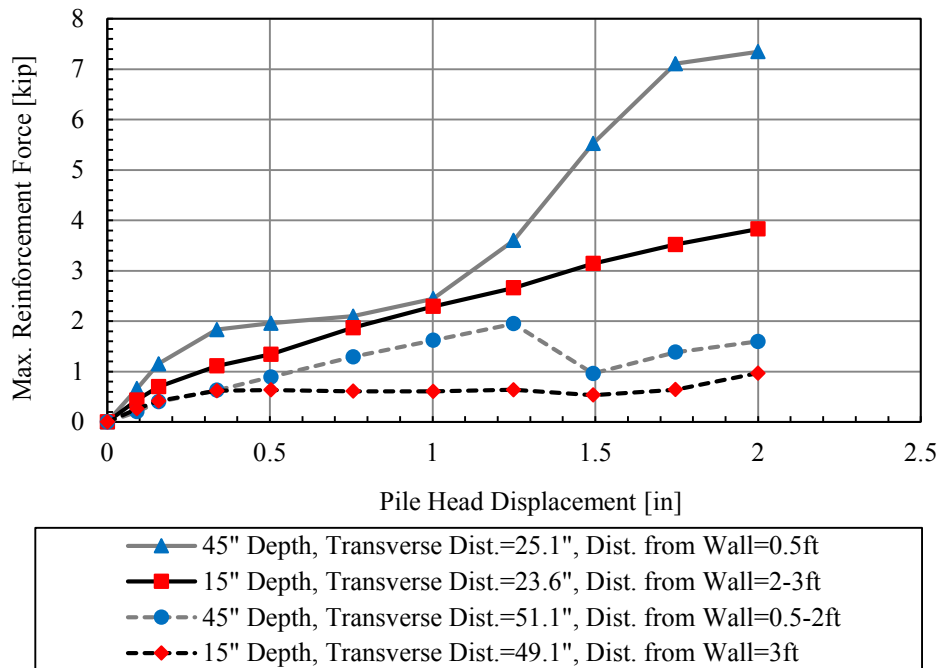


Figure G-4. Maximum reinforcement force for each instrumented ribbed strip versus pile head displacement for H-pile 2.2D.

Square Piles

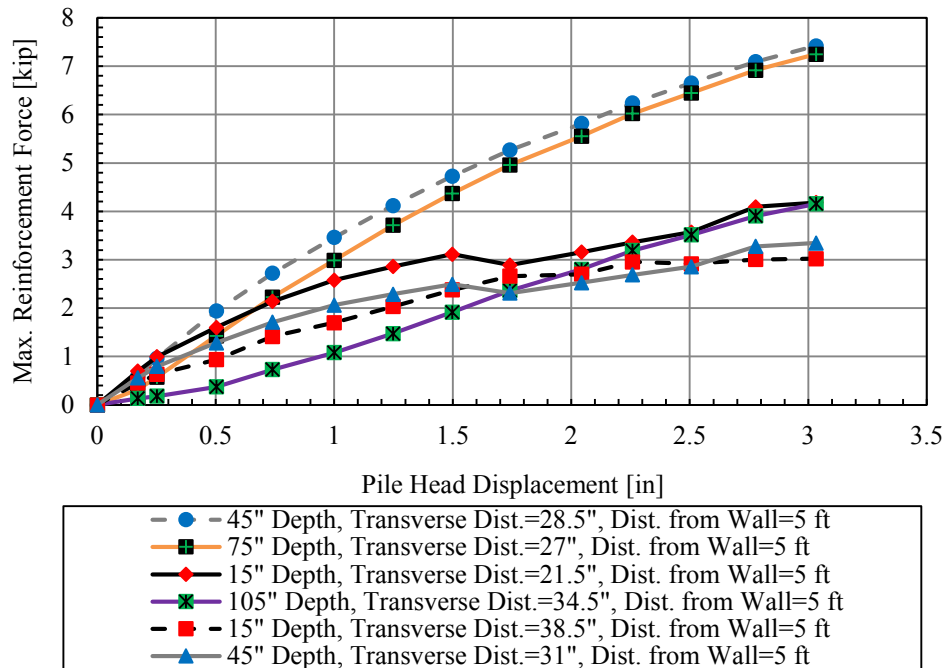


Figure G-5. Maximum reinforcement force for each instrumented welded wire versus pile head displacement for square pile 5.7D.

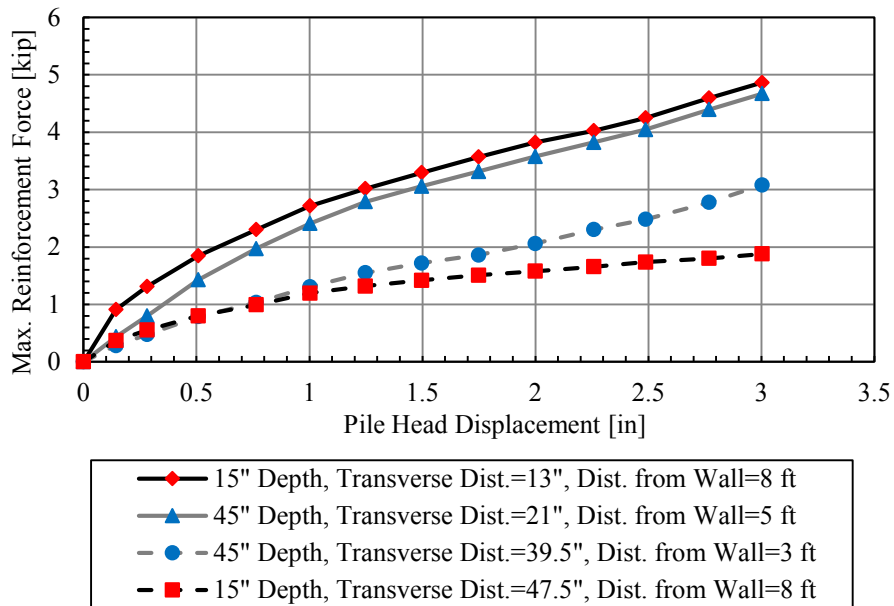


Figure G-6. Maximum reinforcement force for each instrumented welded wire versus pile head displacement for square pile 4.2D.

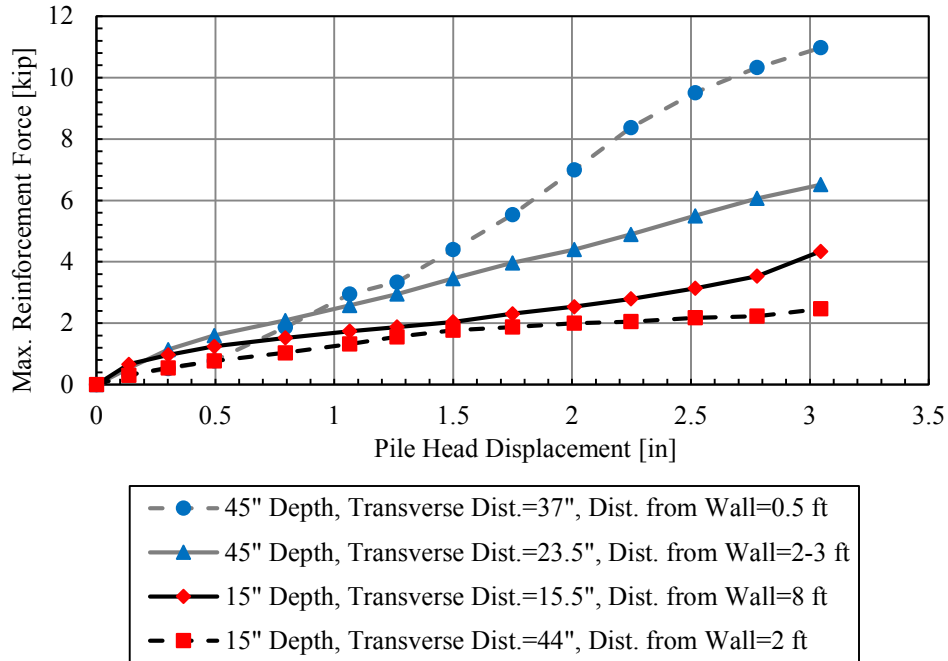


Figure G-7. Maximum reinforcement force for each instrumented welded wire versus pile head displacement for square pile 3.1D.

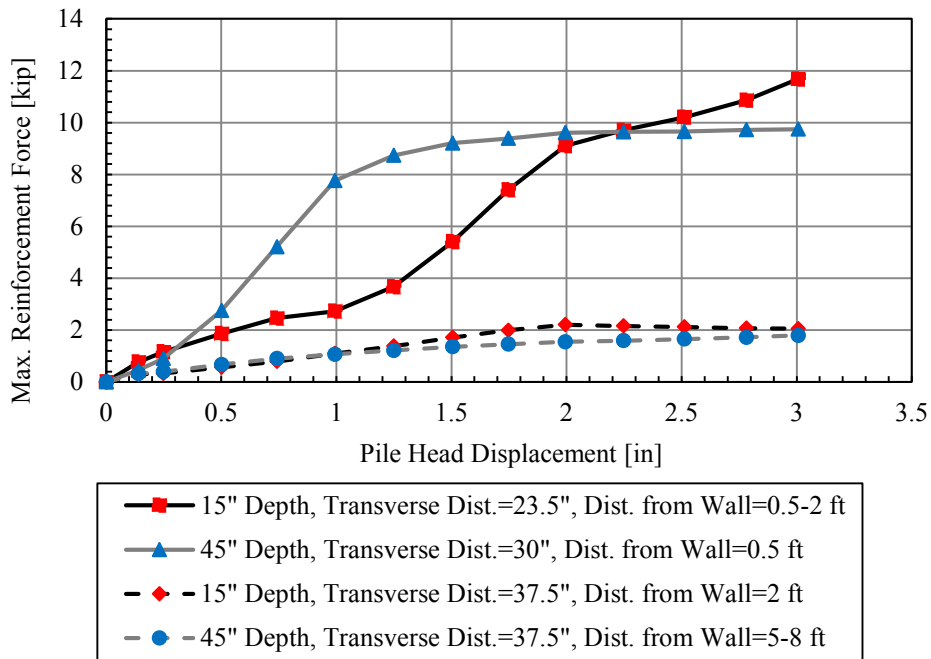


Figure G-8. Maximum reinforcement force for each instrumented welded wire versus pile head displacement for square pile 2.1D.

APPENDIX H. PILE DRIVING BLOWCOUNTS

Table H-1. Pile Driving Blow Counts for the H-piles

Depth (ft)	H-Piles			
	N (Blow Counts)			
	2.2D	2.5D	3.2D	4.5D
1				
2				
3				
4				
4.5		2		
5	2		3	
5.5				3
6				
7				
8		2		
9	3	1	3	2
10	1	1	1	1
11	2	1	2	2
12	2	1	1	1
13	5	7	5	6
14	5	5	5	5
15	4	4	4	4
16	3	4	4	4
17	3	3	4	4
18	3	4	3	4
Total	33	35	35	36

**Table H-2. Pile Driving Blow Counts for
the Square Piles**

Depth (ft)	Square Piles			
	N (Blow Counts)			
	2.1D	3.1D	4.2D	5.7D
1				
2				
3	1			1
4	1	2	2	1
5	1	1	1	1
6	1	1	1	1
7	1	1	1	1
8	1	1	1	1
9	2	1	2	2
10	2	3	5	5
11	5	5	6	6
12	8	7	7	7
13	6	6	6	6
14	5	4	4	4
15	3	4	3	3
16	2	2	2	2
17	3	2	3	3
18	3	3	5	5
Total	45	43	49	49

APPENDIX I. PLUG DEPTHS

Table I-1. Plug Depths for Pipe and Square Piles

Study	Pile Type	Nominal Normalized Spacing	Plug Depth Measured from Bottom of Pile [ft]
Hatch & Budd	Pipe	5D	10.4
		4D	10.5
		3D	10.9
		2D	10.3
Han & Besendorfer	Pipe	5D	11.3
		4D	10.4
		3D	10.6
		2D	12.1
This Study	Square	5D	8.9
		4D	9.8
		3D	9.0
		2D	9.7

APPENDIX J. HORIZONTAL SPACING OF PIPE PILES

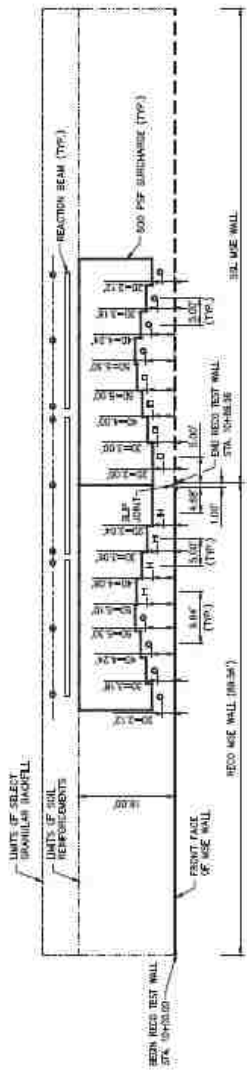
Table J-1. Adjacent Spacing of Pipe Piles on the Ribbed Strip Side

	2D to 3D Pipe (strip side)	3D to 4D Pipe (strip side)	4D to 5D Pipe (strip side)	5D Pipe to 5D H-pile (strip side)
Adjacent Spacing [in]	60	59	62	59

Table J-2. Adjacent Spacing of Pipe Piles on the Welded Wire Side

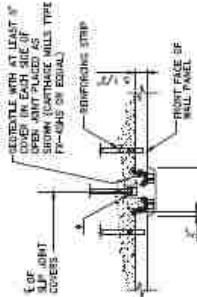
	5D Square to 5D Pipe (wire side)	5D to 4D Pipe (wire side)	4D to 3D Pipe (wire side)	3D to 2D Pipe (wire side)
Adjacent Spacing [in]	68.5	55	55	65

APPENDIX K. RECO MSE WALL PLANS



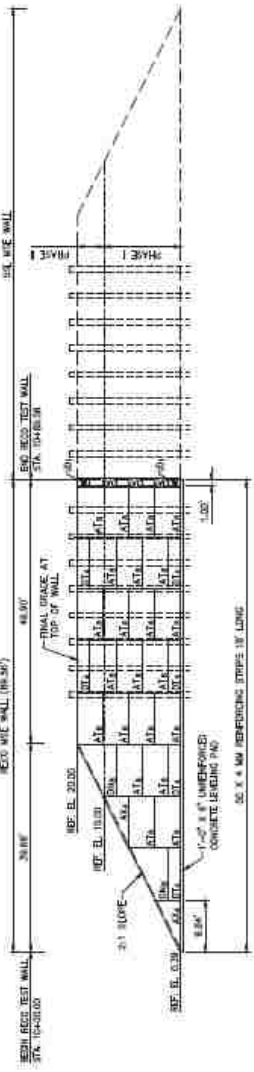
PLAN VIEW — RECO TEST WALL
SCALE: 1" = 10'

RECO TEST WALL
SCALE: NO SCALE



SLIP JOINT COVER DETAIL
SCALE: NO SCALE

THREE BEARING PADS PER UNIT. BASE STRIP OF BEARING PAD SHALL BE FOLDED OUT TO FIT FLAT ON TOP OF SLIP JOINT COVER AS SHOWN.



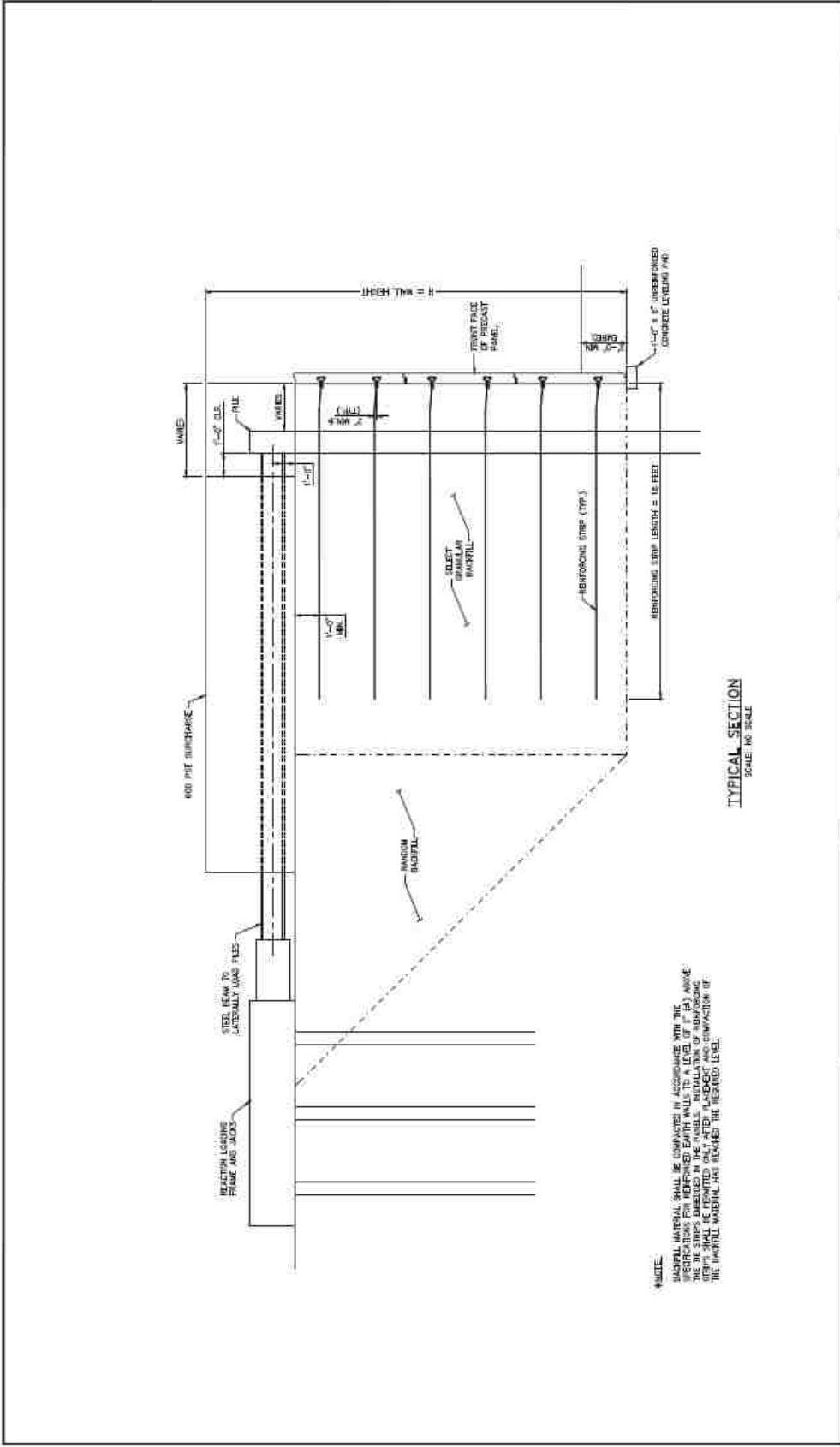
ELEVATION — FRONT FACE — RECO TEST WALL
SCALE: 1" = 30'

NOTE: DURING PHASE I, THE TOP PANELS "ON" IN COLUMN 4, PANEL "A" IN COLUMN 5, AND PANEL "X" IN COLUMN 6 SHALL ONLY HAVE THE BOTTOM REINFORCING STRIP. THE REMAINING REINFORCING STRIPS SHALL BE INSTALLED TO THE PANEL REFERENCE ELEVATION OF 30.00.

The design contained on these drawings is based on the information provided to the Reinforced Earth Company and is not intended to be used for any other project. The Reinforced Earth Company is not responsible for the safety or stability of the structure only. Reinforced Earth Company is not responsible for the safety or stability of the structure only. Reinforced Earth Company is not responsible for the safety or stability of the structure only.

This drawing contains information proprietary to The Reinforced Earth Company, and it is hereby notified that the use of this information without the written consent of The Reinforced Earth Company is prohibited. The Reinforced Earth Company is not responsible for the safety or stability of the structure only. Reinforced Earth Company is not responsible for the safety or stability of the structure only. Reinforced Earth Company is not responsible for the safety or stability of the structure only.

REVISION NO.	DATE	DESCRIPTION	BY	CHK	APP	SCALE
1	05/11/14	ISSUE FOR INTERACTION STUDY	PROJ. MGR.			AS SHOWN
2	05/11/14	ISSUE FOR INTERACTION STUDY	PROJ. MGR.			AS SHOWN
3	05/11/14	ISSUE FOR INTERACTION STUDY	PROJ. MGR.			AS SHOWN
4	05/11/14	ISSUE FOR INTERACTION STUDY	PROJ. MGR.			AS SHOWN
5	05/11/14	ISSUE FOR INTERACTION STUDY	PROJ. MGR.			AS SHOWN



NOTE:
 REINFORCING STRIPS SHALL BE ANCHORED BY ASSUREMENT WITH THE
 REINFORCING STRIPS FROM REINFORCED EARTH WALLS TO A LEVEL WITH THE
 TOP OF THE STRIPS EMBEDDED IN THE MANDL. INSTALLATION OF REINFORCING
 STRIPS SHALL BE PROMPTED ONLY AFTER BACKFILL AND COMPACTION OF
 THE MANDL MATERIAL HAS REACHED THE REQUIRED LEVEL.

TYPICAL SECTION
 SCALE: 1/8" = 1'-0"

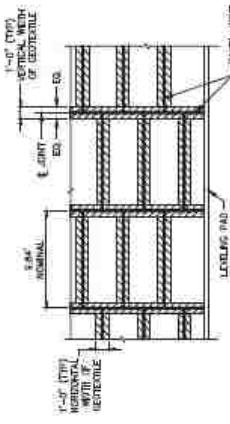
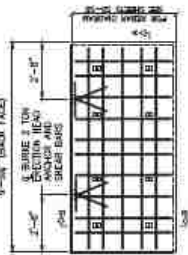
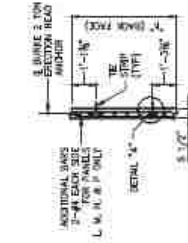
DATE	5/12/24	PROJECT NAME	000000	ISSUED BY	JES	SCALE	AS SHOWN
DRAWN BY	RE-1440	PROJECT NO.	000000	CHECKED BY	JES	DATE	AS SHOWN
DESIGNED BY	RE-1440	PROJECT NO.	000000	APPROVED BY	JES	DATE	AS SHOWN
PROJECT NO.	000000	PROJECT NAME	000000	SCALE	AS SHOWN	DATE	AS SHOWN
PROJECT NAME	000000	PROJECT NO.	000000	SCALE	AS SHOWN	DATE	AS SHOWN
PROJECT NO.	000000	PROJECT NAME	000000	SCALE	AS SHOWN	DATE	AS SHOWN
PROJECT NAME	000000	PROJECT NO.	000000	SCALE	AS SHOWN	DATE	AS SHOWN
PROJECT NO.	000000	PROJECT NAME	000000	SCALE	AS SHOWN	DATE	AS SHOWN
PROJECT NAME	000000	PROJECT NO.	000000	SCALE	AS SHOWN	DATE	AS SHOWN
PROJECT NO.	000000	PROJECT NAME	000000	SCALE	AS SHOWN	DATE	AS SHOWN
PROJECT NAME	000000	PROJECT NO.	000000	SCALE	AS SHOWN	DATE	AS SHOWN
PROJECT NO.	000000	PROJECT NAME	000000	SCALE	AS SHOWN	DATE	AS SHOWN

The design contained on these drawings is based on the information provided to the Reinforced Earth Company by the Owner. The Reinforced Earth Company has no responsibility for the design of the structure or the stability of the structure with existing conditions, and the Reinforced Earth Company is not responsible for the design of the structure or the stability of the structure with existing conditions, and the Reinforced Earth Company is not responsible for the design of the structure or the stability of the structure with existing conditions.

This drawing contains information proprietary to The Reinforced Earth Company, and its use is restricted to the use of the Reinforced Earth Company. The Reinforced Earth Company is not responsible for the design of the structure or the stability of the structure with existing conditions, and the Reinforced Earth Company is not responsible for the design of the structure or the stability of the structure with existing conditions.

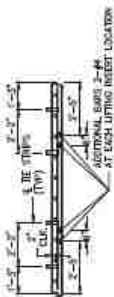
PANEL THICKNESS	3 1/2" (MIN)	REINFORCING BEMBARITY	#4	PANEL DIMENSIONS (FOR PANEL TYPE "A")	5'-0" HORIZONTAL, 5'-0" VERTICAL	MINIMUM FACTORS HORIZONTAL STREES AT FRAMES (MSF)	1.00
-----------------	--------------	-----------------------	----	---------------------------------------	----------------------------------	---	------

- NOTES:**
1. REINFORCING STEEL TO BE A615 GRADE 60.
 2. 1/2" x 1/2" CHAMFER SHALL BE FINISHED ON ALL EXPOSED EDGES (FRONT FACE ONLY).
 3. ALL PANEL TYPES AND OTHER RELATED ELEMENTS WILL BE DETAIL ON SHOP DRAWINGS.
 4. ALL PANELS SHALL HAVE TWO LIFTING KEEPS OF MINIMUM TWO TON CAPACITY EACH.
 5. MINIMUM PANEL DESIGN THICKNESS IS 3 1/2".
 6. COMPLETE FINISHES FOR PANELS SHALL HAVE A MINIMUM COMPRESSIVE STRENGTH AFTER 28 DAYS OF 4000 PSI.
 7. THE STRIPS SHALL BE STEEL ASTM A618 SS, GRADE 30 (FORMERLY ASTM A570) (QUALIFIED PER ASTM A-123).

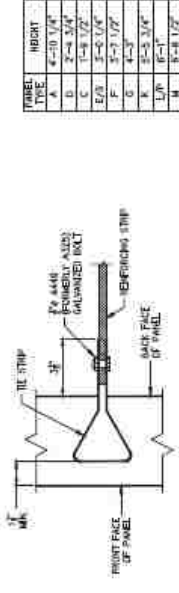


NOTE: STRIPS OF GEOTEXTILE SHALL BE PLACED ON BACK OF PANEL. PANELS SHALL BE KEPT FROM BEING MOVED BY BACK FACE PANELS. THE REINFORCED EARTH COMPANY (OR EQUAL) IS THE RESPONSIBLE PARTY FOR THE REINFORCED EARTH COMPANY (OR EQUAL).

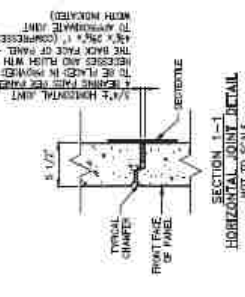
GEOTEXTILE INSTALLATION DETAIL PARTIAL ELEVATION - BACK FACE NOT TO SCALE



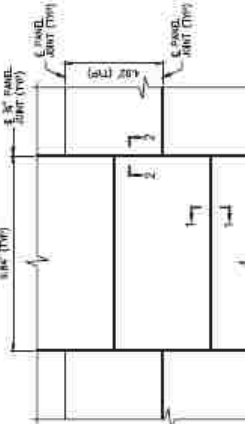
SECTION A-A NOT TO SCALE



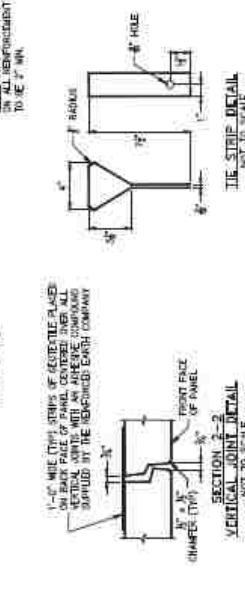
CONNECTION DETAIL 'A' NOT TO SCALE



SECTION 1-1 HORIZONTAL JOINT DETAIL NOT TO SCALE



TYPICAL PANEL LAYOUT PARTIAL ELEVATION - FRONT FACE RECTANGULAR LARGE PANELS NOT TO SCALE



SECTION 2-2 VERTICAL JOINT DETAIL NOT TO SCALE



HIGH ADHERENCE (RIBBED) REINFORCING STRIP - 50MM X 4MM NOT TO SCALE

TARGET TYPE	HIGHT
A	4'-0" 1/4"
D	2'-4" 3/4"
C	1'-8" 1/2"
E/O	3'-5" 1/4"
F	3'-7" 1/2"
G	4'-3"
K	5'-5" 3/4"
L/P	6'-1"
S	7'-3" 3/4"

NOTE: CONCRETE COVER TO BE 2" MIN.

The design contained on these sheets is based on the information provided by the client. The Reinforced Earth Company is not responsible for the design, construction, or performance of the project. The Reinforced Earth Company is not responsible for the design, construction, or performance of the project. The Reinforced Earth Company is not responsible for the design, construction, or performance of the project.

Reinforced Earth Company
 10000 W. 10th Ave., Suite 100, Golden, CO 80401
 Phone: (303) 750-1881 Fax: (303) 750-1881
 www.reinforcedearth.com

DATE	REV	DESCRIPTION
05/11/14	1	ISSUE FOR PERMIT
05/11/14	2	ISSUE FOR PERMIT
05/11/14	3	ISSUE FOR PERMIT
05/11/14	4	ISSUE FOR PERMIT
05/11/14	5	ISSUE FOR PERMIT
05/11/14	6	ISSUE FOR PERMIT
05/11/14	7	ISSUE FOR PERMIT
05/11/14	8	ISSUE FOR PERMIT
05/11/14	9	ISSUE FOR PERMIT
05/11/14	10	ISSUE FOR PERMIT
05/11/14	11	ISSUE FOR PERMIT
05/11/14	12	ISSUE FOR PERMIT
05/11/14	13	ISSUE FOR PERMIT
05/11/14	14	ISSUE FOR PERMIT
05/11/14	15	ISSUE FOR PERMIT
05/11/14	16	ISSUE FOR PERMIT
05/11/14	17	ISSUE FOR PERMIT
05/11/14	18	ISSUE FOR PERMIT
05/11/14	19	ISSUE FOR PERMIT
05/11/14	20	ISSUE FOR PERMIT
05/11/14	21	ISSUE FOR PERMIT
05/11/14	22	ISSUE FOR PERMIT
05/11/14	23	ISSUE FOR PERMIT
05/11/14	24	ISSUE FOR PERMIT
05/11/14	25	ISSUE FOR PERMIT
05/11/14	26	ISSUE FOR PERMIT
05/11/14	27	ISSUE FOR PERMIT
05/11/14	28	ISSUE FOR PERMIT
05/11/14	29	ISSUE FOR PERMIT
05/11/14	30	ISSUE FOR PERMIT
05/11/14	31	ISSUE FOR PERMIT
05/11/14	32	ISSUE FOR PERMIT
05/11/14	33	ISSUE FOR PERMIT
05/11/14	34	ISSUE FOR PERMIT
05/11/14	35	ISSUE FOR PERMIT
05/11/14	36	ISSUE FOR PERMIT
05/11/14	37	ISSUE FOR PERMIT
05/11/14	38	ISSUE FOR PERMIT
05/11/14	39	ISSUE FOR PERMIT
05/11/14	40	ISSUE FOR PERMIT
05/11/14	41	ISSUE FOR PERMIT
05/11/14	42	ISSUE FOR PERMIT
05/11/14	43	ISSUE FOR PERMIT
05/11/14	44	ISSUE FOR PERMIT
05/11/14	45	ISSUE FOR PERMIT
05/11/14	46	ISSUE FOR PERMIT
05/11/14	47	ISSUE FOR PERMIT
05/11/14	48	ISSUE FOR PERMIT
05/11/14	49	ISSUE FOR PERMIT
05/11/14	50	ISSUE FOR PERMIT
05/11/14	51	ISSUE FOR PERMIT
05/11/14	52	ISSUE FOR PERMIT
05/11/14	53	ISSUE FOR PERMIT
05/11/14	54	ISSUE FOR PERMIT
05/11/14	55	ISSUE FOR PERMIT
05/11/14	56	ISSUE FOR PERMIT
05/11/14	57	ISSUE FOR PERMIT
05/11/14	58	ISSUE FOR PERMIT
05/11/14	59	ISSUE FOR PERMIT
05/11/14	60	ISSUE FOR PERMIT
05/11/14	61	ISSUE FOR PERMIT
05/11/14	62	ISSUE FOR PERMIT
05/11/14	63	ISSUE FOR PERMIT
05/11/14	64	ISSUE FOR PERMIT
05/11/14	65	ISSUE FOR PERMIT
05/11/14	66	ISSUE FOR PERMIT
05/11/14	67	ISSUE FOR PERMIT
05/11/14	68	ISSUE FOR PERMIT
05/11/14	69	ISSUE FOR PERMIT
05/11/14	70	ISSUE FOR PERMIT
05/11/14	71	ISSUE FOR PERMIT
05/11/14	72	ISSUE FOR PERMIT
05/11/14	73	ISSUE FOR PERMIT
05/11/14	74	ISSUE FOR PERMIT
05/11/14	75	ISSUE FOR PERMIT
05/11/14	76	ISSUE FOR PERMIT
05/11/14	77	ISSUE FOR PERMIT
05/11/14	78	ISSUE FOR PERMIT
05/11/14	79	ISSUE FOR PERMIT
05/11/14	80	ISSUE FOR PERMIT
05/11/14	81	ISSUE FOR PERMIT
05/11/14	82	ISSUE FOR PERMIT
05/11/14	83	ISSUE FOR PERMIT
05/11/14	84	ISSUE FOR PERMIT
05/11/14	85	ISSUE FOR PERMIT
05/11/14	86	ISSUE FOR PERMIT
05/11/14	87	ISSUE FOR PERMIT
05/11/14	88	ISSUE FOR PERMIT
05/11/14	89	ISSUE FOR PERMIT
05/11/14	90	ISSUE FOR PERMIT
05/11/14	91	ISSUE FOR PERMIT
05/11/14	92	ISSUE FOR PERMIT
05/11/14	93	ISSUE FOR PERMIT
05/11/14	94	ISSUE FOR PERMIT
05/11/14	95	ISSUE FOR PERMIT
05/11/14	96	ISSUE FOR PERMIT
05/11/14	97	ISSUE FOR PERMIT
05/11/14	98	ISSUE FOR PERMIT
05/11/14	99	ISSUE FOR PERMIT
05/11/14	100	ISSUE FOR PERMIT

APPENDIX L. SSL MSE WALL PLANS

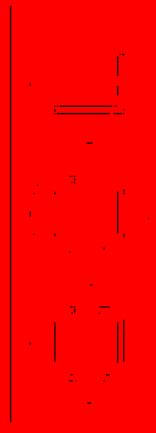


Fig. 1

**PRELIMINARY CONSTRUCTION PROPOSALS
FOR SOUTH VALLEY TREAT PLANT,
SOUTH VALLEY, TEXAS.**
FOR THE CITY OF SOUTH VALLEY, TEXAS
BY THE STATE ENGINEER, TEXAS

RECOMMENDATIONS.

FOR THE SAND FILTER
1. The sand filter should be of the type known as the "gravity" type.
2. The sand filter should be of the type known as the "gravity" type.
3. The sand filter should be of the type known as the "gravity" type.

FOR THE SAND FILTER
1. The sand filter should be of the type known as the "gravity" type.
2. The sand filter should be of the type known as the "gravity" type.
3. The sand filter should be of the type known as the "gravity" type.

FOR THE SAND FILTER
1. The sand filter should be of the type known as the "gravity" type.
2. The sand filter should be of the type known as the "gravity" type.
3. The sand filter should be of the type known as the "gravity" type.

CONCLUSIONS.

1. The sand filter should be of the type known as the "gravity" type.
2. The sand filter should be of the type known as the "gravity" type.
3. The sand filter should be of the type known as the "gravity" type.

ANALYSIS OF SAMPLES

DATE	NO.	DESCRIPTION	TEMPERATURE	PH	TOTAL SOLIDS	COLOUR	CHLORIDE	SULPHATE	CALCIUM	MAGNESIUM	IRON	COPPER	ZINC	LEAD	CHLORINE	FLUORIDE	PHOSPHORUS	NITROGEN	AMMONIA	NITRATE	NITRITES	FREE CHLORINE	TOTAL CHLORINE	TOTAL HARDNESS	CALCIUM HARDNESS	MAGNESIUM HARDNESS
1/1/24	1	Raw water	68	7.2	150	10	100	50	100	50	10	1	1	1	100	1	1	1	1	1	1	1	100	100	50	50
1/1/24	2	Filtered water	68	7.2	10	10	10	10	10	10	1	1	1	1	10	1	1	1	1	1	1	1	10	10	5	5
1/1/24	3	Filtered water	68	7.2	10	10	10	10	10	10	1	1	1	1	10	1	1	1	1	1	1	1	10	10	5	5
1/1/24	4	Filtered water	68	7.2	10	10	10	10	10	10	1	1	1	1	10	1	1	1	1	1	1	1	10	10	5	5
1/1/24	5	Filtered water	68	7.2	10	10	10	10	10	10	1	1	1	1	10	1	1	1	1	1	1	1	10	10	5	5
1/1/24	6	Filtered water	68	7.2	10	10	10	10	10	10	1	1	1	1	10	1	1	1	1	1	1	1	10	10	5	5
1/1/24	7	Filtered water	68	7.2	10	10	10	10	10	10	1	1	1	1	10	1	1	1	1	1	1	1	10	10	5	5
1/1/24	8	Filtered water	68	7.2	10	10	10	10	10	10	1	1	1	1	10	1	1	1	1	1	1	1	10	10	5	5
1/1/24	9	Filtered water	68	7.2	10	10	10	10	10	10	1	1	1	1	10	1	1	1	1	1	1	1	10	10	5	5
1/1/24	10	Filtered water	68	7.2	10	10	10	10	10	10	1	1	1	1	10	1	1	1	1	1	1	1	10	10	5	5

1. The sand filter should be of the type known as the "gravity" type.
2. The sand filter should be of the type known as the "gravity" type.
3. The sand filter should be of the type known as the "gravity" type.

NO.	DESCRIPTION	DATE	BY	REMARKS
1	Raw water	1/1/24	J. H.
2	Filtered water	1/1/24	J. H.
3	Filtered water	1/1/24	J. H.
4	Filtered water	1/1/24	J. H.
5	Filtered water	1/1/24	J. H.
6	Filtered water	1/1/24	J. H.
7	Filtered water	1/1/24	J. H.
8	Filtered water	1/1/24	J. H.
9	Filtered water	1/1/24	J. H.
10	Filtered water	1/1/24	J. H.



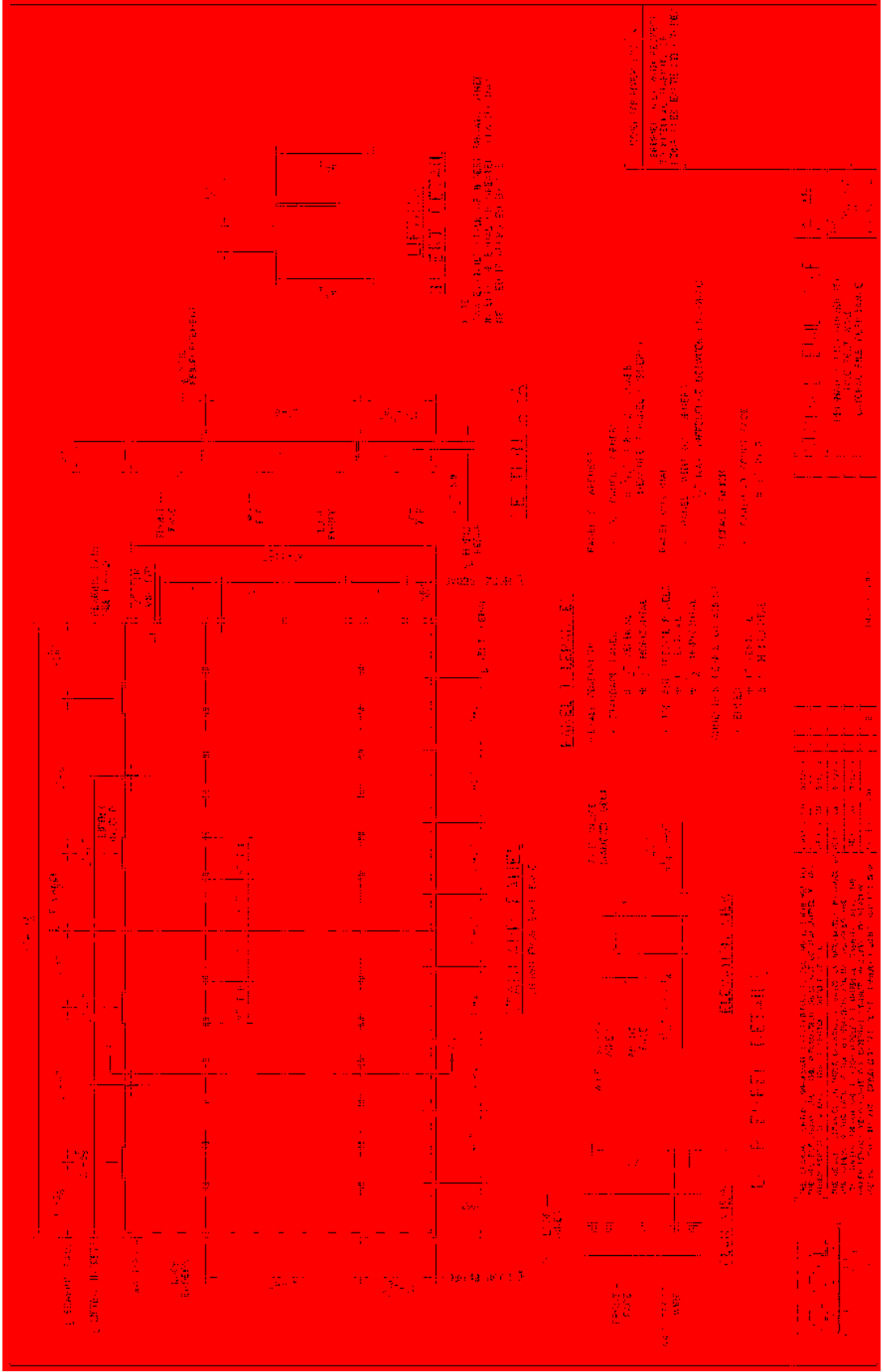


Fig. 10

TABLE I
SCHEDULE OF EQUIPMENT

NO.	DESCRIPTION	QUANTITY	UNIT	REMARKS
1	TRANSFORMER	1	UNIT	
2	MAIN BUSBAR	1	UNIT	
3	DISTRIBUTION BUSBAR	4	UNIT	
4	SWITCH	1	UNIT	
5	CIRCUIT BREAKER	1	UNIT	
6	MOTOR	2	UNIT	
7	LAMP	10	UNIT	
8	WIRE	100	FT.	

TABLE II
BILL OF MATERIALS

NO.	DESCRIPTION	QUANTITY	UNIT	REMARKS
1	TRANSFORMER	1	UNIT	
2	MAIN BUSBAR	1	UNIT	
3	DISTRIBUTION BUSBAR	4	UNIT	
4	SWITCH	1	UNIT	
5	CIRCUIT BREAKER	1	UNIT	
6	MOTOR	2	UNIT	
7	LAMP	10	UNIT	
8	WIRE	100	FT.	



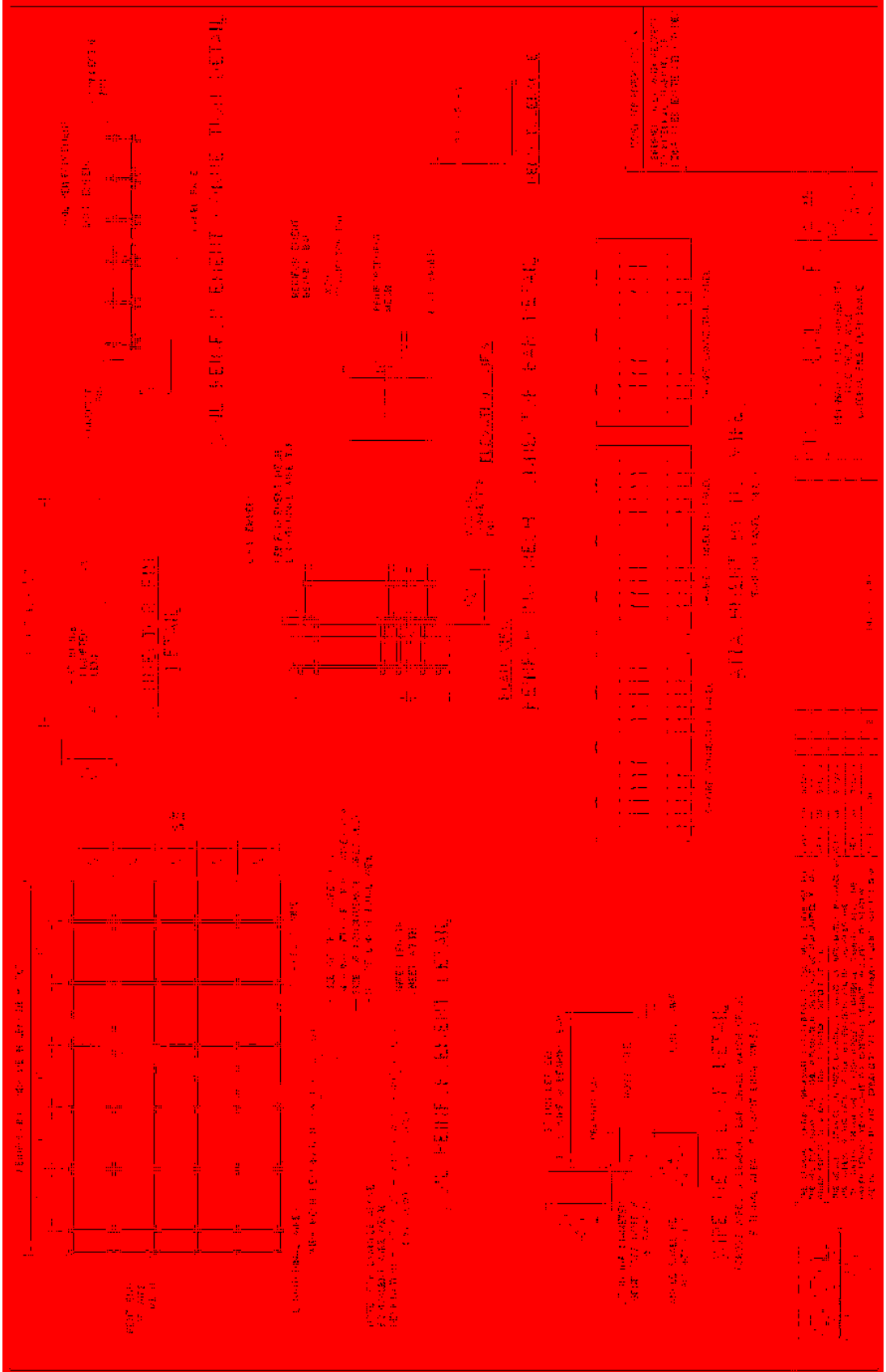
The diagram shows a transformer with a primary winding connected to a switch and a secondary winding connected to a lamp. The switch is controlled by a control circuit. The lamp is connected to the secondary winding of the transformer.

TABLE III
SCHEDULE OF EQUIPMENT

NO.	DESCRIPTION	QUANTITY	UNIT	REMARKS
1	TRANSFORMER	1	UNIT	
2	MAIN BUSBAR	1	UNIT	
3	DISTRIBUTION BUSBAR	4	UNIT	
4	SWITCH	1	UNIT	
5	CIRCUIT BREAKER	1	UNIT	
6	MOTOR	2	UNIT	
7	LAMP	10	UNIT	
8	WIRE	100	FT.	

TABLE IV
BILL OF MATERIALS

NO.	DESCRIPTION	QUANTITY	UNIT	REMARKS
1	TRANSFORMER	1	UNIT	
2	MAIN BUSBAR	1	UNIT	
3	DISTRIBUTION BUSBAR	4	UNIT	
4	SWITCH	1	UNIT	
5	CIRCUIT BREAKER	1	UNIT	
6	MOTOR	2	UNIT	
7	LAMP	10	UNIT	
8	WIRE	100	FT.	



INSTRUMENTS FOR REFLECTING INSTRUMENTS

1. **SCALE**—Four hundredths of an inch of length. The scale is divided into four hundredths of an inch, and the divisions are numbered from 0 to 100. The scale is used to measure the length of the instrument.

2. **BEVEL**—A bevel is used to draw lines at an angle. The bevel is used to draw lines at an angle of 45 degrees, 60 degrees, 75 degrees, 90 degrees, 105 degrees, 120 degrees, 135 degrees, 150 degrees, 165 degrees, and 180 degrees.

3. **PROTRACTOR**—A protractor is used to draw lines at an angle. The protractor is used to draw lines at an angle of 1 degree, 2 degrees, 3 degrees, 4 degrees, 5 degrees, 6 degrees, 7 degrees, 8 degrees, 9 degrees, 10 degrees, 11 degrees, 12 degrees, 13 degrees, 14 degrees, 15 degrees, 16 degrees, 17 degrees, 18 degrees, 19 degrees, 20 degrees, 21 degrees, 22 degrees, 23 degrees, 24 degrees, 25 degrees, 26 degrees, 27 degrees, 28 degrees, 29 degrees, 30 degrees, 31 degrees, 32 degrees, 33 degrees, 34 degrees, 35 degrees, 36 degrees, 37 degrees, 38 degrees, 39 degrees, 40 degrees, 41 degrees, 42 degrees, 43 degrees, 44 degrees, 45 degrees, 46 degrees, 47 degrees, 48 degrees, 49 degrees, 50 degrees, 51 degrees, 52 degrees, 53 degrees, 54 degrees, 55 degrees, 56 degrees, 57 degrees, 58 degrees, 59 degrees, 60 degrees, 61 degrees, 62 degrees, 63 degrees, 64 degrees, 65 degrees, 66 degrees, 67 degrees, 68 degrees, 69 degrees, 70 degrees, 71 degrees, 72 degrees, 73 degrees, 74 degrees, 75 degrees, 76 degrees, 77 degrees, 78 degrees, 79 degrees, 80 degrees, 81 degrees, 82 degrees, 83 degrees, 84 degrees, 85 degrees, 86 degrees, 87 degrees, 88 degrees, 89 degrees, 90 degrees, 91 degrees, 92 degrees, 93 degrees, 94 degrees, 95 degrees, 96 degrees, 97 degrees, 98 degrees, 99 degrees, and 100 degrees.

4. **COMPASS**—A compass is used to draw circles and arcs. The compass is used to draw circles and arcs of any radius.

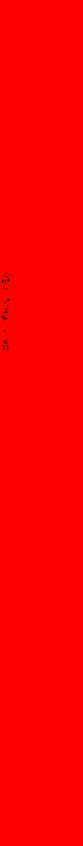
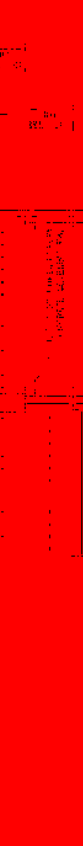
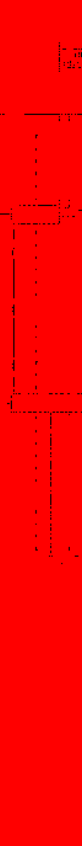
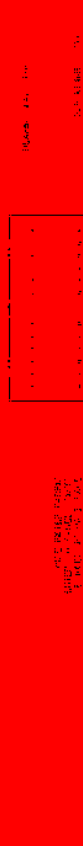
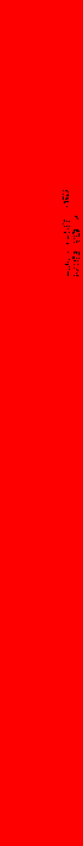
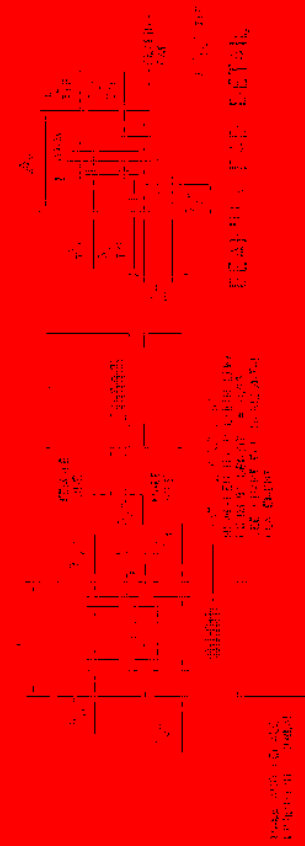
5. **TRACING BOARD**—A tracing board is used to draw lines. The tracing board is used to draw lines of any length and width.

6. **TRACING PAPER**—Tracing paper is used to draw lines. The tracing paper is used to draw lines of any length and width.

7. **TRACING PEN**—A tracing pen is used to draw lines. The tracing pen is used to draw lines of any length and width.

8. **TRACING BOARD**—A tracing board is used to draw lines. The tracing board is used to draw lines of any length and width.

9. **TRACING PAPER**—Tracing paper is used to draw lines. The tracing paper is used to draw lines of any length and width.



10. **TRACING BOARD**—A tracing board is used to draw lines. The tracing board is used to draw lines of any length and width.

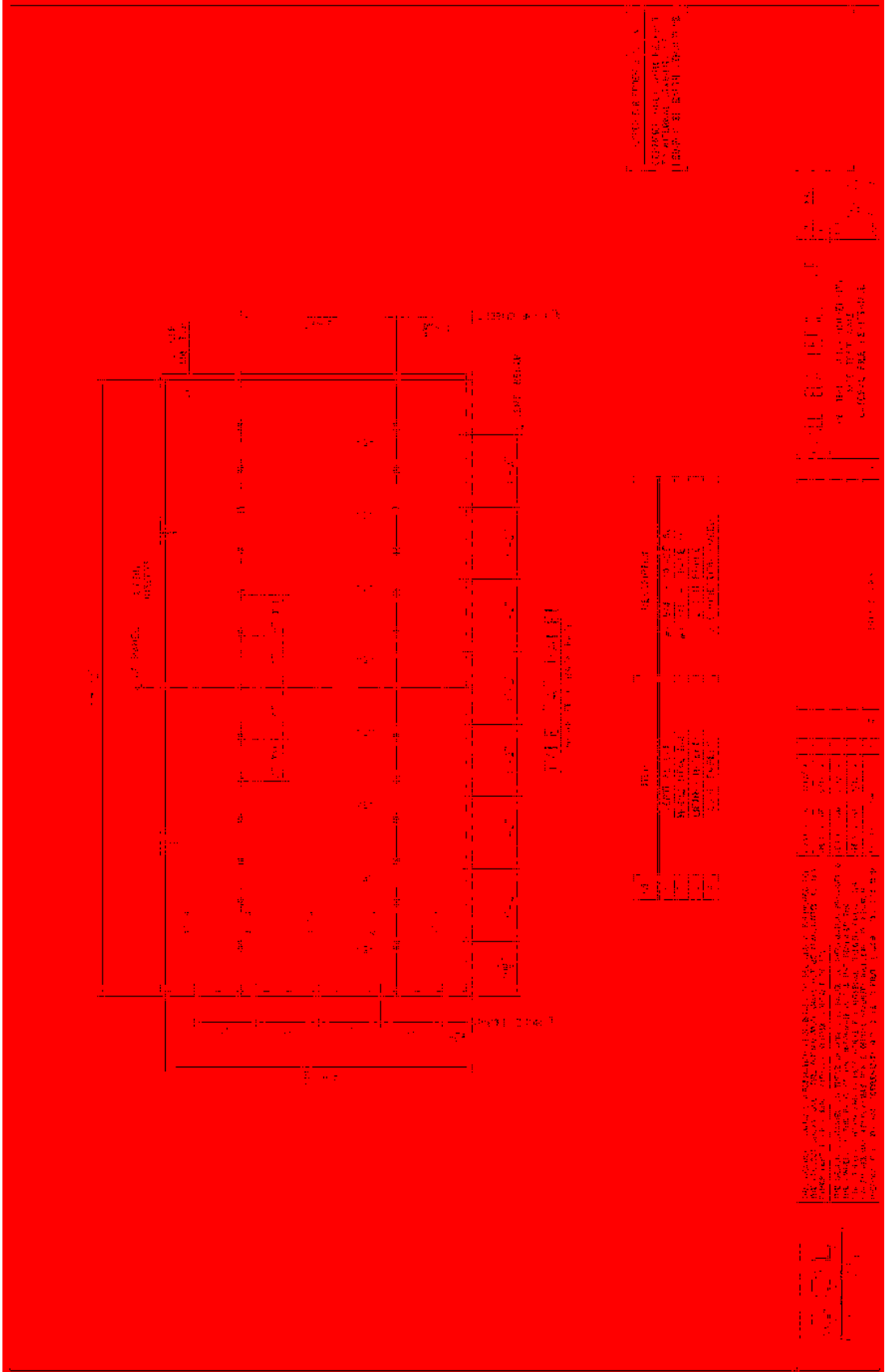
11. **TRACING PAPER**—Tracing paper is used to draw lines. The tracing paper is used to draw lines of any length and width.

12. **TRACING PEN**—A tracing pen is used to draw lines. The tracing pen is used to draw lines of any length and width.

13. **TRACING BOARD**—A tracing board is used to draw lines. The tracing board is used to draw lines of any length and width.

14. **TRACING PAPER**—Tracing paper is used to draw lines. The tracing paper is used to draw lines of any length and width.

15. **TRACING PEN**—A tracing pen is used to draw lines. The tracing pen is used to draw lines of any length and width.



1000 BROADWAY, N. Y.
 THE NEW HOTEL
 FIRST FLOOR PLAN

NO.	DESCRIPTION	AREA	REMARKS
1	RESTAURANT	1,200	
2	BAR	150	
3	LOBBY	300	
4	THEATRE	1,500	
5	STAIR	100	
6	OFFICE	200	
7	REAR	100	
8	STAIR	100	
9	STAIR	100	
10	STAIR	100	
11	STAIR	100	
12	STAIR	100	
13	STAIR	100	
14	STAIR	100	
15	STAIR	100	
16	STAIR	100	
17	STAIR	100	
18	STAIR	100	
19	STAIR	100	
20	STAIR	100	
21	STAIR	100	
22	STAIR	100	
23	STAIR	100	
24	STAIR	100	
25	STAIR	100	
26	STAIR	100	
27	STAIR	100	
28	STAIR	100	
29	STAIR	100	
30	STAIR	100	
31	STAIR	100	
32	STAIR	100	
33	STAIR	100	
34	STAIR	100	
35	STAIR	100	
36	STAIR	100	
37	STAIR	100	
38	STAIR	100	
39	STAIR	100	
40	STAIR	100	
41	STAIR	100	
42	STAIR	100	
43	STAIR	100	
44	STAIR	100	
45	STAIR	100	
46	STAIR	100	
47	STAIR	100	
48	STAIR	100	
49	STAIR	100	
50	STAIR	100	

1000 BROADWAY, N. Y.
 THE NEW HOTEL
 FIRST FLOOR PLAN

1000 BROADWAY, N. Y.
 THE NEW HOTEL
 FIRST FLOOR PLAN

